NAM

# Evaluation of Liquefaction-Induced Settlements of typical Residential Buildings on Shallow Foundations Groningen, The Netherlands


## Fugro

**Jacob Chacko, A. Giannakou, V. Drosos and P. Tasiopoulou**



Datum August 2018

## General Introduction

The soils in Groningen contain deposits of saturated sands. Therefore, the possibility of earthquake-induced liquefaction also needs to be considered. Potentially, liquefaction could be important for critical infra-structure like dikes and levees (Ref. 1).

A methodology for evaluation of liquefaction triggering more appropriate for the Groningen region was developed (Ref. 2) and a Liquefaction Hazard Assessment (Ref. 3) carried out or a pilot area in the area of largest seismic hazard and saturated sand with largest liquefaction potentials (Ref. 4) in the Groningen area.

To provide an indication of the impact liquefaction could have on the foundations of residential buildings a modelling study was carried out.

## References


1. Code calibration for coupled, effective stress FEM-assessments of the primary flood defenses at Eemshaven-Delfzijl, RMC & Fugro, R. Jongejans, Jacob Chacko, A. Giannakou, V. Drosos and P. Tasiopoulou, February 2017
2. Unbiased Cyclic Resistance Ratio Relationships for Evaluating Liquefaction Potential in Groningen, Russell Green, Adrian Rodriguez-Marek, Peter Stafford, Julian Bommer, April 2016.
3. Liquefaction Hazard Pilot Study for the Groningen Region of the Netherlands due to Induced Seismicity, R.A. Green, J.J. Bommer, P.J. Stafford, B.W. Maurer, B. Edwards, P.P. Kruiver, A. Rodriguez-Marek, G. de Lange, S.J. Oates, T. Storck, P. Omidi, S.J. Bourne, and J. van Elk, August 2018
4. Liquefaction sensitivity of the shallow subsurface of Groningen, Deltares, November 2016

NAM

| | | | | |
|---|---|---|---|---|
| **Title** | **Evaluation of Liquefaction-Induced Settlements of typical Residential Buildings on Shallow Foundations Groningen, The Netherlands** | | **Date** | August 2018 |
| | | | **Initiator** | NAM |
| **Author(s)** | Jacob Chacko, A. Giannakou, V. Drosos and P. Tasiopoulou | **Editor** | | |
| **Organisation** | Fugro | **Organisation** | | |
| **Place in the Study and Data Acquisition Plan** | The soils in Groningen contain deposits of saturated sands. Therefore, the possibility of earthquake-induced liquefaction also needs to be considered. Potentially, liquefaction could be important for critical infra-structure like dikes and levees .<br>A methodology for evaluation of liquefaction triggering more appropriate for the Groningen region was developed and a Liquefaction Hazard Assessment carried out or a pilot area in the area of largest seismic hazard and saturated sand with largest liquefaction potentials (Ref. 4) in the Groningen area.<br>To provide an indication of the impact liquefaction could have on the foundations of residential buildings a modelling study was carried out. | | | |
| **Directly linked research** | 1. Site Response of shallow subsurface and soils.<br>2. Ground Motion Prediction. | | | |
| **Used data** | | | | |
| **Associated organisation** | Fugro | | | |
| **Assurance** | | | | |

FUGRO

# EVALUATION OF LIQUEFACTION-INDUCED SETTLEMENTS OF TYPICAL RESIDENTIAL BUILDINGS ON SHALLOW FOUNDATIONS GRONINGEN, THE NETHERLANDS

Prepared for:
NPR TG2

APRIL 2018
Report No. 2017.0057-00

**CONTENTS**

## TABLES

Page



## APPENDICES

# 1.0 INTRODUCTION

## 1.1 BACKGROUND

Gas-extraction-induced earthquakes occur in the Groningen area. Consequently earthquake effects are to be considered for existing residential houses in the Groningen Province.

The current state-of-the practice in the Netherlands as implemented in NPR 9998 2017 guidelines for addressing liquefaction under shallow building foundations involves the performance of bearing capacity checks through the use of: a) simplified liquefaction triggering methods for the estimation of reduced/residual shear strength of sand layers (e.g., Idriss and Boulanger 2007); and b) the use of empirical procedures developed to calculate post-liquefaction, one-dimensional, reconsolidation settlement in the free-field away from buildings (e.g., Ishihara and Yoshimine 1992). Numerical and experimental studies have shown that these simplified analyses cannot possibly capture the magnitude of shear-induced deformations in the soil beneath shallow foundations (Dashti et al 2010, Bray and Dashti 2014, Bray and Macedo 2017).

Nonlinear effective stress fully coupled soil-structure interaction dynamic analyses were performed to develop estimates of liquefaction-induced settlements of typical residential buildings on shallow foundations covering a range of soil, ground motion and structural characteristics that are typically encountered in Groningen.

This report outlines the procedures followed, includes background information on constitutive model calibration and validation, describes the parametric numerical analyses performed to evaluate the influence of various parameters on the results, and presents a summary of the results and regression analyses performed to develop a simplified equation to estimate shallow foundation settlements of typical residential buildings in Groningen.

## 1.2 PURPOSE

Recent centrifuge tests (Dashti et al 2010, Bray and Dashti 2014) and parametric numerical analyses (Dashti and Bray, 2013, Bray and Macedo 2017) have shed light into the mechanisms involved in liquefaction-induced building settlement which are controlled primarily by shear-induced ground deformations as a result of soil-structure interaction (SSI-induced) ratcheting and bearing capacity-type movements (Figure 1-1). Volumetric-strain induced ground deformations resulting from localized partial drainage, sedimentation, and post-liquefaction reconsolidation can also contribute in addition to the possible removal of materials beneath a foundation due to the formation of sediment ejecta.

Recent research (i.e. Bray and Macedo 2017) has led to recommendations (in the form of simplified equations based on regressions of numerical results) for evaluating building settlements at liquefiable sites. However, these efforts are focused on buildings resting on continuous rigid slab foundations (i.e. minimum footing widths of about 6 meters) under relatively large earthquake events (i.e. corresponding to magnitudes larger than $M_w$ 6). By contrast for the Groningen case, typical spread footings supporting residential buildings may exhibit different behavior in terms of deformations than those evaluated by Bray and Macedo (2017). Additionally the ground motion characteristics in Groningen (i.e. energy, number of cycles and duration) are different than those in the centrifuge tests and case histories examined (i.e. from Turkey, Japan and New Zealand earthquakes with magnitudes larger than $M_w$ 7) may affect the dynamic behavior of the shallow foundation performance.

To address the above an approach for evaluating the behavior of shallow foundations of typical residential buildings in Groningen on liquefiable soils has been developed adopting similar advanced numerical methodologies as those used for the evaluation of buildings on rigid mat foundations from the researchers above. The approach has been validated against centrifuge tests and case histories of buildings on spread footings underlain by liquefiable sand. Parametric analyses were performed for the typical range of variables that affect foundation settlement (related to soil conditions, ground motion characteristics and structural characteristics) that are encountered in Groningen. The results of the parametric studies were regressed to develop a design equation that can be used to derive estimates of liquefaction-induced settlements under typical residential buildings in Groningen.

In addition, a "worst-case" scenario was developed based on the results of the parametric analyses in terms of building differential settlements. The differential settlements were imposed through springs onto a detailed 3D structural model in order to evaluate the building response.

## 1.3 APPROACH

Fugro has recently completed advanced nonlinear effective stress analyses for the dynamic performance evaluation of the Eemshaven- Delfzijl (Fugro, 2016; Tasiopoulou et al 2017 and 2018) and the Eemskanaal (Fugro, 2017; Tasiopoulou et al 2018) levees in Groningen province. The evaluations were conducted using advanced constitutive models (i.e. PM4Sand and UBCSand) to simulate the effective stress behavior of liquefiable sands.

Similar advanced numerical analyses methodology were adopted for this study of the dynamic performance of typical shallow foundations encountered in residential houses in Groningen on liquefiable deposits. The following steps outline the procedure adopted:

- *Development of idealized soil profiles and structural characteristics for parametric analyses.* Idealized soil profiles (i.e. stratigraphy and dynamic properties) were developed for use in the parametric numerical evaluations. A range of soil conditions was selected to develop idealized stratigraphy and dynamic properties for areas where screening studies have indicated the presence of thick liquefiable soils (extending from ground surface to about -15 NAP), and relatively high seismic demand. These are areas such as the town of Zandeweer where relatively high Liquefaction Potential Index/Liquefaction Potential Index-Ishihara ($LPI/LPI_{ISH}$) values were estimated by Russel Green (2018) and Deltares (2018). CPTs available in these areas were used as a basis for the development of idealized stratigraphy, properties, and the definition of scenarios for parametric studies. For the structures in the 2D effective stress analyses, equivalent frame models were developed by BICL based on typical single-storey and two-storey (i.e. terrace house) residential unreinforced masonry houses. Structural characteristics (i.e. foundation pressure and dimension) were varied based on input received by the NPR TG2 for typical ranges encountered in Groningen residential houses.
- *Development of input ground motions for 2D analyses.* Acceleration time histories were developed at El. -25m NAP for use in the 2D numerical analyses. The seismic hazard for the area of the Eemskanaal levee that crosses the Groningen field, has been assessed by the Royal Dutch Meteorological Institute (KNMI) using the latest v4 Ground Motion Prediction Equations (GMPEs) for Groningen and provided to Fugro in the form of design spectra at selected locations along the levee at the base of the North Sea formation (NS_B). The North Sea formation is the

reference “rock” horizon encountered at a depth of about 800 to 900 meters with a $V_{s30}$ of about 1400 m/s. Eleven time histories (one horizontal component) from earthquake recordings were selected for the Eemskanaal levee following the recommendations of Jongejan et al (2017) and spectrally matched to the KNMI bedrock design spectra. One-dimensional (1D) site response analyses were performed using “best-estimate” properties to propagate the design ground motions from bedrock level to about El –25 m NAP for use as input in the 2D numerical analyses. A location along the Eemskanaal levee was selected where the deep soil profile from El –25 m NAP to the base of the North Sea formation (NS_B) was similar to the Zandeweer deep soil profile. Factors of 1.15 and 0.75 were applied on the ground motions at El. -25 m NAP to account for the ground motion amplitude variability across the Groningen field.

- *Dynamic effective-stress parametric numerical analyses.* Two dimensional, effective-stress, dynamic analyses were performed using the finite difference code FLAC v8.0 (Itasca, 2016). The PM4Sand constitutive model, developed by Professor Ross Boulanger and Dr Katerina Ziotopoulou at UC Davis, was used to model the effective stress behavior of coarse-grained layers. The model parameters were calibrated in order to capture soil triggering and strain accumulation behavior for both level (no-bias) and sloping ground (with static-bias) conditions. In addition centrifuge experiments and case histories involving shallow spread foundations on liquefiable soils were analyzed to validate the ability of the model to predict liquefaction induced settlements. Two dimensional models were developed considering a range of key parameters that affect the system behavior such as thickness of non-liquefiable crust, liquefiable layer thickness, liquefiable layer relative density etc. Both dynamic liquefaction-induced (co-seismic) and volumetric post-liquefaction reconsolidation foundation settlements (post-seismic) were estimated from these analyses. A total of about 450 parametric numerical analyses were performed. Input provided by NEN TG2 was considered in selecting the cases analysed.
- *Evaluation of structural performance for “worst-case” scenario*. A “worst-case” scenario was developed based on the results of the parametric analyses in terms of building differential settlements. The differential settlements were imposed through “offset” springs on a detailed 3D structural model in order to evaluate the building response. Differential settlements of about 4.0 cm to 8.0 cm were imposed on the building through “offset” springs due to assumed differential soil conditions under the building. Sensitivity analyses were performed to evaluate building performance for different scenarios of soil variability under the building.
- Regression analysis of numerical results. Regression analyses were performed using the numerical analyses results for a total of 7 parameters associated with soil characteristics (relative density, thickness of liquefiable sand, thickness of non-liquefiable crust), structural characteristics (foundation width and foundation pressure) and ground motion characteristics (significant duration, $D_{5\text{-}75}$, and spectral acceleration at 0.7 seconds)

## 1.4 KEY PERSONNEL

Key personnel associated with the numerical analyses presented in this report are identified in the following table.

**Table 1-1. Key Project Personnel**

| **FUGRO *(2D Effective Stress Numerical Evaluations)*** | **NAME** |
|---|---|
| Technical Manager | Dr Amalia Giannakou |
| Technical Reviewer | Jacob Chacko |
| 2D Effective Stress Numerical Evaluations | Dr Ioannis Chaloulos, Dr Panagiota Tasiopoulou, Dr Vasileios Drosos, Dr Spyros Giannakos |
| Regression of Numerical Analyses Results | Dr Vasileios Drosos |
| **BICL *(Structural Evaluations)*** | **NAME** |
| Technical Managers | Rob Jury, Phil Clayton |
| Structural Evaluations of Worst-Case Scenario / Structural Input | Arun Mankavu-Puthanpurayil, Viranchi Patel |

## 1.5 REPORT ORGANIZATION

The report is organized in nine main sections. Following this introductory section:

- Section 2 presents an overview of the development of idealized soil profiles and structural characteristics for the parametric analyses
- Section 3 presents a summary for the development of input time histories for the 2D numerical analyses
- Section 4 presents the numerical approach adopted for the 2D effective stress numerical analyses
- Section 5 presents the calibration and validation of the effective stress constitutive models used in numerical analyses
- Section 6 summarizes the results from the parametric numerical analyses
- Section 7 presents the results of “worst-case” scenario evaluations
- Section 8 presents the regression analysis of the numerical results and
- Section 9 lists the references.

# Section 1

# *Shallow Foundation Study – Literature Review*

## *Mechanisms of settlement Accumulation*

1. **Ejecta-Induced**
   - **Localised, when it occurs**

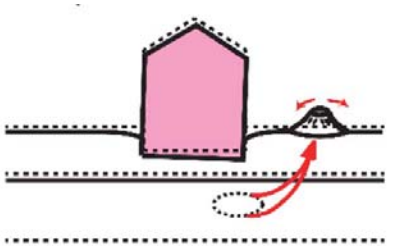

2. **Volumetric-Induced (Sedimentation, Consolidation)**
   - **Occurs after strong shaking subsides**
   - **Simplified methodologies for free-field volumetric deformations cannot capture the total settlements**

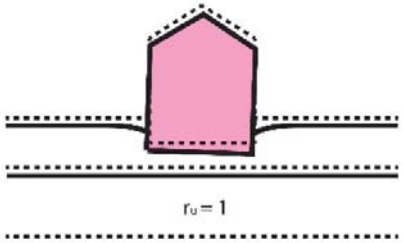


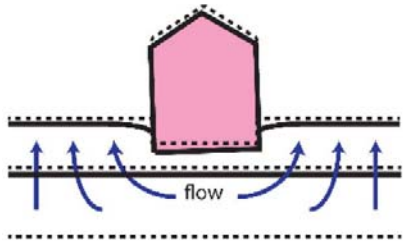


3. **Shear-Induced (Punching, SSI Ratcheting)**
   - **No simplified methodology exists**
   - **Currently can be predicted only through advanced numerical analyses**

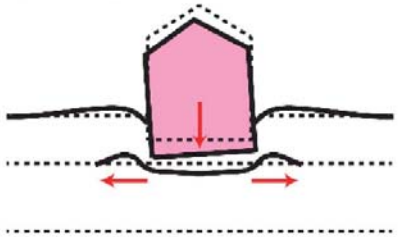

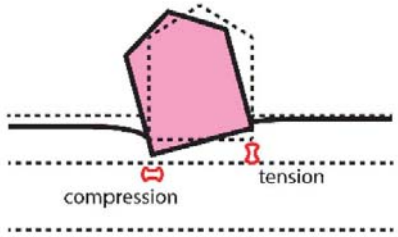


*Dashti et al (2010)*

Figure 1-1

# 2.0 DEVELOPMENT OF IDEALIZED SOIL PROFILES AND STRUCTURAL CHARACTERISTICS

Experimental studies (e.g. Liu & Dobry, 1997; Dashti et al, 2010; Popescu et al, 2010), numerical evaluations (e.g. Dashti & Bray, 2013; Elgamal et al, 2005; Bray & Macedo, 2017; Shahir & Pak, 2010) and case histories (e.g. Cubrinovski et al, 2010; Bray & Luque, 2017; Yasuda, 2012; Cetin et al, 2002) have highlighted that the major factors affecting settlements of shallow foundations on liquefiable deposits include:

- Density and Thickness of liquefiable layer
- Thickness of non-liquefiable crust
- Building pressure and foundation width; and
- Inertial forces from the structure

Based on the above, a range of soil profiles and properties as well as building pressures and foundation widths that bracket the conditions typically encountered in residential houses in Groningen were considered.

## 2.1 IDEALIZED STRATIGRAPHY AND DYNAMIC PROPERTIES

Areas where previous studies (presented at the Workshop in Schiphol in January 2018 by R. Green, and M. Korff) had highlighted high LPI/$LPI_{ISH}$ values, were reviewed to develop idealized stratigraphy and dynamic properties due to the presence of thick liquefiable sand layers.

Figure 2-1a presents a map of estimated $LPI_{ISH}$ values from available CPTs in Zandeweer using:

- Green et al (2018) Groningen-specific liquefaction triggering method to estimate factor of safety against liquefaction
- PGA of 0.25g from v4 GMM in Zandeweer for 2475-year return period based on the NPR webtool
- A scenario earthquake of magnitude $M_w$ 5

Figure 2-1b presents similar results using Idriss and Boulanger (2008) liquefaction triggering method that is currently in NPR9998 2017. As shown on these figures $LPI_{ISH}$ values estimated with the two methods are largely similar with the Green et al (2018) method resulting is slightly higher LPIish values (i.e. 6 to 14 compared to 2 to 12).

Typical liquefaction-triggering logs in this area are shown on Figures 2-2a to 2-2d. The left plot on these figures shows the measured tip resistance and the tip resistance required to preclude liquefaction (i.e. required to result in a factor of safety against liquefaction of 1). When the tip resistance required to preclude liquefaction is higher than the measured tip resistance the area between the two lines is shaded blue (i.e. to the right of the measured tip resistance). The colors shown on the left of the measured tip resistance (i.e. yellow, green, pink and red) correspond to the different zones according to Robertson (1990) classification chart shown on Figure 2-2a. The second plot from the left shows the estimated factor of safety against liquefaction (black dots) and the Ic factor (red line) versus depth. The third plot from the left shows the estimated Cyclic Resistance Ratio (CRR, red line) and the Cyclic Stress Ratio (CSR, blue line). The fourth plot shows the friction ratio.

A review of Figures 2-2a to 2-2d shows that:

- Lower $LPI_{ISH}$ values are generally associated with presence of non-liquefiable soils near the surface (Figure 2-2a)
- Higher $LPI_{ISH}$ values are generally associated with presence of liquefiable coarse-grained layers near the ground surface (Figure 2-2b to 2-2d)
- The presence of laminated sand and clay deposits (as evidenced by Ic values close to 2.6) near the ground surface tends to result in low estimates of cyclic resistance and therefore higher $LPI_{ISH}$ values
- Another factor contributing to higher $LPI_{ISH}$ values is the increased thickness of liquefiable deposits (Figure 2-2d) which in many cases are laminated sands and clays

It is noted that the presence of clay laminations increases the liquefaction triggering resistance (Figure 2-3) relative to that of homogenous sand, while at the same time producing lower tip resistance than would typically be measured in a homogenous sand (Fugro 2016; Tasiopoulou et al 2017). This is due to the fact that the sand layers within the interlayered deposits are thin (perhaps 1 to 20 cm thick) and the tip resistances do not fully develop to a level that would provide a meaningful representation of the soil density. However, the signature of the CPT data which is essentially showing an averaged response of multiple layers is often similar to that of a loose silty sand or a sandy silt. In this study, laminated deposits are conservatively treated as homogenous when considering ranges of relative density or in the definition of worst case scenarios.

Figure 2-4 presents cumulative frequency distributions of relative densities estimated through qc1Ncs from all CPTs available in Zandeweer using Boulanger and Idriss (2014) procedure. The grey lines represent cumulative frequency distributions of relative densities from 1 m to 6 m depth from individual CPTs and the red line represent cumulative frequency distribution of relative densities from 1 m to 6 m depth from all available CPTs. The blue line on this plot represents cumulative frequency distribution of relative densities from 1 m to 2 m depth from all available CPTs. As shown on this figure, the median relative density is about 50%, while a relative density of about 40% represents a 3rd percentile value. As noted above the laminated deposits are conservatively treated as silty sands in these evaluations (as discussed above).

Figure 2-5 presents an example of soil variability encountered in Zandeweer from two adjacent CPTs under the same building, where in one CPT the liquefiable soils extend up to the ground water table elevation (i.e. assumed at 1 meter depth) while in the adjacent CPT a clay crust is present up to about 4 m depth.

Based on the above the following idealized stratigraphy and properties was developed for the parametric evaluations (Figure 2-8) in descending sequence:

- Top soil consisting of non-saturated sand extending from ground surface (assumed at El. 0 m NAP) to base of foundation
- Non-liquefiable crust layer of varying thickness, $H_{crust}$, ($H_{crust}$ varies from 0 to 1 meter in the parametric analyses) consisting of clay. Parametric analyses were performed for various clay undrained shear strength values where the clay static strength is varied as a function of the foundation pressure, q, as $S_{u,crust} = \alpha\ (q/5.14)$, where $\alpha$ varies between 1 and 6
- Liquefiable layer of varying thickness, $H_{liq}$, ($H_{liq}$ varies from 0.5 to 10 meters). Parametric analyses were performed for relative densities between 30% and 50%.

- Holocene clay layer extending to El. -15 m NAP. The static undrained shear strength of the clay increases with depth.
- Pleistocene Sand extending from El. -15 m NAP to El. -25 m NAP.

Figure 2-6 presents plots of idealized shear wave velocity and static shear strength parameters for an example profile analyzed. Shear wave velocity estimates were developed from typical CPTs shown on Figure 2-6. Shear wave velocity was estimated as the average of published correlations with CPT data. For fine-grained layers the average of the Mayne and Rix (1995), Andrus et al. (2007), and Robertson (2009) correlations was used while for sands the average of the Rix and Stokoe (1991), Andrus et al. (2007), and Robertson (2009) correlations was used.

Static undrained shear strength estimates for the Holocene clay layer were estimated from typical CPTs shown on Figure 2-6 using an $N_k$ factor of 15. A 20% increase was used for the dynamic undrained shear strength of fine-grained layers to account for strain rate effects.

The hydraulic conductivity of the liquefiable sand layers was assumed to be anisotropic and equal to 1e-6m/s and 0.5e-6m/s for horizontal and vertical drainage respectively.

## 2.2 STRUCTURAL CHARACTERISTICS

Two structures have been analyzed in the study presented herein: a) a 1-storey detached house with an attic and b) a 2-storey terraced house. These types of structure were considered representative of the building stock in Groningen (Figure 2-7a).

The 1-storey structure has plan-view dimensions of about 7.8 m by 10.7 m and it is made of masonry (Figure 2-7b). The foundation system consists of strip footings, mainly along the perimeter of the building. The footings are embedded about 0.9 m and the space between the foundation base and the ground floor has been assumed to be empty (crawl space). Since the out-of-plane stiffness/strength of the masonry walls is limited, it is assumed that the lateral loads can only be carried by the perimeter walls (i.e. the walls parallel to the direction of movement/loading).

BICL developed an equivalent frame model of the building that was used in the 2D effective stress parametric analyses with FLAC performed by Fugro. Luque and Bray (2015) showed that the primary aspects of the dynamic response of a three-dimensional (3D) system in terms of liquefaction-induced building settlement can be captured in two-dimensional (2D) analyses by using tributary mass and stiffness with the primary goals being to capture the mass and stiffness, and hence the correct fundamental period of the structural system for one-directional shaking as well as the contact pressure transmitted to the foundation system. For the development of the equivalent frame model the location, dimensions and properties of the masonry piers and spandrels were taken into consideration (Figure 2-7c). The mass of the building that participates into the inertial load due to earthquake was estimated and assigned to the perimeter walls. An effective mass of 30 tons was assigned to the equivalent frame model. It is noted that this mass provides solely inertial load and does not contribute to the vertical loading of the footing. The vertical loads were assigned directly onto the footings as vertical distributed forces and were varied in the parametric evaluations as discussed in Section 6.0. The natural period of the fixed-base equivalent frame has been calculated to be about 0.11 sec in the short direction and 0.13 sec in the long direction.

For the 2D analysis, the frame is considered to rest on two strip foundations, at the two ends, running out of plane. As shown on Figure 2-7c, the strip footing section is 0.7 m wide and 0.45 m tall. In order to transform the 3-dimensional building geometry into 2 dimensions,

loads and stiffnesses were scaled by the tributary out-of-plane length of the equivalent frame (i.e. 5.5m in the short direction and 3.9m in the long direction).

Similarly, an equivalent frame model was developed by BICL for the 2-storey masonry building (Figure 2-7d). The building model is 7.8m-wide and it is assumed to rest on two strip foundations with dimensions of 0.7m (width) and 0.35m (height). Effective masses of about 60 tons and 36 tons were assigned to the first and second floor level, respectively, of the equivalent frame model. It is noted that the masses provide solely inertial load and do not contribute to the vertical loading of the footings. The vertical loads were assigned directly onto the footings as vertical distributed forces and were varied in the parametric evaluations as discussed in Section 6.0. A tributary out-of-plane length of 6.3 m has been assigned to the equivalent frame. The natural period of the fixed-base equivalent frame has been calculated to be about 0.1 sec, similar to that of the 1-storey building. This is primarily because these types of structures are relatively stiff in the transverse direction.

# Section 2

# Liquefaction Triggering Evaluations in Zandeweer

## $LPI_{ish}$ values [Green et al., 2018] – $M_w$ 5 , PGA = 0.25 g [V4 GMM, 2475 yrs]

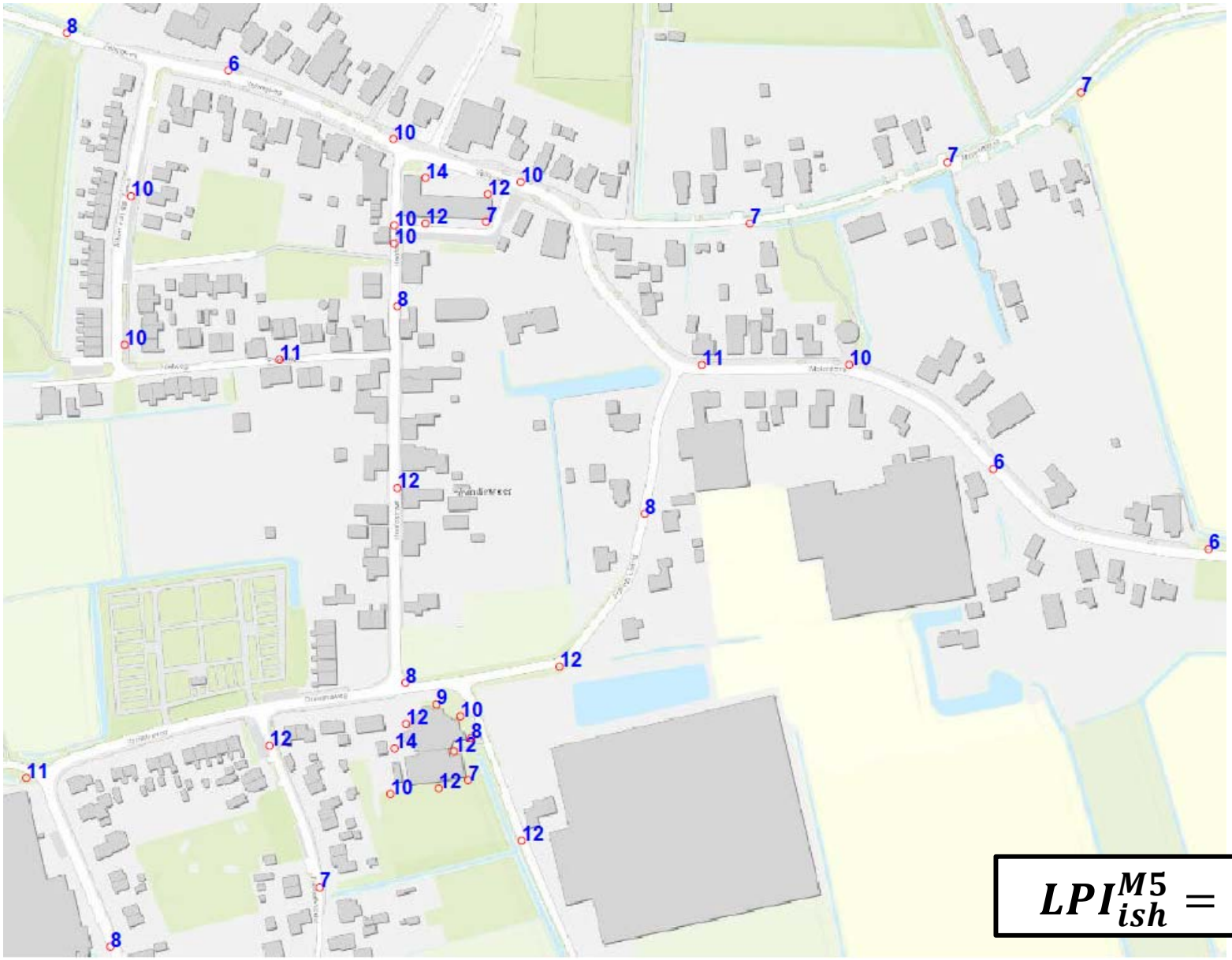


$$LPI_{ish}^{M5} = 6 - 14$$

Figure 2-1a

# *Liquefaction Triggering Evaluations in Zandeweer*

## *$LPI_{ish}$ values [Idriss & Boulanger, 2008] – $M_w$ 5 , PGA = 0.25 g [V4 GMM, 2475 yrs]*

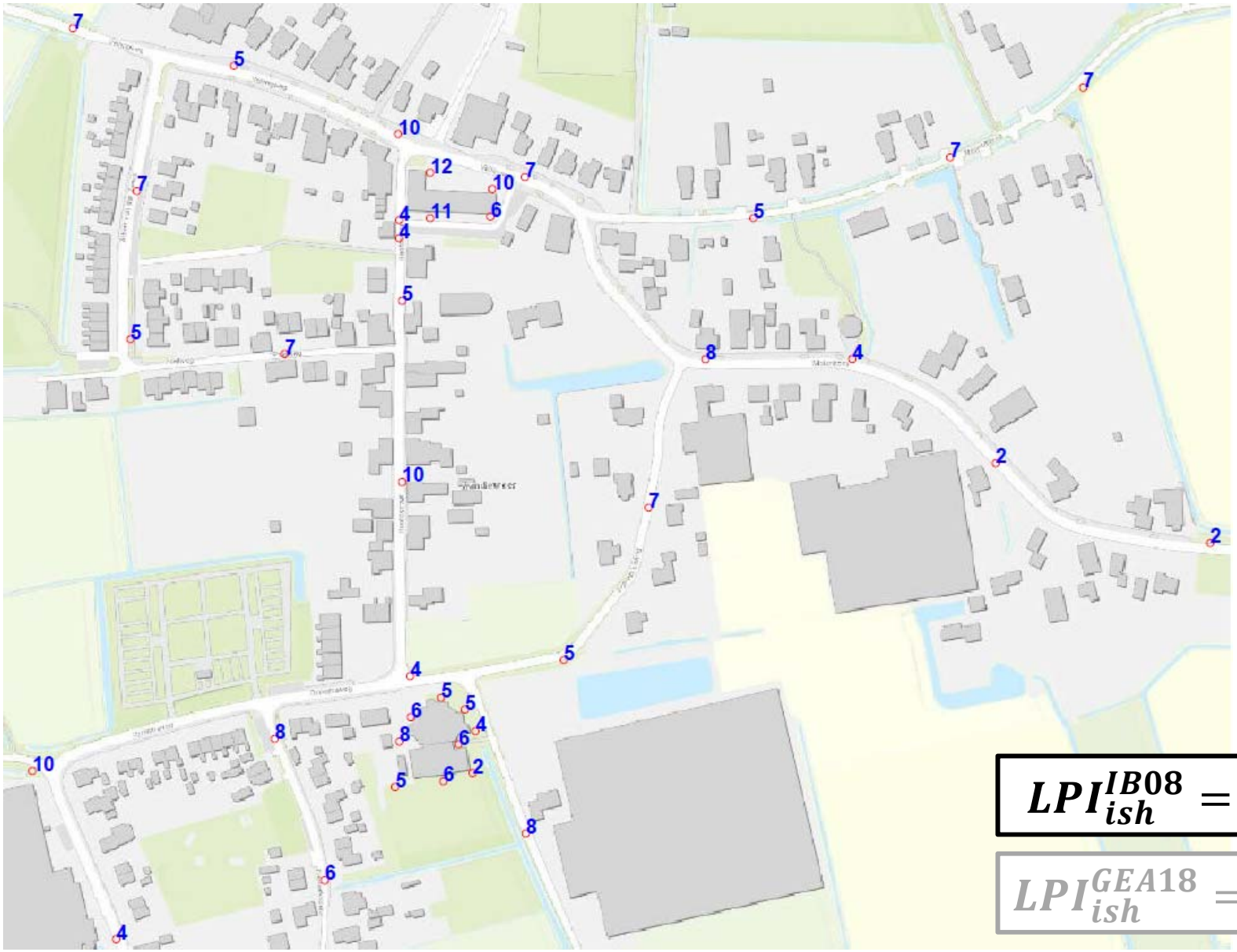


$$LPI_{ish}^{IB08} = 2 - 12$$

$$LPI_{ish}^{GEA18} = 6 - 14$$

Figure 2-1b

# *Liquefaction Triggering Evaluations in Zandeweer – Typical Site Conditions*

**$LPI_{ish}$ = 6** *(9017-0068-000_DKMP16_20170316)*

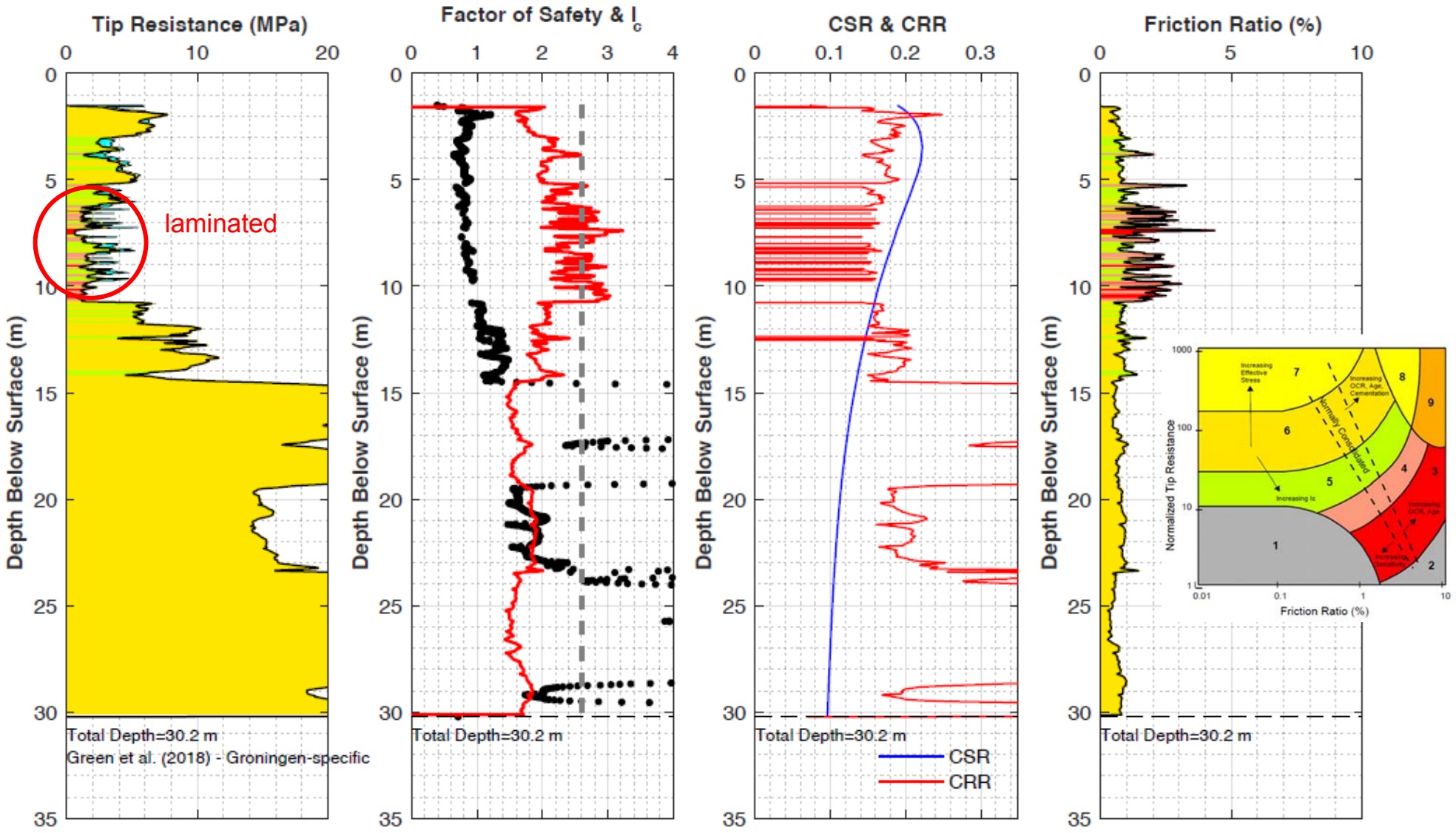


Figure 2-2a

# *Liquefaction Triggering Evaluations in Zandeweer – Typical Site Conditions*

**$LPI_{ish}$ = 10** *(9017-0068-000_DKMP10_20170316)*

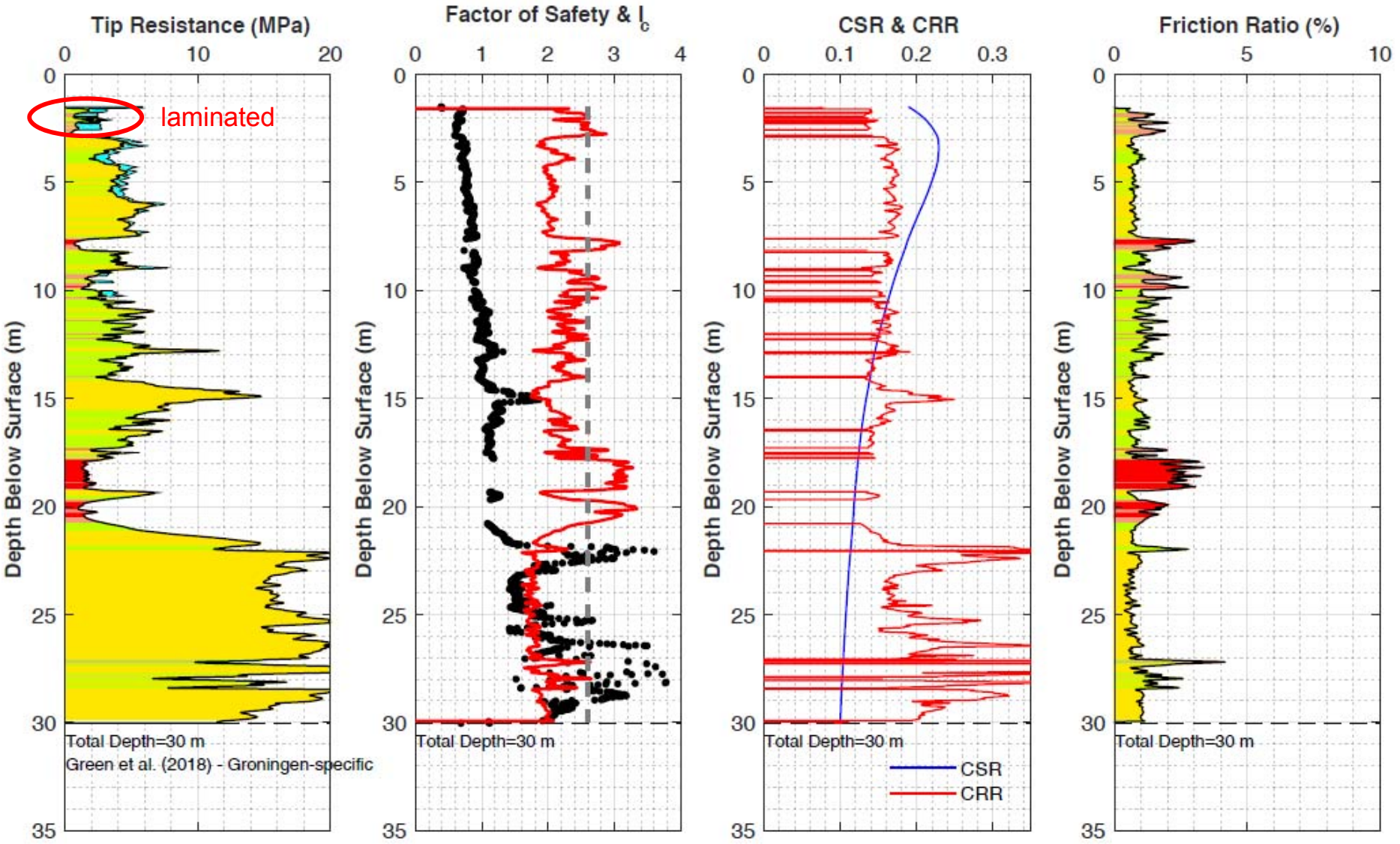


Figure 2-2b

# *Liquefaction Triggering Evaluations in Zandeweer – Typical Site Conditions*

**$LPI_{ish}$ = 14** *(66754_DKP004_20161213)*

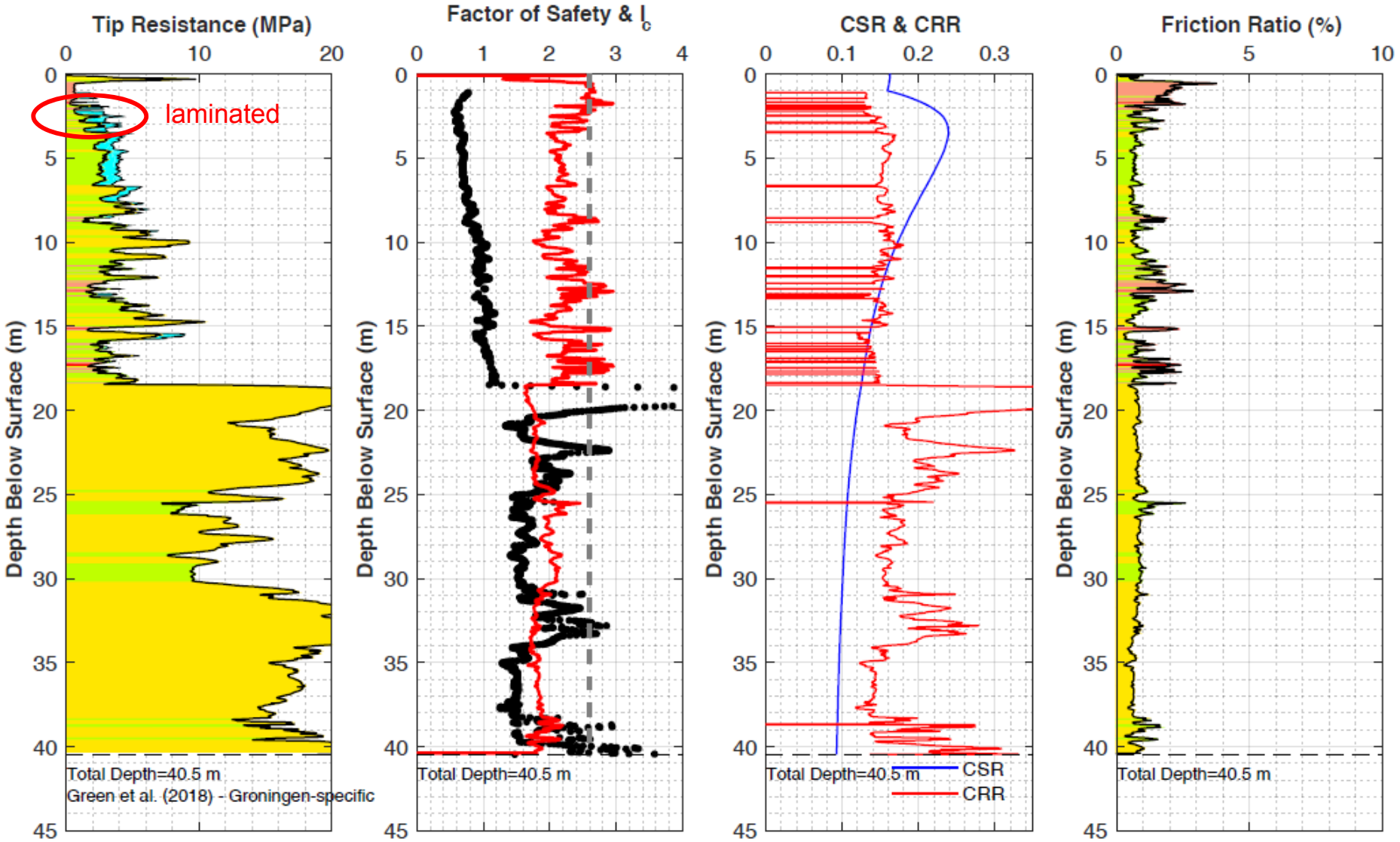


Figure 2-2c

# *Liquefaction Triggering Evaluations in Zandeweer – Typical Site Conditions*

**$LPI_{ish}$ = 14** *(1601765_S064-4_20160826)*

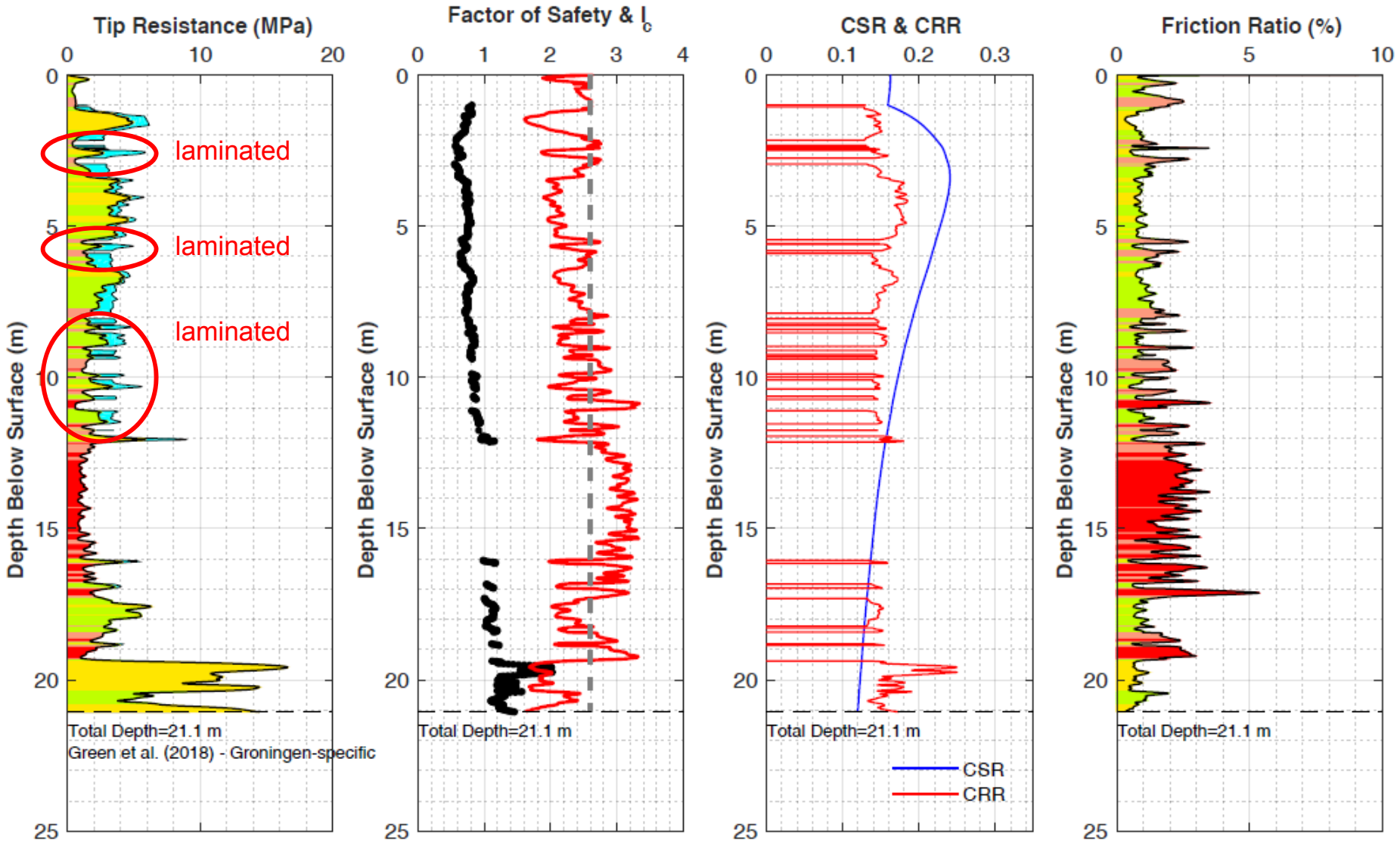


Figure 2-2d

# *Liquefaction Triggering Resistance of Laminated Deposits*

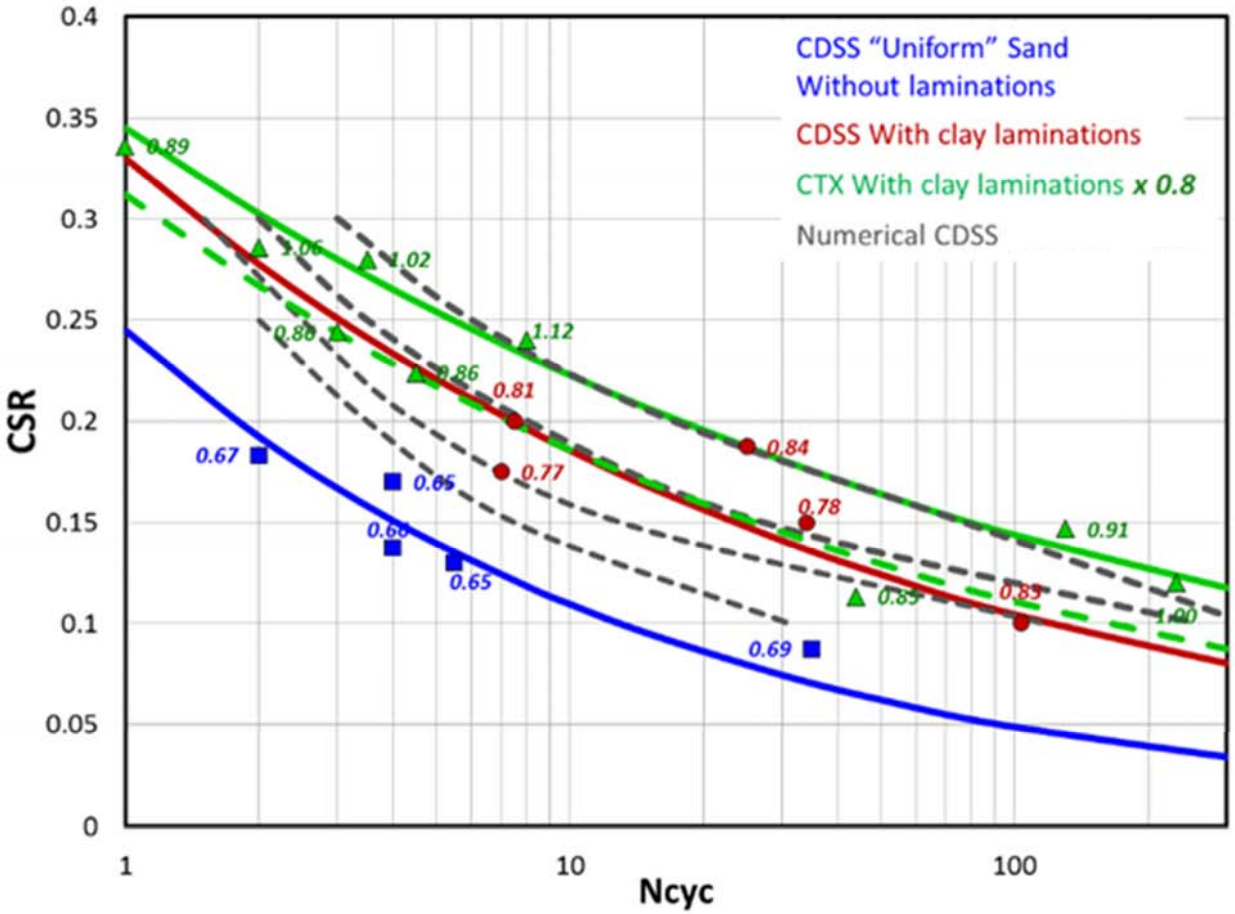


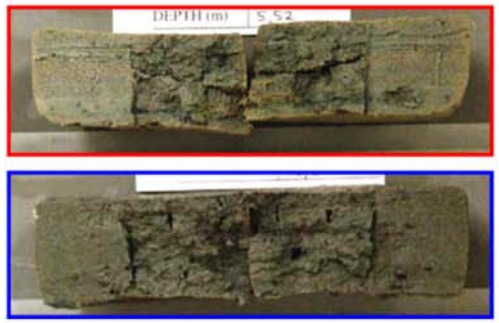

Figure 2-3

# Site Conditions - Zanderweer

## Zandeweer CPTs cumulative frequency distribution of Dr

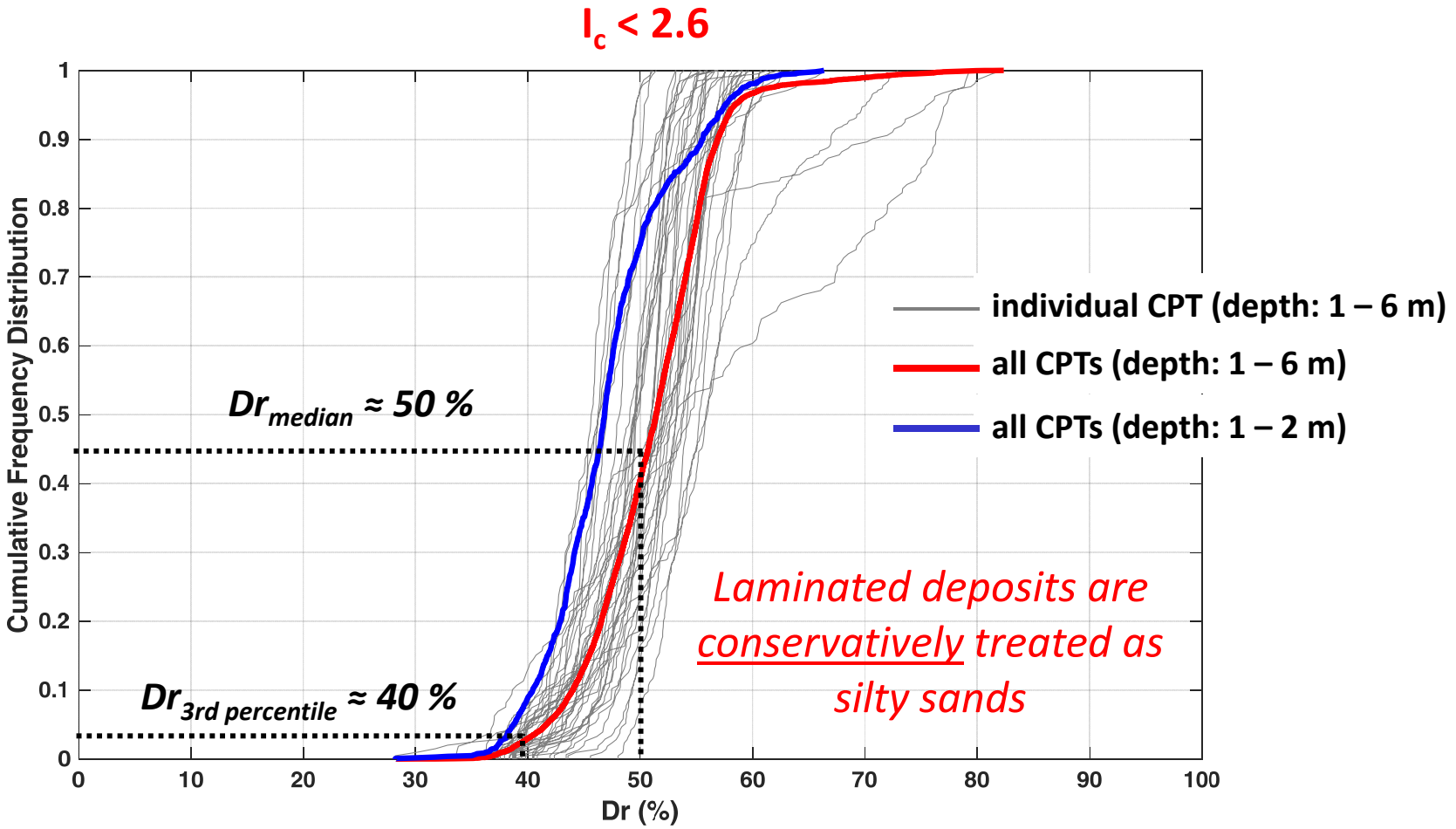


Figure 2-4

# *Soil Variability in Zanderweer*

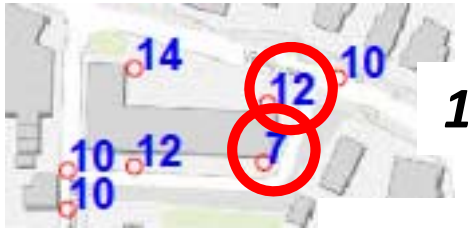


***15 m apart***

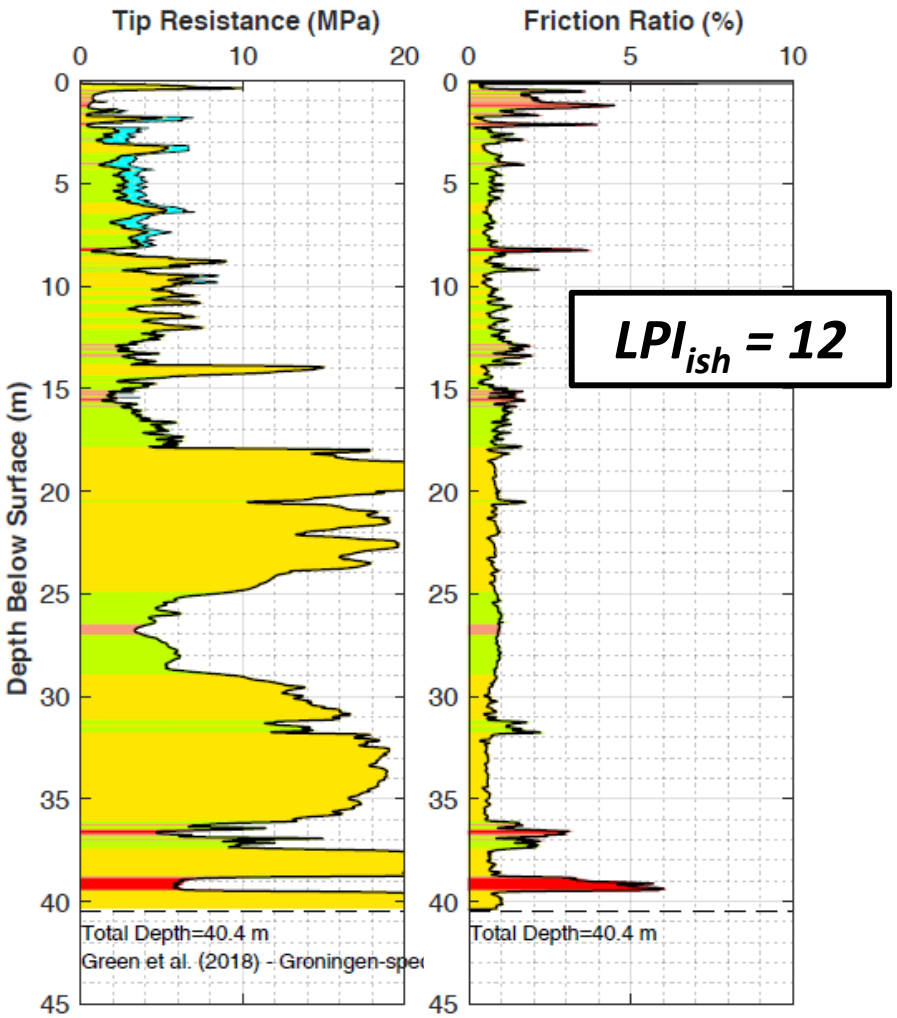


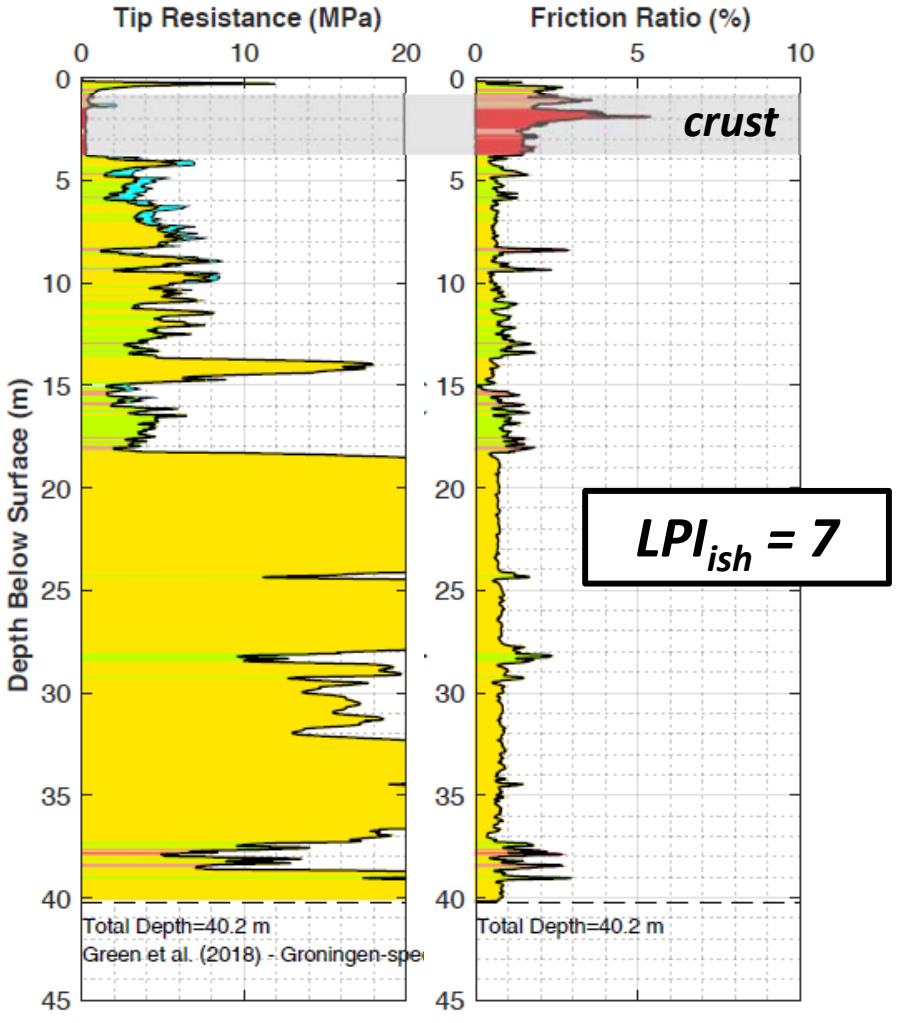


Figure 2-5

# Idealized Dynamic Profile

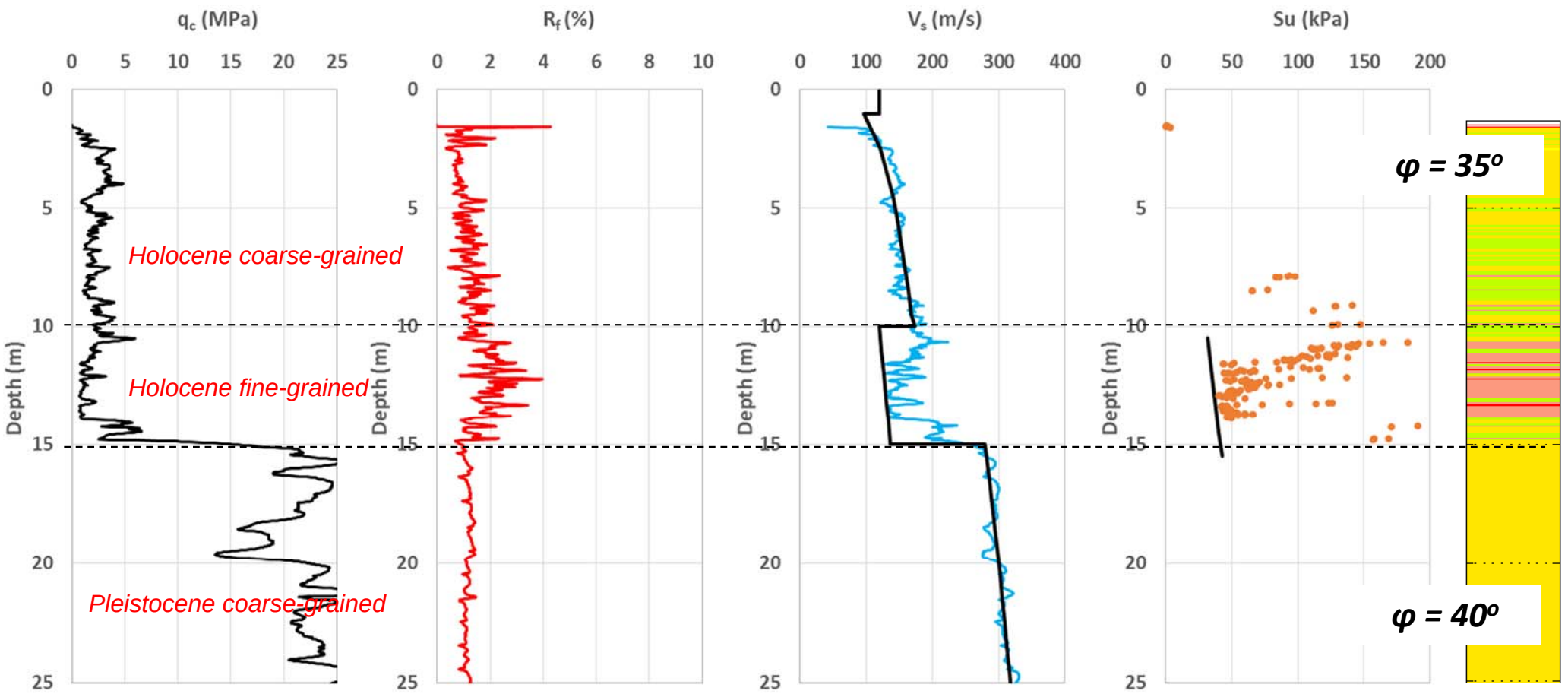


Figure 2-6

# *Typical Groningen buildings examined*

**1-storey building**

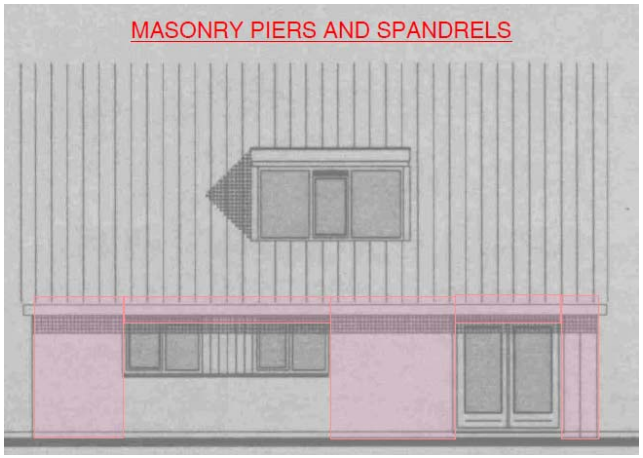


**Longitudinal direction**

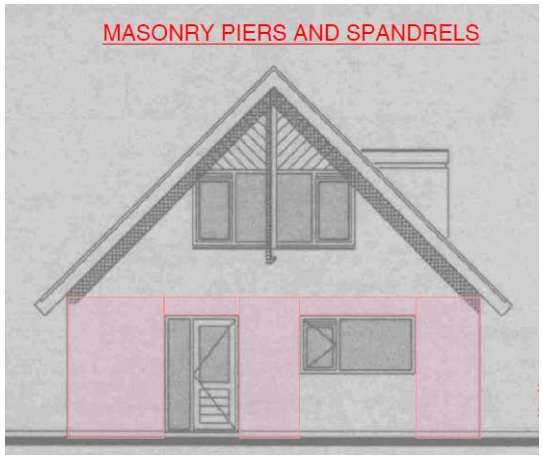


**Transverse direction**

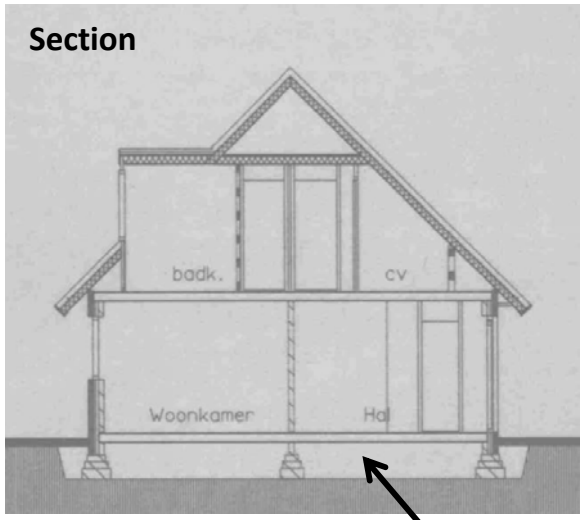


**Crawling space**

**2-storey building**

**Plan view**

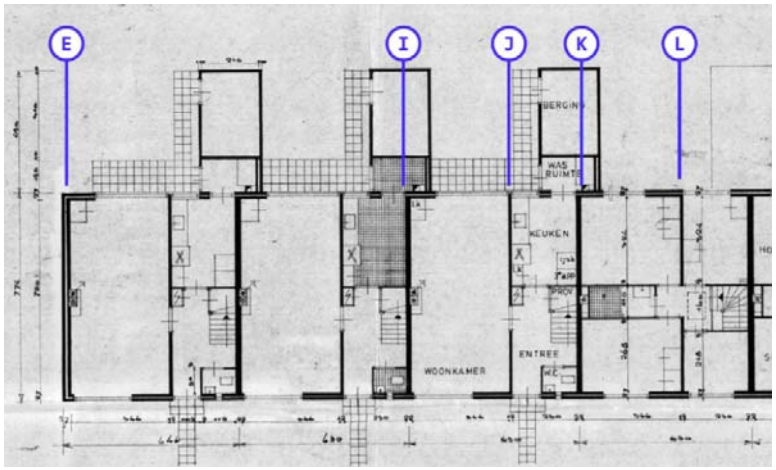


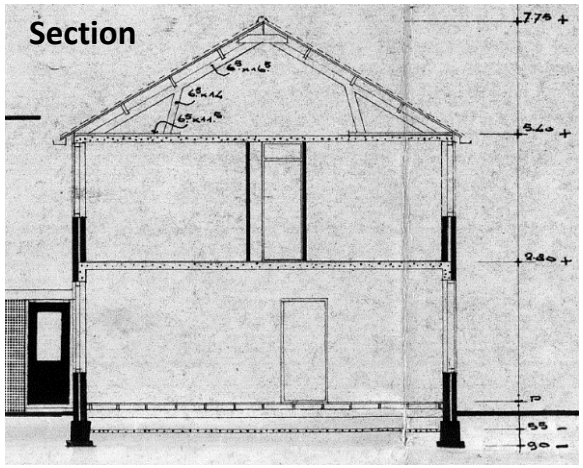


- **Residential buildings of masonry**
- **Foundation : strip footing along the perimeter**
- **Out-of-plane strength of the masonry walls is negligible**

Figure 2-7a

# *Superstructure Modeling – 1-storey building*

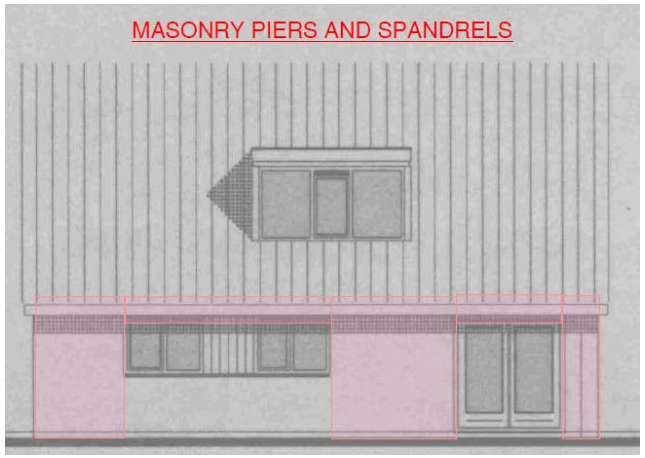


Longitudinal direction

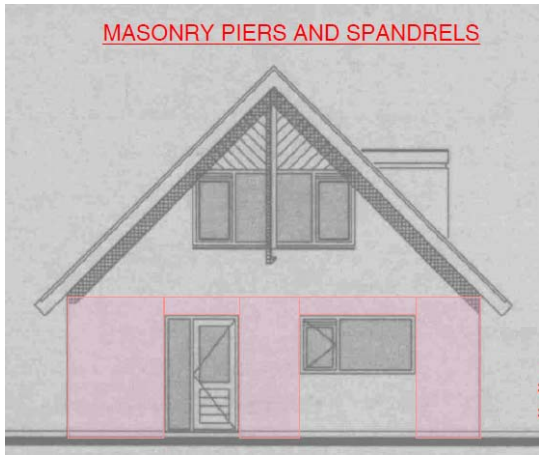


Transverse direction

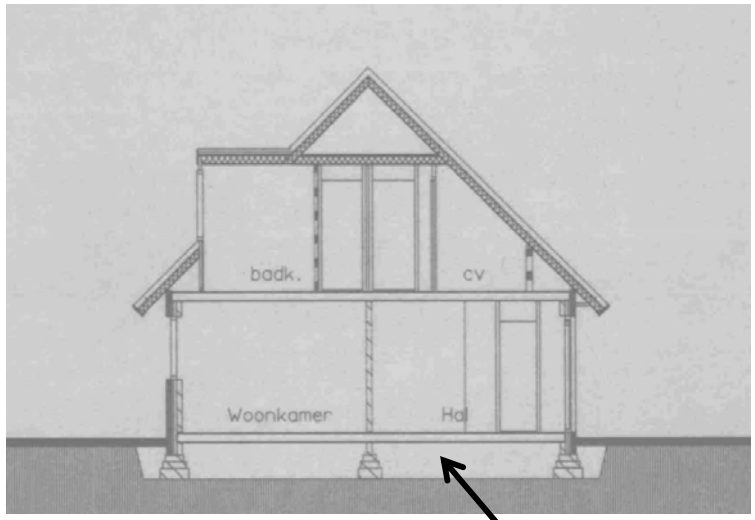


Crawling space

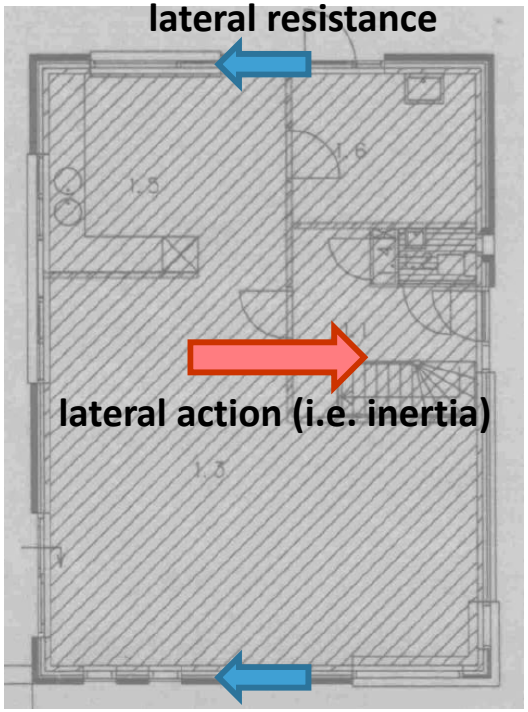


- **Residential building of masonry**
- **Foundation : strip footing along the perimeter**
- **Out-of-plane strength of the masonry walls is negligible**
- **Lateral loads can only be delivered by the walls in the perimeter (in-plane action)**
- **Crawling space height : 0.9 m**

Figure 2-7b

# *Superstructure Modeling – 1-storey building*

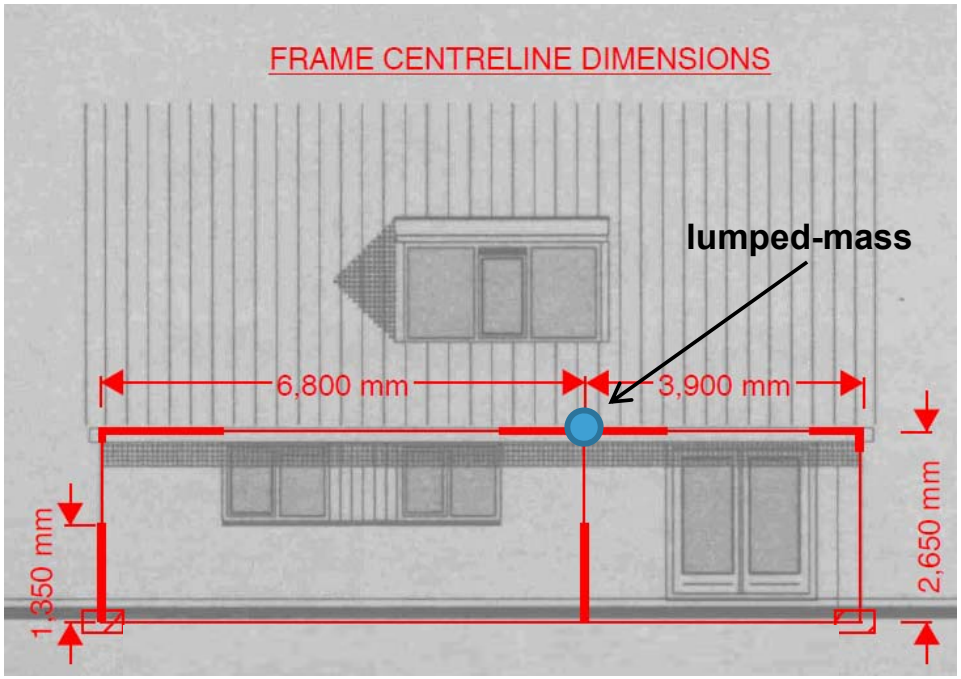


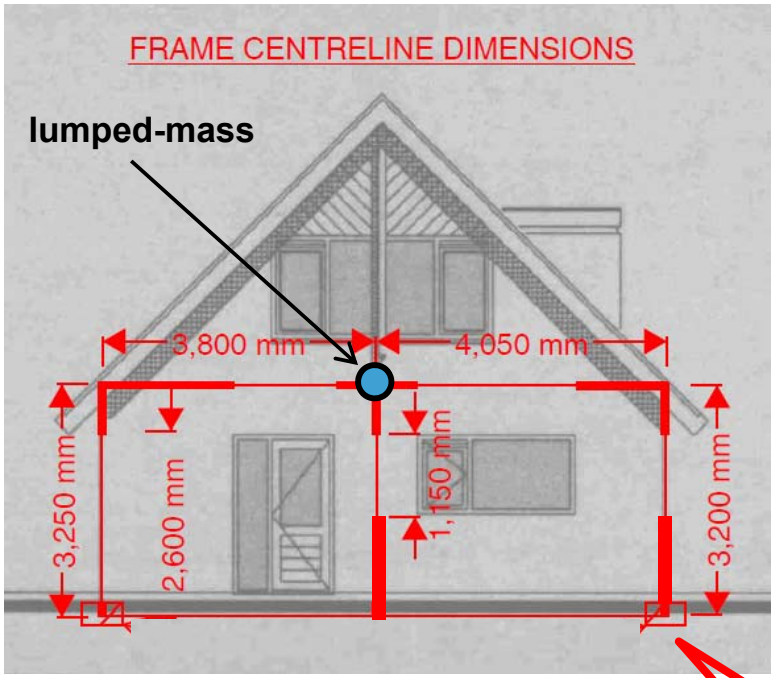


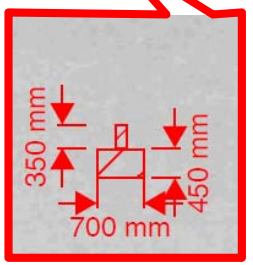


**Foundation cross-section geometry**

- **An equivalent frame model was developed and provided by BICL**
- **An effective mass of 30 tons is assigned only for inertial load (it does not contribute to vertical loading of the footing)**
- **$T_{short}$ ≈ 0.11 sec ; $T_{long}$ = 0.13 sec (fixed-base periods)**
- **Out-of-plane tributary length : $L_{short}$ = 5.5 m ; $L_{long}$ = 3.9 m**
- **Load on soil ≈ 25 kN/m**

Figure 2-7c

# *Superstructure Modeling – 2-storey building*

**Plan view**

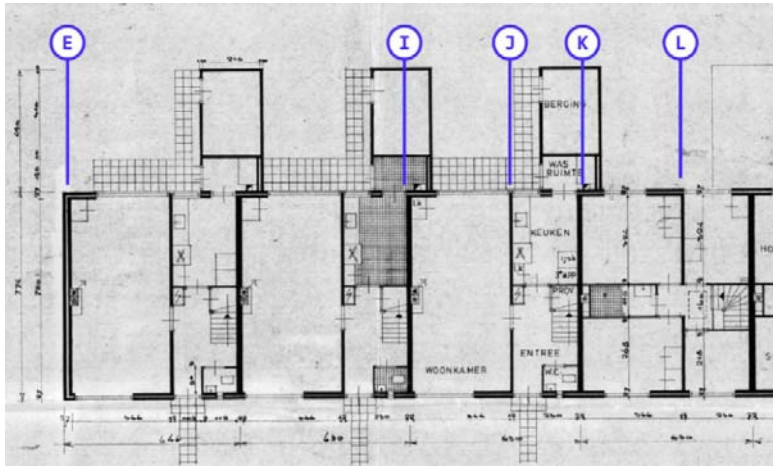


**Section**

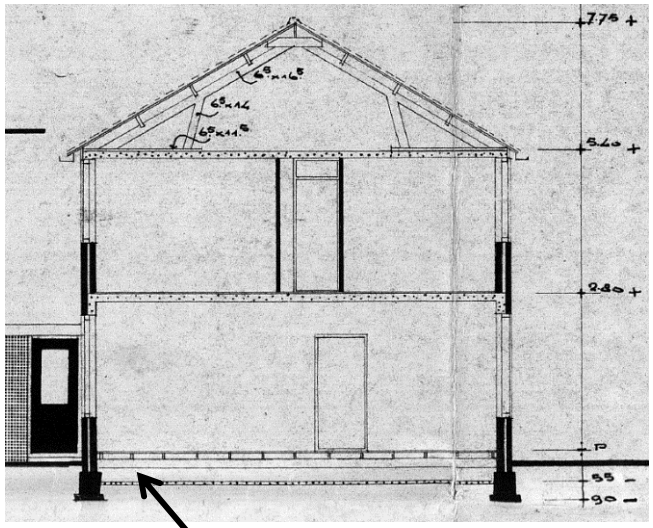

**Crawling space**

**Equivalent frame @ line K**

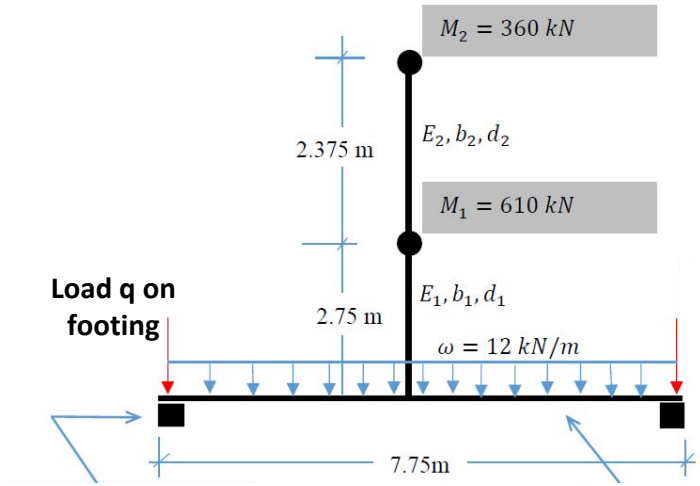


**Load q on footing**

**B = 0.7 m, H = 0.35 m**

**rigid beam**

Figure 2-7d

# Numerical Model Geometry

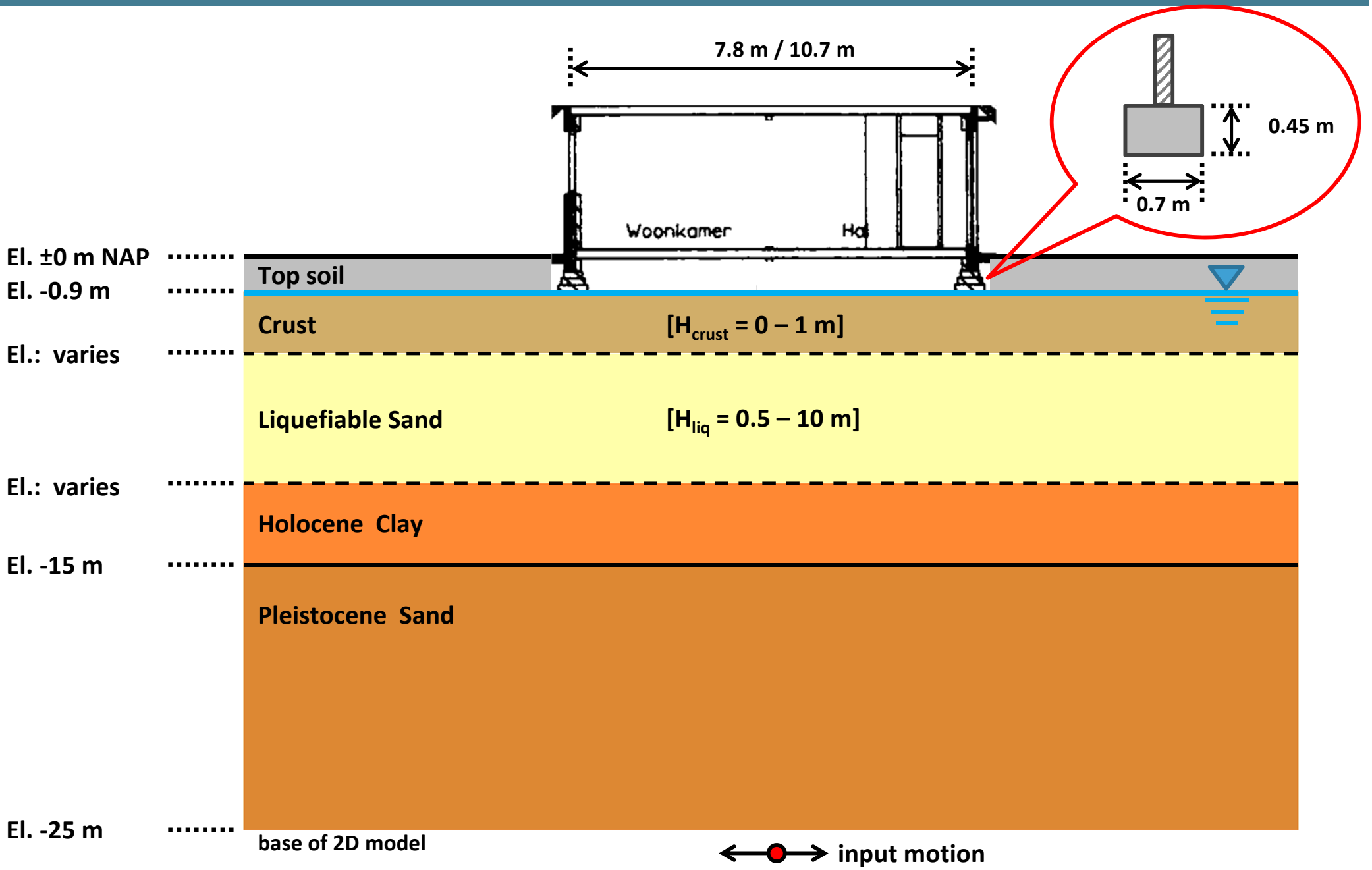


Figure 2-8

## 3.0 DEVELOPMENT OF INPUT TIME HISTORIES FOR 2D NUMERICAL ANALYSES

Acceleration time histories were developed at El. -25m NAP for use in the 2D numerical analyses (Figure 3-1). The seismic hazard at reference bedrock level with v4 GMM for the Eemskanaal project was used to develop input time histories (Fugro 2017). A return period of 2475-years was used in accordance with NPR9998 2017 provisions.

The seismic hazard for the area of the Eemskanaal levee was assessed by the Royal Dutch Meteorological Institute (KNMI) using the latest v4 Ground Motion Prediction Equations (GMPEs) for Groningen (Bommer et al 2017) and provided to Fugro in the form of design spectra at select locations along the levee at the base of the North Sea formation (NS_B). The North Sea formation is the reference "rock" horizon encountered at a depth of about 800 to 900 meters with a Vs30 of about 1400 m/s. Eleven time histories (one horizontal component) from earthquake recordings were selected for the Eemskanaal levee following the recommendations of Jongejan et al (2017) and spectrally matched to the KNMI bedrock design spectra.

One-dimensional (1D) site response analyses were performed using "best-estimate" properties to propagate the design ground motions from bedrock level to about El –25 m NAP for use as input in the 2D numerical analyses. A location along the Eemskanaal levee was selected where the deep soil profile from El –25 m NAP to the base of the North Sea formation (NS_B) was similar to the idealized profile evaluated (Figure 3-2). Scale factors of 1.15 and 0.75 were applied on the ground motions at El. -25 m NAP to account for the ground motion amplitude variability across the Groningen field.

We note that while the ground motions use a limited number of subsurface conditions, subsequent parametric analyses considered a range of shaking levels, above and below the typical one for Zandeweer. The intent of this approach was to eventually evaluate variations in liquefaction-induced settlement as a function of ground shaking levels. The key objective thus was to have ground motions at the base of the numerical analyses model at El. -25 meters that would produce similar response spectra at the surface as are computed using the V4 model if liquefiable soils were absent. The procedure adopted for the time history development at El. -25 m NAP is described in this section

### 3.1 SELECTION AND MODIFICATION OF TIME HISTORIES

Eleven independent time histories (one horizontal component) from earthquake recordings were selected following the recommendations of Jongejan et al (2017) and were spectrally matched to the KNMI reference bedrock design spectra (i.e. applicable at 800 meters depth) developed in accordance with v4 GMM.

Overall, the criteria considered in selecting optimal seed motions included: seismotectonic setting, magnitude and site-to-source distance, frequency content (i.e., spectral shape), and significant duration ($D_{5\text{-}75}$). In general, because the motions will be modified through spectral matching (i.e., not amplitude scaling only) a wider range of recorded peak amplitudes can be used. Secondary criteria were related to the fault mechanism and site class. Care was taken to select motions with usable periods as high as 2 to 3 seconds.

Figure 3-3 summarizes the selected records and their key characteristics. It is noted that the significant duration, $D_{5\text{-}75}$, included in this figure corresponds to the significant duration of the spectrally matched signals after being propagated with site response analyses to El. -25 m NAP following procedures described below. For reference it is noted that the median

significant duration, $D_{5-75}$, for a magnitude 5 earthquake at 3 km distance according to the v5 GMM is about 3 seconds for a $V_{s-30}$ of about 200 m/s (Figure 3-4).

The seed acceleration time histories were modified by adding wavelets in the time domain to obtain response spectra compatible with the target spectra. A time-domain spectral matching procedure was used to preserve the non-stationary characteristics of the seed time histories to the extent possible.

The time-domain spectral matching was accomplished using the computer code RSPMATCH written by Abrahamson (2003), which generally follows the algorithm set forth by Lilhanand and Tseng (1988). As stated above, this code calculates the spectral differences between a response spectrum and a target spectrum, and then adds wavelets in the time domain to alter the frequency content to reduce the differences. A 10% tolerance for maximum mismatch was used. An overall match for all structural periods from PGA to approximately 2 to 3 seconds was targeted.

A final baseline correction was necessary to remove any permanent offset imposed on the time history through the spectral matching procedure. This baseline correction was carried out by fitting an $n^{th}$ order polynomial (where n = 3 to 10) to the displacement time history. The second derivative of this polynomial is then subtracted from the acceleration time history. An attempt was made to preserve the distribution of energy throughout the record of the input acceleration, velocity, and displacement time histories.

The spectrally modified design ground motions in terms of acceleration, velocity, and displacement time histories and 5%-damped acceleration response spectra normalized by the PGA for the seed are included in Appendix A.

### 3.2 SITE RESPONSE ANALYSES

For the development of input ground motions at El. -25 m NAP, 1D site response analyses were conducted using “best-estimate” shear wave velocity profiles at a location along Eemskanaal where the deep soil profile resembles the deep soil profile conditions encountered near Zandeweer (Figure 3-2). Analyses were conducted for motions with a return period of 2475-years.

Free-field equivalent linear site response analyses were performed using the computer code STRATA (Kottke et al., 2013). The 11 design spectrum compatible bedrock motions were input at a depth of about 800 to 900 meters as outcropping motions and propagated up to the surface using a frequency-domain solution.

Ground motions were extracted at an elevation of about -25 m NAP as “outcrop” motions. Scale factors of 1.15 and 0.75 were applied on the motions at El. -25m NAP to capture a range of amplitudes that are representative of the ground motion variation in the Groningen field for a 2475-year return period (Figure 3-5a).

As an example 1D total stress site response analyses were performed for a typical soil profile in Zandeweer using the ground motions at El -25m NAP developed with the procedure described above and a scaling factor of 1.15. Figure 3-5b presents a comparison of the acceleration response spectra at the ground surface from total stress site response analyses (grey lines) and the surface spectrum at Zandeweer from the webtool provided with the v4 GMM (solid black line). As discussed in Section 6 for the spectral periods of interest (i.e. between 0.5 to 1 second) the spectral accelerations of the ground motions used in this study are on the high side when compared with the design spectrum in Zandeweer.

# Section 3

## Geological cross-section at Zandeweer (from Dinoloket)

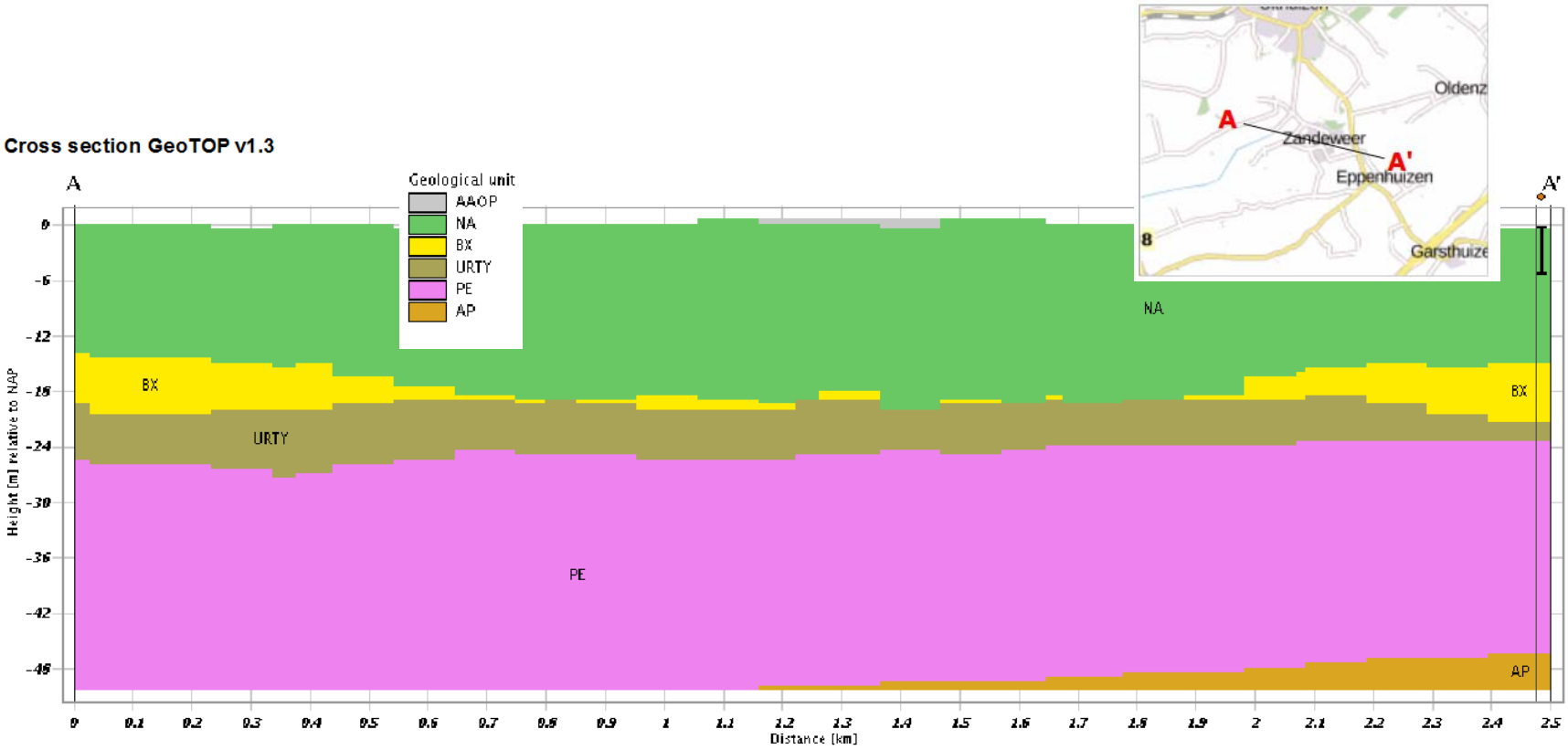


Figure 3-1

# Development of Input Time Histories

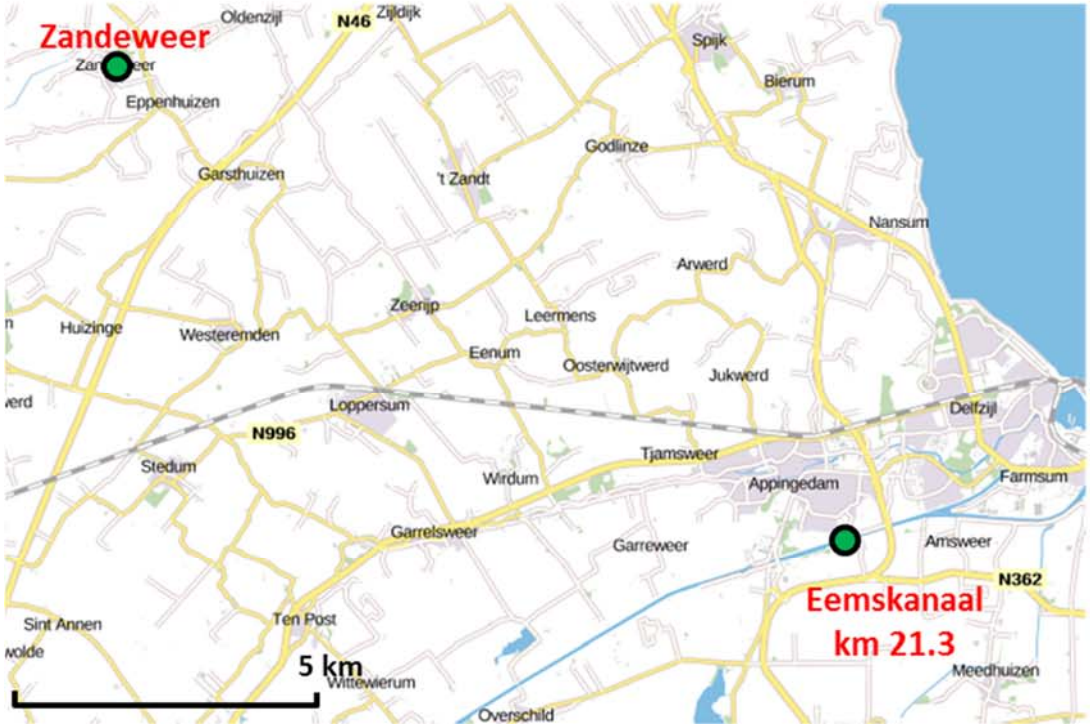


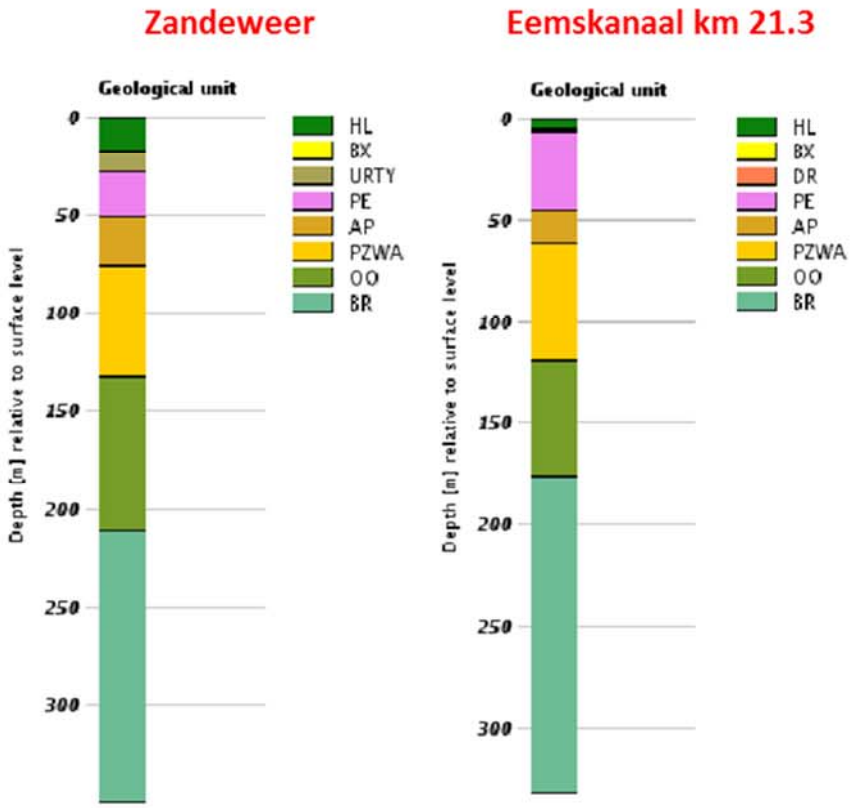


Figure 3-2

# *Motion Selection for Bedrock at 800 m depth*

| Motion No | Record Sequence Number | Earthquake Name | Year | Station Name | Magnitude | Mechanism | $R_{rup}$ (km) | $V_{s30}$ (m/sec) | 5-75% Duration *at -25 m NAP (sec)* |
|---|---|---|---|---|---|---|---|---|---|
| 1 | 419 | Coalinga-07 | 1983 | Sulphur Baths (temp) | 5.21 | Reverse | 12 | 617 | 2.3 |
| 2 | 1312 | Ano Liosia _ Greece | 1999 | Athens 2 (Chalandri District) | 6 | Normal | 9 | 411 | 5.1 |
| 3 | 2021 | Kalamata _ Greece (aftershock) | 1986 | Kalamata-OTE Building | 4.1 | Normal | 8 | 399 | 2.4 |
| 4 | 2426 | Chi-Chi_ Taiwan-02 | 1999 | TCU137 | 5.9 | Reverse | 23 | 635 | 5.1 |
| 5 | 4284 | Basso Tirreno_ Italy | 1978 | Naso | 6 | Strike Slip | 19 | 620 | 6.8 |
| 6 | 4312 | Umbria-03_ Italy | 1984 | Gubbio | 5.6 | Normal | 16 | 922 | 3.8 |
| 7 | 4369 | Umbria Marche _ Italy (aftershock 1) | 1997 | Nocera Umbra-Salmata | 5.5 | Normal | 12 | 694 | 2.8 |
| 8 | 4520 | L'Aquila _ Italy (aftershock 1) | 2009 | Sulmona | 5.6 | Normal Oblique | 42 | 612 | 4.8 |
| 9 | 6093 | Kozani _ Greece (aftershock) | 1995 | Karpero-Town Hall | 5.2 | Normal | 16 (epic.) | 665 | 4.2 |
| 10 | 6434 | Izmit _ Turkey (aftershock) | 1999 | LDEO Station No. C1058 BV | 4.9 | Thrust | 26 (epic.) | 502 | 4.0 |
| 11 | 8775 | 14383980 | 2008 | Chilao Flat Rngr Sta | 5.39 | Reverse Oblique | 50 | 927 | 8.6 |

Figure 3-3

# *Significant Duration $D_{5\text{-}75}$*

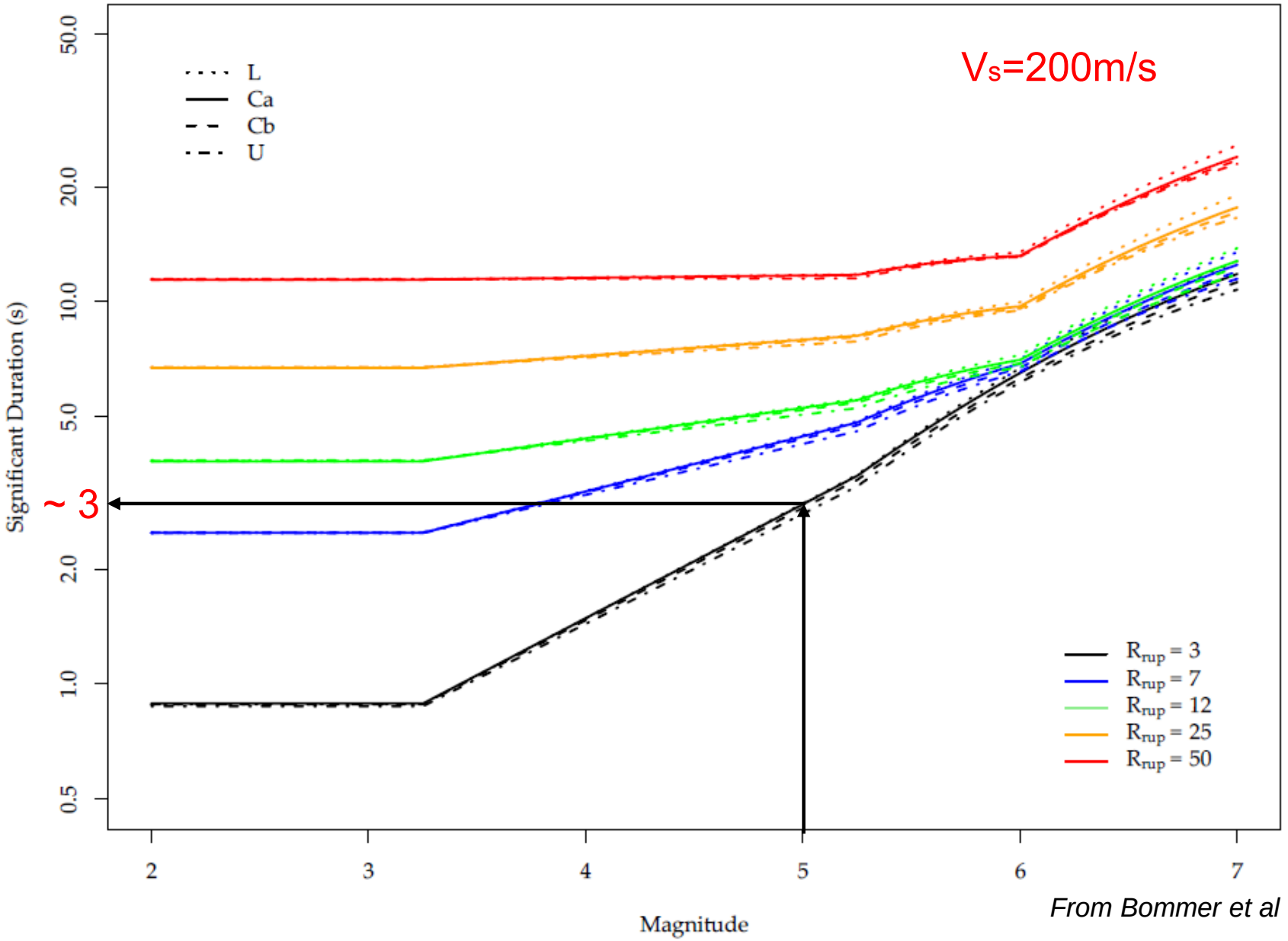


*From Bommer et al (2017)*

Figure 3-4

# Development of Input Time Histories

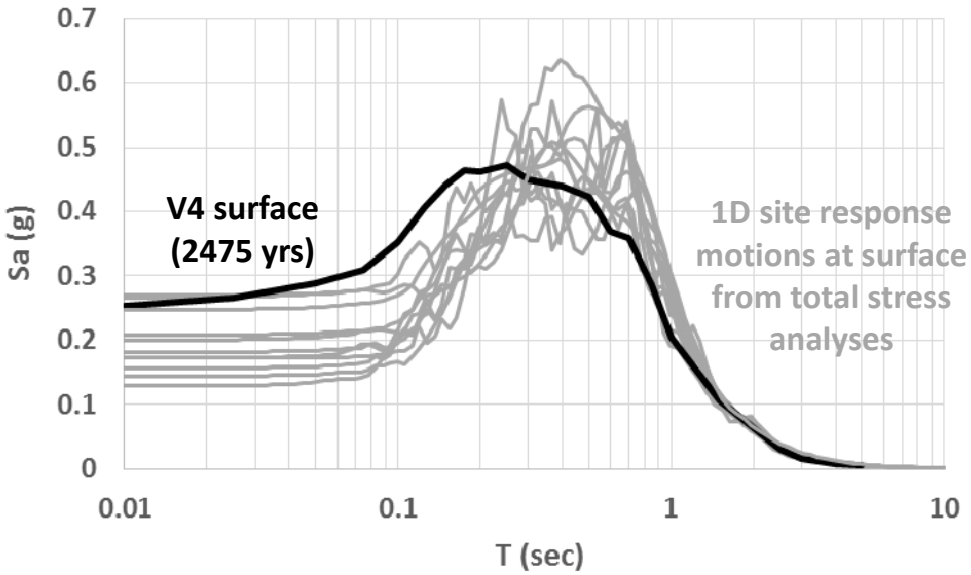


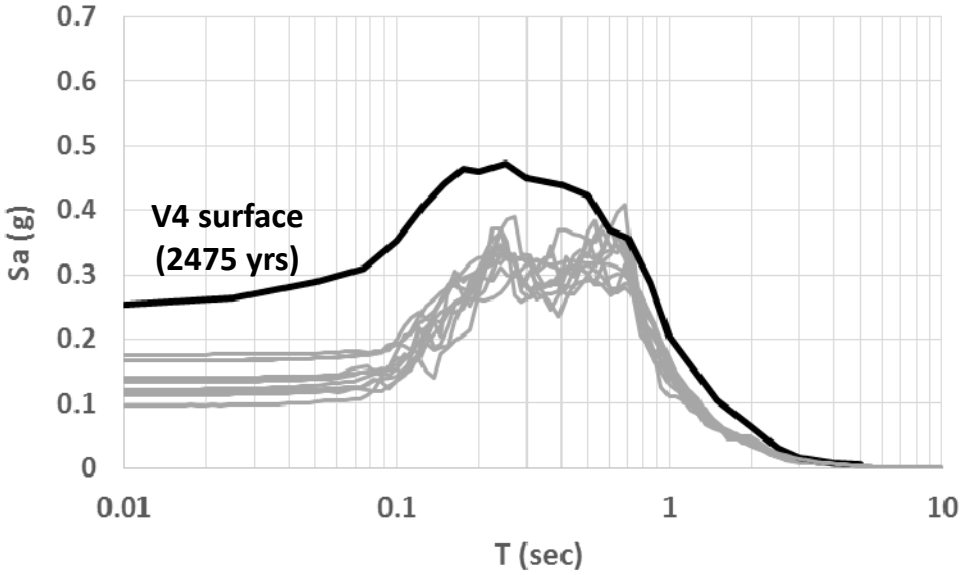


$PGA_{model\_base} = 1.15\ PGA_{-25m\ NAP}$

$PGA_{model\_base} = 0.75\ PGA_{-25m\ NAP}$

Figure 3-5a

# Development of Input Time Histories

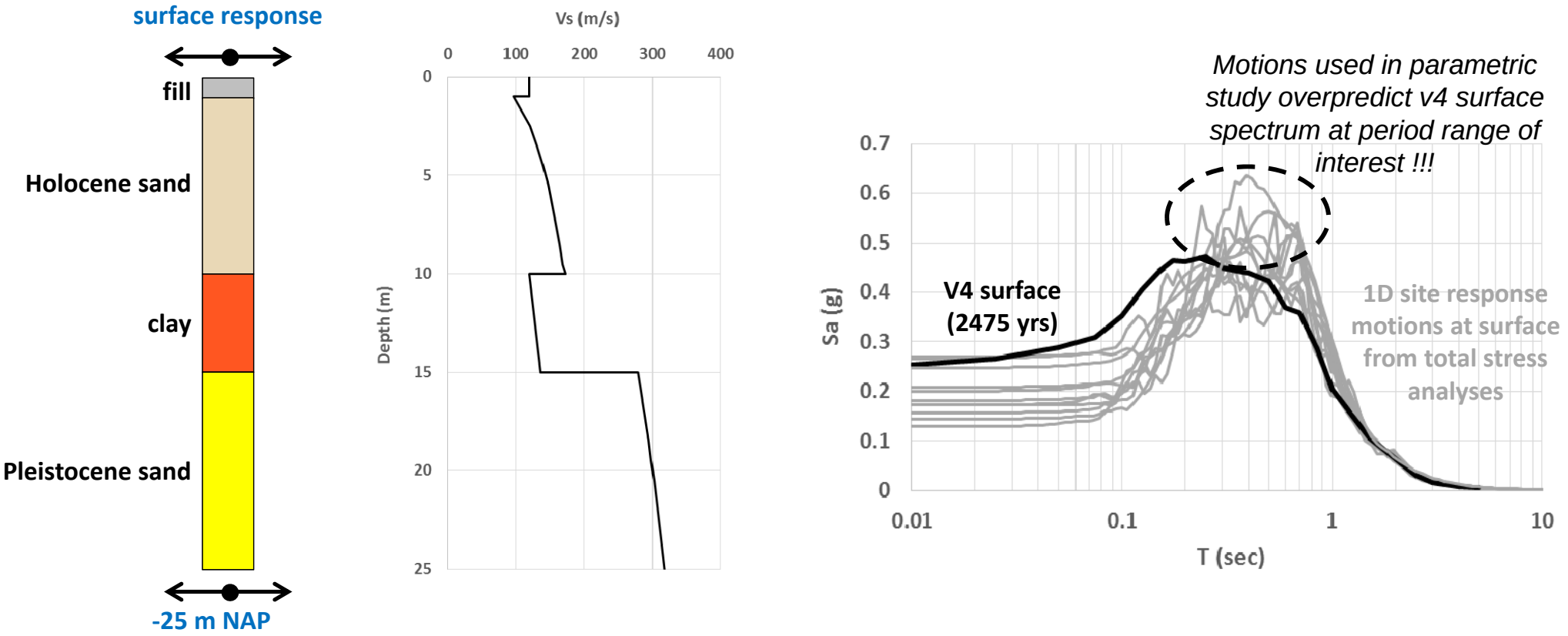


Figure 3-5b

# 4.0 MODELING APPROACH AND METHODOLOGY

## 4.1 MODELING APPROACH

Two dimensional, effective-stress, dynamic analyses were performed using the finite difference code FLAC (Itasca, 2016). FLAC2D is a two-dimensional explicit finite difference program (Itasca, 2016). FLAC2D incorporates the ability to model groundwater flow and pore pressure dissipation, and the full coupling between the deformable porous soil skeleton and the viscous fluid flowing within the pore space. The FLAC2D analyses were intended to realistically model the time-dependent, nonlinear behavior associated with liquefaction of sandy loose materials, as well as nonlinear behavior of non-liquefiable clay-type materials that were identified in site characterization.

The intent of these analyses was to provide estimates of foundation settlements for typical residential buildings in Groningen under a 2475-year event using an advanced 2D effective stress approach for modeling soil behavior. The seismic performance of the foundation was evaluated for two stages: a) during seismic shaking (i.e. co-seismic); and b) after the end of seismic shaking (i.e. post-seismic). The first stage analyses (co-seismic) involves performing dynamic, nonlinear, effective stress analyses to estimate the liquefied zones and the deformations that occur during strong shaking (primarily shear-induced settlements). Two types of analyses were performed for the second stage (post-seismic), both of which are static analyses under gravity loads performed for conditions after the end of strong shaking with the following objectives: i) estimate the post liquefaction volumetric-strain-induced settlements (i.e. settlement analyses) and ii) assess the foundation stability assuming residual undrained shear strength conditions in the liquefied zones under the foundation (i.e. stability analyses).

Post-earthquake volumetric-strain induced reconsolidation settlement analyses included the following steps: a) monitoring the maximum shear strain developed in the liquefiable zones during shaking, b) terminating the dynamic analyses at the end of shaking, c) for areas where the maximum excess pore pressure during shaking exceeded a specified threshold indicative of significant pore pressure generation (e.g., typically assumed 70 percent) update the constitutive model to Mohr-Coulomb and assign stiffness parameters by assuming a constrained modulus corresponding to consolidation strains estimated from the maximum shear strains that developed during the earthquake using the relationship suggested by Ishihara and Yoshimine (1992) (Figure 4-1), a Poisson's ratio of 0.3 and the initial static vertical effective stress, and d) conducting static analyses under gravity loads with the revised constitutive model and stiffness parameters to obtain estimates of post-earthquake volumetric reconsolidation settlements. We note that Fugro used this procedure to estimate free-field reconsolidation settlements observed in the Port Island Case Study (Ishihara et al, 1996; Ziotopoulou & Boulanger, 2013 and predicted reconsolidation settlements on the order of 30 cm which are within the range of the reported reconsolidation settlement range of 20 to 50 cm (Figure 4-2a). Note that for 2D Soil-Structure Interaction problems like the one addressed herein, a simplified 1D estimation of post-earthquake volumetric reconsolidation settlements through monitoring of maximum shear strains during shaking and subsequently integration of the associated Ishihara and Yoshimine volumetric strains below the foundation i.e., without performing a numerical analysis, may underestimate settlements associated with reconsolidation. This is demonstrated in Figure 4-2b which shows results from the parametric analyses presented in Section 6.0. The horizontal axis shows volumetric settlements as obtained by simple integration of volumetric strains, while the vertical axis shows volumetric settlements as obtained with the numerical procedure outlined above. In the latter case,

volumetric settlements are considerably larger, indicating that additional mechanisms (e.g. 2D effects, soil-structure interaction etc.) also affect the development of shear strains and the associated accumulation of volumetric settlements.

Post-earthquake stability analyses included the following steps: a) monitoring the maximum excess pore water pressure developed in the liquefiable zones during shaking, b) terminating the dynamic analyses at the end of shaking, c) for areas where the maximum excess pore pressure during shaking exceeded a specified threshold indicative of liquefaction (e.g., typically assumed 70 percent) update the constitutive model to Mohr-Coulomb and assign residual strength [using the empirical relationship for residual strength as a function of $q_{c1Ncs}$ proposed by Idriss and Boulanger (2008), Figure 4-3], and d) conducting static analyses under gravity loads with the revised constitutive model and properties until equilibrium is reached. This procedure has been outlined by Naesgaard and Byrne (2007) and has been used successfully to predict post shaking slope failures (e.g. Naesgaard and Byrne, 2007).

We note that similar approach has been adopted by Fugro for a number of important peer-reviewed projects in the Groningen area (i.e. Eemshaven-Delfzijl levee and Eemskanaal levee) and around the world (for example BART Transbay Tube in California, Wheatstone LNG facilities in Australia, Izmit Bay Bridge and Canakkale Bridge in Turkey).

## 4.2 BOUNDARY CONDITIONS

The model was subjected to one-directional horizontal dynamic loading using outcrop time histories developed from 1D site response analyses as described in Section 3.0. A compliant base was used at the bottom of the model (through the use of quiet boundaries in FLAC) to model the half space. Dynamic excitation to the FLAC model was specified using the compliant-base deconvolution procedure proposed by Mejia and Dawson (2006) and implemented in FLAC version 7.0 (Itasca, 2016). In this procedure a shear stress time history compatible with the half space stiffness is applied to the base of the model. This is derived by multiplying the outcrop velocity time history by the half-space shear wave velocity and density.

Appropriate kinematic constraints were applied to the two lateral sides of the model to simulate shear-box type boundary conditions.

The ground water table was assumed to be at the base of the foundation.

## 4.3 CONSTITUTIVE MODELS

### 4.3.1 Liquefiable Soils

Liquefiable sands were modeled with the PM4Sand (Boulanger and Ziotopoulou, 2015) constitutive model developed by Drs Ross Boulanger and Katerina Ziotopoulou at the University of California at Davis. The PM4Sand (version 3) model follows the basic framework of the stress-ratio controlled, critical state compatible, bounding surface plasticity model for sand developed by Dafalias and Manzari (2004). Modifications to the Dafalias-Manzari model were developed and implemented to improve its ability to approximate engineering design relationships that are used to estimate the stress-strain behaviors that are important to predicting liquefaction-induced ground deformations during earthquakes. The basic features of the PM4Sand model are shown on Figure 4-4. The three primary input properties in PM4Sand are the sand's apparent relative density $D_R$, the shear modulus coefficient $G_o$, and the contraction rate parameter $h_{po}$. Detailed descriptions of the model parameters and its calibration procedure can be found in Ziotopoulou and Boulanger (2013), and Boulanger and Ziotopoulou (2015).

### 4.3.2 Non-Liquefiable Soils

Non-Liquefiable soils were modeled with the Mohr-Coulomb failure criterion in combination with a nonlinear stress-strain behavior characterized by a three-parameter sigmoidal shaped backbone curve (Itasca, 2011). This model is referred to as Itasca-S3 in this report. The model parameters were fit to approximate target shear modulus reduction curves selected from the available literature for similar soil types, plasticity characteristics and depth. For the Holocene clay layer, Darendeli (2001) curves for PI=40 were used while for the Pleistocene sand layer Darendeli (2001) curves for PI=0 were used.

## 4.4 MODELING OF STRUCTURE AND SOIL-STRUCTURE INTERACTION

The structural members were simulated with linear beam elements, which are described in terms of four parameters: mass density, $\rho$; Young's modulus, $E$; cross-section area, $A$, and moment of inertia, $I$. The properties of the beams are summarized in Figures 4-5a and 4-5b for the single-storey and the 2-storey building, respectively. The footings were simulated as elastic solid elements, rigidly connected with the frame. Furthermore, in order to simulate the relative movement between the foundation and the surrounding soil, interface elements were placed both at the base and at the vertical side of each footing. Interface elements in FLAC follow an elastic-perfectly plastic constitutive law, while selection of proper values is based both on physical and numerical criteria. For the elastic stiffness an adequately large value (to avoid interface deformation and at the same time do not excessively reduce the timestep of the analysis) was selected based on recommendation in FLAC's manual as well as experience from previous projects. For the plastic parameters, based on the results of sensitivity analyses which indicated negligible effects of interface properties on settlement accumulation, a value of 35 degrees (approximately equal to the friction angle of the sand) was assigned. The above formulation and calibration was further verified with respect to a case study and a centrifuge as described in Section 5.2.

# Section 4

# Post-liquefaction free-field volumetric strains

## Volumetric Strains

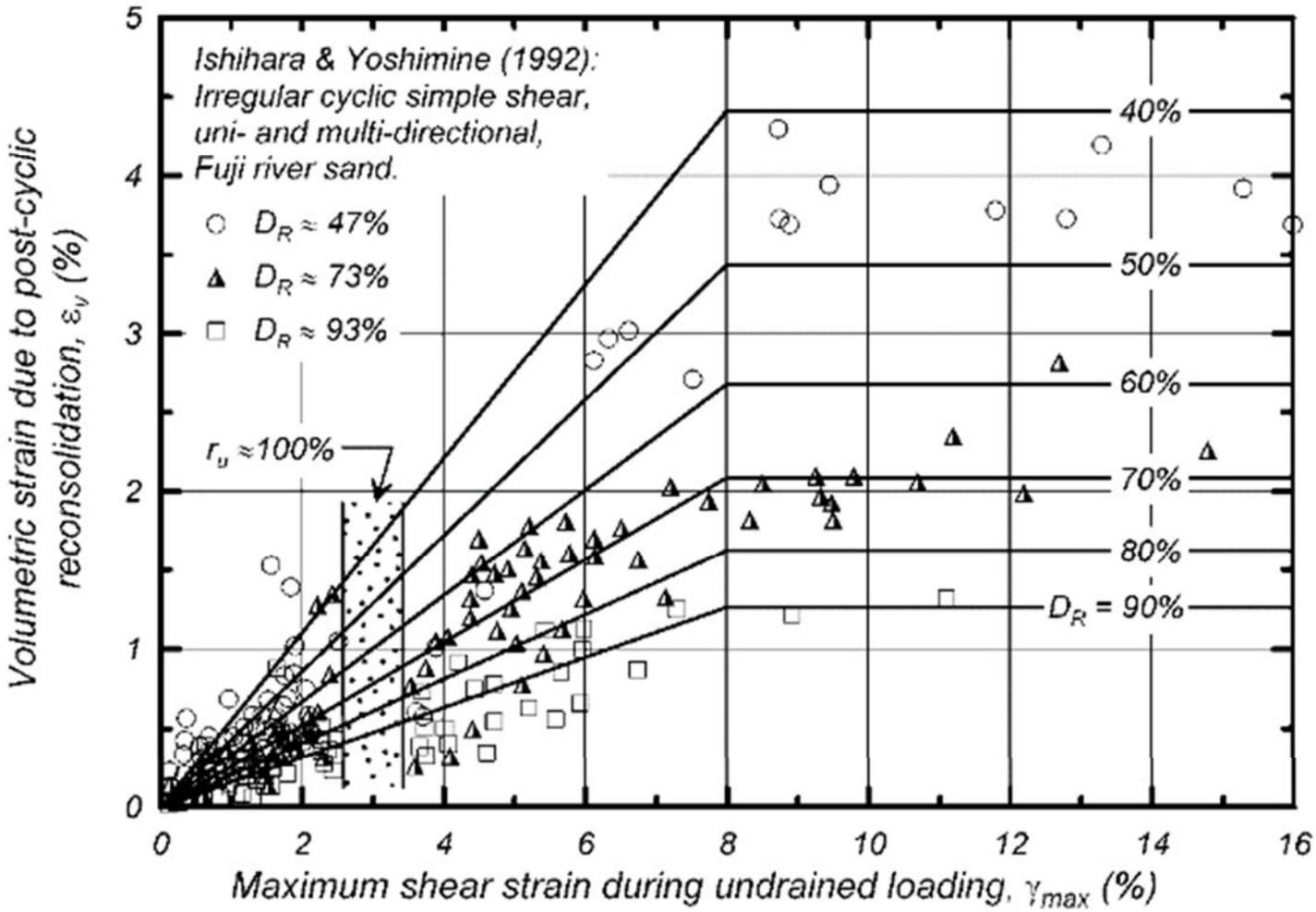


***Ishihara & Yoshimine, 1992***

Figure 4-1

# Port Island Case History of Free-Field Reconsolidation Settlements

## Volumetric Strains

**Port Island Case Study**

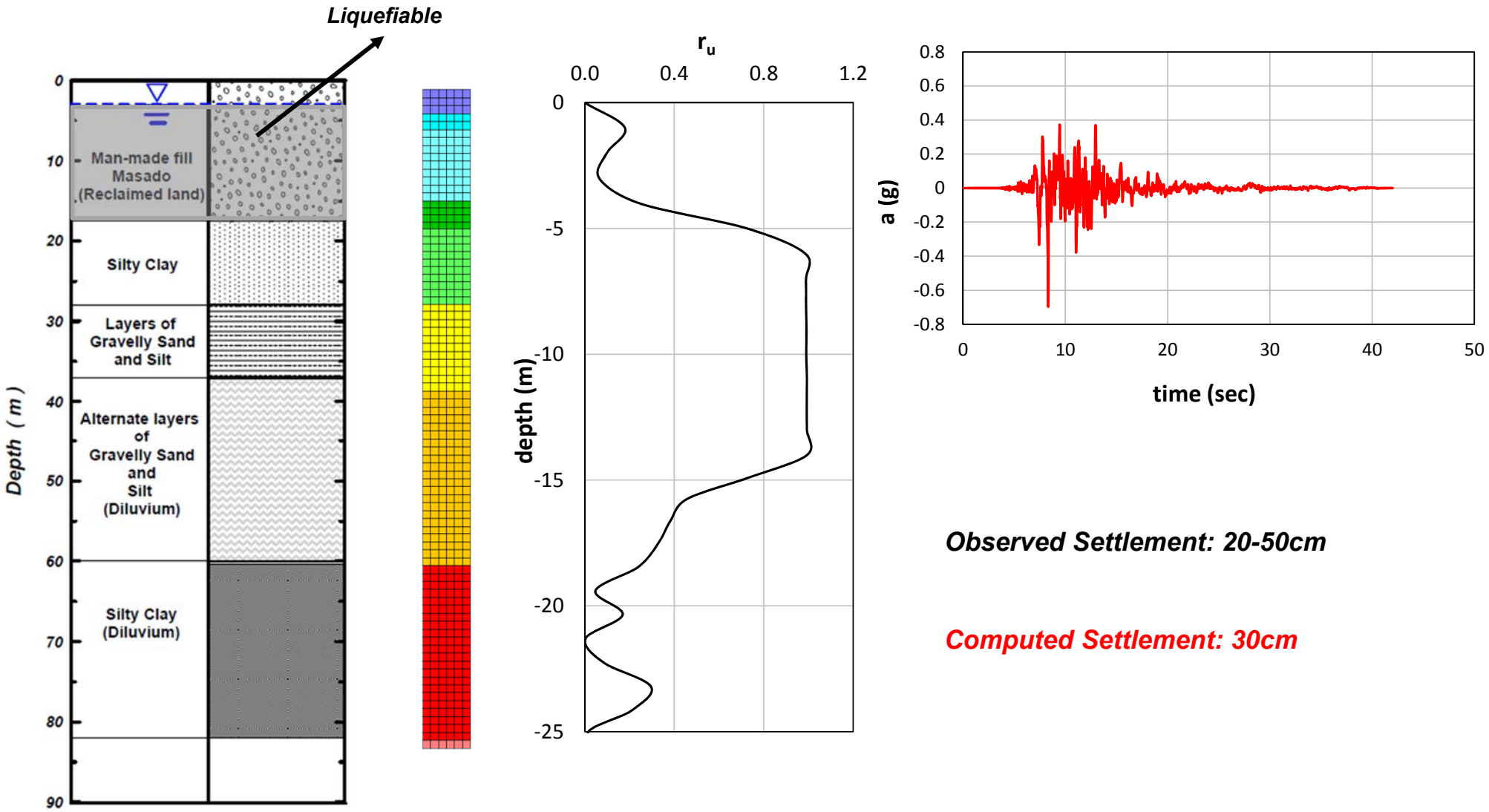


***Observed Settlement: 20-50cm***

***Computed Settlement: 30cm***

Figure 4-2a

# Contribution of Volumetric Settlements

## Volumetric Strains

***Simplified 1-D vs Numerical 2D Calculation***

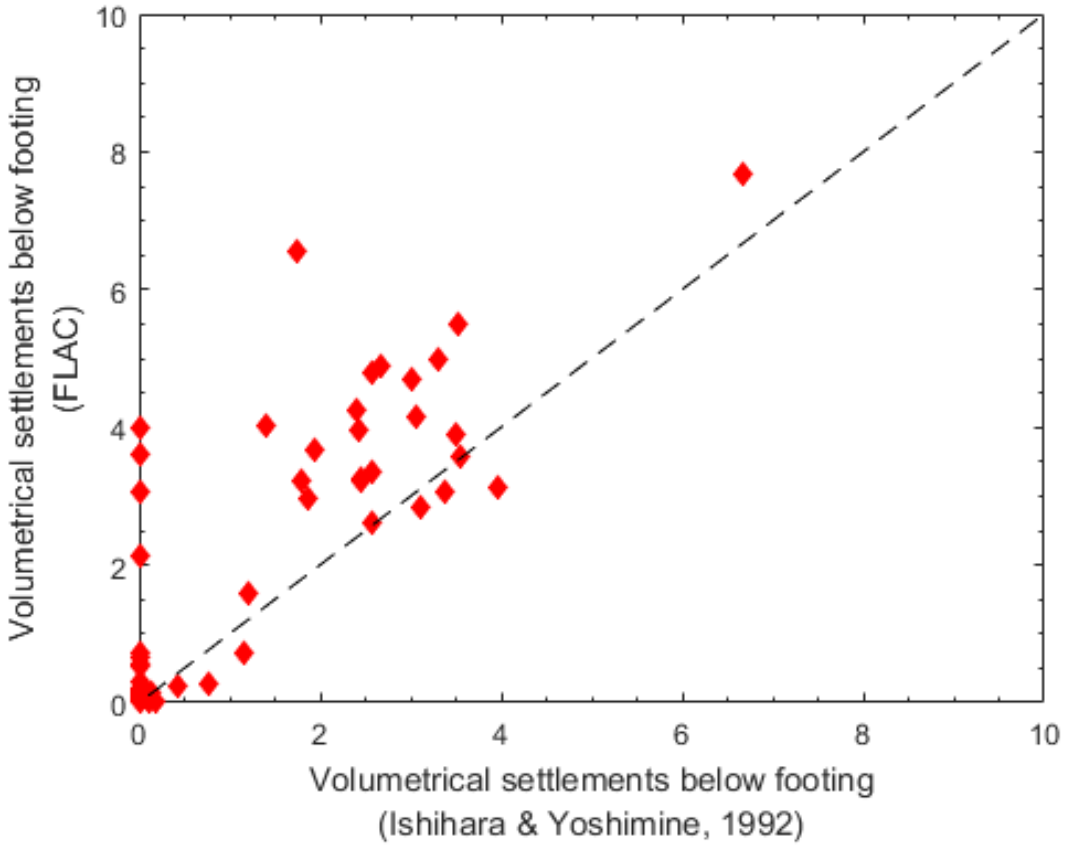


Figure 4-2b

# Residual Undrained Shear Strength

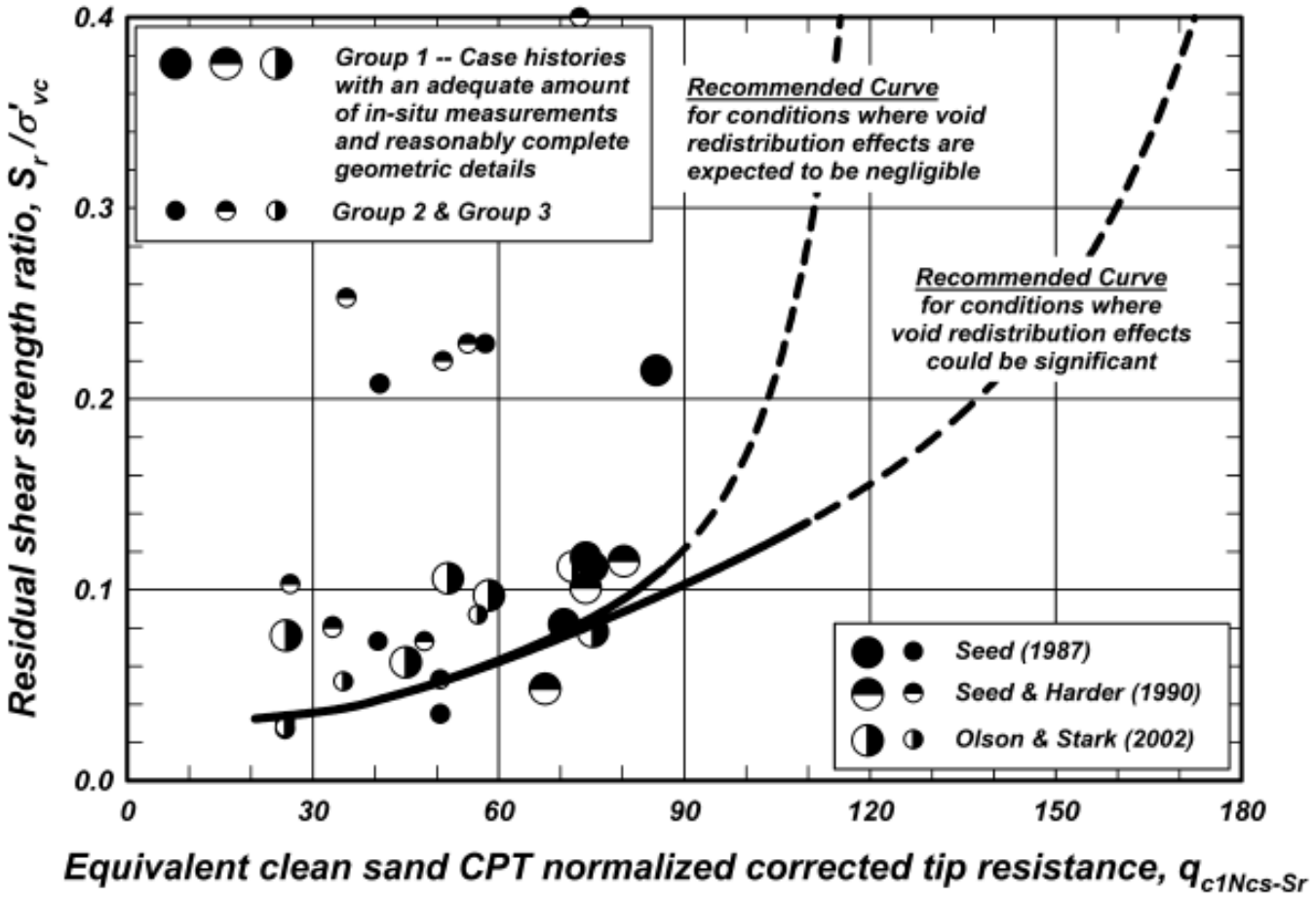


***Idriss and Boulanger (2008)***

Figure 4-3

# Constitutive Model for Liquefiable Sands

## PM4Sand (Boulanger and Ziotopoulou 2015)

**Bounding Surface Plasticity**
**Critical State Compatible**
**Stress ratio Controlled → plastic deformations**
**Accounting for fabric effects on plastic modulus, plastic volumetric strains**

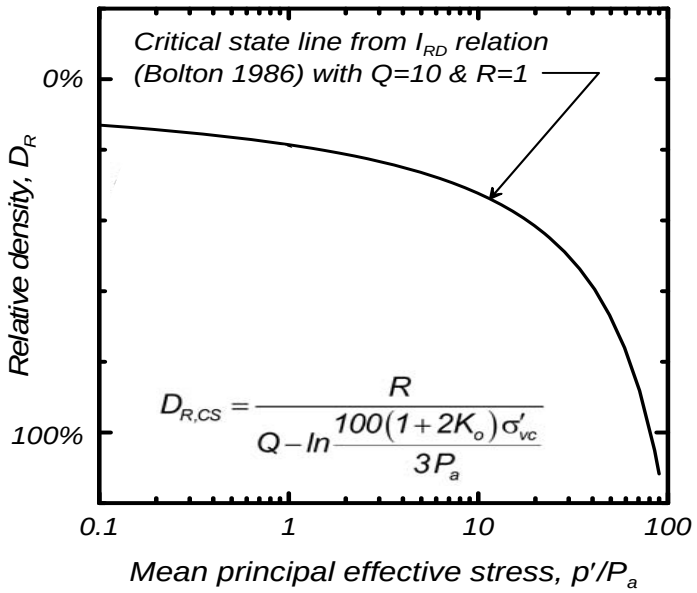


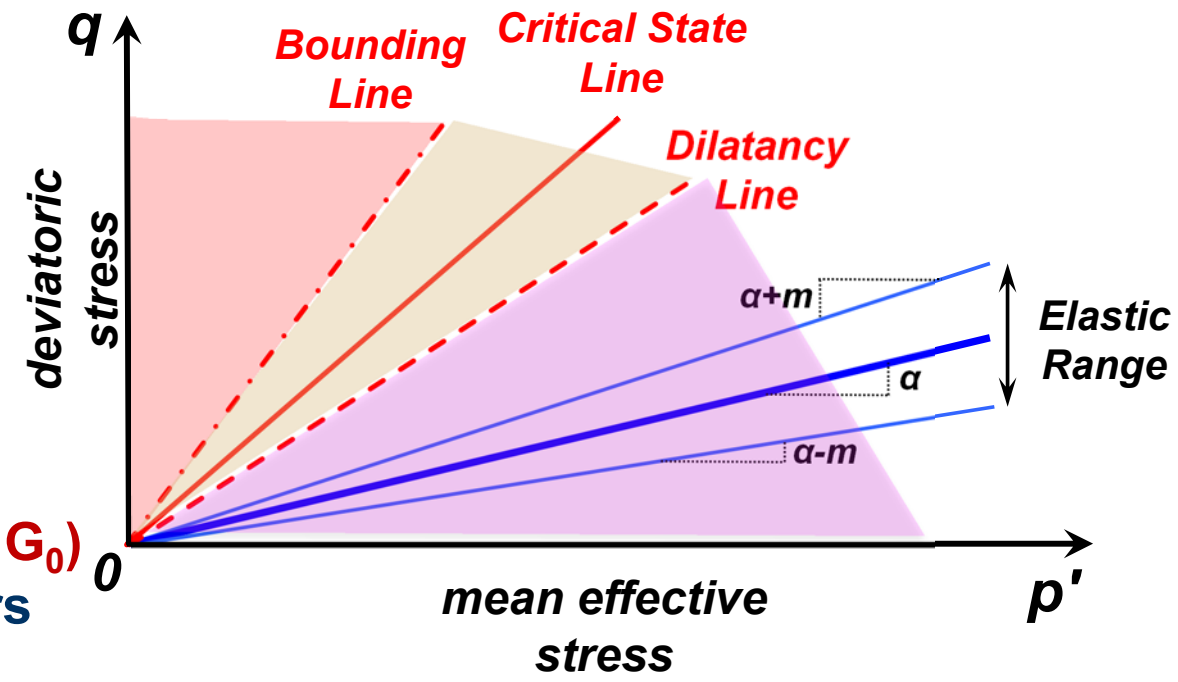


**Input parameters:**

**3 primary parameters ($D_R$ , $h_{p0}$, $G_0$)**
**18 secondary model parameters**
***(default values)***

Figure 4-4

# *Superstructure Modeling – 1-storey building*

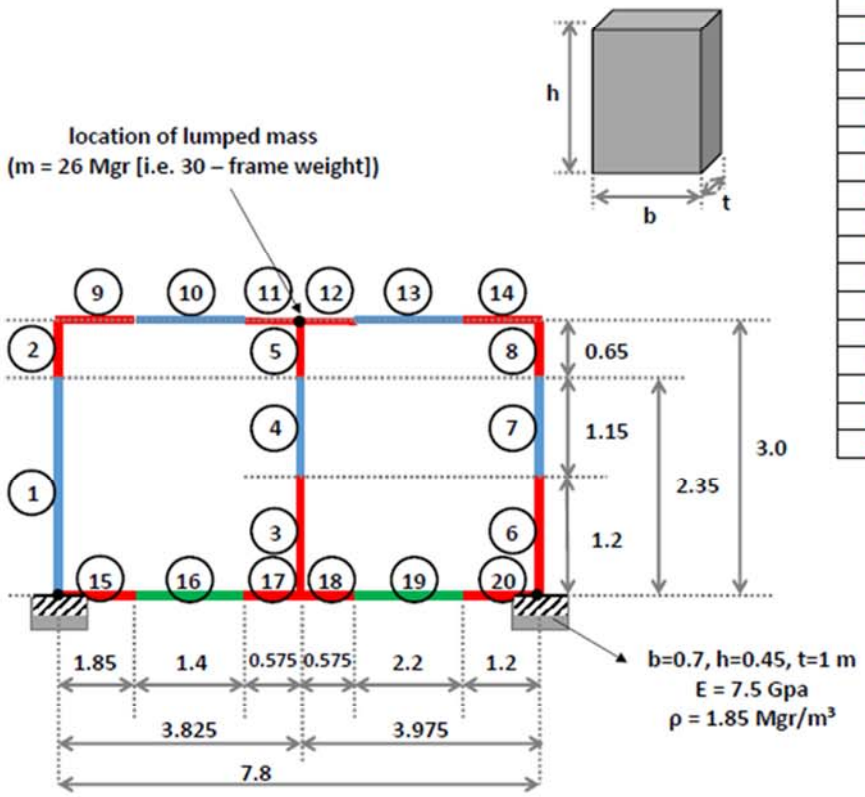


| Element | b (m) | h (m) | t (m) | A (m2) | I (m4) | ρ (Mgr/m3) | E (GPa) |
|---|---|---|---|---|---|---|---|
| 1 | 1.85 | 2.35 | 0.1 | 0.185 | 0.04870 | 1.85 | 7.5 |
| 2 | 1.85 | 0.65 | 0.1 | 0.185 | 0.04870 | 0.925 | 750 |
| 3 | 1.15 | 1.2 | 0.1 | 0.115 | 0.01170 | 1.85 | 750 |
| 4 | 1.15 | 1.15 | 0.1 | 0.115 | 0.01170 | 1.85 | 7.5 |
| 5 | 1.15 | 0.65 | 0.1 | 0.115 | 0.01170 | 1.2 | 750 |
| 6 | 1.2 | 1.2 | 0.1 | 0.12 | 0.01329 | 1.85 | 750 |
| 7 | 1.2 | 1.15 | 0.1 | 0.12 | 0.01329 | 1.85 | 7.5 |
| 8 | 1.2 | 0.65 | 0.1 | 0.12 | 0.01329 | 0.925 | 750 |
| 9 | 1.85 | 0.65 | 0.1 | 0.065 | 0.00211 | 0.925 | 750 |
| 10 | 1.4 | 1.2 | 0.1 | 0.12 | 0.01329 | 1.85 | 7.5 |
| 11 | 0.575 | 1.2 | 0.1 | 0.12 | 0.01329 | 1.2 | 750 |
| 12 | 0.575 | 1.2 | 0.1 | 0.12 | 0.01329 | 1.2 | 750 |
| 13 | 2.2 | 1.2 | 0.1 | 0.12 | 0.01329 | 1.85 | 7.5 |
| 14 | 1.2 | 0.65 | 0.1 | 0.065 | 0.00211 | 0.925 | 750 |
| 15 | 1.85 | 0.35 | 0.1 | 0.035 | 0.00033 | 1.85 | 750 |
| 16 | 1.4 | 0.35 | 0.1 | 0.035 | 0.00033 | 1.85 | 7.5 |
| 17 | 0.575 | 0.35 | 0.1 | 0.035 | 0.00033 | 1.85 | 750 |
| 18 | 0.575 | 0.35 | 0.1 | 0.035 | 0.00033 | 1.85 | 750 |
| 19 | 2.2 | 1.3 | 0.1 | 0.13 | 0.01690 | 1.85 | 7.5 |
| 20 | 1.2 | 0.35 | 0.1 | 0.035 | 0.00033 | 1.85 | 750 |

out-of-plane length = 5.5 m

Figure 4-5a

# *Superstructure Modeling – 2-storey building*

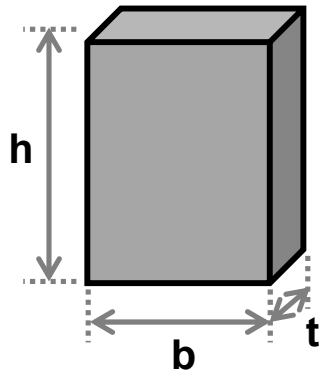


| Element | b (m) | h (m) | t (m) | A (m2) | Iy (m4) | ρ (Mgr/m3) | E (GPa) |
|---|---|---|---|---|---|---|---|
| 1 | 3.875 | 1 | 1 | 1 | 0.08333 | 0.63 | 100 |
| 2 | 3.875 | 1 | 1 | 1 | 0.08333 | 0.63 | 100 |
| 3 | 7.55 | 2.75 | 0.24 | 1.812 | 8.60738 | 1.85 | 3 |
| 4 | 7.55 | 2.375 | 0.24 | 1.812 | 8.60738 | 1.85 | 3 |

**out-of-plane length = 6.3 m**

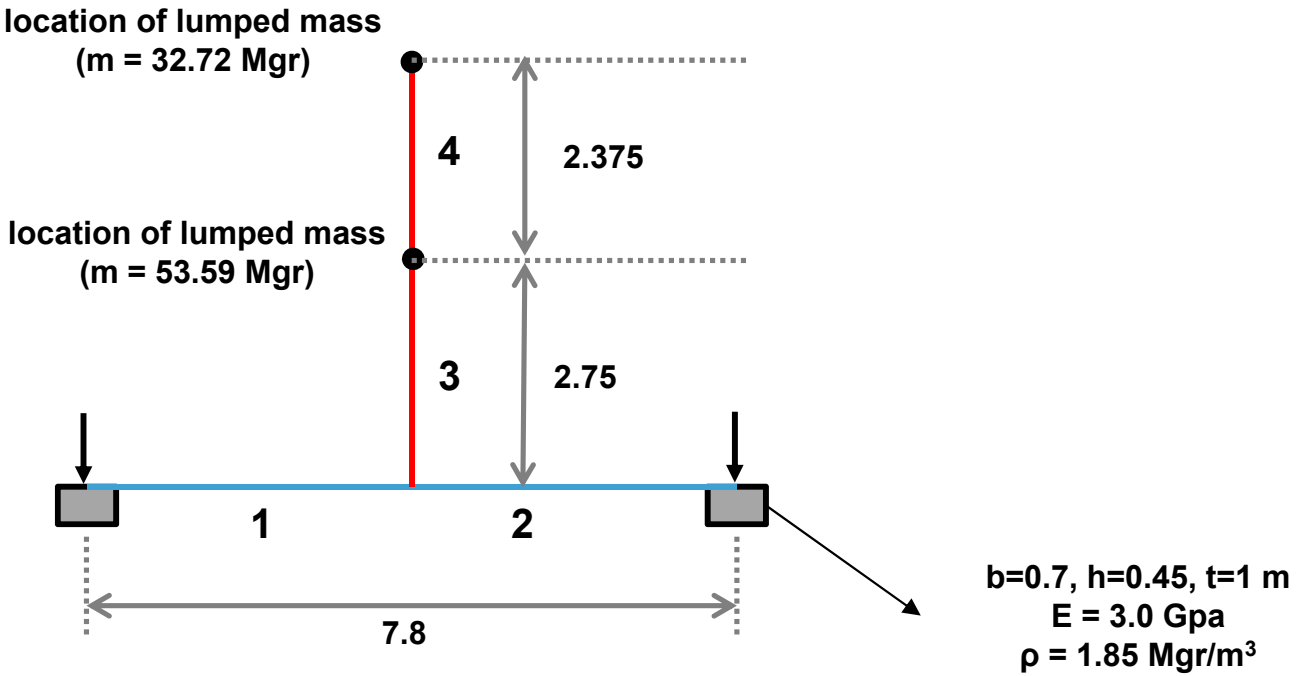


Figure 4-5b

# 5.0 MODEL CALIBRATION AND VALIDATION

## 5.1 MODEL CALIBRATION

The problem under consideration involves the effective stress behavior of loose sands with and without initial static shear stress conditions. The undrained behavior of loose sands under initial static shear stress has been studied by various researchers (Vaid and Finn 1979, Vaid and Chern 1985, Boulanger et al 1991, Sriskandakumar 2004, Kammerer et. al. 2000, Wu 2002) and it has been found that the existence of an initial static shear can have a significant effect on the liquefaction resistance, pore pressure generation, and shear strain accumulation of cohesionless soils.

PM4Sand was calibrated in order to capture soil triggering and strain accumulation behavior for both level (no-bias) and sloping ground (bias) conditions. For the parametric study, liquefaction triggering curves from Green et al (2018) were used to calibrate the constitutive model parameters. In addition, recommendations by Idriss and Boulanger (2008) were used to capture the effect of static bias. Figure 5-1 presents the liquefaction triggering curves for no bias (α=0) and with bias (α=0.1 and 0.2) with the calibrated PM4Sand model (red lines) and the liquefaction triggering curve (no bias) suggested by Green et al (2018) (black line).

Constitutive model parameters of liquefiable sands were also calibrated to capture the accumulation of post liquefaction shear strains. Post-liquefaction response in terms of the rate and magnitude of accumulation of plastic shear strains is equally critical for the proper estimation of liquefaction induced demands. The value of shear strain developed at a specified number of cycles for a specific CSR and specific initial conditions, such as relative density and confining pressure, can be an index of the rate of accumulation of plastic shear strain.

In the absence of soil-specific experimental data, a database of published results from stress-controlled direct cyclic simple shear laboratory tests on sands exhibiting post-liquefaction deformations, compiled by Giannakou et al. (2011) and Giannakou et al (2012), was used.

An example comparison between the shear strain accumulation predicted by a calibrated effective stress constitutive model and the results from the compiled database from Giannakou et al. (2012) without static bias and for 5 cycles is shown on Figure 5-2. The figure presents the cyclic stress ratio versus the estimated SPT $N_{1,60}$ value for all tests with initial static bias from the database compiled (grey triangle). The value of $N_{1,60}$ was calculated based on the reported relative density for each sample using the correlations proposed by Idriss and Boulanger (2008) and Kulhawy and Mayne (1990) with equal weights. The figure also presents the value of the shear strain accumulated at 5 cycles, as a number (*in italics*) next to the grey triangle corresponding at any given test. For cases where the test was terminated at a number of cycles less than 5 the shear strain developed at test termination is reported with the “>” sign preceding. On the same figures the accumulated strains predicted by the calibrated PM4Sand model are also plotted in green circles.

The reasonable comparison between observed and simulated behavior suggests that the calibrated constitutive models can be tailored to adequately simulate cyclic soil behavior at the element level both in terms of liquefaction triggering and in terms of post-liquefaction shear strain accumulation.

## 5.2 MODEL VALIDATION AND VERIFICATION

Validation is the process of determining a degree to which a model is an accurate representation of the real world from the perspective of the intended uses of the model. Validation procedures are used to provide evidence that the selected models are capable of capturing the key phenomena of the problem in question (Tasiopoulou 2015).

In order to validate the constitutive models used for the liquefiable sands and evaluate the predictability of the implemented constitutive model, numerical simulations of a centrifuge experiment and a case history were performed and numerical results were compared with recorded measurements in the centrifuge and in the field, respectively. The cases considered in the validation involved liquefaction induced spread footing settlement.

### 5.2.1 Centrifuge Test of Building on Spread Footings on Liquefiable Sand

A series of centrifuge tests of a frame structure resting on two spread foundations overlying Fraser River sand was performed at C-CORE's geotechnical centrifuge facility (Chakrabortty and Popescu 2010). One of these tests was performed on a 16-m-thick homogenous Frasier River sand with 55% relative density, overlying a 4-m-thick dense sand (Dr=75%) as shown on Figure 5-3. This test was selected for the validation of the numerical approach described above.

The characteristic frequency of the structure is 2.1 Hz (at prototype scale). The two footings are 1.8m wide with a bearing pressure of 110 kPa at 70g below each. A rigid box was used in the experiment and a 5.4-cm-thick (model scale) Duxseal (a relatively soft material) was placed at each end wall of the box to create absorbing boundaries.

The input ground motion was applied at the base of the box in horizontal direction. A synthetic earthquake time history was used corresponding to the 2475-year design event for the Vancouver area (in Canada) based on the firm ground target spectrum in NBCC (2005), amplified by 1.46 to obtain a peak ground acceleration of 0.25g in the centrifuge tests (Figure 5-3).

In order to simulate the structural period and foundation pressure in the numerical analyses we used beam elements with stiffness of 3e7 kPa, cross-sectional area 0.252 $m^2$ and 0.3414$m^2$ (columns and top slab respectively), moment of inertia $1.33 \cdot 10^{-3} m^4$ and $3.32 \cdot 10^{-3} m^4$ (columns and top slab respectively). Interface elements were placed under the foundations as described in the numerical approach section above.

The PM4Sand constitutive model was used to model the sand layers. The model parameters were calibrated to match Cyclic Simple Shear test results under level and sloping ground conditions performed by Sivathayalan (1994) and Vaid et al (2001). The calibrated PM4Sand model is compared with the lab results on Fraser River sand on Figure 5-4 in the form of CSR versus number of cycles to liquefaction for no bias (upper left graph) and for initial static bias α of 0.05 (upper right graph), 0.11 (lower left graph) and 0.2 (lower right graph). Onset of liquefaction was considered at shear strain of 3% single amplitude and 6% double amplitude.

The Duxseal placed in the walls of the box was modeled as elastic with a Young's Modulus of 8 MPa and a Poisson's ratio 0.46 (Chakrabortty and Popescu 2012).

Figure 5-5 presents numerical analyses results in the form of excess pore water pressure ratio. As shown on this figure the 55% relative density Frasier River sand liquefies under the imposed shaking. However, there is no liquefaction observed (although excess

pore pressures develop) in a zone directly under the foundation. This is in line with observations from other experimental tests (Dashti et al, 2010; Bertalot and Brennan, 2015; Popescu et al, 2010; Liu and Dobry, 1997).

Figure 5-6 presents comparisons of excess pore water pressure ratio measurements and numerical predictions in the free field and under the foundation. As discussed above although the excess pore water pressure ratio reaches values near 1 in the free field, under the foundation limited excess pore water pressures develop.

Figure 5-7 presents comparisons of foundation settlement measurements and numerical predictions for the two footings.

In general the numerical model predictions compared well with the measured response both in terms of excess pore water pressures and in terms of foundation settlements.

### 5.2.2 Case History of Residential Building at Kaiapoi, New Zealand

A case history of a residential building with largely similar structural and foundation characteristics with residential buildings in Groningen subjected to liquefaction-induced settlements during the 2010 $M_w$ 7.1 Darfield (Canterbury) earthquake was selected as a validation case. Information about the building characteristics, observed settlements and geotechnical conditions were gathered by BICL (2018).

The 2010-2011 Canterbury earthquake sequence includes the 4 September 2010 $M_w$ 7.1 Darfield earthquake and the 22 February 2011 $M_w$ 6.2 Christchurch earthquake among other events. Widespread liquefaction in Christchurch and surrounding areas were reported after these events.

According to BICL (2018) the residential building is a two storey unreinforced masonry and timber framed construction founded on strip footings along the perimeter of the building (Figure 5-8). It is located at 188 Williams street at Kaiapoi, approximately 16 km north of the Christchurch Central Business District. The building suffered differential settlement during the Darfield earthquake event (September 2010). The Eastern side of the building was reported to have sustained a settlement of about 5-10 cm. No settlement data were attributed to the subsequent Christchurch earthquake event (February 2011).

Liquefaction assessment performed by BICL (2018) of 4 CPT logs located close to the corners of the building, resulted in LPI and $LPI_{ish}$ indices greater than 15 for the Darfield event and between 5 and 15 for the Christchurch earthquake event (Figure 5-8). The values of the estimated volumetric-strain induced settlements using simplified Ishihara and Yoshimine (1992) methodology were similar for both events, indicating greater settlement at the Eastern side. Indeed, as shown in Figure 5-9, a comparison of the $qc_{1ncs}$ values from CPT001 (Eastern corner) and CPT003 (northern corner) reveals different soil conditions. The surficial liquefiable deposits at the Eastern corner of the building exhibit lower values of $qc_{1ncs}$ at a greater depth than the ones at the Northern corner. Based on the CPT data and the observed settlements at the site, the Northeastern section of the building was selected for numerical analyses.

The acceleration response spectra (Figure 5-10) of the ground motions recorded at Kaiapoi North School (KPOC) station, situated about 700 m north of the building, during Darfield event indicate much higher spectra values than the ones predicted by empirical models (Cubrinovski et al., 2010). As also shown on Figure 5-10, a map with PGA contours from Smyrou et al. (2011) demonstrates, that during the Darfield event, the Kaiapoi area experienced unusually high PGA values, contrary to the trend of PGA attenuation with source-to-site distance that would be predicted by empirical ground motion prediction models. This

site amplification at the Kaiapoi area is attributed to basin effects resulting in significant amplitude of long period (6-8 sec) surface waves, as observed by Bradley (2012) and shown in Figure 5-11a. A comparison of the acceleration response spectrum of KPOC depicted in Figure 5-11b with other spectra at various locations, indicates high frequency amplification in the range between 0.2 and 0.8 sec.

The general geology of this area comprises of distinct layers of gravels interbedded with layers of finer sediments to a depth of over 500 m below the ground surface according to the geological section by Brown and Weeber (1992), shown on Figure 5-12. Due to lack of outcropping “rock” recordings and the large depth to bedrock, which is hard to estimate accurately, a deconvolution process of strong ground motions at locations where no significant soil nonlinearity was anticipated, was chosen as an alternative. Markham et al. (2014) suggest that Riccarton Gravel formation, which is encountered at depths less than 40m from the ground surface, can be considered stiff enough to be selected as engineering bedrock. The top of Riccarton gravel can be identified at a depth of 18 m below the ground surface at KPOC location, as shown by the shear wave velocity (Vs) profile shown on Figure 5-12. Markham et al. (2014) followed the deconvolution process illustrated as a sketch in Figure 5-13 for two records, CACS and RHSC for all main seismic events including the Darfield and Christchurch earthquakes. The deconvolved Riccarton ground motions were used as input motions for 1D site response analysis for the rest of the recording stations after being scaled by a factor obtained by the New Zealand specific ground motion prediction equation outlined in Bradley (2013), shown on the table of Figure 5-13.

The deconvolved Riccarton ground motions (fault-normal and fault parallel components) obtained from CACS recording were used as input motions for the numerical analyses. However, it was observed that the proposed scaling factor equal to 0.47 for the Darfield event used by Markham et al. (2014), resulted in large residual values as shown by the black line on the upper plots of Figure 5-14a and 5-14b (this was also confirmed by personal communication with Prof Jon Bray who provided the ground motions to Fugro). To improve the prediction for the Darfield event at KOPC, a scaling factor equal to 1 was used in order to achieve lower residual values. Fugro performed parametric 1D site response analyses using the KPOC soil profile shown on Figure 5-12 and then compared the acceleration response spectra at the surface. A better agreement with the acceleration spectrum of the recorded motion is achieved with the higher scaling factor for the Darfield event, as shown by the spectra plot at the bottom of Figure 5-14a and 5-14b.

The devoncolved Riccarton ground motions obtained from CACS were rotated to the building coordinates and the component parallel to the Northeastern section was selected for the analyses (Figure 5-15). A scaling factor equal to 1 was used for the Darfield event, as described above. For the Christchurch event, analyses were performed using two different scaling factors: a) 1 (i.e. same as the scaling factor used for the Darfield event) and b) 0.73 as suggested by Markham et al (2014), shown on the table of Figure 5-13. It should be mentioned that the scaling factor suggested by Markham et al (2014) for the Christchurch event results in lower residual values and thus, better agreement with the spectra of the recorded motion at KPOC (Markham et al., 2014).

Numerical modeling of the structure involved the development of an equivalent frame model based on input from BICL. The equivalent frame is shown on Figure 5-16. Lumped masses were assigned only for inertial loading. The out-of-plane tributary length is 7 m and the load exerted on the soil is estimated to be 45 kN/m approximately (foundation width is 0.8 m).

Idealized soil profiles were obtained based on the CPT data at the northern (CPT003) and eastern (CPT001) corners of the building for depths 10m and 7m below the ground surface, respectively. For greater depths up to 18m (i.e. top of Riccarton gravel and the base of the numerical model), the soil profile of KPOC was used. The values of relative density, Dr, assumed for the soil profiles at each corner were based on Boulanger and Idriss (2014) correlation with CPT data and they are plotted on Figure 5-17. The numerical model along with the stratigraphy, the groundwater level, the structure and the base input motions for the Darfield and Christchurch events using a scaling factor equal to 1 are shown on Figure 5-18. The liquefaction triggering curve for the critical surficial layer with the least relative density of 40-45% was obtained based on laboratory data on Christchurch fluvial silty sand by Taylor et al. (2013), shown on Figure 5-19. Calibration of PM4Sand was based on the lab data for this layer and judgment was used to scale up the resistance to liquefaction triggering of the layers with higher relative density.

Figures 5-20a to 5-20e present numerical results for the Darfield event. Figure 5-20a shows the contours of maximum excess pore pressure ratio, $Ru_{max}$, during shaking indicating that liquefaction occurs below the footing at the eastern corner of the building and in the free field at the eastern side within the layer with Dr=40-45%. Layers with higher relative densities do not liquefy. The settlement time histories and contours plotted on Figure 5-20b show that the right (eastern) footing settles 26 cm and the left (northern) one settles only 8 cm resulting in a differential settlement of about 18 cm. Observing the shear strain contours shown on Figure 5-20c, a characteristic shear zone develops starting from the right (eastern) footing and moving deeper and towards the free field within the liquefied layer, almost in parallel to the interface with the underlying non-liquefiable layer. Figure 5-20d depicts the settlements after reconsolidation indicating an extra settlement of the right (eastern) footing in the order of 5 cm and no additional settlement for the left (northern) footing. Figure 15-20e depicts the contours of $Ru_{max}$ at the top and reconsolidation volumetric strains, $\varepsilon_{vol}$, at the bottom. It is evident that volumetric strains develop only at the right (eastern) side within the liquefied layer close to the footing, indicating an increase of differential settlement. The total (co-seismic and reconsolidation) differential settlement is estimated to be 23 cm compared to a measured range on the site of between 5 and 10 cm.

Figures 5-21a to 5-21c present numerical results for the Christchurch event using a scaling factor equal to 1. Figure 5-21a shows the contours of maximum excess pore pressure ratio, $Ru_{max}$, during shaking indicating that no significant excess pore pressures develop ($Ru_{max} < 0.6$); thus, liquefaction wasn't triggered. The settlement time histories and contours plotted on Figure 5-21b show that the right (eastern) footing settles about 6 cm and the left (northern) one settles only 3 cm resulting in an additional differential settlement of about 3 cm. Due to the lack of significant excess pore pressure development, practically no additional settlements due to reconsolidation occur, as indicated by Figure 5-21c.

Figures 5-22a to 5-22c present numerical results, in the same fashion as previously, for the Christchurch event using a scaling factor equal to 0.73 suggested by Markham et al. (2014). The numerical results are similar to the ones described above, indicating even less excess pore pressure development ($Ru_{max} < 0.5$) and less differential settlement in the order of 1.3 cm. We note that little additional differential settlement was reported for this building after the Christchurch event.

The comparison of field observation during the different earthquake events with numerical model predictions is considered satisfactory (however conservative) considering the uncertainties and subsequent simplifications involved (ground motions, site conditions,

structural characteristics etc.). It should be noted also that these results are unrestrained differential settlements and the presence of a continuous foundation under the footing may in some cases reduce the observed differential displacements from those predicted using 2D plane strain analyses.

# Section 5

# Model Calibration

- ***Triggering:*** based on CSR versus Number of Cycles to Liquefaction from Green et al (2018), Kα based on Idriss and Boulanger (2008)

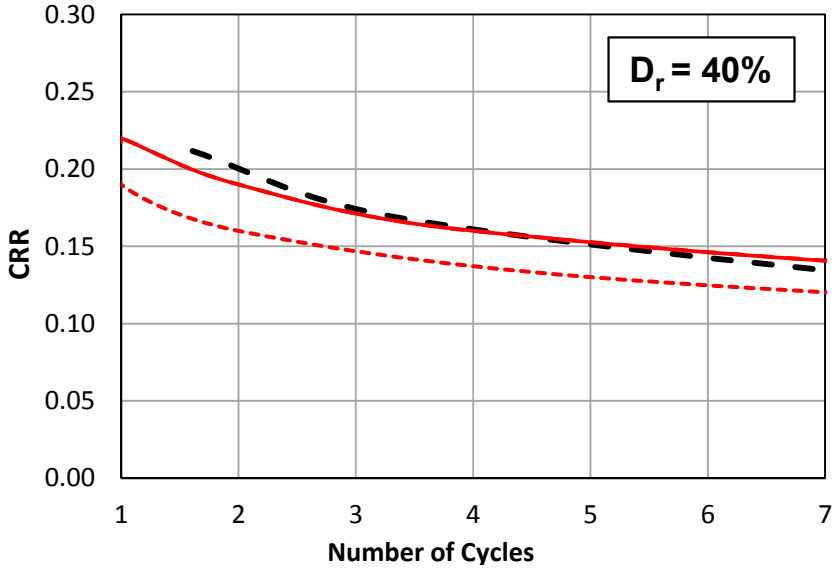


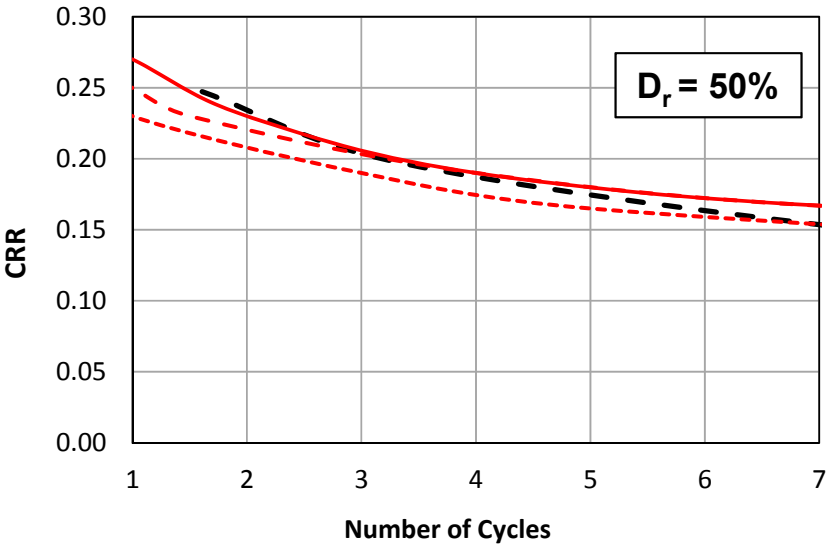


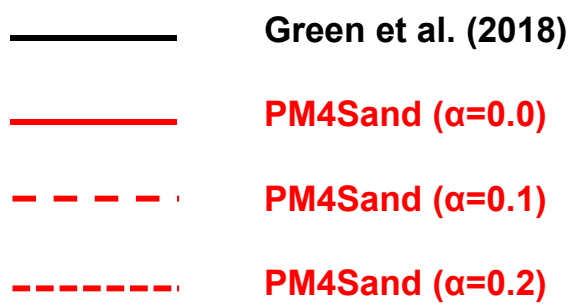


***Idriss and Boulanger (2008)***

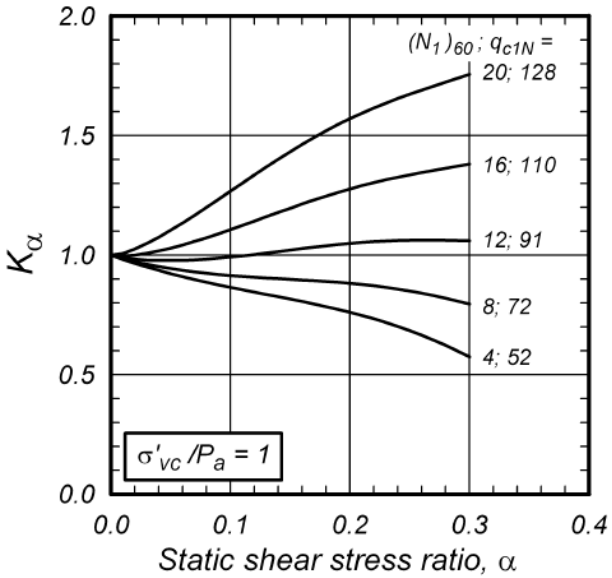


Figure 5-1

# Model Calibration

- ***Post-Liquefaction Shear Strain Accumulation:*** based on procedure and lab testing database presented in Giannakou et al (2015)

## Level Ground Conditions (5 cycles)

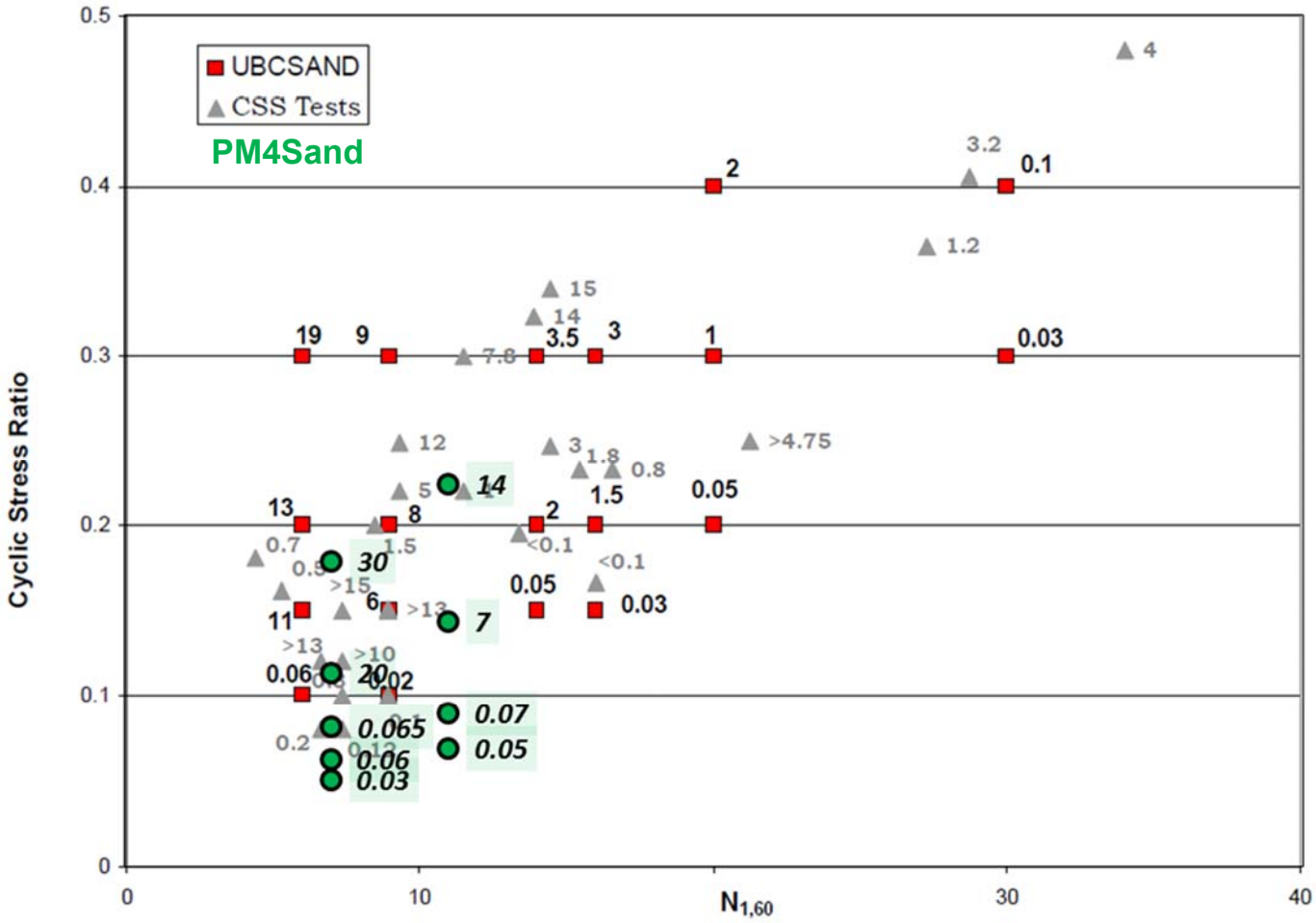


Figure 5-2

# Model Validation

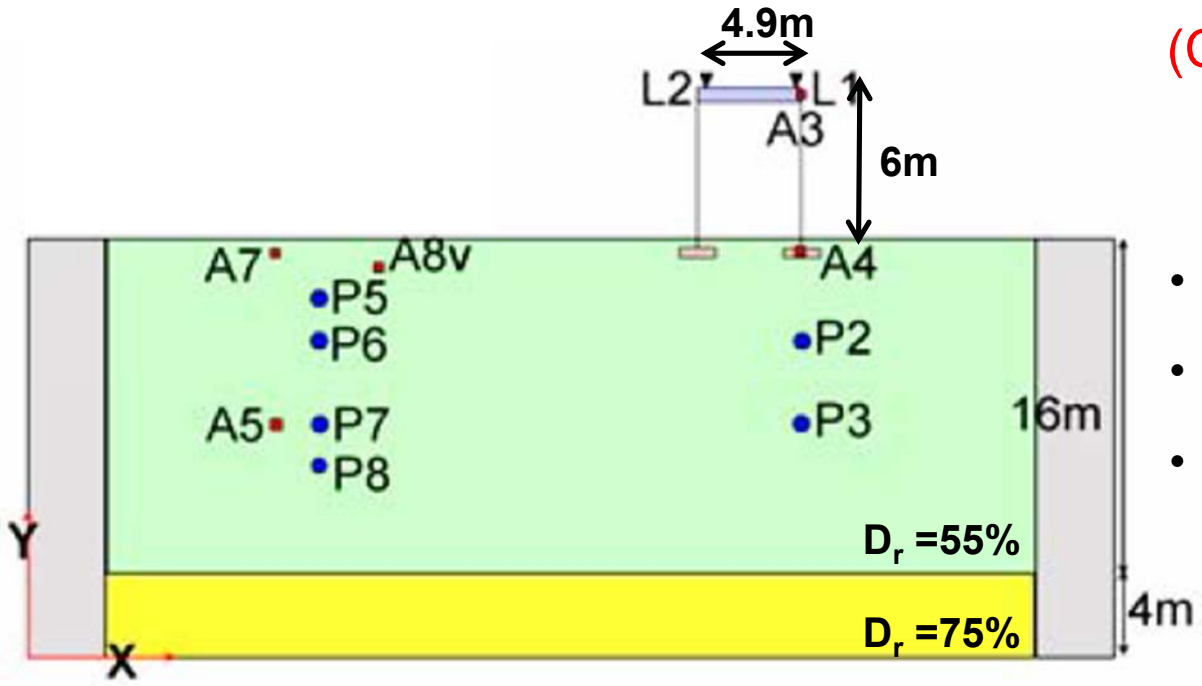


(Chakrabortty & Popescu, 2010)

- **Structure: $T_{str}$=0.47s**
- **Footings: B=1.8m, q=110kPa**
- **Soil: Fraser River Sand, $D_r$=55, 75%**

## Input Motion

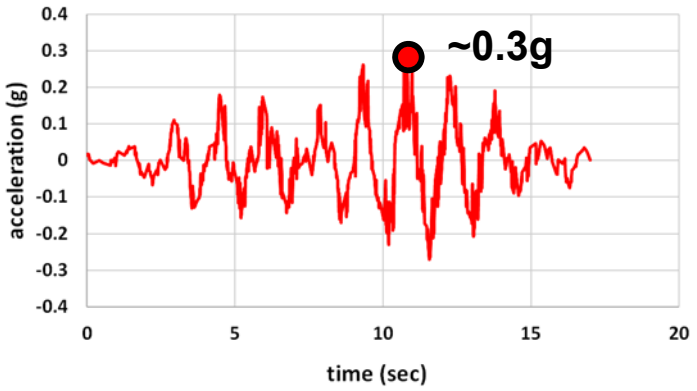


## Numerical Model

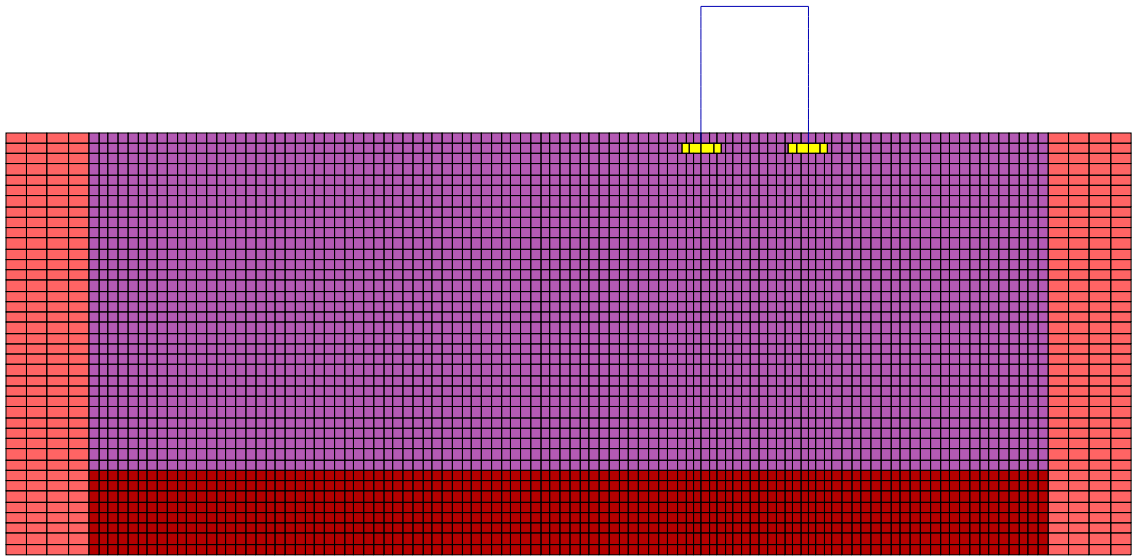

Figure 5-3

# *Constitutive Model Calibration – PM4Sand*

Fraser River Sand – Liquefaction Curves

Experimental
$D_r$ = 59%

PM4Sand
$D_r$ = 55%

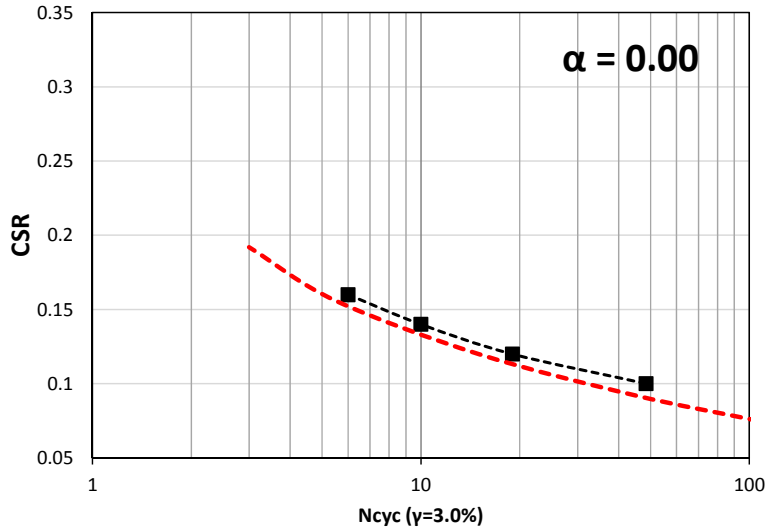


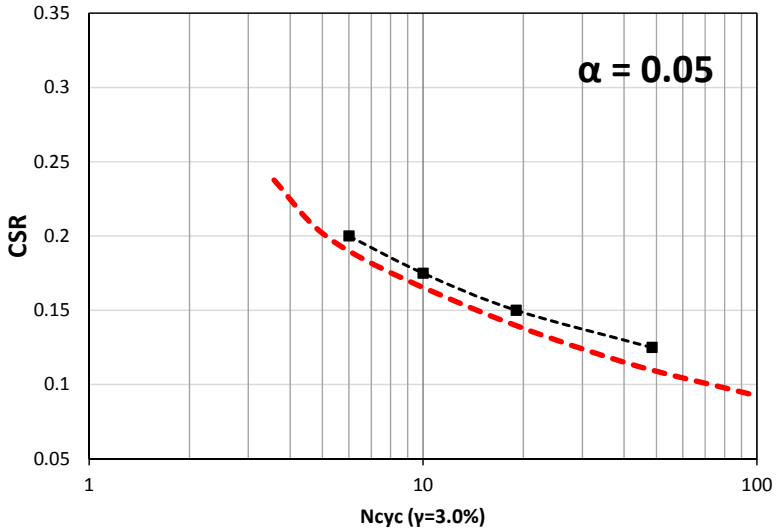


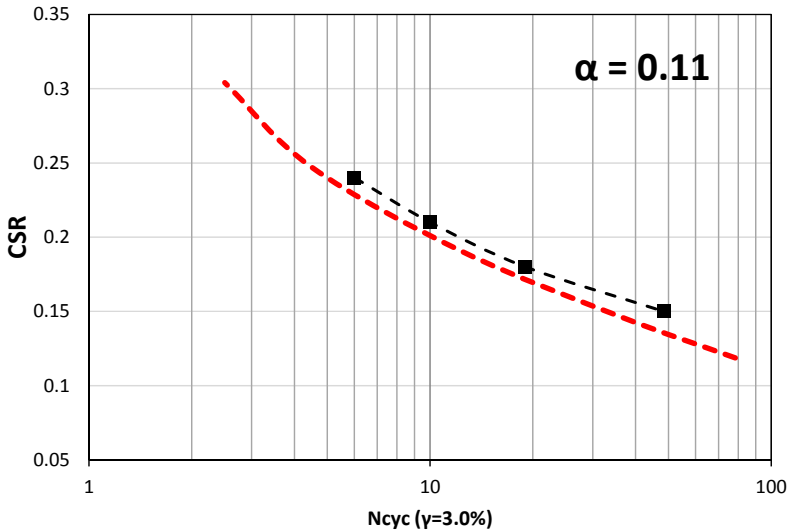


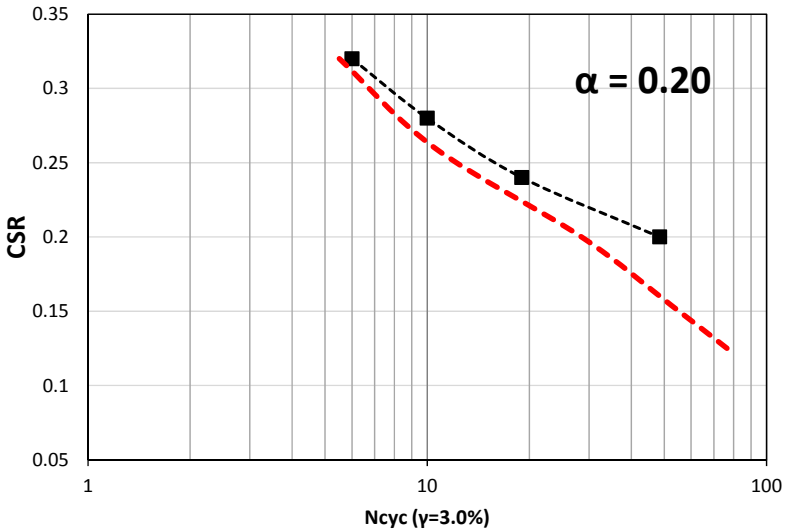


Figure 5-4

# *Excess Pore Pressure Ratio*

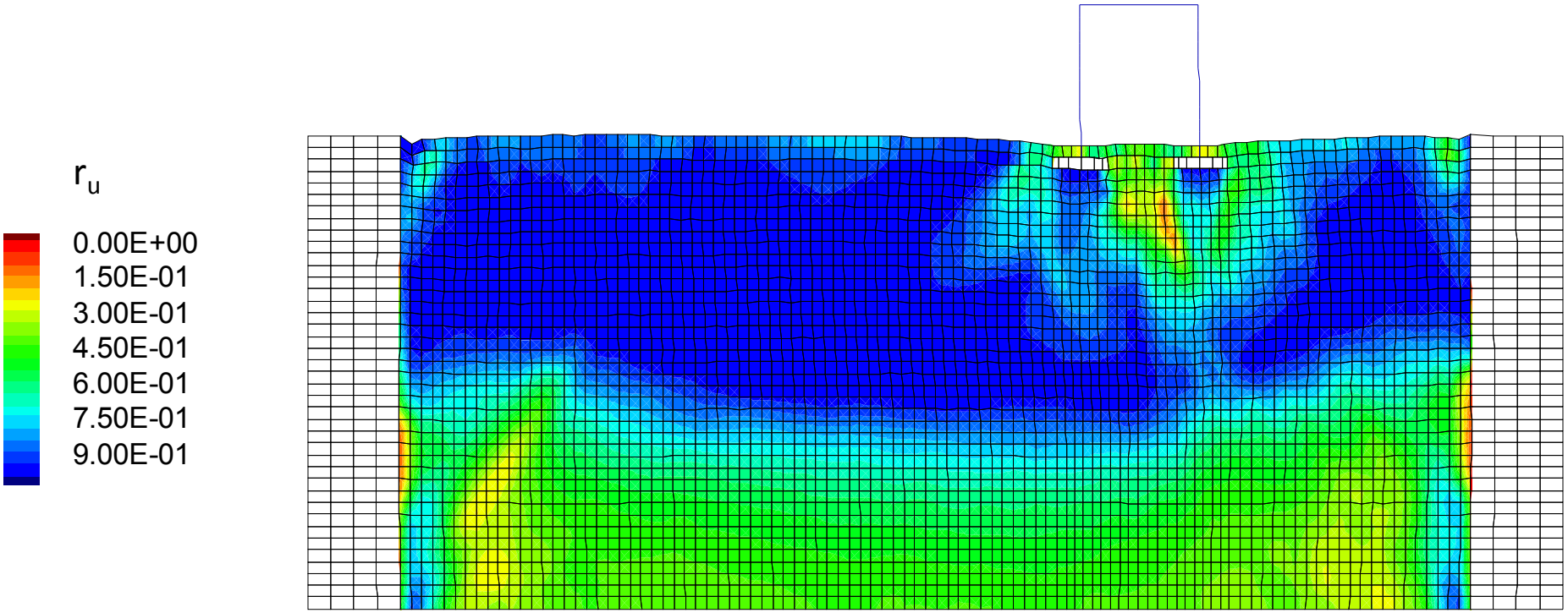


Figure 5-5

# *Excess Pore Pressure ratio*

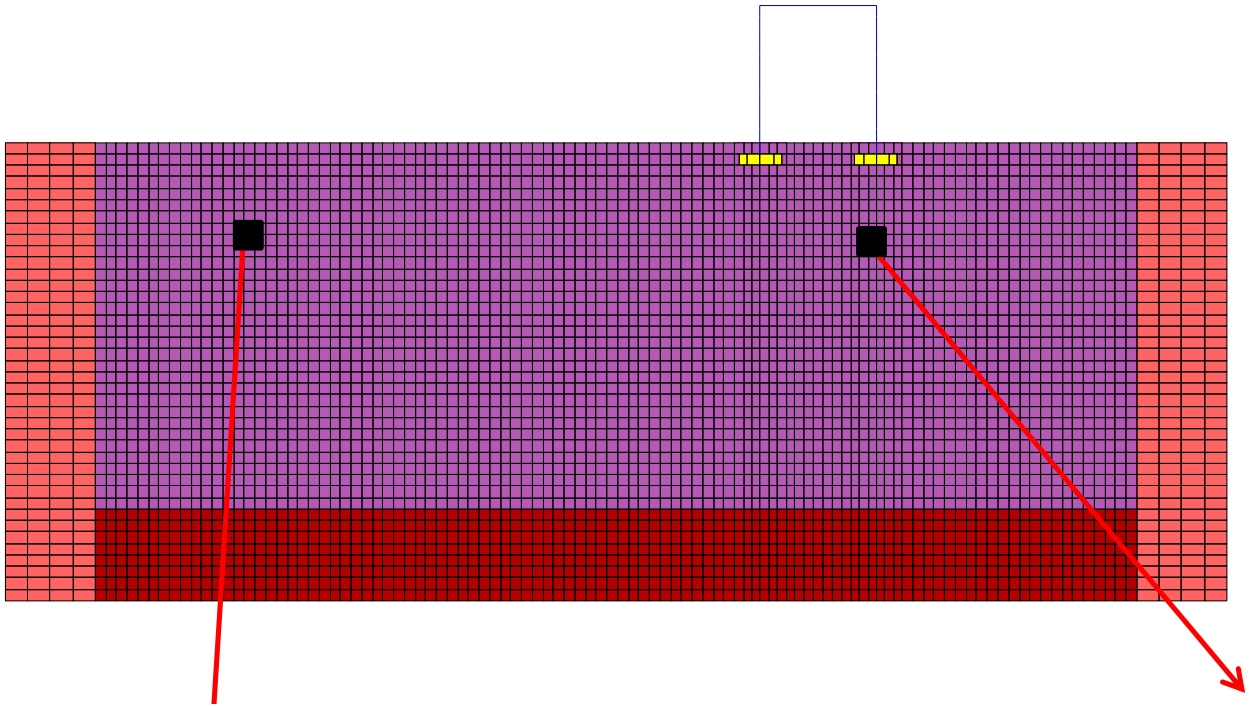

Experimental

Numerical

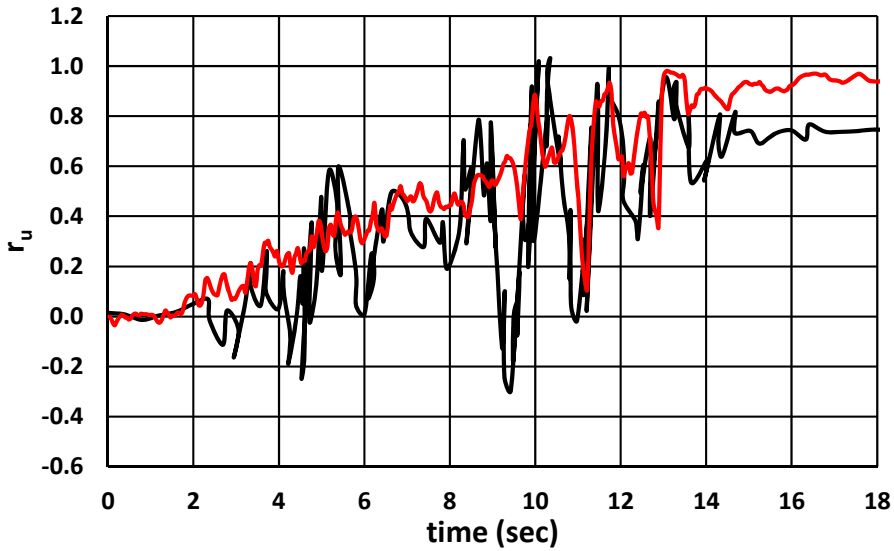


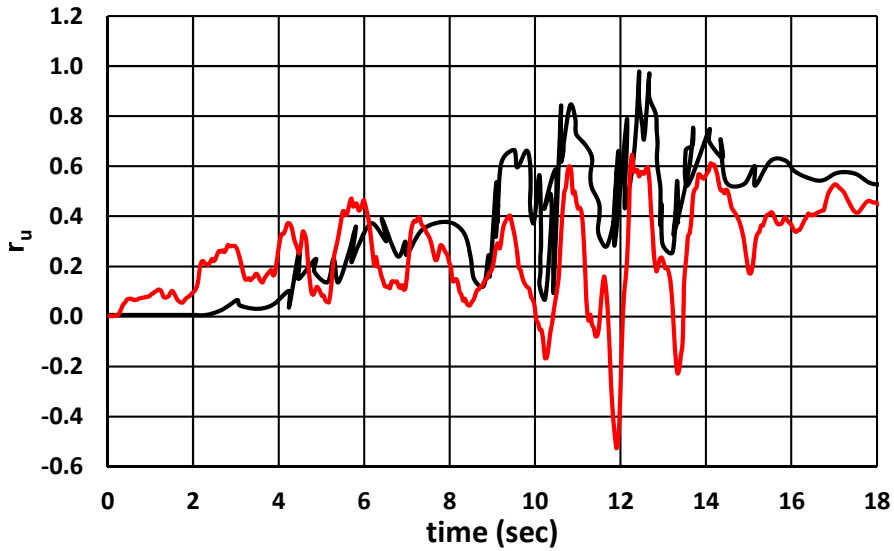


Figure 5-6

# *Footing Settlements*

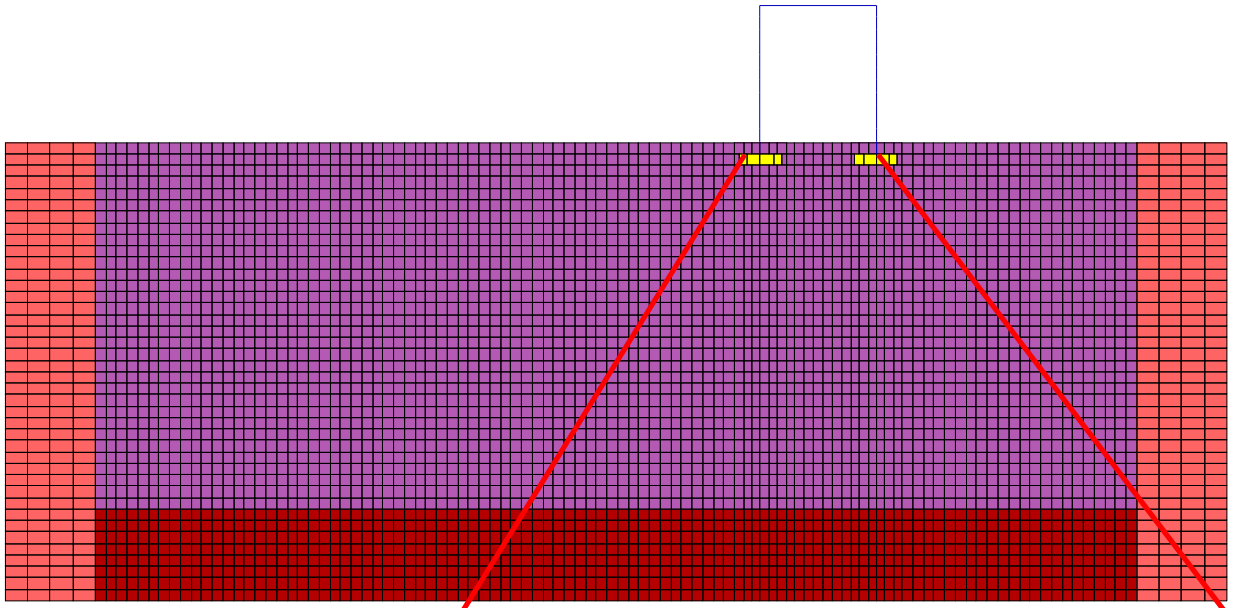

Experimental

Numerical

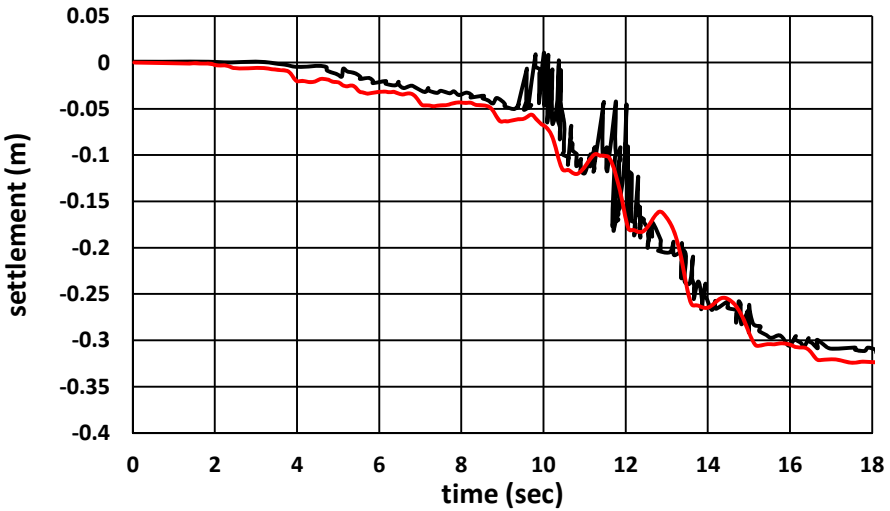


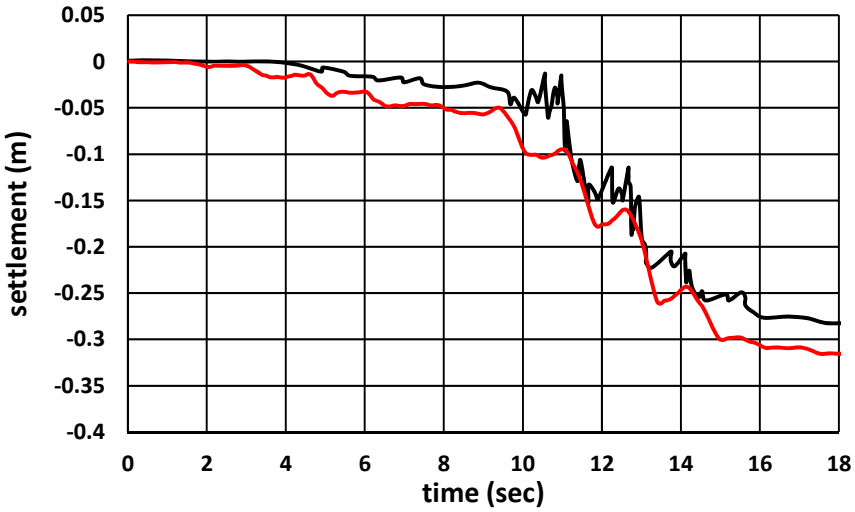


Figure 5-7

# *Case History: Residential Building in Kaiapoi, New Zealand*

- The LPI (Liquefaction Potential Index) for CPT1 to 4 under September 2010 Darfield event is LPI > 15 and under February 2011 Christchurch event is 5< LPI < 15
- $LPI_{ISH}$ (LPI Ishihara) generally falls within the same range as the LPI

## 7.2 Observed Differential Settlement

On 13 September 2010, the building was inspected by TMCO Consulting Engineers, who reported 50-100mm settlement on the East side. We believe this settlement represents the settlement of the building relative to the surrounding ground level. On 21 January 2011, an inspection carried out by MWH had noted that while there was no noticeable change to the building attributable to the recent 2011 aftershocks, the building had settled a little further since 13 September 2010.

We have found no settlement data attributed to the 22 February 2011 earthquake.

| Test ID | Depth of Test (m) | 4 September 2010 Mw=7.1, PGA=0.23g | | 22 February 2011 Mw=6.2, PGA=0.19g | |
|---|---|---|---|---|---|
| | | Total Settlement (mm) [1] | Extent of Liquefaction (m bgl) [2] | Total Settlement (mm) [1] | Extent of Liquefaction (m bgl) [2] |
| CPT001 | 8.59 | 170 | 1.0 - 8.5 | 160 | 1.0 - 8.5 |
| CPT002 | 6.46 | 160 | 0.5 - 6.5 | 150 | 0.5 - 6.5 |
| CPT003 | 10.08 | 110 | 0.0 - 2.5<br>3.5 - 7.0<br>8.0 - 9.5 | 90 | 0.0 - 2.5<br>4.5 - 5.0<br>6.0 - 7.0<br>8.5 - 9.2 |
| CPT004 | 8.56 | 80 | 0.0 - 2.5<br>3.75 - 4.0<br>6.5 - 7.0<br>8.0 - 8.5 | 70 | 0.0 - 2.5<br>8.0 - 8.5 |


***from BICL (2018)***

Figure 5-8

# Case History: Residential Building in Kaiapoi, New Zealand

## Differential Soil Conditions between CPTs 1 and 3

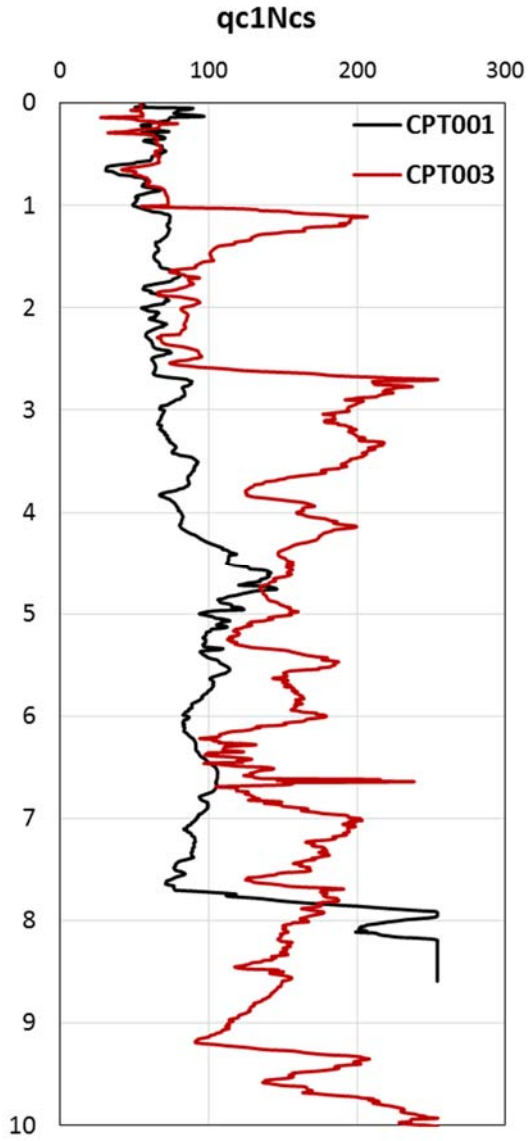



Figure 5-9

# Case History: Residential Building in Kaiapoi, New Zealand

## Ground Motion at Kaiapoi – Darfield Event

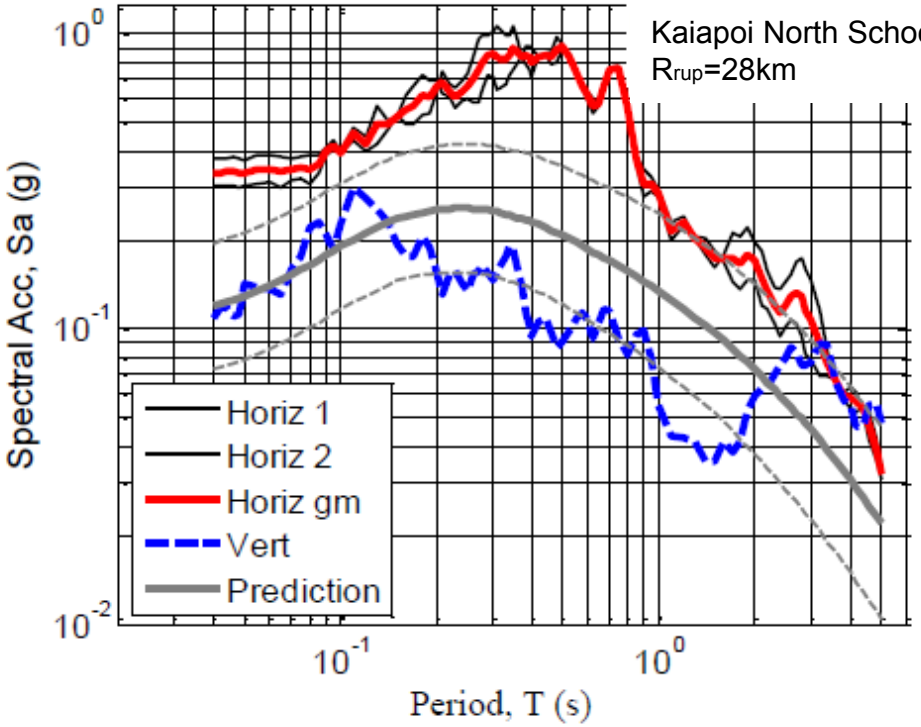


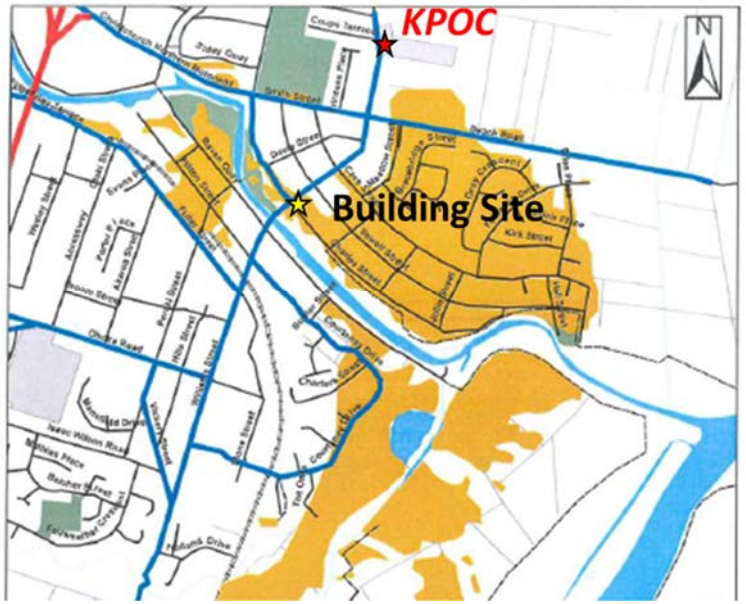


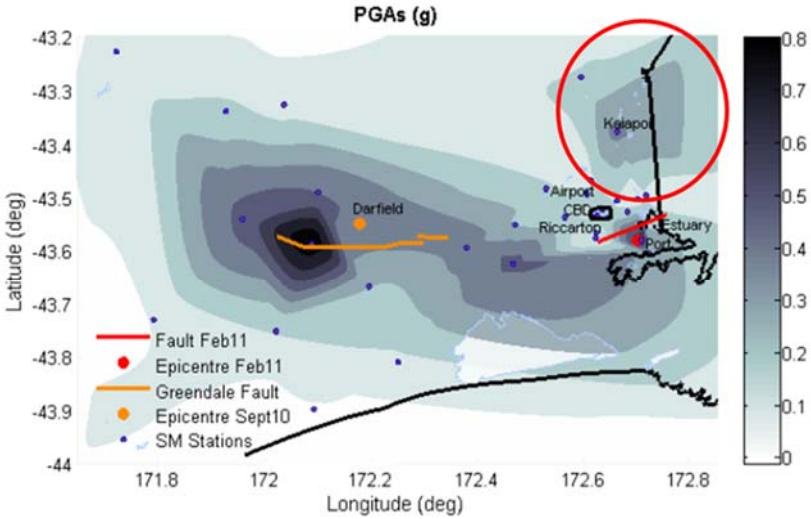


Figure 5-10

# Case History: Residential Building in Kaiapoi, New Zealand

## Ground Motion at Kaiapoi – Darfield Event

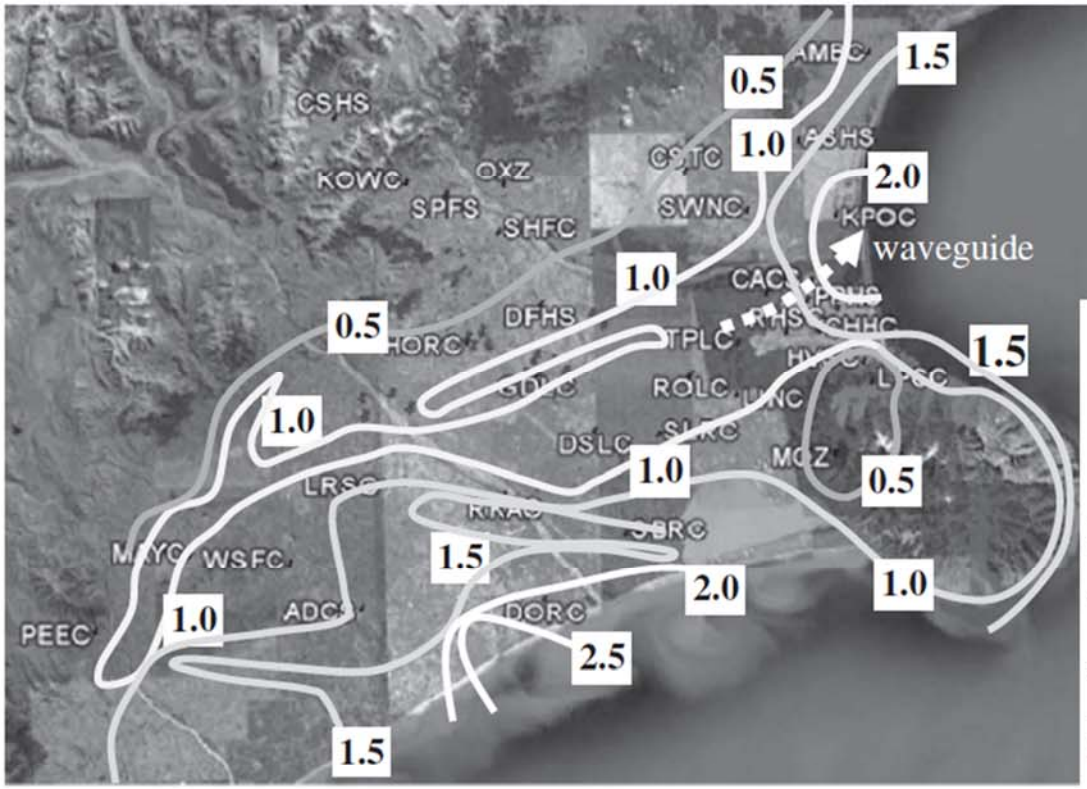


**Fig. 9.** Depth to basement rock (in km) in the Canterbury region [23], relationship to observed waveguide effects.

*significant amplitude of long period surface waves as a result of waveguide effects*

*Significant Basin Effects on long period content (6-8s)*

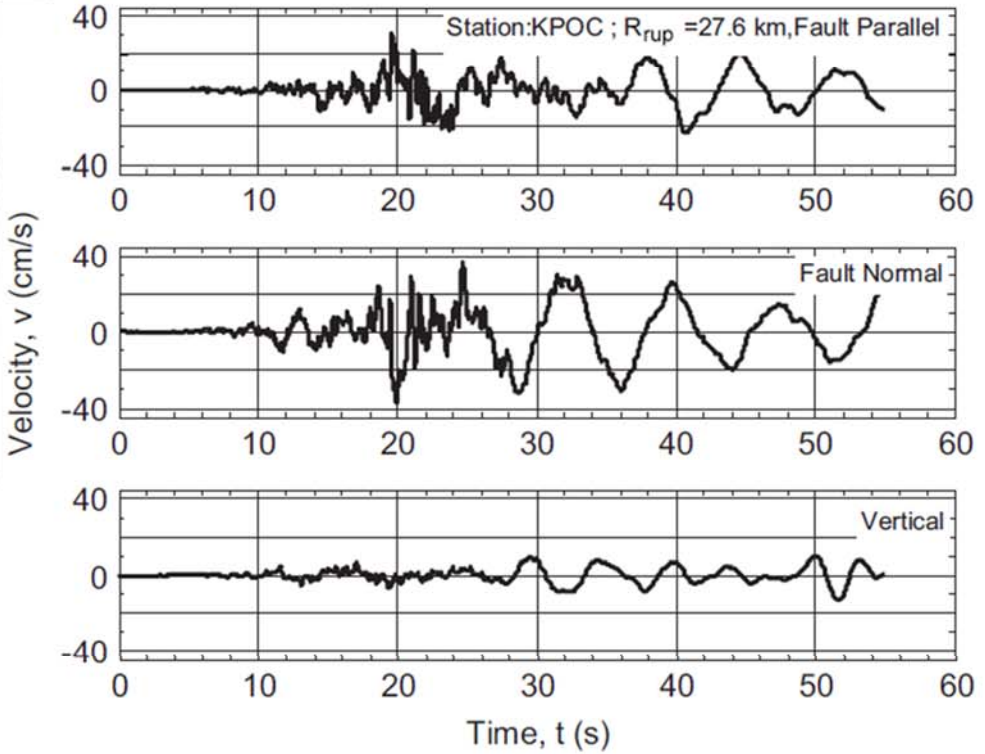


**Fig. 10.** Illustration of significant basin generated surface waves at: (a) Styx Mill (SMTC) and(b) Kaiapoi (KPOC).

***from Bradley (2012)***

Figure 5-11a

# Case History: Residential Building in Kaiapoi, New Zealand

## Ground Motion at Kaiapoi – Darfield Event

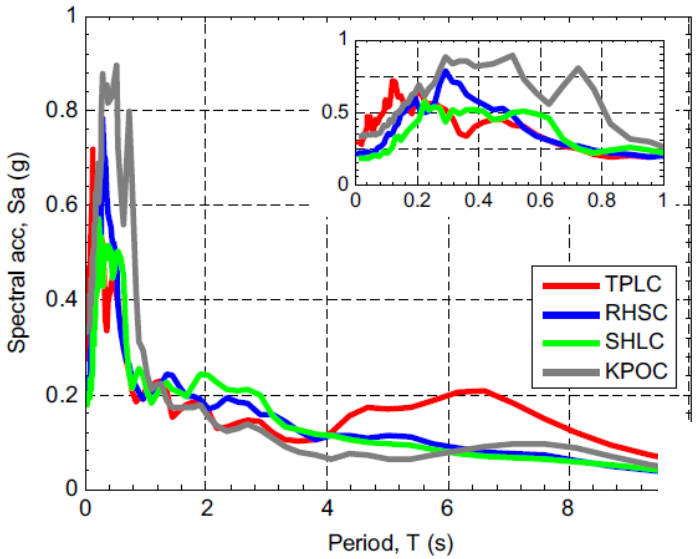


*Near Surface Effects*
*High frequency amplification*

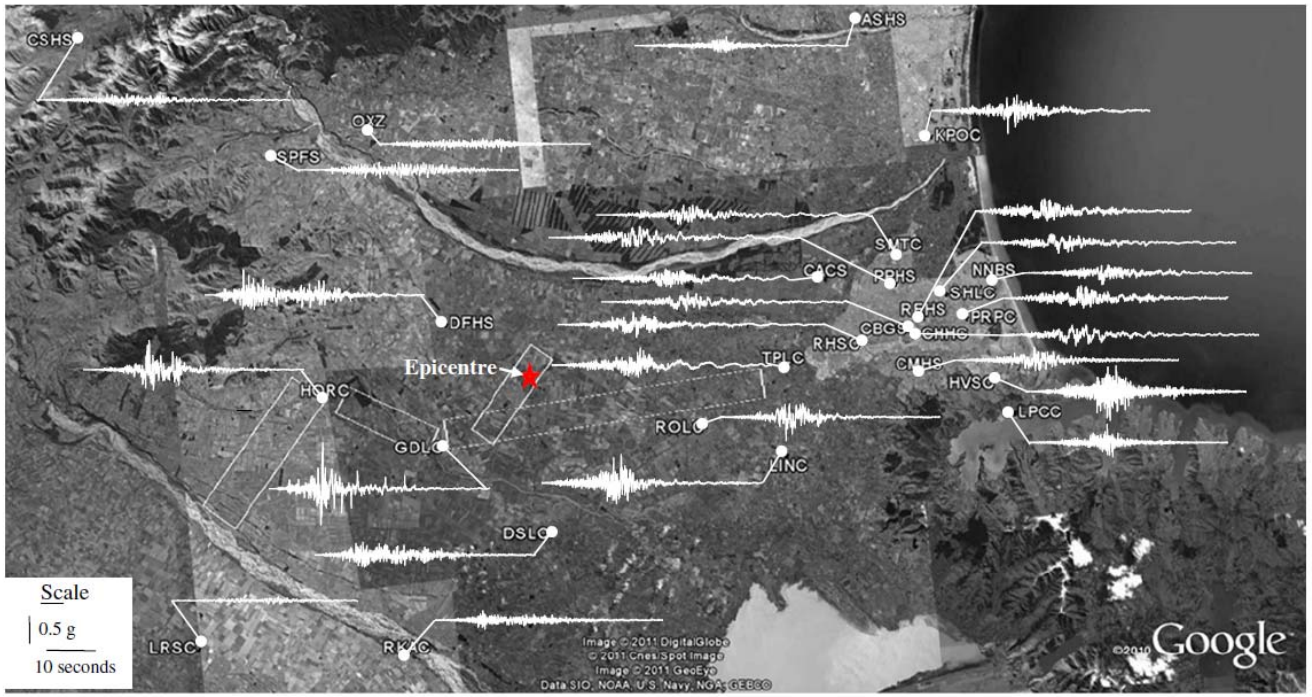


***from Bradley (2012)***

**1.** Observed fault-normal horizontal acceleration time series at various locations in the Canterbury region from the 4 September 2010 earthquake.

Figure 5-11b

# Case History: Residential Building in Kaiapoi, New Zealand

## Ground Motion at Kaiapoi – Darfield Event

A.8 Kaiapoi North School (KPOC)

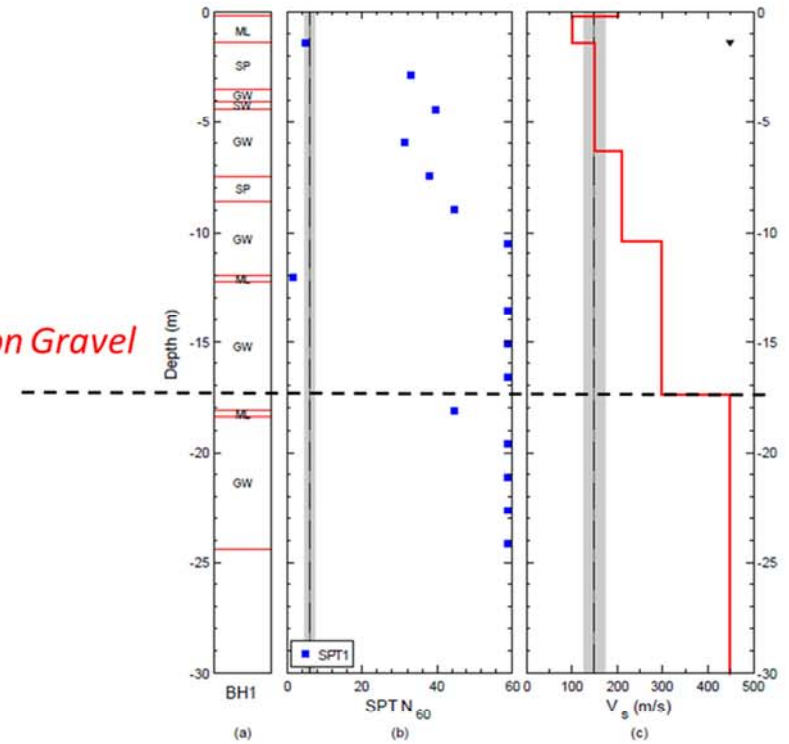


Figure 13 KPOC geotechnical site investigation summary (a) borehole BH1 log, (b) SPT blow counts, (c

52

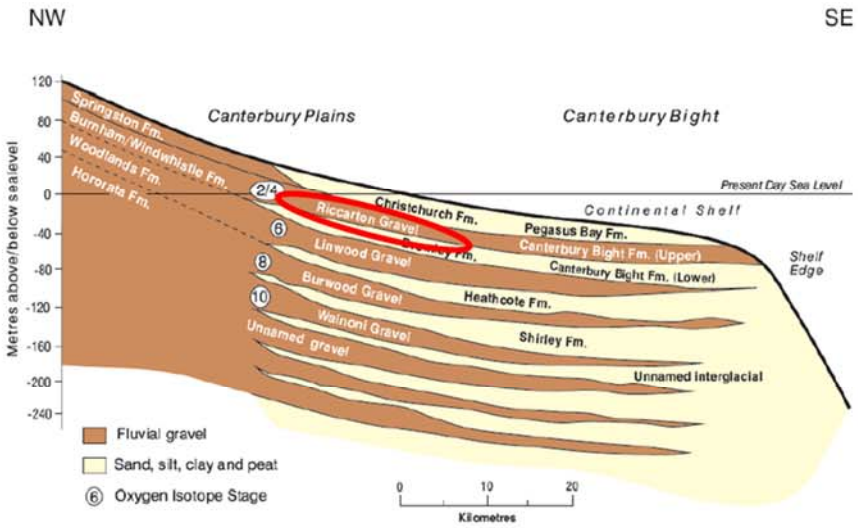


Figure 5: Geologic Cross section of the Christchurch area (from Forsyth et al. 2008; orig. from Brown & Weeber (1992) and Browne & Naish (2003))

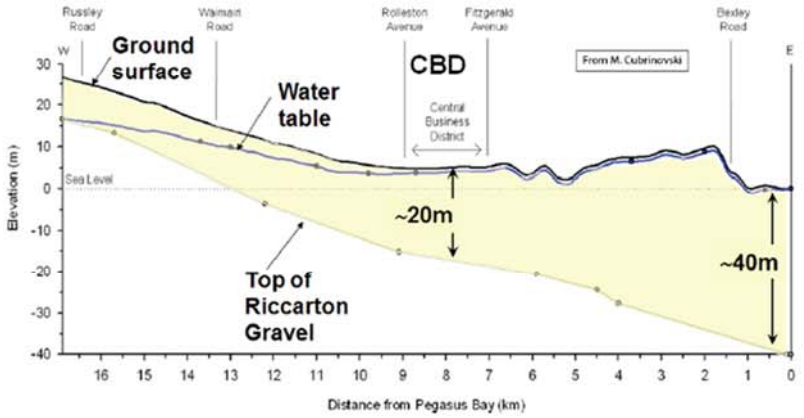


Figure 3: Simplified subsurface profile for Christchurch (from Cubrinovski et al. 2011.)

Figure 5-12

# Case History: Residential Building in Kaiapoi, New Zealand

## Ground Motion at Kaiapoi – Darfield Event

**Use deconvoluted motions by Markham et al (2014) at top of Riccarton Gravel by Markham et al with modified scaling factors for KOPC for the Darfield event**

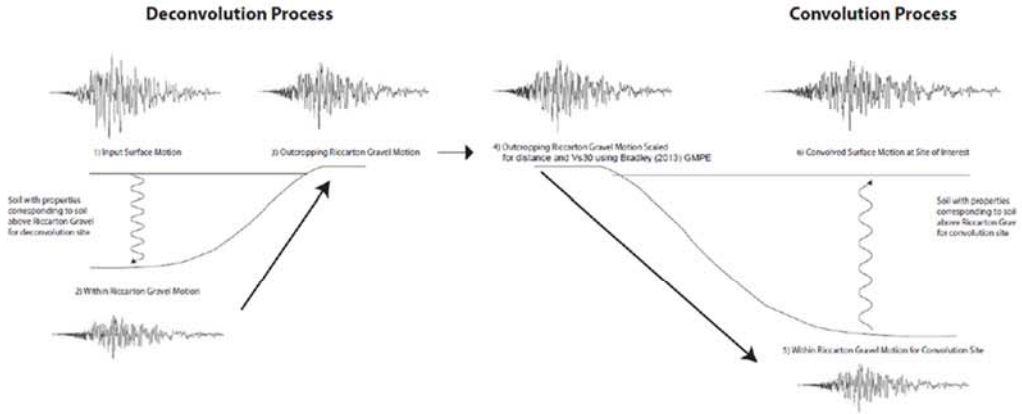


Figure 7: Overview of deconvolution process to obtain input motions for seismic site response analyses (convolution analyses)

Factors recommended in Markham et al are primarily function of Rrup!!

Table 4: Scale factors for input motions at strong motion stations for seismic site response analyses

| Station | 4Sep11 $M_w$7.1 | | 22Feb11 $M_w$6.2 | | 13Jun11 $M_w$6.0 | | 23Dec11 $M_w$5.8 | | 23Dec11 $M_w$5.9 | | 26Dec10 $M_w$4.7 | |
|---|---|---|---|---|---|---|---|---|---|---|---|---|
| | CACS | RHSC | CACS | RHSC | CACS | RHSC | CACS | RHSC | CACS | RHSC | CACS | RHSC |
| CBGS | 0.85 | 0.76 | 2.15 | 1.22 | 2.08 | 1.48 | 1.61 | 1.40 | 1.69 | 1.45 | 3.20 | -- |
| CCCC | 0.78 | 0.69 | 2.74 | 1.55 | -- | -- | 1.90 | 1.65 | 1.98 | 1.70 | 4.59 | -- |
| CHHC | 0.93 | 0.83 | 2.61 | 1.47 | 2.53 | 1.79 | 1.90 | 1.65 | 1.94 | 1.67 | 4.32 | -- |
| HPSC | 0.63 | 0.56 | 2.48 | 1.40 | 2.80 | 1.98 | 3.37 | 2.92 | 3.96 | 3.39 | 2.42 | -- |
| KPOC | 0.47 | 0.42 | 0.73 | 0.42 | 0.82 | 0.58 | -- | -- | -- | -- | 0.47 | -- |
| NNBS | 0.61 | 0.54 | 2.57 | 1.45 | 2.83 | 2.00 | -- | -- | -- | -- | 2.11 | -- |
| PPHS | 0.81 | 0.73 | 1.44 | 0.82 | 1.69 | 1.19 | 1.57 | 1.36 | 1.75 | 1.50 | 1.93 | -- |
| PRPC | 0.78 | 0.70 | 3.16 | 1.78 | 3.77 | 2.67 | 3.05 | 2.64 | -- | -- | 4.55 | -- |
| REHS | 0.92 | 0.82 | 2.45 | 1.38 | 2.66 | 1.89 | 2.21 | 1.92 | 2.30 | 1.97 | 3.98 | -- |
| SHLC | 0.68 | 0.61 | 2.07 | 1.17 | 2.42 | 1.71 | 2.31 | 2.01 | 2.62 | 2.25 | 2.65 | -- |
| SMTC | 0.76 | 0.68 | 1.25 | 0.71 | 1.47 | 1.04 | 1.69 | 1.46 | 1.77 | 1.52 | 1.44 | -- |

# Case History: Residential Building in Kaiapoi, New Zealand

## Ground Motion at Kaiapoi – Darfield Event

**Site response at KOPC – Fault Normal**

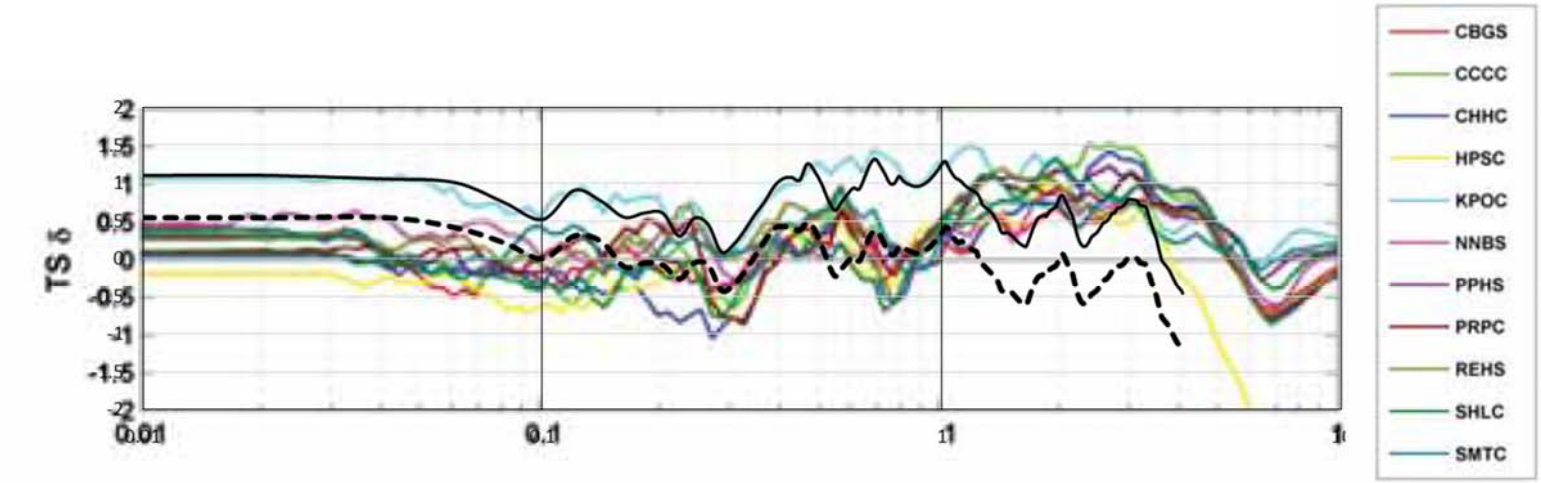


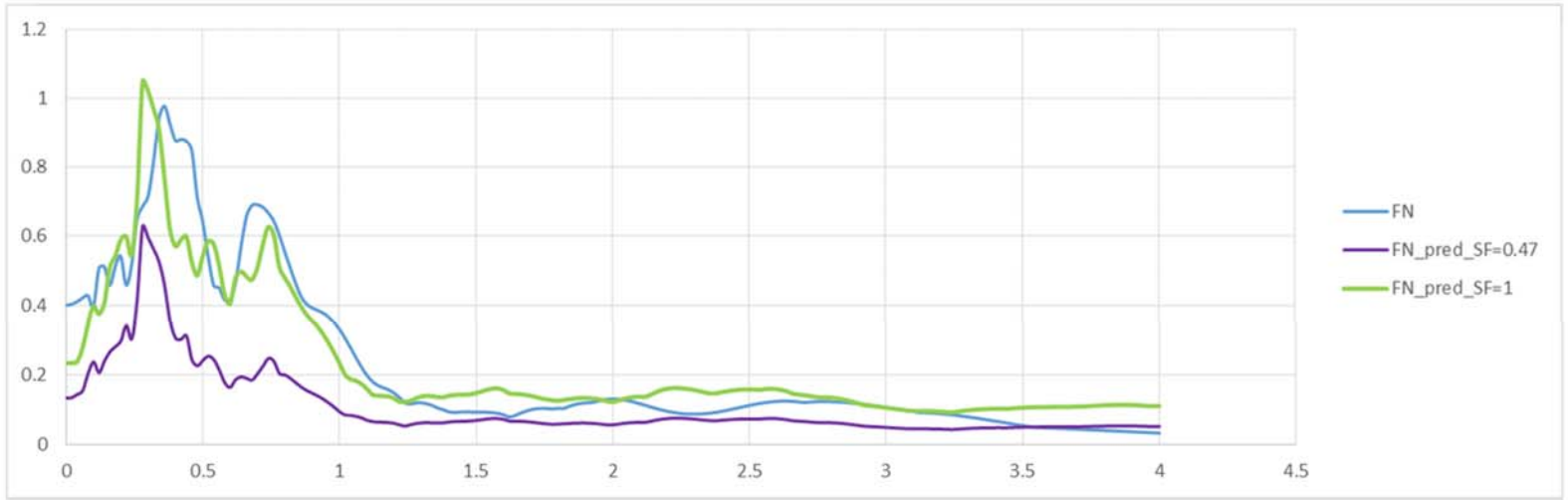


Figure 5-14a

# Case History: Residential Building in Kaiapoi, New Zealand

## Ground Motion at Kaiapoi – Darfield Event

**Site response at KOPC – Fault Parallel**

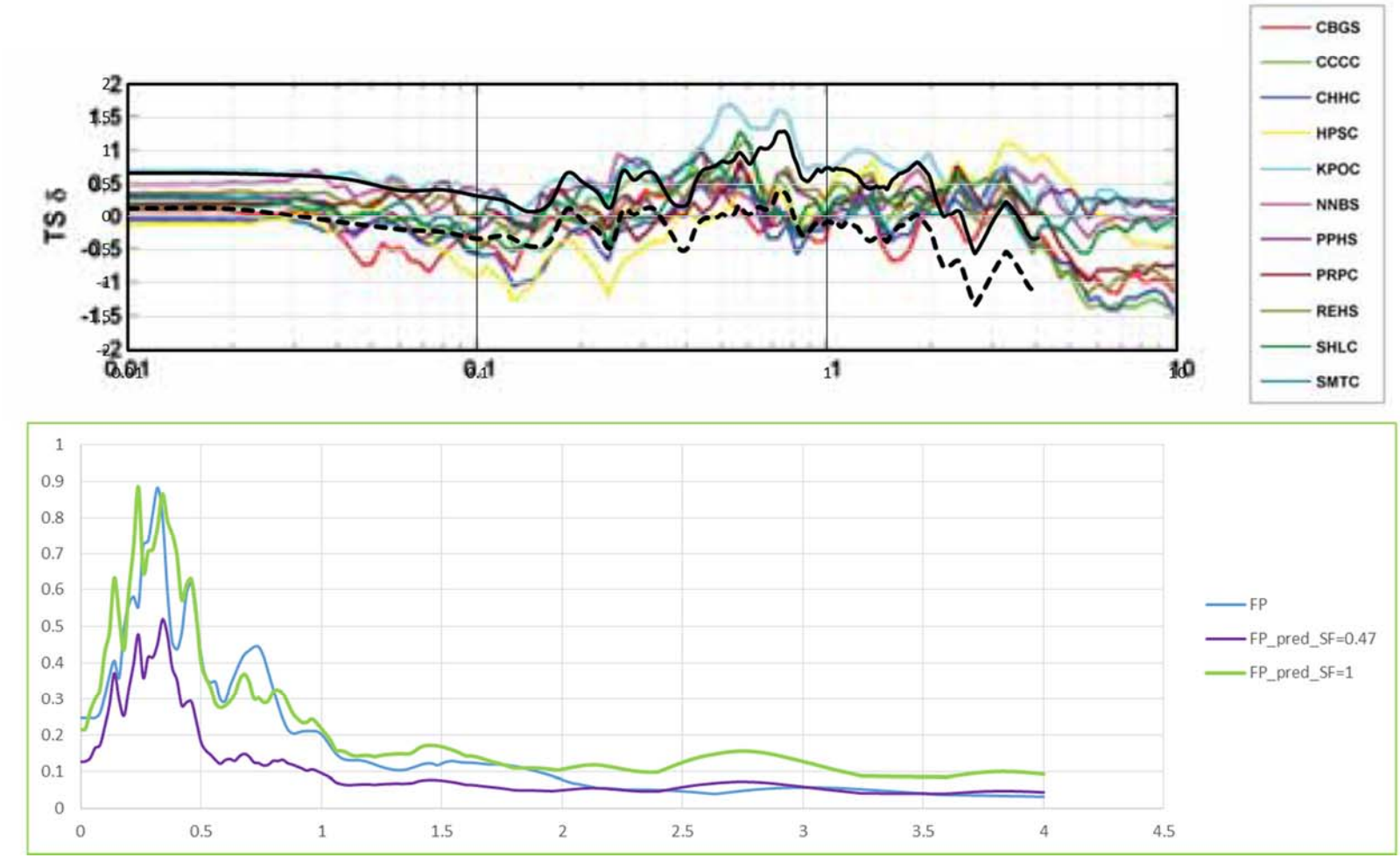


Figure 5-14b

# Case History: Residential Building in Kaiapoi, New Zealand


***Eastern Corner CPT001***

***Nothern Corner CPT003***

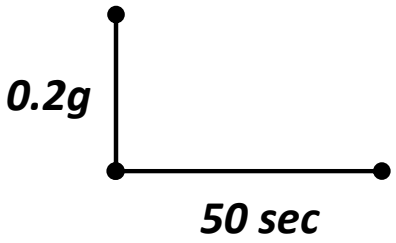


***Rotation of ground motions (Darfield EQ)***

Figure 5-15

# Case History: Residential Building in Kaiapoi, Christchurch

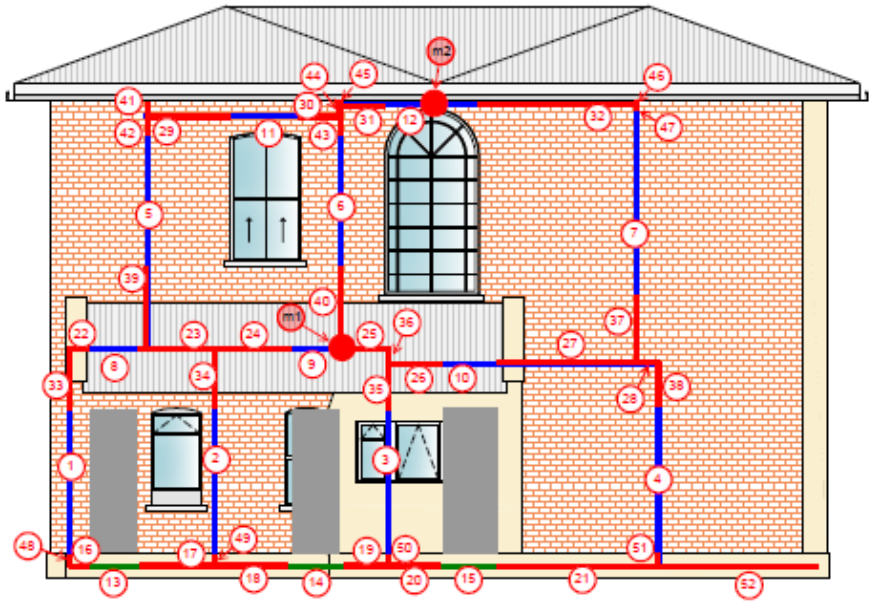

*Equivalent frame model (developed by BICL)*

≈

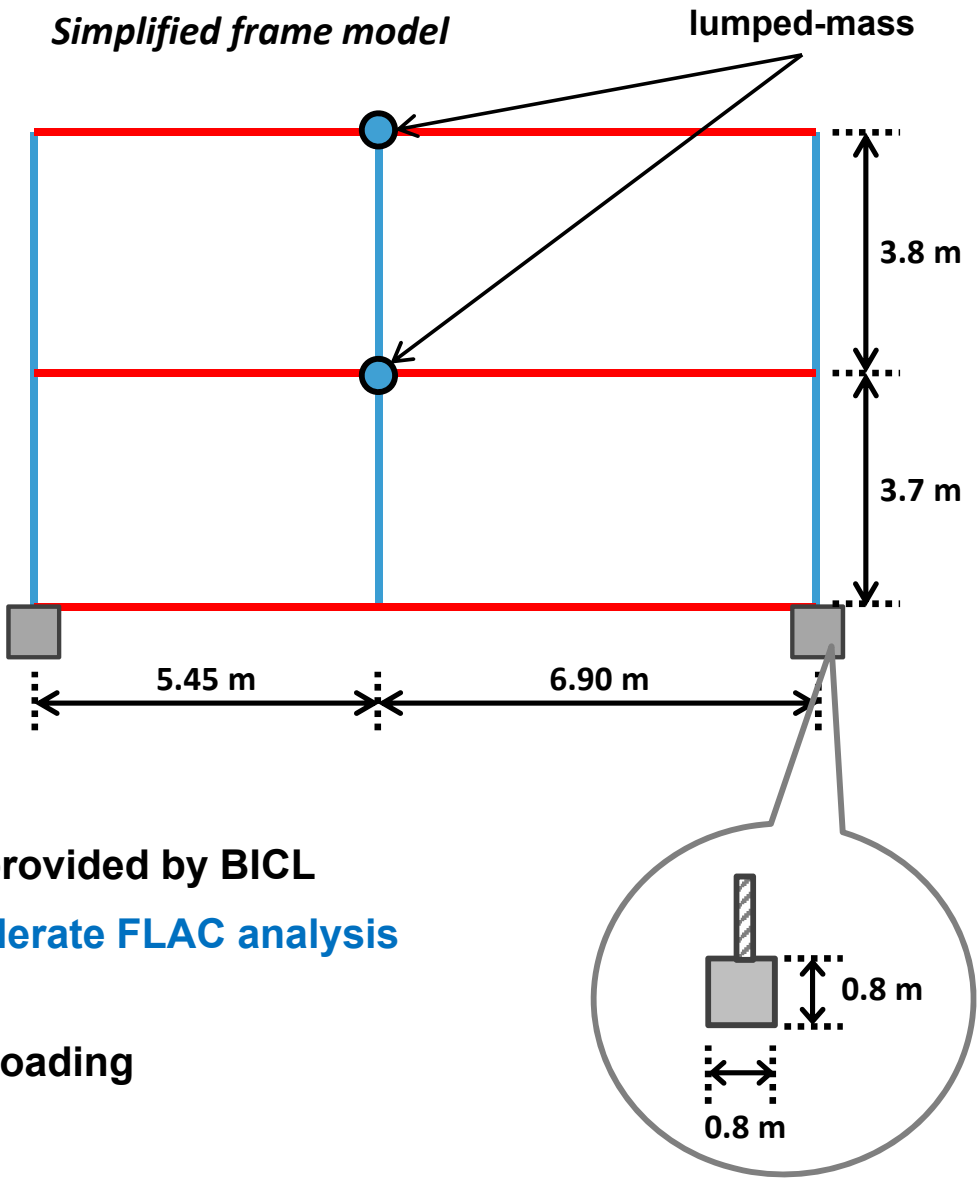


- An equivalent frame model was developed and provided by BICL
- A simplified frame model was developed to accelerate FLAC analysis (same mass; same period)
- Lumped masses were assigned only for inertial loading
- T ≈ 0.08 sec (fixed-base period)
- Out-of-plane tributary length : L = 7 m
- Load on soil ≈ 45 kN/m

Figure 5-16

# Case History: Residential Building in Kaiapoi, New Zealand

## Idealized Soil Profile at 188 Williams St Building

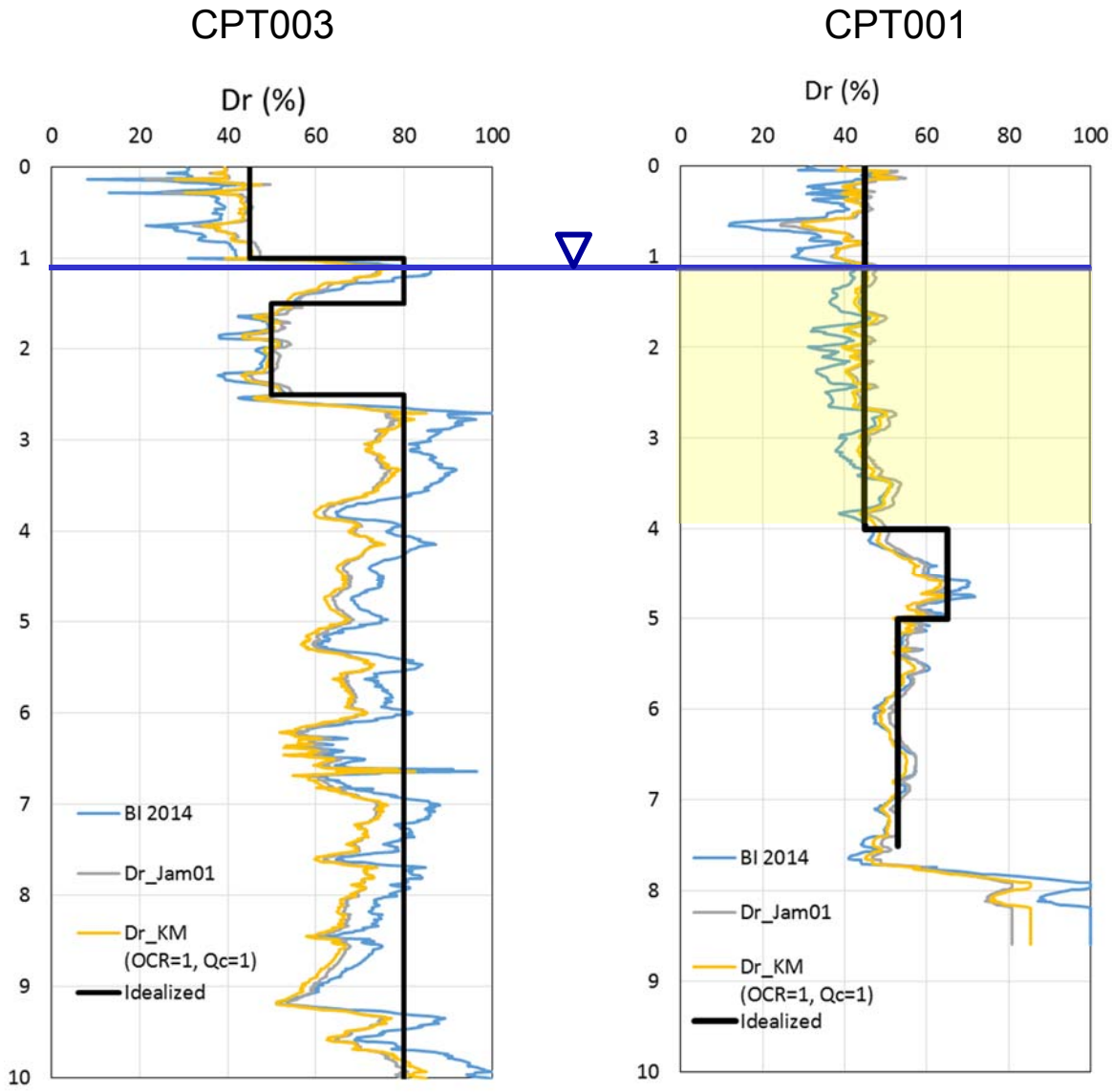


***Nothern Corner CPT003***

***Eastern Corner CPT001***

***Depth : 10.5 – 18.5 m (top of Riccarton Gravel) the soil profile of KPOC was used.***

Figure 5-17

# Case History: Residential Building in Kaiapoi, New Zealand

## Numerical Model and Input Ground Motions

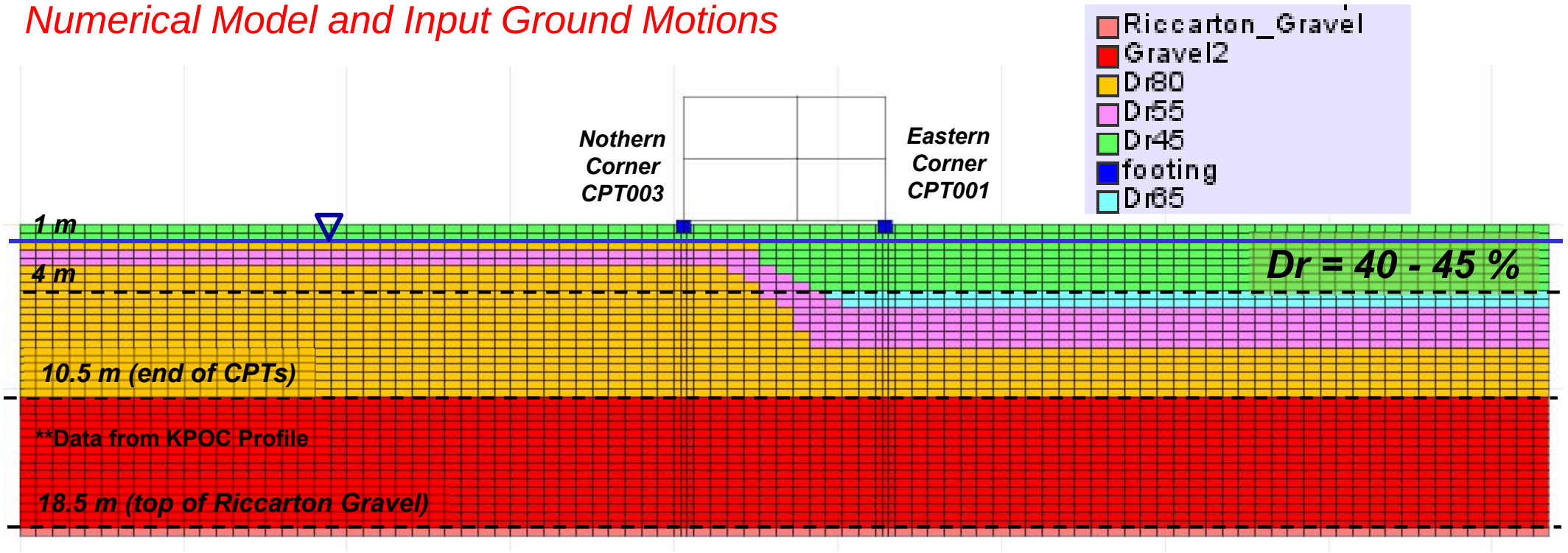


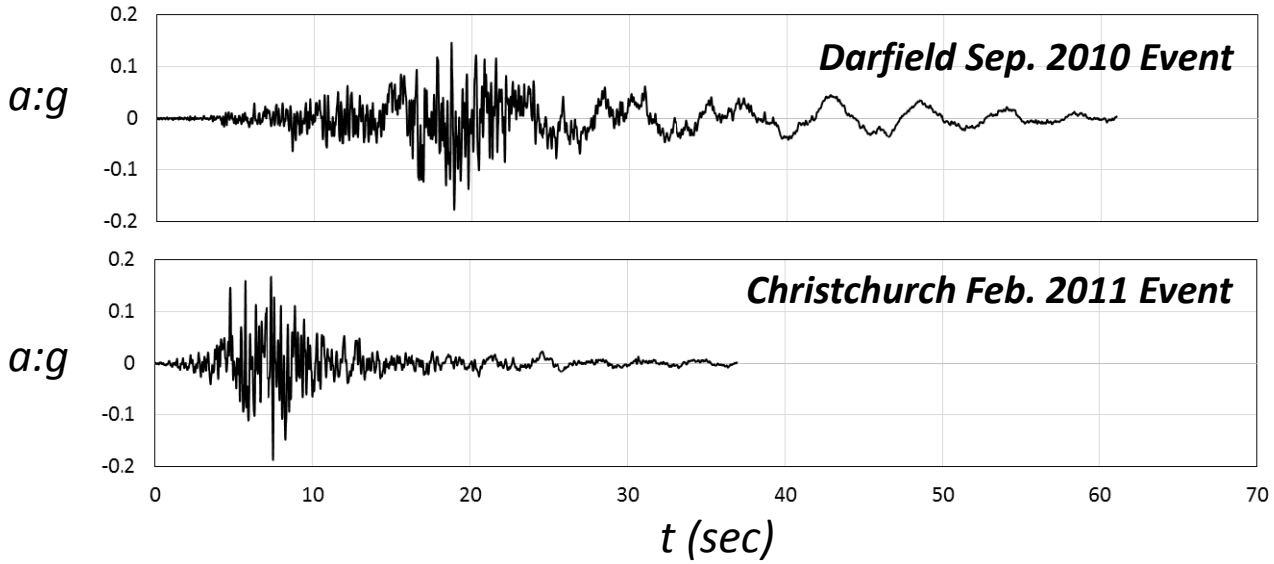


***Input as outcrop motions at the compliant base of the model (top of Riccarton Gravel)***

Figure 5-18

# Case History: Residential Building in Kaiapoi, New Zealand

*Calibration of CSR curves based on lab data (Taylor et al., 2013) on Christchurch fluvial silty sand*

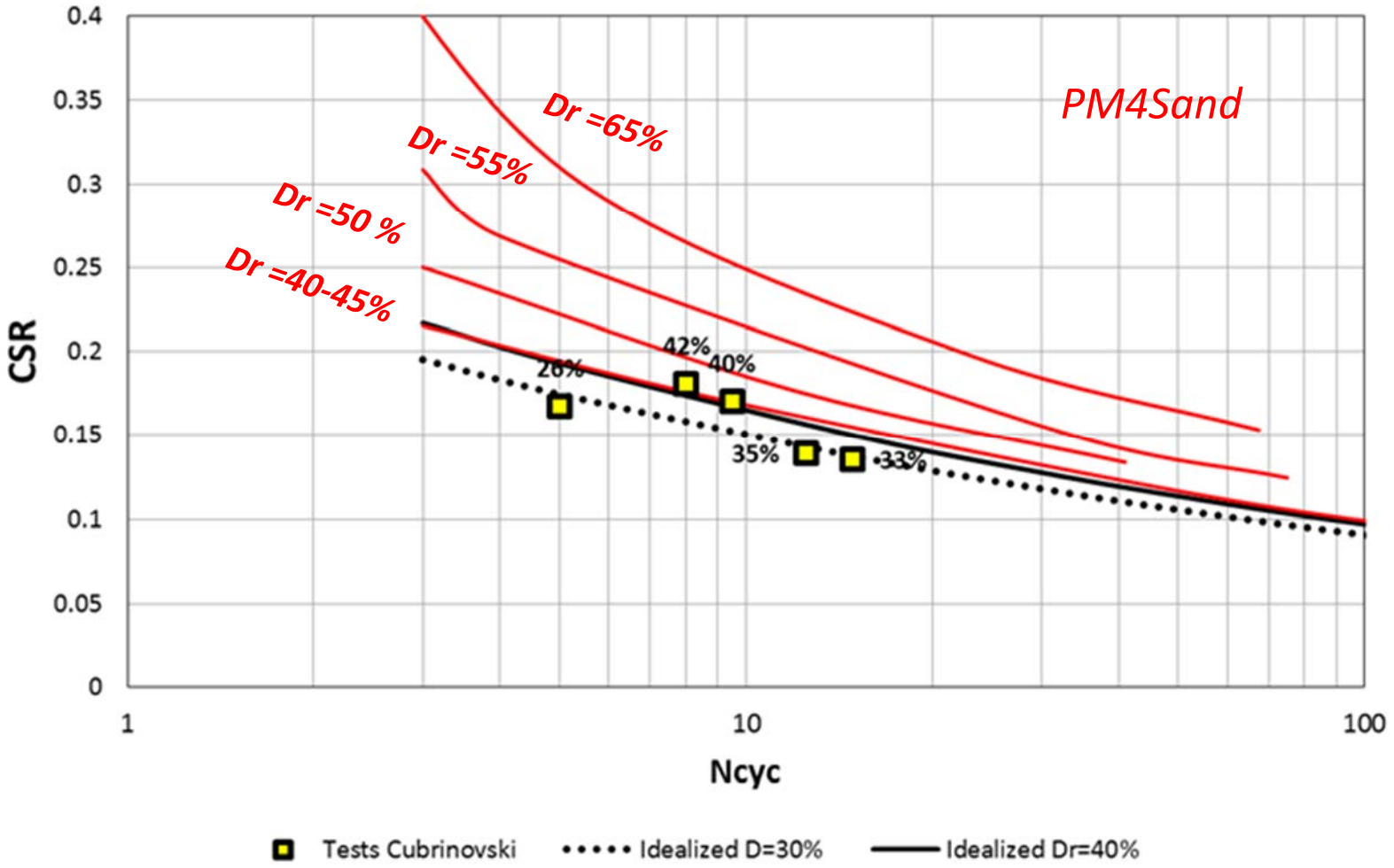


Figure 5-19

# Case History: Residential Building in Kaiapoi, New Zealand

## Darfield Sep. 2010 Event : $Ru_{max}$ contours

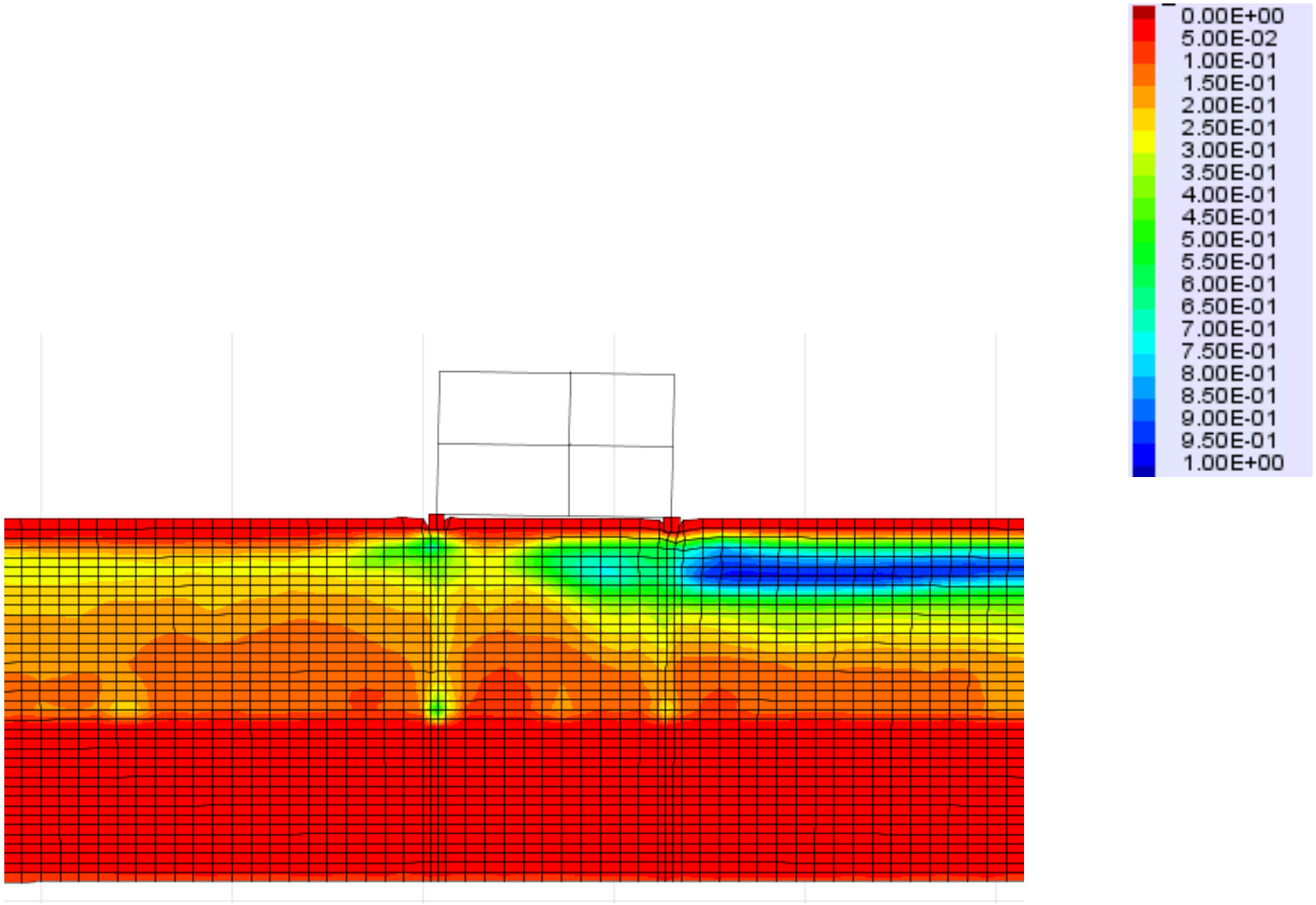


Figure 5-20a

# Case History: Residential Building in Kaiapoi, New Zealand

## Darfield Sep. 2010 Event : settlement contours (m) at the end of shaking

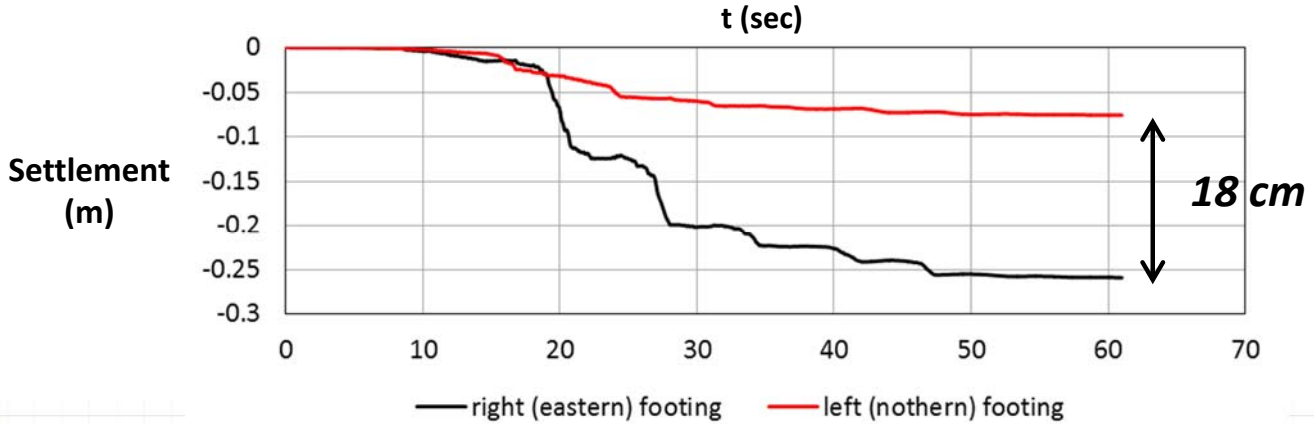


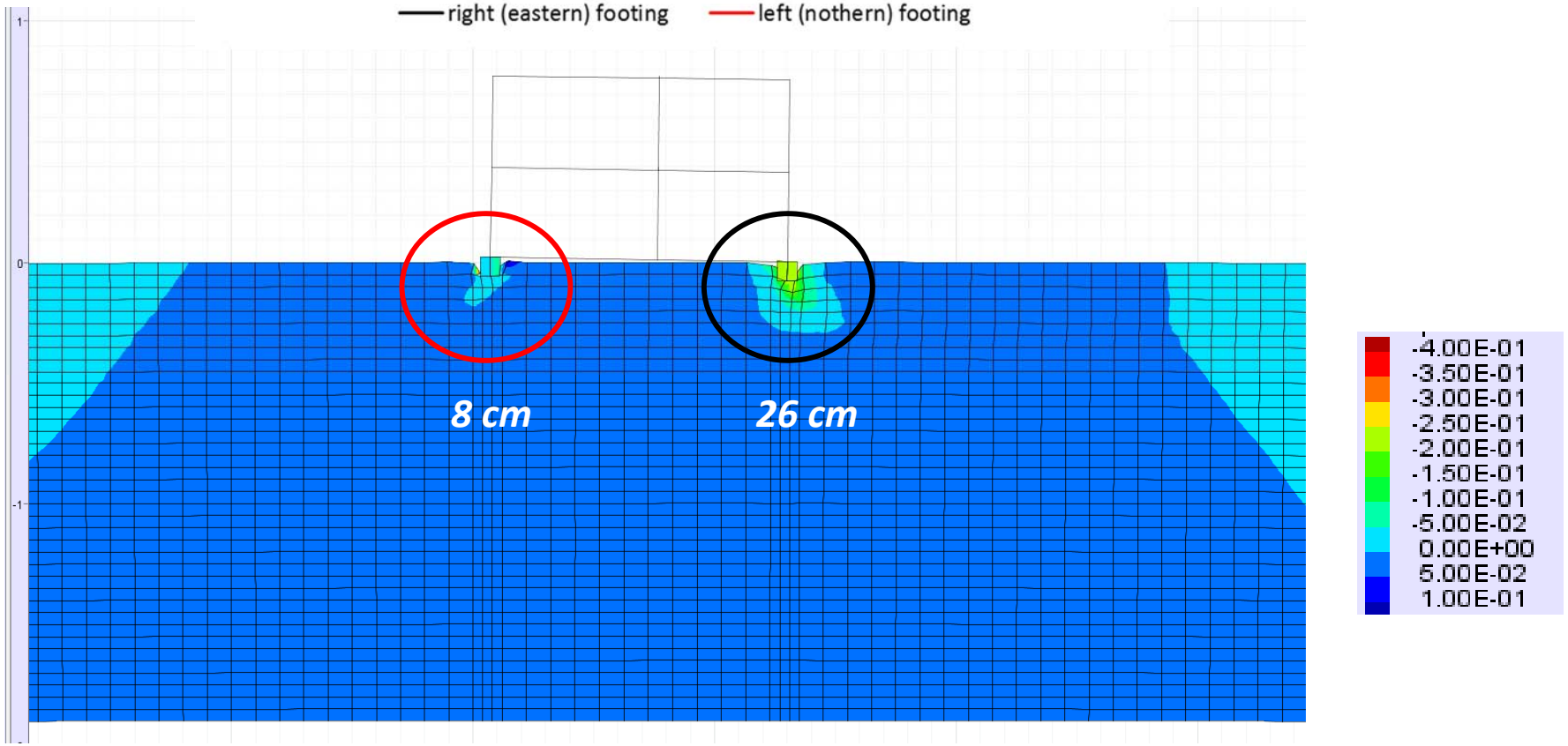


Figure 5-20b

# Case History: Residential Building in Kaiapoi, New Zealand

## Darfield Sep. 2010 Event : shear strain contours at the end of shaking

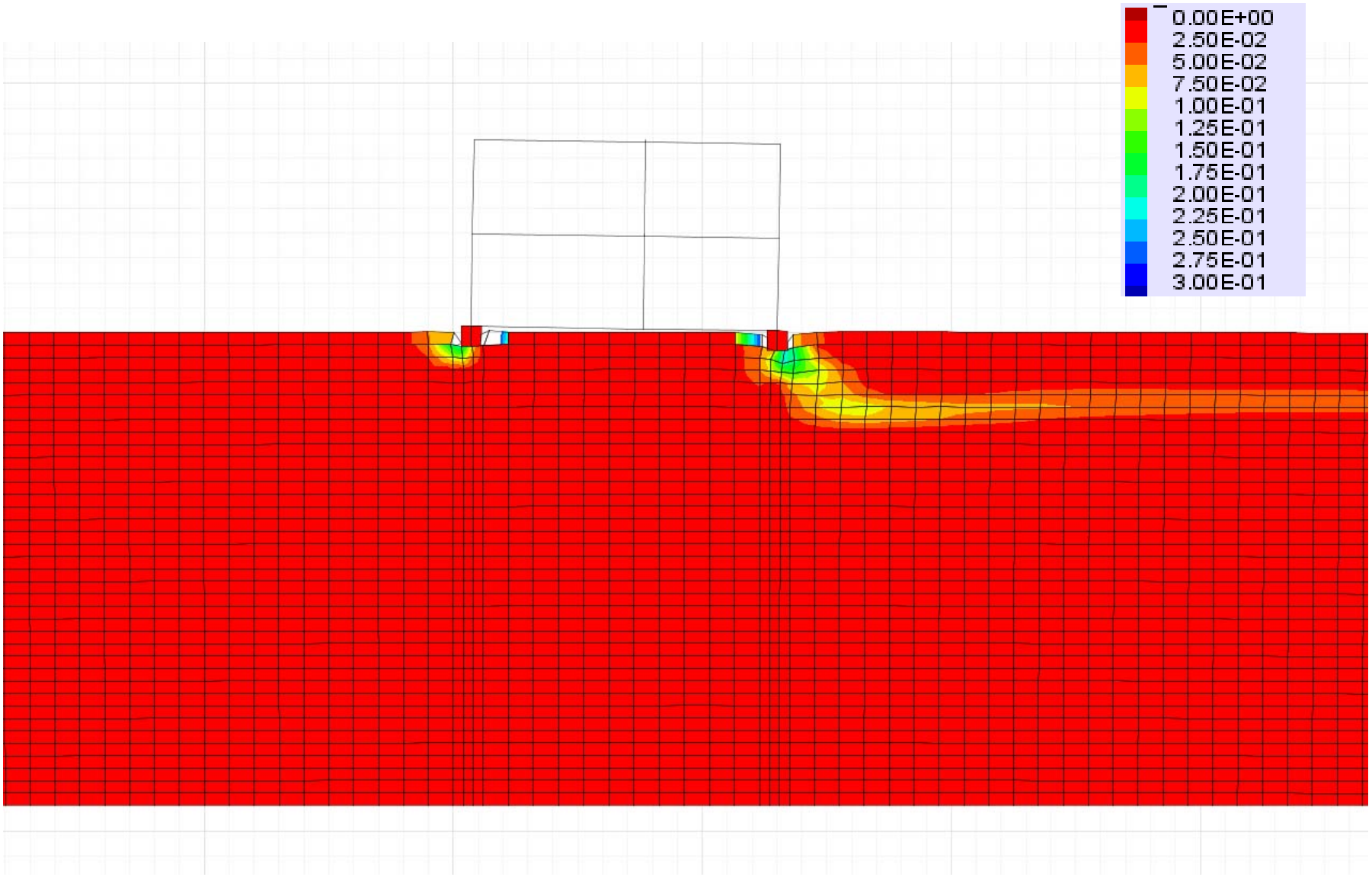


Figure 5-20c

# Case History: Residential Building in Kaiapoi, New Zealand

## Darfield Sep. 2010 Event : settlement contours (m) after reconsolidation

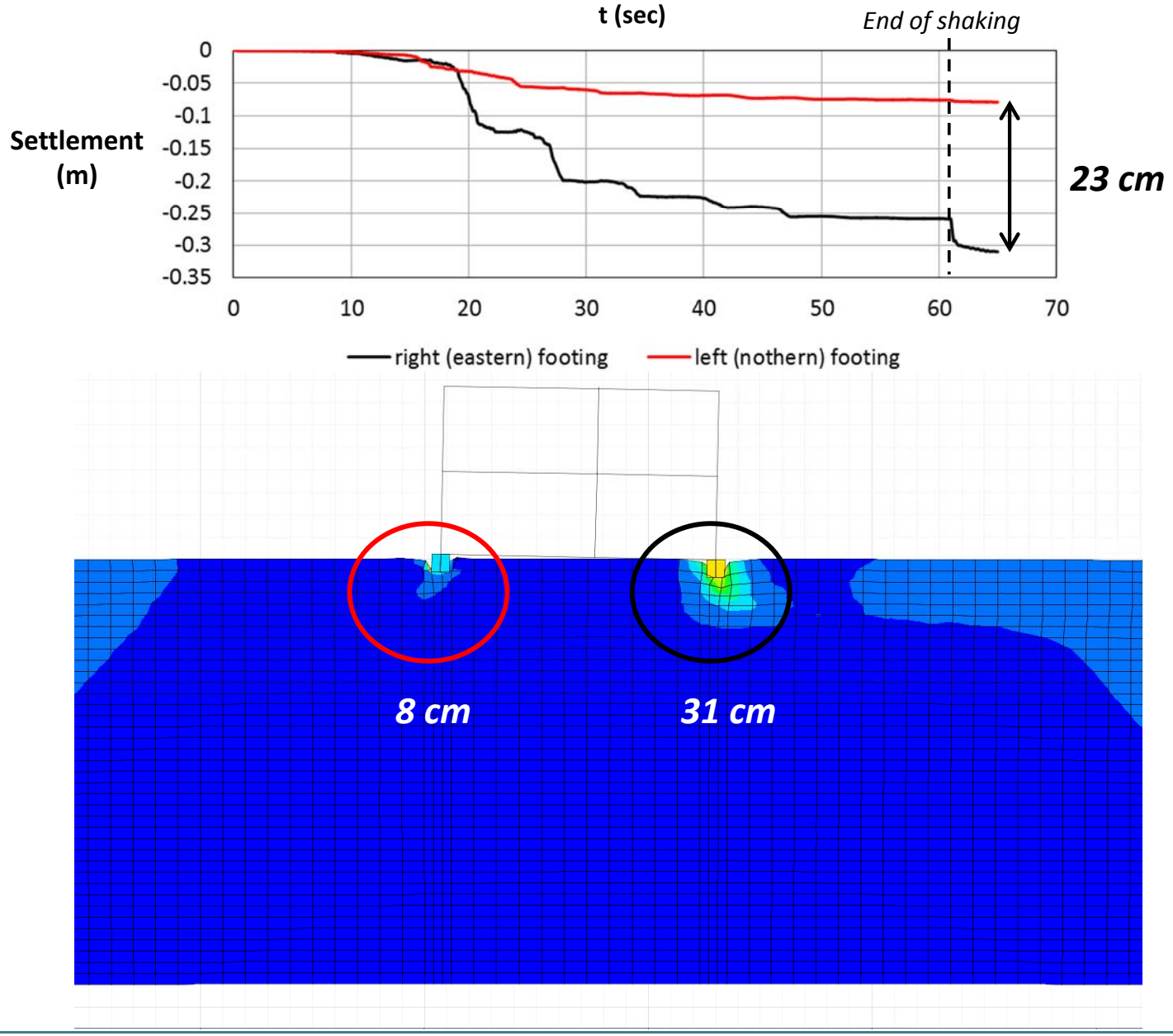


Figure 5-20d

# *Case History: Residential Building in Kaiapoi, New Zealand*

*Darfield Sep. 2010 Event : volumetric strain contours due to reconsolidation*

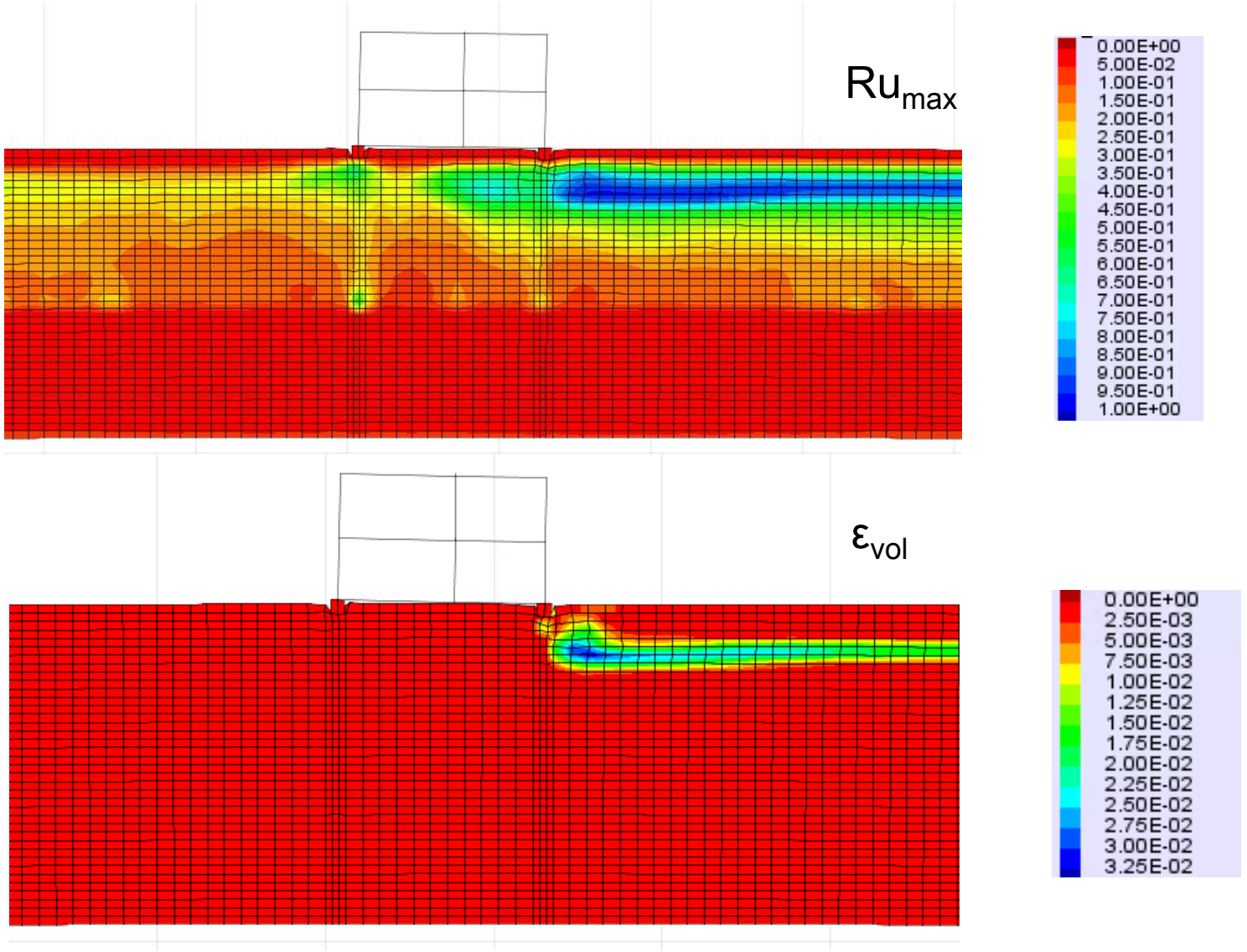


Figure 5-20e

# Case History: Residential Building in Kaiapoi, New Zealand

## Christchurch Feb. 2011 Event (scaling factor=1) : $Ru_{max}$ contours

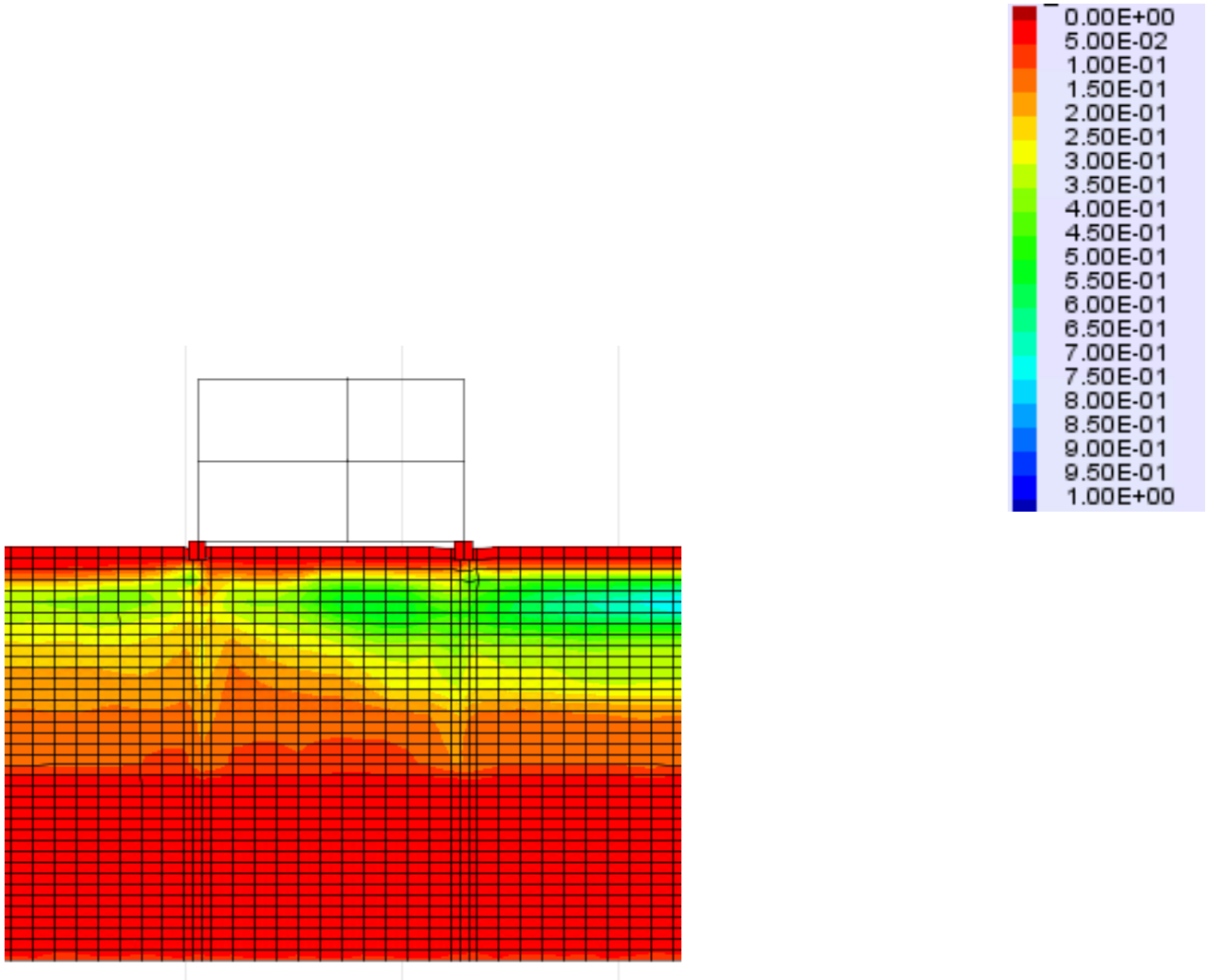


Figure 5-21a

# Case History: Residential Building in Kaiapoi, New Zealand

## Christchurch Feb. 2011 Event (scaling factor=1) : settlement contours (m) at the end of shaking

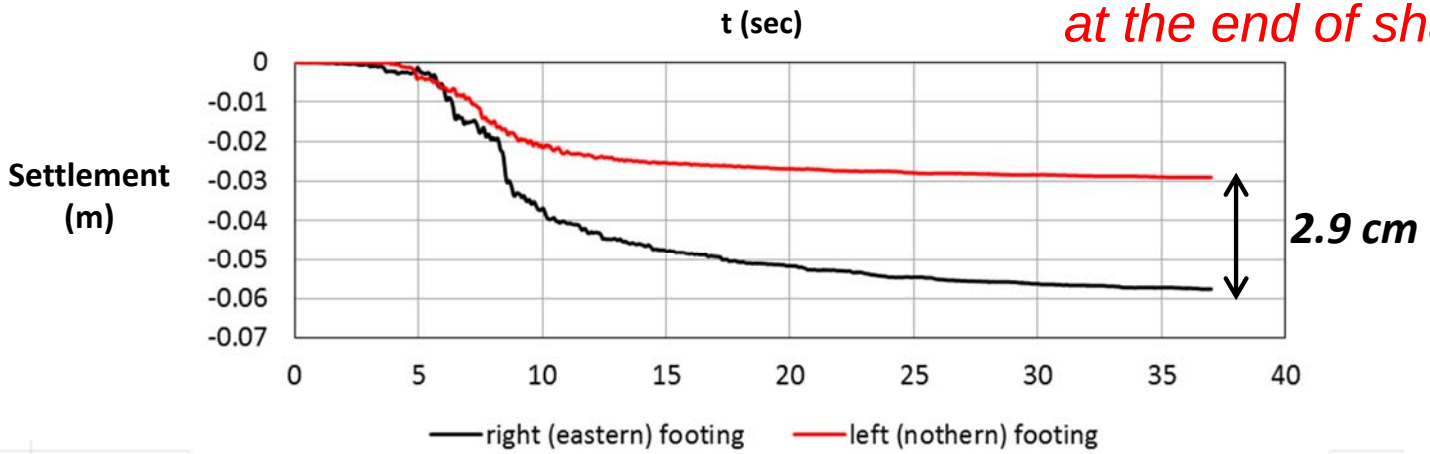


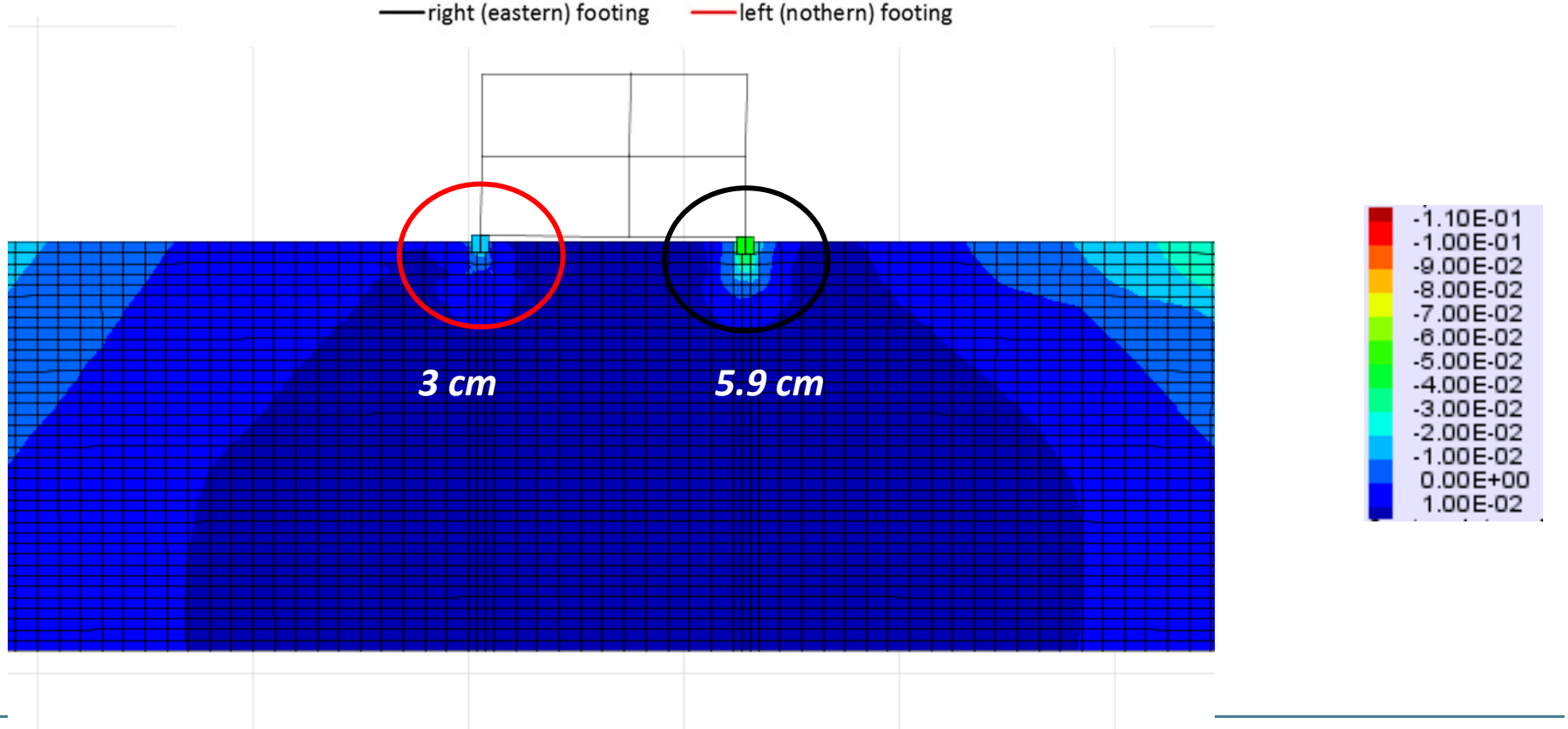


Figure 5-21b

# Case History: Residential Building in Kaiapoi, New Zealand

## Christchurch Feb. 2011 Event (scaling factor=1): settlement contours (m) after reconsolidation

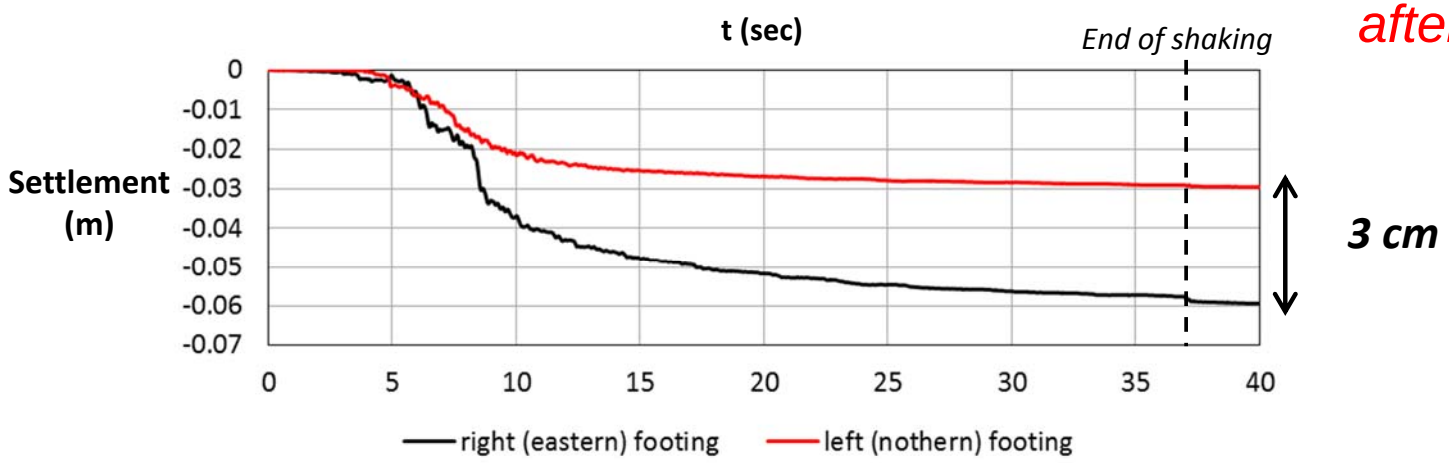


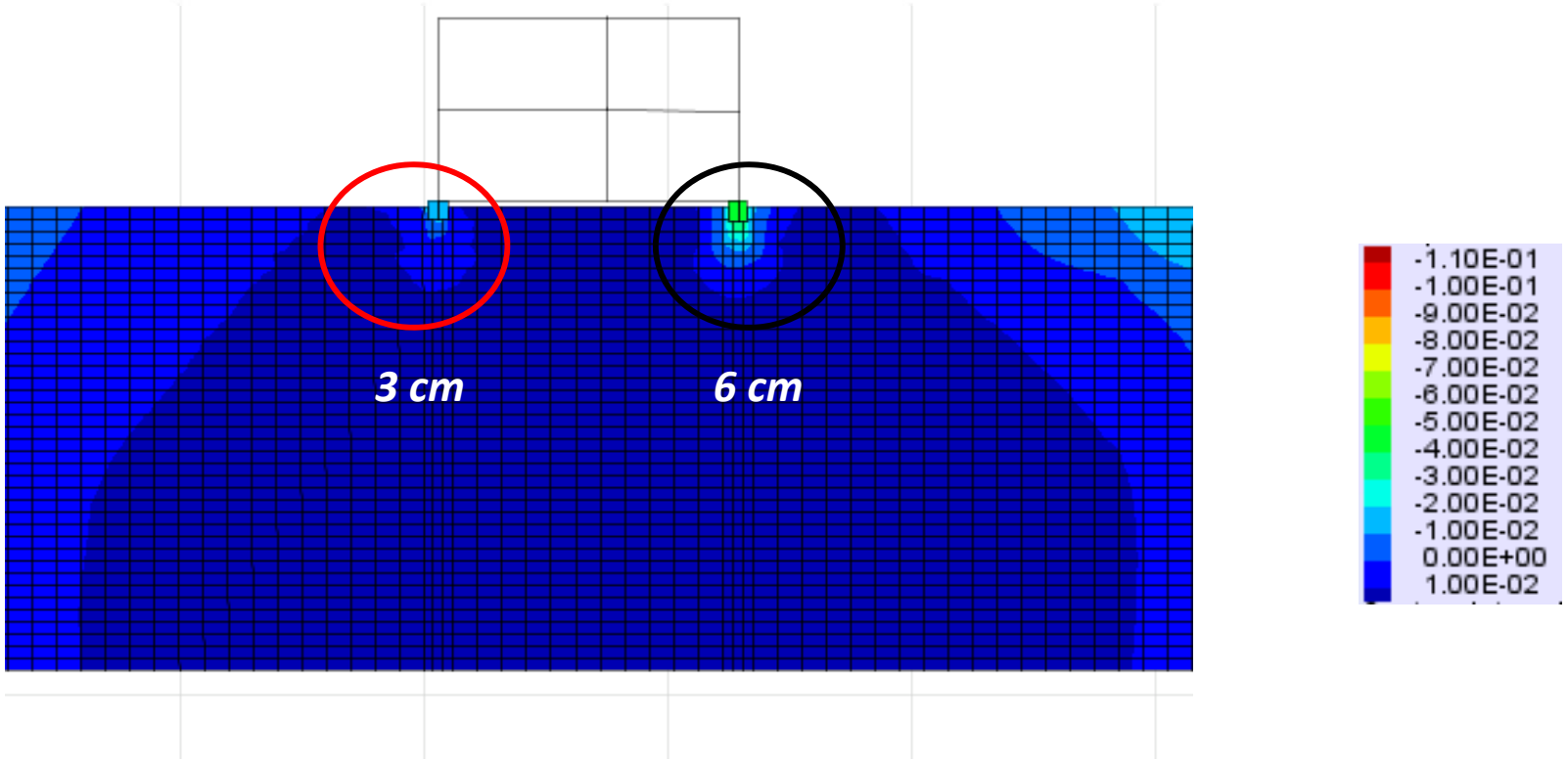


Figure 5-21c

# Case History: Residential Building in Kaiapoi, New Zealand

## Christchurch Feb. 2011 Event (scaling factor=0.73) : $Ru_{max}$ contours

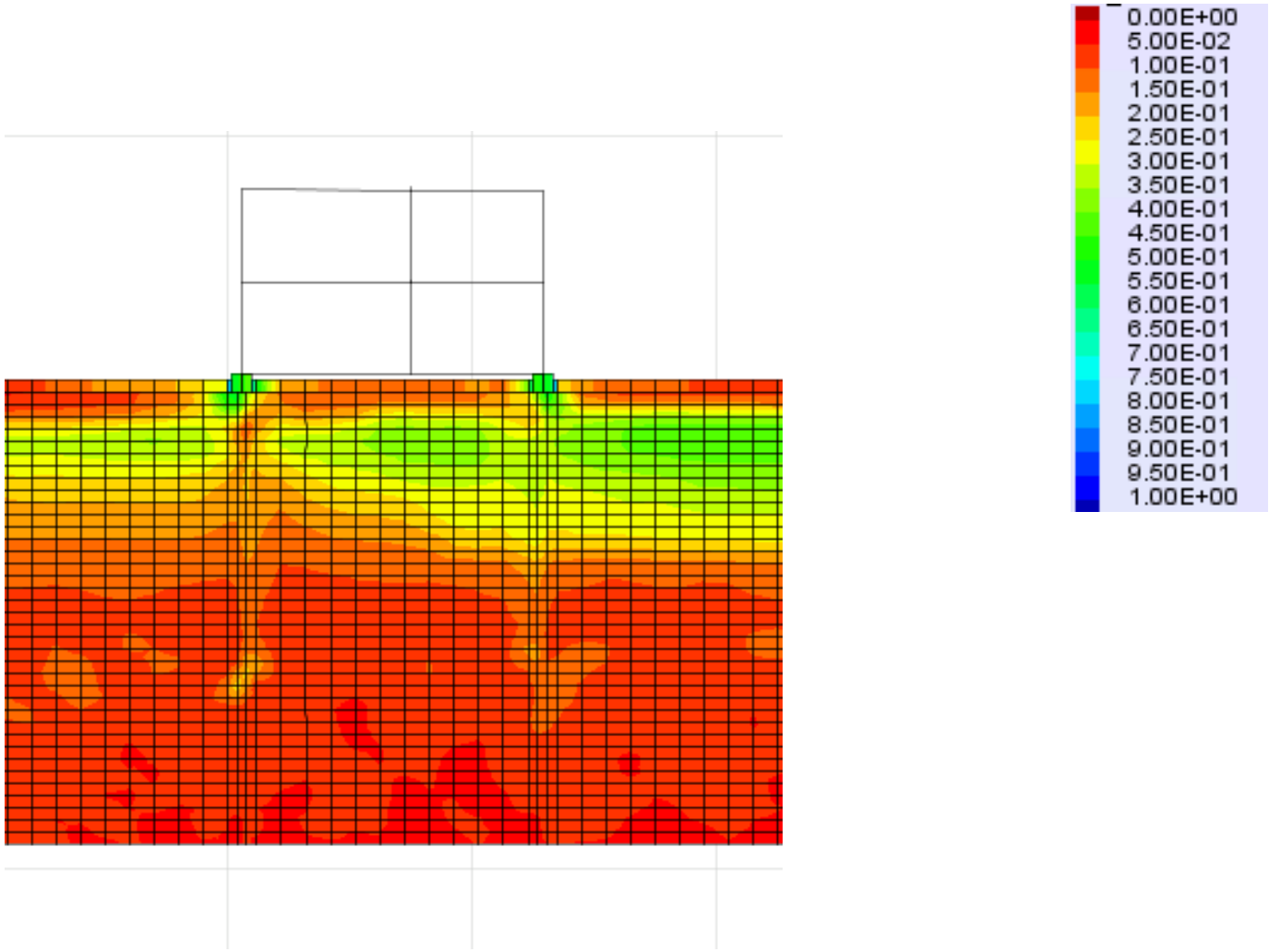


Figure 5-22a

# Case History: Residential Building in Kaiapoi, New Zealand

*Christchurch Feb. 2011 Event (scaling factor=0.73) : settlement contours (m) at the end of shaking*

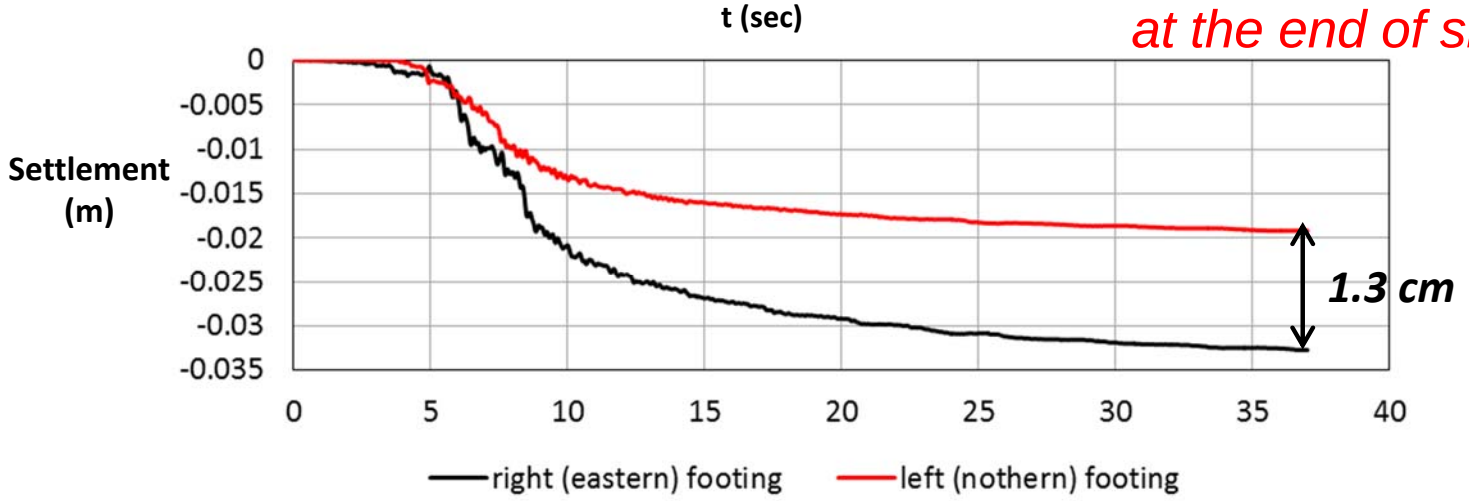


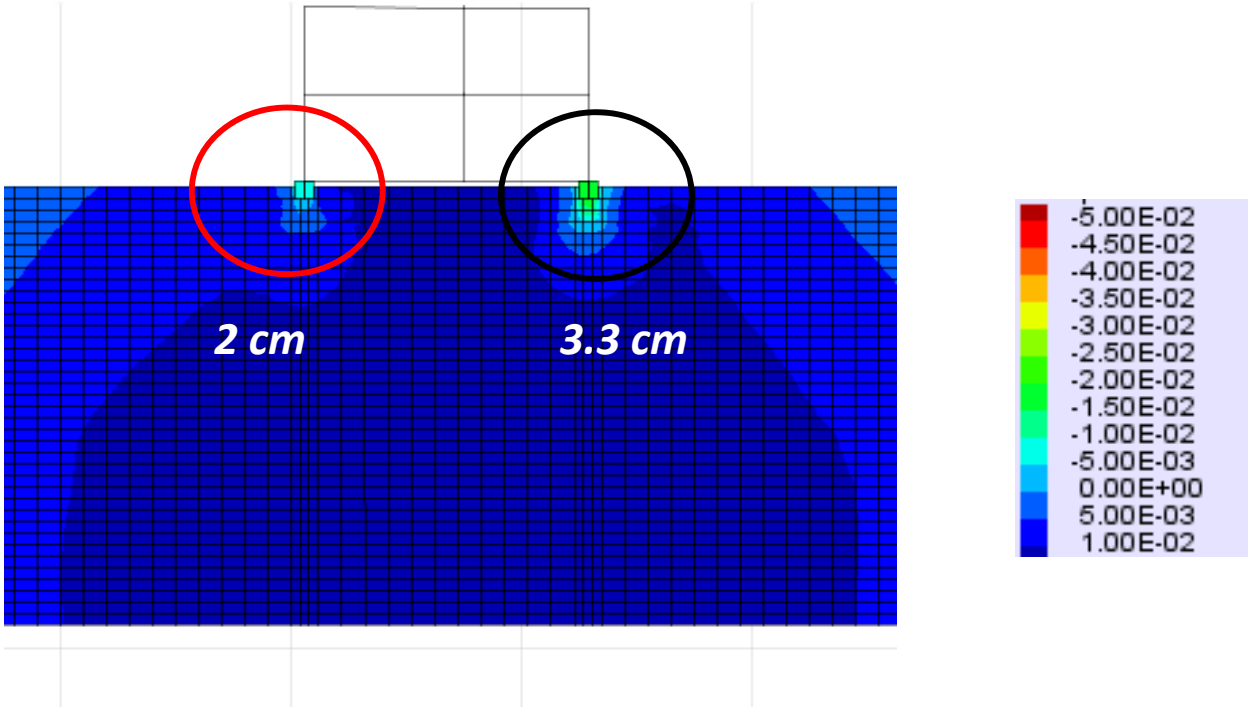


Figure 5-22b

# Case History: Residential Building in Kaiapoi, New Zealand

## Christchurch Feb. 2011 Event (scaling factor=0.73) : settlement contours (m) after reconsolidation

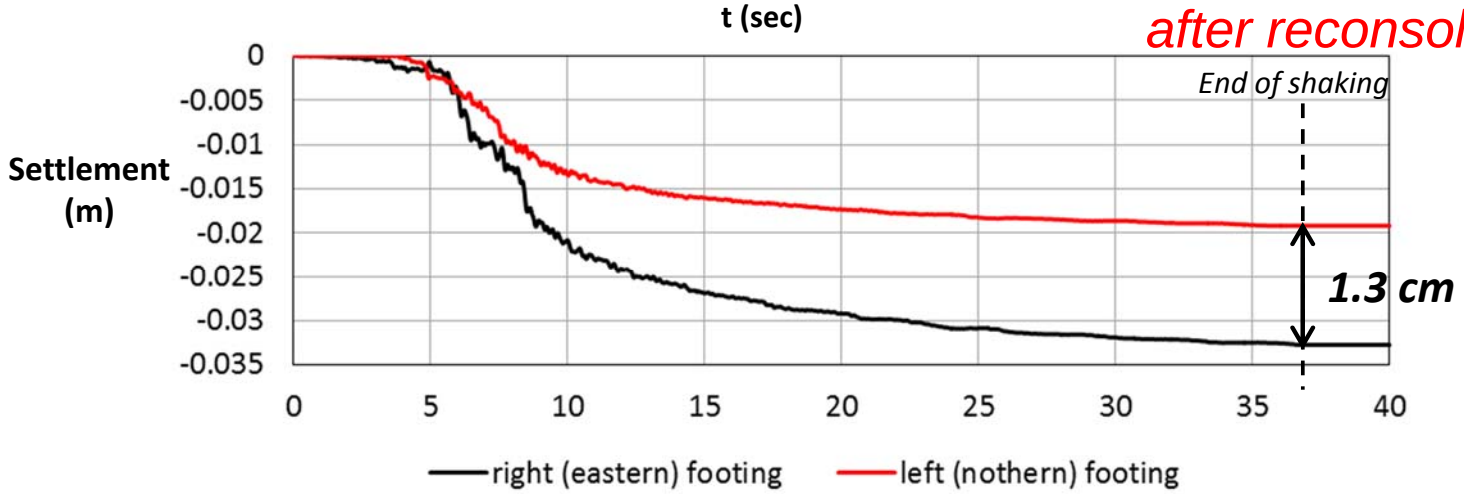


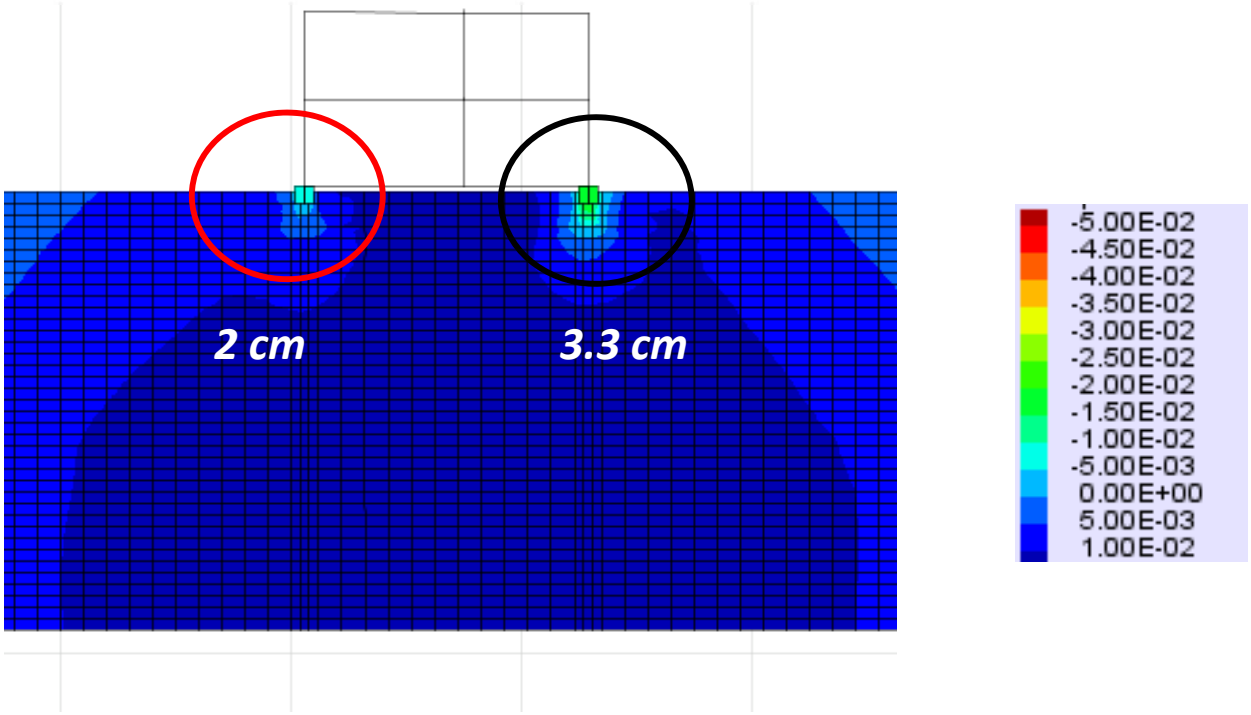


Figure 5-22c

# 6.0 PARAMETRIC NUMERICAL ANALYSES

Parametric 2D dynamic Soil Structure Interaction analyses were performed for typical residential buildings in Groningen by varying key parameters that affect the system behavior such as:

- non-liquefiable crust thickness, $H_{cr}$
- liquefiable layer thickness, $H_{liq}$
- liquefiable layer relative density, $D_r$
- undrained shear strength of liquefiable crust, $S_{u,crust}$
- foundation pressure, q
- foundation width, B
- building typology
- ground motion characteristics

In total, about 450 analyses were performed for the parameter values presented in Table 6-1.

This section presents the results of the parametric investigation in terms of foundation settlements and highlights the influence of the different parameters mentioned above. In addition, a series of sensitivity analyses/scenarios were performed (some upon the request of NPR TG2) and the results are also presented in this section.

**Table 6-1. Range of Values Considered in the Parametric Study**

| Parameter | Description | Range |
|---|---|---|
| $H_{liq}$ (m) | Liquefiable layer thickness | 0.5 - 10.0 |
| $D_r$ (%) | Liquefiable layer relative density | 30 - 50 |
| $H_{cr}$ (m) | Non-liquefiable crust thickness | 0.5 - 1.0 |
| $\alpha = (\pi+2)\, S_{u,crust} / q$ | Undrained shear strength of crust as a function of the foundation pressure, q | 1.0 - 10.0 |
| B (m) | Foundation width | 0.25 - 0.70 |
| Embedment Depth (m) | Foundation Embedment Depth | 0.45 - 0.90 |
| Q (kPa) | Foundation pressure | 20 - 120 |
| $PGA_{,surf}$ / $Sa_{0.7\ sec,\ surf}$ (g) | Ground Motion Spectral Accelerations | 0.10 – 0.30 / 0.27 – 0.55 |
| $D_{5-75}$ (s) | Ground Motion Significant Duration | 2.6 - 10.4 |
| $LPI_{ISH}$ | Liquefaction Potential Index | <1 - 22 |
| $T_{st}$ (s) | Fundamental Structural Period | 0.11 – 0.22 |
| Number of Storeys | Structure | 1 – 2 |

## 6.1 MAIN MECHANISMS IDENTIFIED THROUGH EXAMPLE ANALYSES RESULTS

Parametric analyses were performed to investigate the influence of different ground motion characteristics, site conditions, and building configurations on the amount of liquefaction-induced building settlement. The site conditions and building configurations considered for the sensitivity analyses are listed in Table 6-1 and the finite difference mesh

used for an example case is shown on Figure 6-1. This is a case of a single-storey residential building, with footing width of 0.7m, footing embedment depth 0.9 m, and no backfill in the crawl space under the building.

Example results are presented here to identify key mechanisms that influence the foundation settlements. Analyses results are shown for one motion, motion 4312 discussed in Section 3.0 with a scaling factor of 1.15. The foundation pressure, q, is 36 kPa and the structural fundamental period is 0.11 seconds. A rigid connection is used between the foundation and the superstructure.

Figure 6-2a presents contours of excess pore water pressure ratio, $r_u$, for cases where the foundation rests directly on top of liquefiable sand (i.e. no crust), the sand relative density is 50% (i.e. median value based on Zandeweer CPTs shown on Figure 2-4) and the thickness of the liquefiable sand is 1.5 m (upper left illustration), 3.0 m (upper right illustration), 5.0 m (lower left illustration), 10.0 m (lower right illustration). Excess pore pressure ratio, is estimated as the difference between the initial and the current vertical effective stress over the initial one. The initial vertical effective stress is estimated for each element in the model under gravity load (also including presence of the footing load) through a user-defined subroutine. As shown on this figure the liquefiable sand of 50% relative density develops excess pore pressures (i.e. excess pore water pressure ratios of up to 60%) but does not liquefy. As a result, the foundation seismic settlements are limited to less than 2 cm as shown on Figure 6-2b, where contours of vertical settlements are presented. It is noted that settlements shown on Figure 6-2b do not include reconsolidation volumetric settlements. Superimposed on this figure are total displacement vectors indicating a tendency of the excavation to cave into the crawl space under the building and resulting in upward soil movement under the building.

Figure 6-3a presents contours of excess pore water pressure ratio, $r_u$, for cases where the foundation rests directly on top of liquefiable sand (i.e. no crust), the sand relative density is 40% (i.e. 3$^{rd}$ percentile based on Zandeweer CPTs shown on Figure 2-4) and the thickness of the liquefiable sand is 1.5 m (upper left illustration), 3.0 m (upper right illustration), 5.0 m (lower left illustration), 10.0 m (lower right illustration). As shown on this figure the liquefiable sand of 40% relative density liquefies both under the foundation and in the free-field (i.e. blue contour colors indicate excess pore water pressure ratios larger than 0.7) for some of the cases shown. As a result, the foundation seismic settlements shown on Figure 6-3b are increased compared to the 50% relative density case but are still relatively small and generally less than 4 cm.

The effect of the thickness of liquefiable sand without crust for different relative densities in terms of foundation settlements (co-seismic, mainly shear-induced) is shown on Figure 6-4. Beyond a certain point, the increase in thickness of the liquefiable layer does not result in increased foundation settlements. This is due to the relatively small size of foundation width that is typical for the buildings in Groningen, which results in a limited zone of influence under the foundation as shown on Figure 6-5. Figure 6-5 presents the increase in vertical effective stress due to foundation load. As shown on this figure, for a footing width of 0.7 m (closer to the upper bound of foundation widths encountered in Groningen) and foundation pressure of 36 kPa, the depth of influence of the stress bulbs is limited to the upper 3 meters of the soil profile, in essence implying that liquefaction that occurs at larger depths does not contribute to shear-induced foundation settlements. Furthermore, liquefaction that occurs at deeper elevations in some cases may act as an isolation mechanism de-amplifying the motion as it propagates upwards, thus reducing the seismic demand on the foundation.

Figure 6-6 presents a summary of co-seismic (primarily shear-induced, black lines) and post-seismic reconsolidation settlements (volumetric, red lines) for the different cases presented above and the total settlements (green lines) estimated as the sum of the two. As shown on this figure the post-seismic reconsolidation settlements are on the order of 1 to 3 cm for the 40% relative density and less than about 0.5 cm for the 50% relative density cases. In general, post-seismic reconsolidation settlements are comparable in magnitude with the shear induced co-seismic settlements since they are both relatively small but are much less than what would be estimated from simplified triggering analyses based on CPT data. In the cases presented here the total foundation settlements are less than 7 cm.

Figure 6-7a presents analyses results in the form of contours of excess pore water pressure ratio and settlements for cases where a non-liquefiable crust is present under the footing. The illustrations on the left present results for a crust thickness of 0.5 meters, liquefiable layer thickness of 2.5 meters and relative density of 40% (top illustration of model geometry) in the form of the contours of excess pore water pressure ratio (middle illustration) and settlements (bottom illustration). The illustrations on the right present similar results for crust thickness of 1.0 meter, liquefiable layer thickness of 2.0 meters and relative density of 40%. The crust undrained shear strength in the cases presented on Figure 6-7a is 40kPa. As shown on this figure and on Figure 6-7b the presence of non-liquefiable crust results in reduced foundation settlements: from about 3.5 cm for the no crust case shown on Figure 6-3b to less than 2 cm for a 0.5-m-thick crust less than 1 cm for a 1.0-m-thick crust. This effect of settlement reduction even for small crust thicknesses (i.e. 0.5 meters) is due to the relatively small footing width that is typical for Groningen residential houses. So even the 0.5 meter thick crust is comparable in size to the foundation width in these cases and is therefore is effective in reducing foundation settlements.

Figure 6-8 presents example results for the post-seismic stability check using residual undrained shear strength for the zones that liquefied for a case where there is a crust under one foundation and no crust under the other and sand relative density of 40%. Post seismic stability checks indicate that the foundation remains stable after the end of shaking.

## 6.2 FINDINGS FROM OTHER STUDIES

It is noted that the main observations described above are in line with findings from other researchers. In particular according to Dashti et al (2010): *"If there is a sufficient thickness of liquefiable soil present under building foundations, significant liquefaction-induced building settlements can occur that are not proportional to the thickness of the liquefying layer. Liquefaction-induced building settlements in these cases are governed by shear strains. Structural settlement is not governed by volumetric strains. Therefore, building settlement is not proportional to the thickness of the liquefiable layer as would be suggested if it were governed by volumetric strains. These results indicate that normalizing building settlement by the thickness of the liquefiable layer is misleading in understanding the response of different structures founded on relatively thin, shallow deposits of saturated granular soils"*.

In addition, Dashti et al (2010) notes: *"A thicker liquefiable soil layer might de-amplify accelerations at the foundation level, depending on the fundamental period of the site and structure, and hence, reduce SSI-induced building ratcheting"*

Also according to Bray and Dashti (2014): *"Building displacement largely occurs during earthquake strong shaking, and the governing mechanisms are largely shear-induced when the liquefiable soil layer is close to the building foundation. Methods that estimate free-field settlement (e.g., Tokimatsu and Seed 1987; Ishihara and Yoshimine 1992) cannot be used to*

*estimate liquefaction-induced building settlements for this case (i.e., shallow foundation atop a shallow layer of liquefiable soil)."*

Figure 6-9 from Bray and Macedo (2017) illustrates the effect of relative density (upper left illustration), thickness of liquefiable sand layer (upper right illustration) and crust thickness (lower illustration) on co-seismic settlements (i.e. shear-induced). The analyses in that study were performed for slab foundations and the plots shown on Figure 6-9 are for foundation widths of 6 meters (upper illustrations) and 12 m (lower illustration). Similar trends are observed of decreasing settlements with increase in relative density and increase of crust thickness (note that the plot on the influence of crust thickness of foundation settlements examines crust thicknesses of only up to 0.5B). These are similar to the observations presented by Bray and Macedo (2017) who showed that the foundation settlement does not increase beyond a certain point with increase in thickness of liquefiable layer (upper left illustration where settlements remain constant or even decrease when the thickness of the layer becomes equal to about one foundation width).

Luque and Bray (2015) noted that (Figure 6-10): *"Liquefaction, defined in terms of maximum pore pressure ratio, is triggered where lowest FS were calculated. However, FS below unity did not always mean liquefaction was triggered. As an example, the simplified procedure predicts liquefaction triggering (FS < 1) from 2 to 7.25 m and from 9 to 14 m for the Darfield event. However, numerical analysis shows high pore pressures (>50%) only from 3.75 to 7.25 m."*

## 6.3 INFLUENCE OF VARIOUS PARAMETERS ON FOUNDATION SETTLEMENT FOR GRONINGEN RESIDENTIAL BUILDINGS

**Thickness and Relative Density of Liquefiable Sand.** The effect of the thickness of liquefiable sand for different relative densities is shown on Figure 6-4. As discussed above beyond a certain point, the increase in thickness of the liquefiable layer does not result in an increase of foundation settlements. In addition the increase in relative density results in a decrease of foundation settlements.

**Thickness of Non-Liquefiable Crust.** The effect of the thickness of non-liquefiable crust is shown on Figure 6-7b ($S_{u,crust}$=40kPa) As discussed above the increase in thickness of non-liquefiable crust results in reduced foundation settlements.

**Ground Motion Characteristics.** Figure 6-11a presents the effect of different *input* ground motion characteristics at El. -25m (i.e. Arias Intensity, CAV, $CAV_{dp}$ and significant duration $D_{5-75}$) on foundation settlements (co-seismic, shear-induced). Figure 6-11b presents the same results for different *surface* motion characteristics (from total stress 1D site response analyses).

Results are presented for all 11 ground motions presented in Section 3.0 for the following cases:

- $H_{liq}$=1.5 m, $D_r$=40%, $H_{cr}$=0.0 m, q=36 kPa, input ground motion scaling factor 1.15 (black symbols)
- $H_{liq}$=3.0 m, $D_r$=40%, $H_{cr}$=0.0 m, q=36 kPa, input ground motion scaling factor 1.15 (red symbols)
- $H_{liq}$=2.0 m, $D_r$=40%, $H_{cr}$=1.0 m, q=36 kPa, input ground motion scaling factor 1.15 (blue symbols)

- $H_{liq}$=2.0 m, $D_r$=40%, $H_{cr}$=1.0 m, q=72 kPa, input ground motion scaling factor 1.15 (green symbols)
- $H_{liq}$=3.0 m, $D_r$=40%, $H_{cr}$=0.0 m, q=36 kPa, input ground motion scaling factor 0.75 (pink symbols)

As shown on these figures foundation settlements increase with increase in ground motion characteristics such as Arias Intensity, CAV, $CAV_{dp}$ and significant duration. It is noted that the scatter observed in significant duration is a bit larger than the other intensity measures because it does not change with the scaling of the motions (i.e. the motion amplitude changes but not the significant duration).

Figure 6-12 presents the effect of spectral accelerations at the ground surface from total stress 1D site response analyses at different spectral periods (i.e. PGA, $Sa_{0.3sec}$, $Sa_{0.7sec}$, and $Sa_{0.9sec}$) on foundation settlements. Results are presented for all 11 ground motions for the cases described above. As shown on this figure foundation settlements do not correlate well with PGA since the high-frequency components do not affect liquefaction related phenomena (we note here that the PGA used in simplified triggering calculations is a proxy for overall seismic demand and not a metric of good correlation of this metric with liquefaction phenomena). A better correlation is observed with spectral accelerations at longer spectral periods (i.e. 0.7 seconds).

We note that the observations presented herein on the effect of ground motion characteristics on shallow foundation settlements are in line with findings from Bray and Macedo (2017).

**Foundation Width.** Figure 6-13 presents the effect of foundation width on foundation settlements (co-seismic, shear-induced). Results are presented for crust thicknesses, $H_{cr}$, varying between 0 and 1.0 meter and liquefiable layer thicknesses, $H_{liq}$, varying between 1.5 m to 10 m. The relative density of the sand is 40%, the foundation pressure is 36 kPa, the undrained shear strength of the crust is 40 kPa and the ground motion scaling factor is 1.15. As shown on this figure footing width appears to have a relatively small influence on foundation settlements for the types of foundations (i.e. spread footings) and range of footing widths considered in this study (i.e. 0.2 to 0.7 meters).

**Foundation Load.** Figure 6-14 presents the effect of foundation load on foundation settlements (co-seismic, shear-induced). Results are presented for crust thicknesses, $H_{cr}$, varying between 0 and 1.0 meter and liquefiable layer thicknesses, $H_{liq}$, varying between 2.0 m to 3.0 m, $D_r$=40%, $S_{u,crust}$ = 40 kPa and B=0.4 and 0.7 m.

As shown on this figure settlements increase with increasing foundation load.

**Undrained Shear Strength of Non-liquefiable Crust.** Figure 6-15 presents the effect of undrained shear strength of non-liquefiable crust on foundation settlements (co-seismic, shear-induced). Results are presented for $H_{cr}$=0.5m and $H_{liq}$=2.5 m (left illustration) and $H_{cr}$=1.0m and $H_{liq}$=2.0 m (right illustration), $D_r$=40%, B=0.7 m and various foundation loads (ground motion scaling factor 1.15).

As shown on this figure settlements increase with a decrease in undrained shear strength of the crust.

## 6.4 ADDITIONAL SENSITIVITY ANALYSES / SCENARIOS CONSIDERED

A series of sensitivity analyses were performed for a number of scenarios some of which were requested by NPR TG2 group and the results are presented here.

**Longitudinal Building Direction / Structural Period.** Figure 6-16 summarizes the foundation settlements (co-seismic, shear-induced) from sensitivity analyses performed: i) in the longitudinal direction of the building ($T_{st}$=0.13, distance between foundations 10.7 meters compared to 7.8 in the transverse direction) and ii) in the transverse building direction for structural period $T_{st}$=0.22 (compared to 0.11 which is the reference structural period used in the analyses). Analyses were performed for $H_{cr}$=0.0m and $H_{liq}$=1.5 m (longitudinal) and 3 m (transverse), $D_r$=40%, B=0.7 m and ground motion scaling factor 1.15. As shown on this figure foundation settlements in the longitudinal direction are somewhat larger than in the transverse mainly due to the larger distance between the foundations which also results in a smaller restraining effect from the superstructure. In addition the evaluated range of building fundamental periods does not appear to influence the estimated settlements.

**20% Load Variability between Footings.** Per the request from NPR TG2 a scenario was analyzed where the foundation load between the two spread footings was varied by 20%. Figure 6-17 presents the two footing settlement curves for foundation loads of 36kPa and 36*1.2 kPa (upper illustration) and 72kPa and 72*1.2 kPa (lower illustration). Analyses were performed for $H_{cr}$=0.0m and $H_{liq}$=3.0 m, $D_r$=40%, B=0.7 m and a ground motion scaling factor 1.15. As shown on this figure a 20% variation in foundation load results in 0.5 to 1 cm of differential settlements depending on the foundation pressure.

**Foundation on Soft Clay.** Per the request from NPR TG2 a scenario was analyzed where the foundation rests on a 1-m-thick soft clay layer with an undrained shear strength of 10 kPa without any liquefiable sand present. Analyses were performed for B=0.5 m, embedment depth 0.5 m, footing load q=5*Su=50kPa and ground motion scaling factor 1.15. Figure 6-18 presents the model geometry and contours of vertical displacement. As shown on this figure foundation settlements are limited to less than 1 cm at the end of shaking. In addition to this analysis, Fugro conducted a comprehensive numerical investigation of the seismic performance of foundations on soft clay for typical residential buildings in Groningen and the results are reported in Fugro (2018).

**Foundation on Extremely Loose Sand.** Per the request from NPR TG2 two scenarios were analyzed involving an extremely loose sand with relative density 30%. In the first case, the foundation rests on a 1-m-thick 30% relative density liquefiable sand, underlain by a 4-m-thick 40% relative density liquefiable sand layer. Analyses were performed for B=0.5 m, embedment depth 0.9 m, footing load q=50kPa and ground motion scaling factor 1.15. Figure 6-19a presents the model geometry and the PM4Sand calibration to match the liquefaction triggering curves of 30% and 40% according to Green et al (2018). Figure 6-19b presents results in terms of contours of maximum excess pore water pressure ratio during shaking (upper illustration) and vertical displacements (lower illustration) at the end of shaking. As shown on this figure foundation settlements are about 3 cm at the end of shaking.

In the second case, the 1-m-thick 30% relative density liquefiable sand rests directly on the Holocene clay formation. Figure 6-19c presents the numerical model (upper illustration) as well as the results in terms of contours of maximum excess pore water pressure ratio during shaking (middle illustration) and vertical displacements (lower illustration) at the end of shaking. As shown on this figure foundation settlements are about 2.5 cm at the end of shaking.

**Connection between Foundation and Superstructure.** Per the request from NPR TG2 a scenario was analyzed where the connection between the foundation and the superstructure was modeled with a hinge instead of as rigid (Figures 6-20a). An additional case was examined where the superstructure was not included in the analyses (i.e. only the

individual foundations with the foundation pressure were modeled, Figures 6-20a). Analyses were performed for B=0.5 m, embedment depth 0.9 m, footing load q=90kPa, $D_r$=40%, $H_{liq}$=5.0 m and ground motion scaling factor 1.15. Figure 6-20b presents results in terms of contours of excess pore water pressure ratio for the three cases (i.e. fixed connection, hinge connection, no superstructure). Figure 6-20c shows the vertical displacements and Figure 6-20d shows the horizontal displacements at the end of shaking for the three cases considered. As shown on Figure 6-20c foundation settlements are similar for the three cases analyzed (about 3 cm), however larger foundation rotations are observed for the hinged connection and the individual footings compared to the fixed connection. In addition as shown on Figure 6-20c in the case of the individual footings larger horizontal displacements are observed compared to the cases with the superstructure, due to the effect of the excavation on the foundations and the absence of the superstructure. We note, however that such displacements are likely unrealistic since there is a constraint from the peripheral strip footing under the building.

**Soil Variability under the Building.** From the sensitivity analyses performed it was observed that the total foundation settlements for all cases considered are relatively small (i.e. less than 4 cm) and perhaps most importantly the differential settlements between the two foundations due to ground motion, variation in footing load etc. were limited to about 1 cm. Sensitivity analyses were performed to evaluate the effect of soil variability under the building on foundation differential settlements.

A “worst-case” scenario was analyzed where a 1-m-thick crust exists under one footing (with high undrained shear strength so as to limit settlements) while no crust exists under the other footing that rests directly on a 40% liquefiable sand layer (Figure 6-21a). In these analyses the footing pressure was 36kPa, the footing width was 0.7 m, and the ground motion scaling factor was 1.15. Different thicknesses of liquefiable sand were considered varying from 1.5 to 5 meters. Figure 6-21b presents results for a 3-m-thick liquefiable layer thickness in the form of excess pore pressure ratio (upper illustration) and foundation settlements (lower illustration, co-seismic/shear induced, and post-seismic/reconsolidation volumetric). As shown on this figure this scenario results in about 4 cm differential settlements between the foundations.

The effect of the foundation differential settlements on building performance is discussed in the next section.

**Two-Storey Terraced Houses.** In addition to the analyses performed for the single-storey detached houses, a series of analyses were conducted for a typical two-storey terraced house encountered in Groningen. The basic geometric data of the considered building and the equivalent frame model that was used for the analyses have been presented in Sections 2 and 4 (Figures 2-7a, 2-7d, and 4-5b).

Parametric analyses were performed to investigate the influence of different ground motion characteristics, and site conditions on the liquefaction-induced building settlement. The site conditions and building configurations considered for the sensitivity analyses are listed in Table 6-1 and the finite difference mesh used for an example case (footing width 0.7m, footing embedment depth 0.9 m, and 30cm backfill in the crawl space under the building) of the two-storey house is shown on Figure 6-22.

Results of the numerical analyses of the two-storey building showed that the same mechanisms govern the seismic behavior of the soil-structure system as in the single-storey building case. Example results are presented on Figure 6-23a and 6-23b in terms of excess

pore pressure ratio and settlement contours respectively for one motion, motion 4312 discussed in Section 3.0 with a scaling factor of 1.15. The thickness of the 40% relative density liquefiable sand layer is 3 m and the footings rest directly on this layer (i.e. no crust case). The foundation pressure, q, is 36.7 kPa and the structural fundamental period is 0.10 second in this example so that the results are directly comparable with the single-storey house. A rigid connection is used between the foundation and the superstructure. Results are presented in terms of contours of maximum excess pore water pressure ratio during shaking (upper illustration) and vertical displacements (lower illustration) at the end of shaking. The results from the analysis of the single-storey structure are also presented for comparison. As shown on this figure foundation settlements of the terraced house are about 2 cm at the end of shaking and are slightly lower than for the detached house (about 3 cm).

The influence of the different structure and the presence of the second storey on the settlements of the building is illustrated on Figure 6-24 where the settlement of both the one-storey and the two-storey structures are plotted against different values of load on footings and different crust thicknesses. It is generally observed that the two-storey building exhibits less settlement than the single-storey structure.

A sensitivity analysis was also performed on the effect of the structural fundamental period (fixed-base) on the earthquake-induced settlements. A longer period (0.22 sec) was assigned to the two-storey building model (as requested in the terraced house scenario provided by NPR TG2). Analysis of the more flexible structure demonstrated that there is practically no effect of on the settlements. This is illustrated in Figure 6-25a which shows footing settlements in terms of footing load for the case of no crust and crust thickness of 0.5m and 1.0m. Furthermore, Figure 6-25b presents a one-to-one comparison between the settlements of the two-storey building with a longer period (i.e. 0.22 sec) against the settlements calculated for the base-case two-storey building with a shorter period (i.e. 0.1 sec) while all other parameters remain the same. It is observed that the points plot along the 1:1 diagonal revealing little or no effect of fixed-base structural fundamental period on the settlements.

**Foundation Embedment Depth.** Sensitivity analyses were performed to evaluate the effect of foundation embedment depth on liquefaction induced settlements of typical residential houses in Groningen. Results presented above for single-storey and two-storey houses assumed embedment depths on the order of 0.9 m. Additional analyses were performed for single and two-storey houses assuming an embedment depth of 0.45m. Analyses were performed for a range of foundation loads up to 86.7 kPa (i.e. Static Factor of Safety close to unity). Note that for the 2-storey building the FS is higher for the same foundation load due to the presence of backfill within the crawl space. Results are presented on Figure 6-26 in the form of settlement versus foundation load for single and two storey houses with foundation embedment depths of 0.45 m and 0.9 m. Analyses were performed for B=0.7 m, $D_r$=40%, $H_{liq}$=3.0 m and ground motion scaling factor 1.15. As shown on this figure, for the same foundation pressure, smaller embedment depths result in slightly larger foundation settlements.

# Section 6

# Finite Difference Mesh

## Parametric Analyses Results

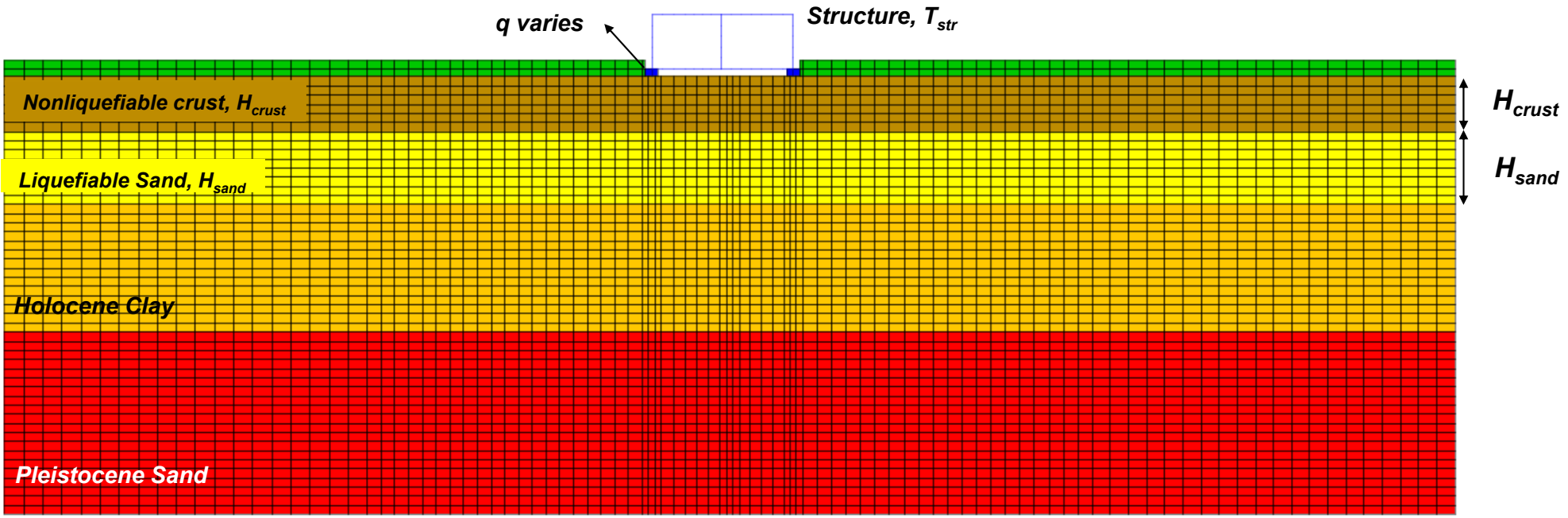


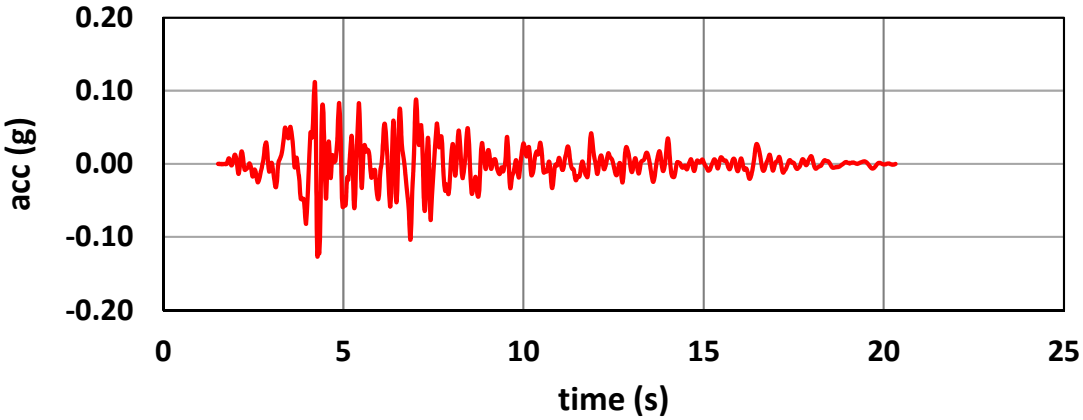


Figure 6-1

# Contours of Excess Pore Water Pressure, $D_r$ = 50%, $H_{cr}$ = 0.0

## Analyses Results

***Excess Pore Pressure Ratio, $r_u$***

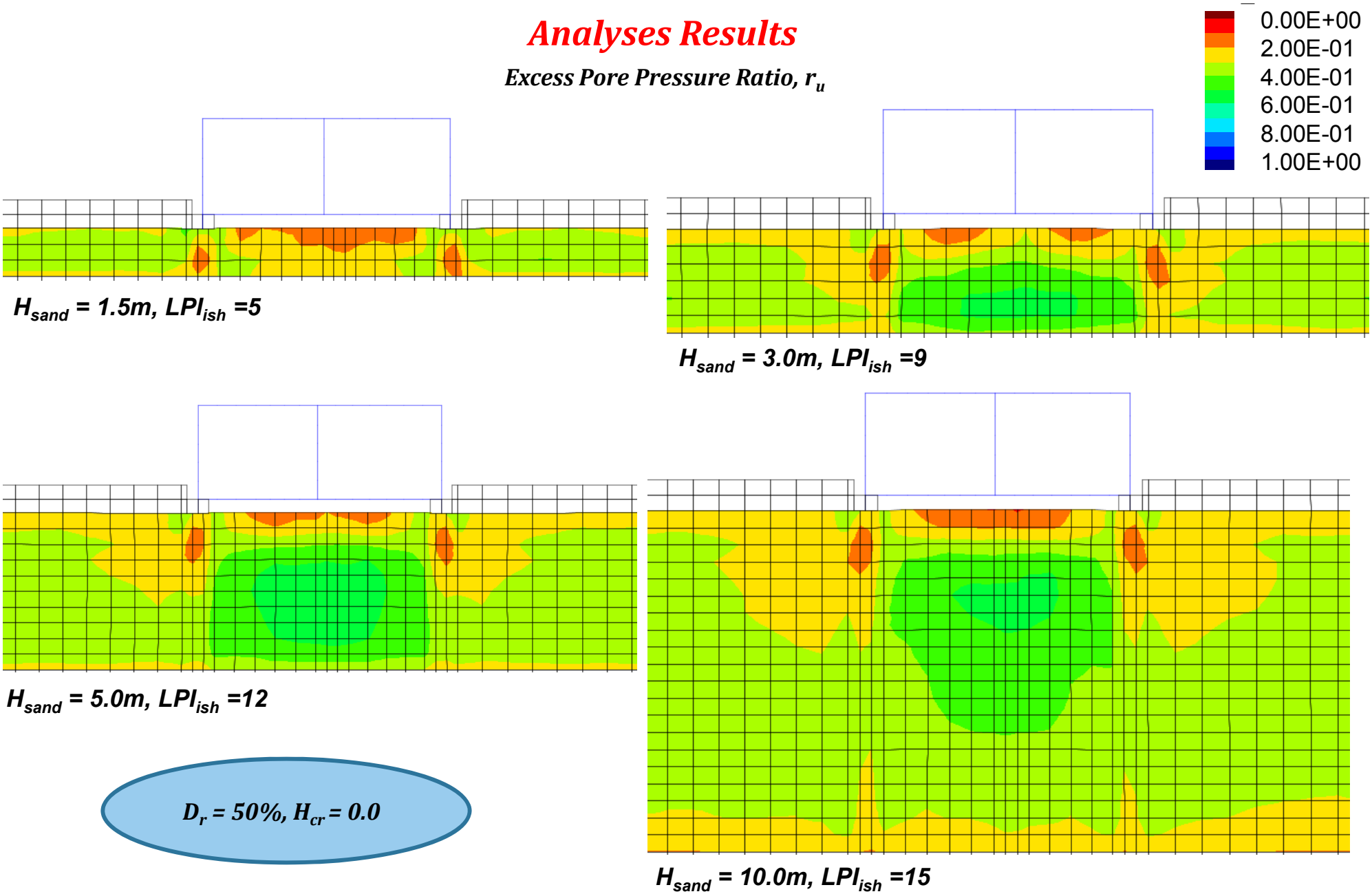


Figure 6-2a

# Contours of Vertical Displacement, $D_r$ = 50%, $H_{cr}$ = 0.0

## Analyses Results

*Settlements (m)*

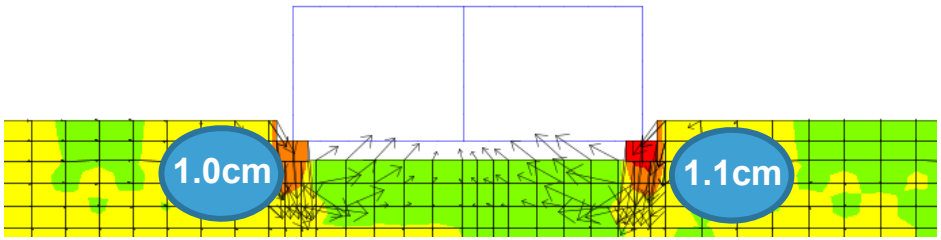


$H_{sand}$ = 1.5m, $LPI_{ish}$ =5

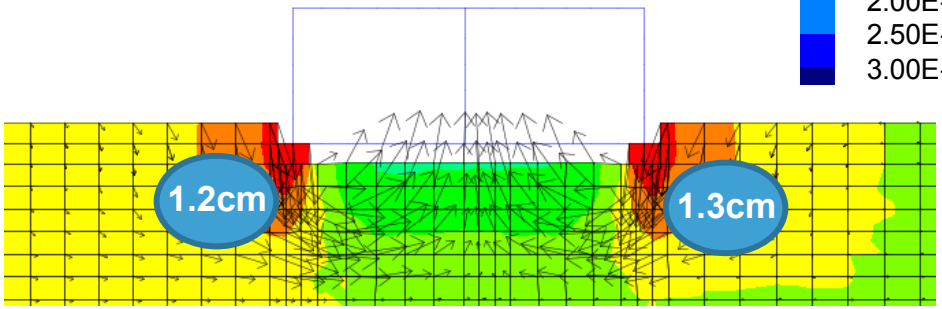


$H_{sand}$ = 3.0m, $LPI_{ish}$ =9

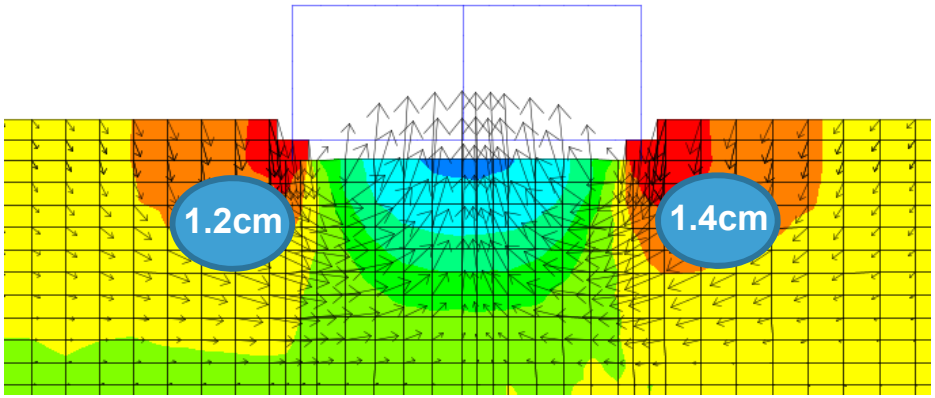


$H_{sand}$ = 5.0m, $LPI_{ish}$ =12

$D_r$ = 50%, $H_{cr}$ = 0.0

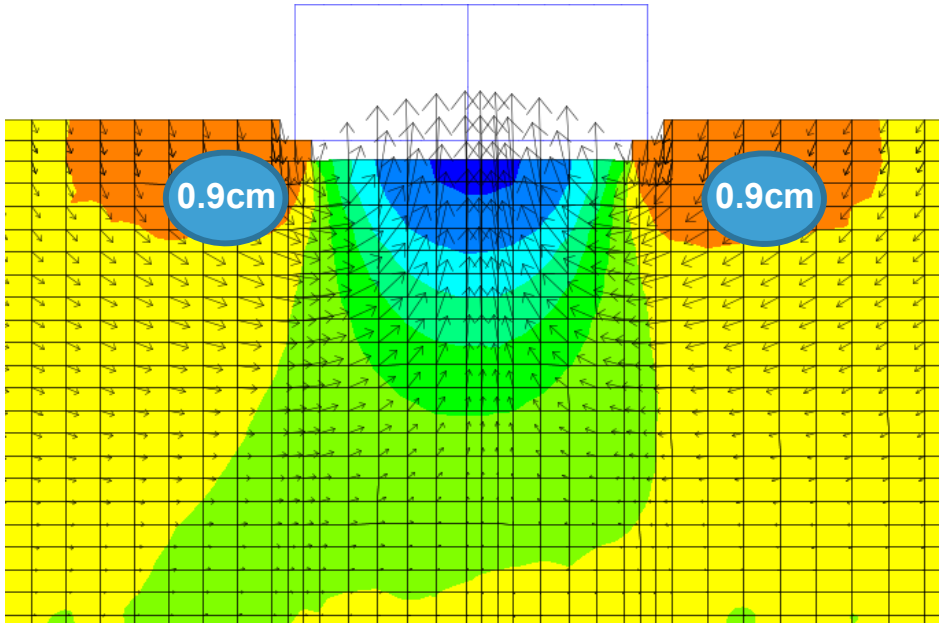


$H_{sand}$ = 10.0m, $LPI_{ish}$ =15

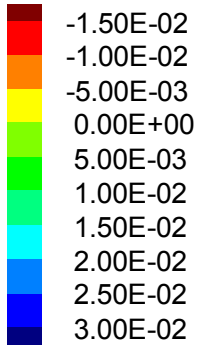


Figure 6-2b

# Contours of Excess Pore Water Pressure, $D_r = 40\%$, $H_{cr} = 0.0$

## Analyses Results

***Excess Pore Pressure Ratio, $r_u$***

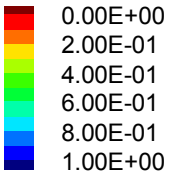


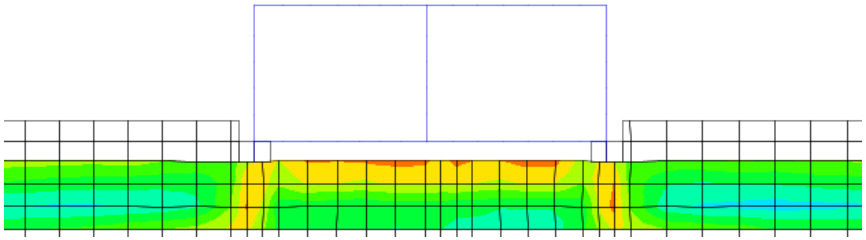

***$H_{sand}$ = 1.5m, $LPI_{ish}$ =8***

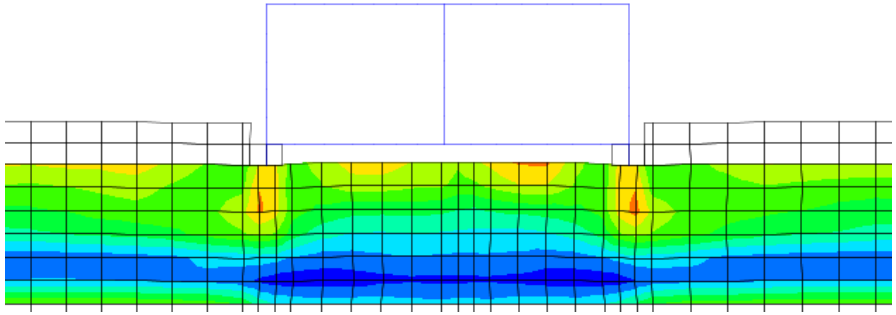

***$H_{sand}$ = 3.0m, $LPI_{ish}$ =13***

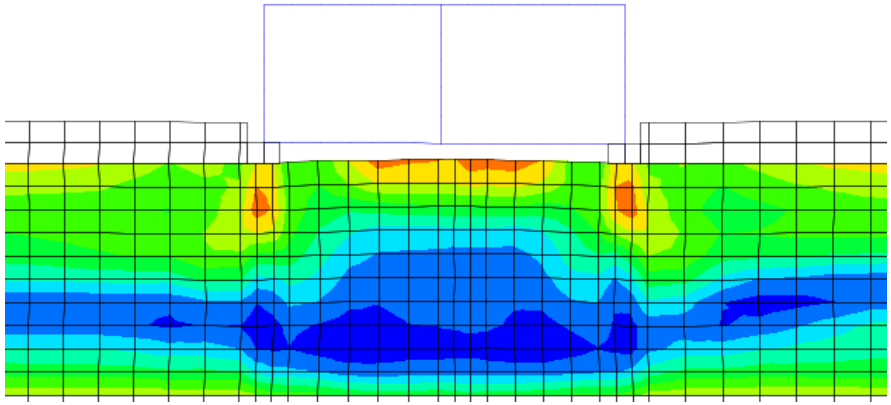

***$H_{sand}$ = 5.0m, $LPI_{ish}$ =17***

***$D_r = 40\%$, $H_{cr} = 0.0$***

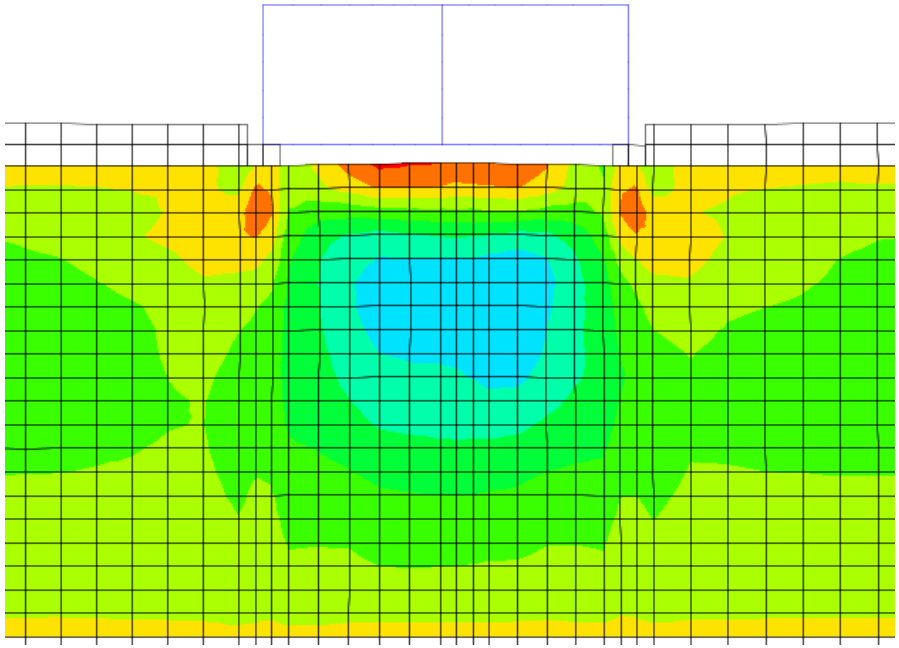

***$H_{sand}$ = 10.0m, $LPI_{ish}$ =22***

Figure 6-3a

# Contours of Vertical Displacement, $D_r = 40\%$, $H_{cr} = 0.0$

## Analyses Results

*Settlements (m)*

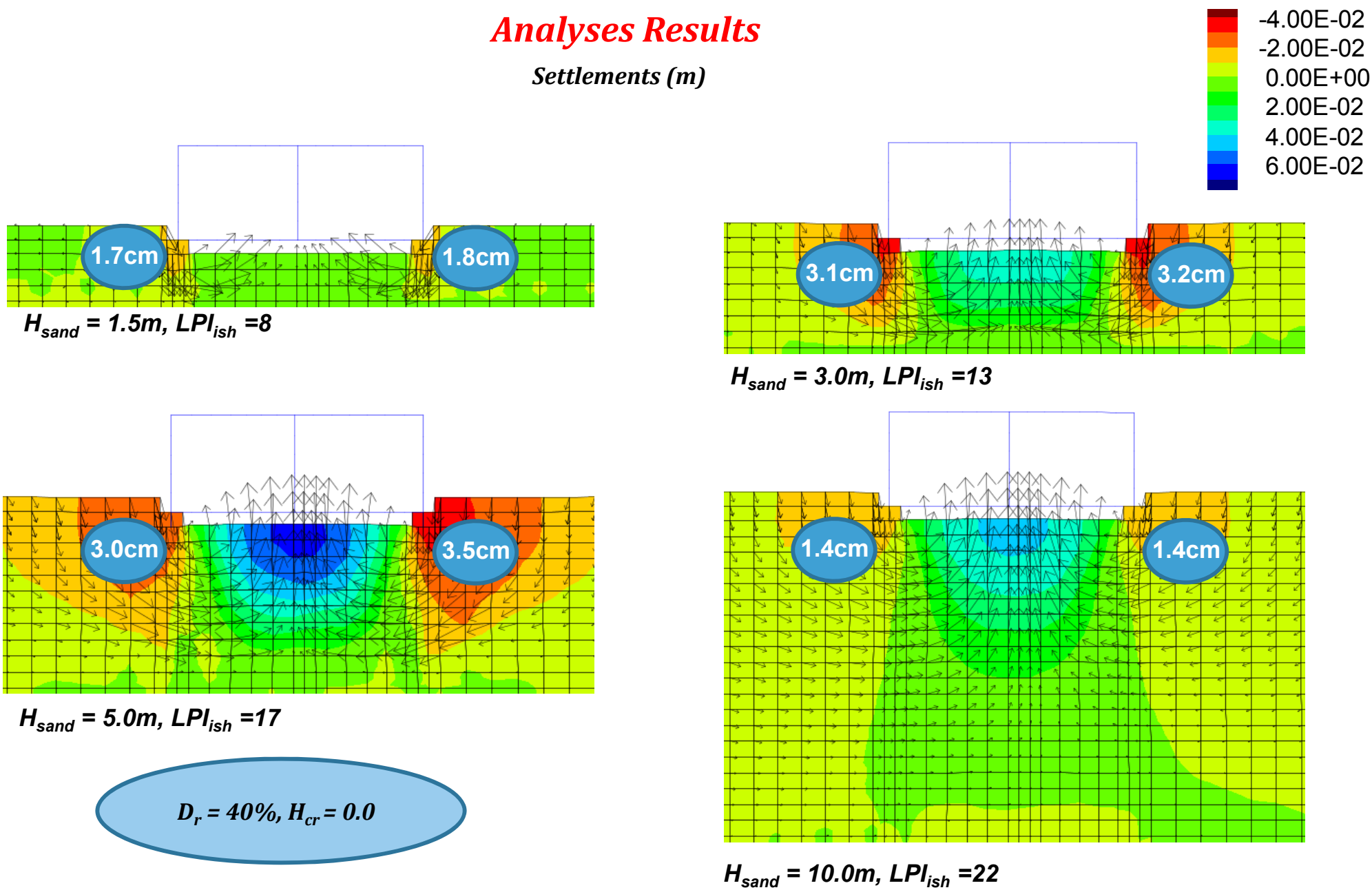


Figure 6-3b

# *Effect of Liquefiable Sand Thickness and Relative Density (No Crust)*

## *Analyses Results*

***Effect of Liquefiable Sand thickness and Relative Density (No Crust)***

***B=0.7m, q=36.5kPa***

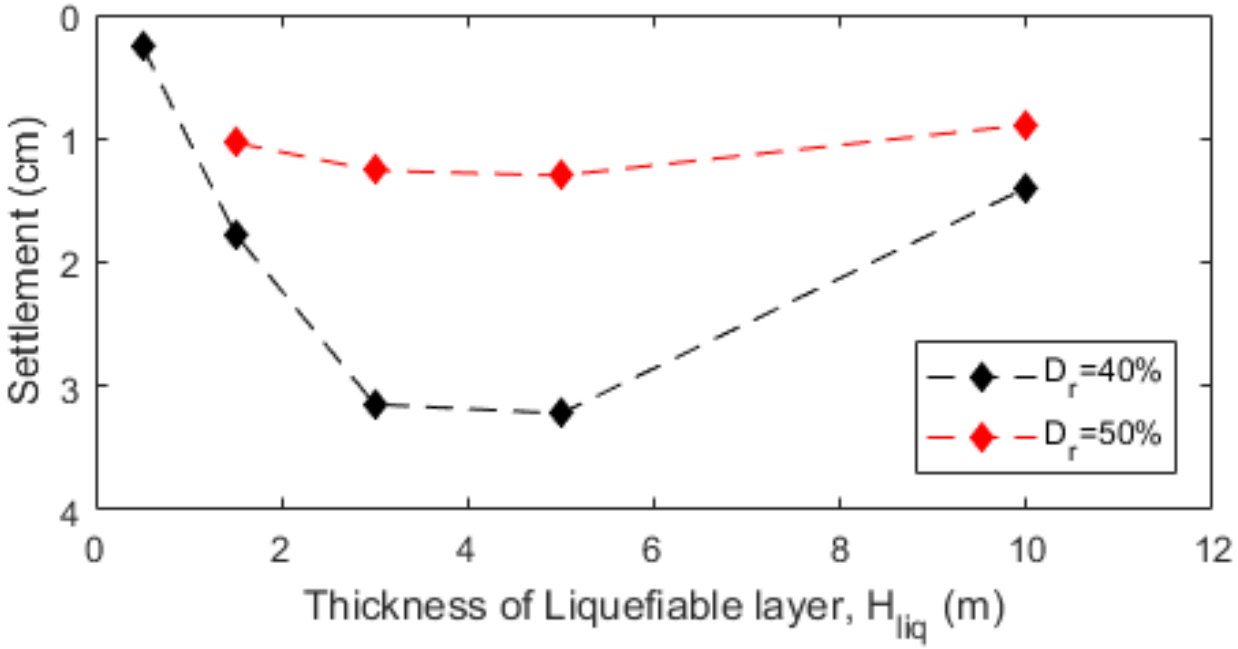


**$D_r$ = 40%**

**$D_r$ = 50%**

Figure 6-4

# Effective Vertical Stress Increase due to Foundation Load

## Analyses Results

***Stress bulbs due to structural load***

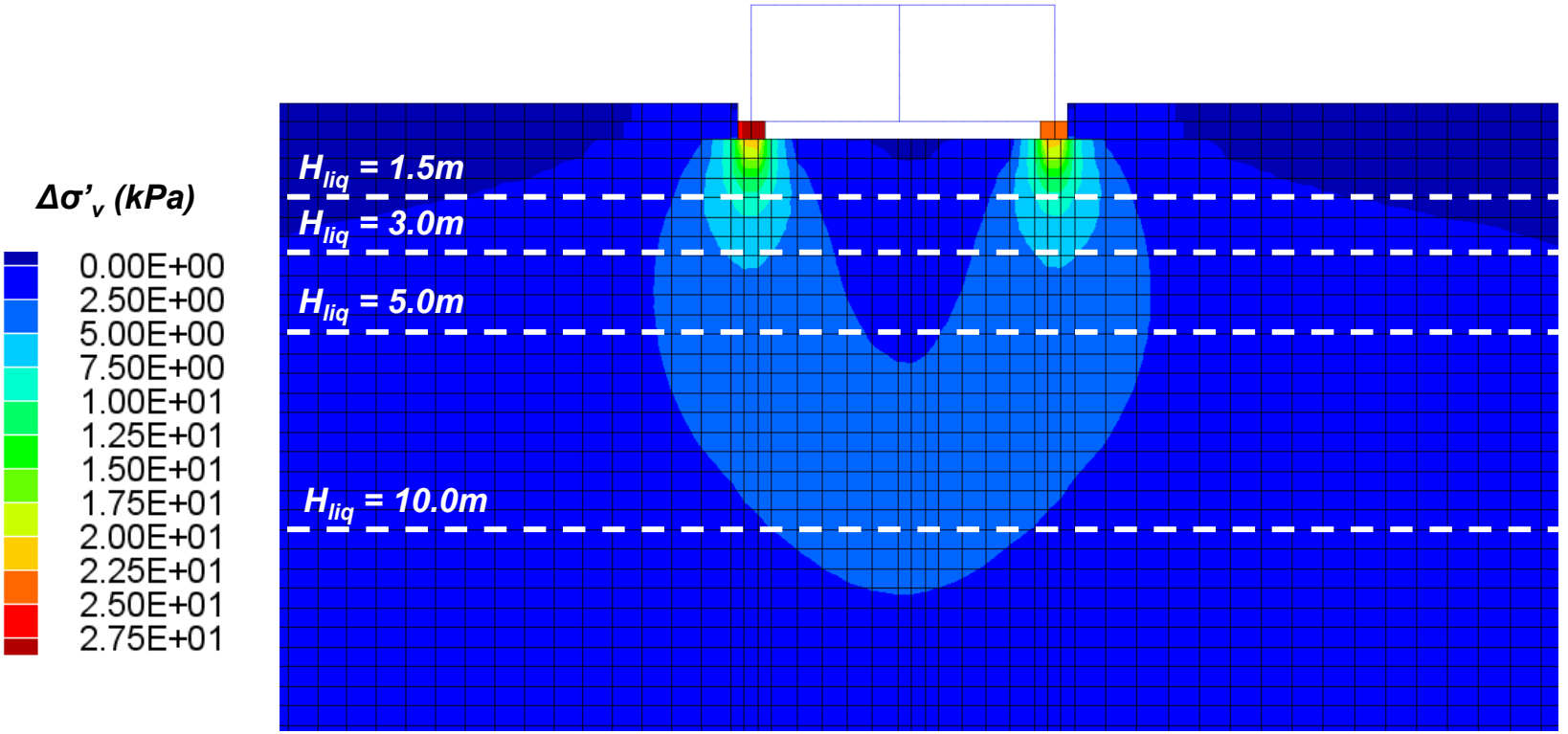


Figure 6-5

# Contribution of Volumetric Settlements

## Analyses Results

**Contribution of Volumetric Settlements**

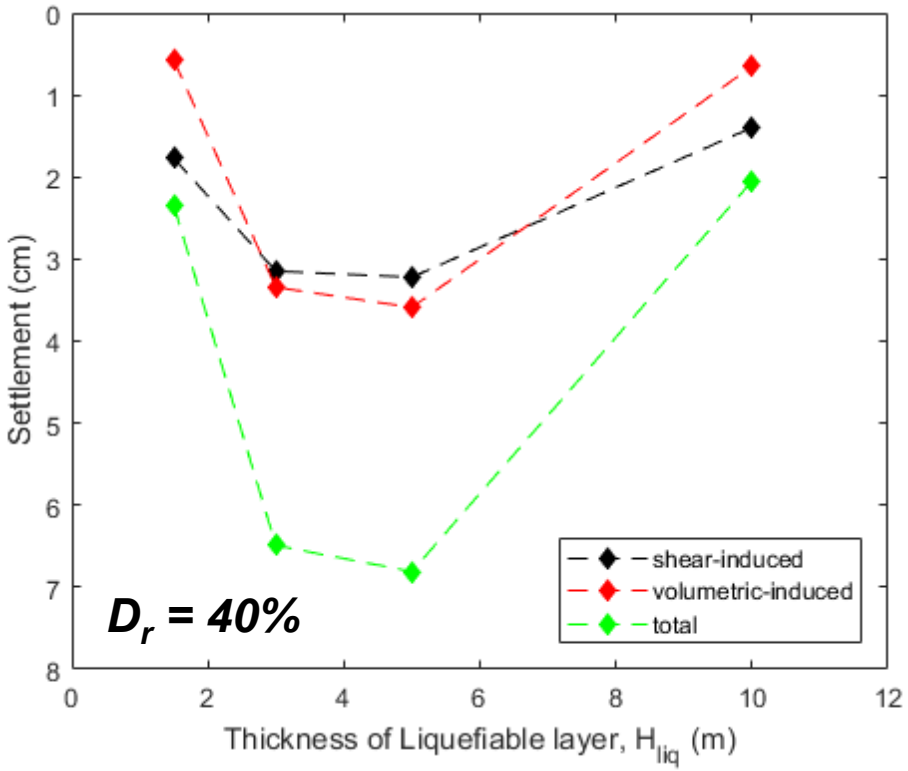


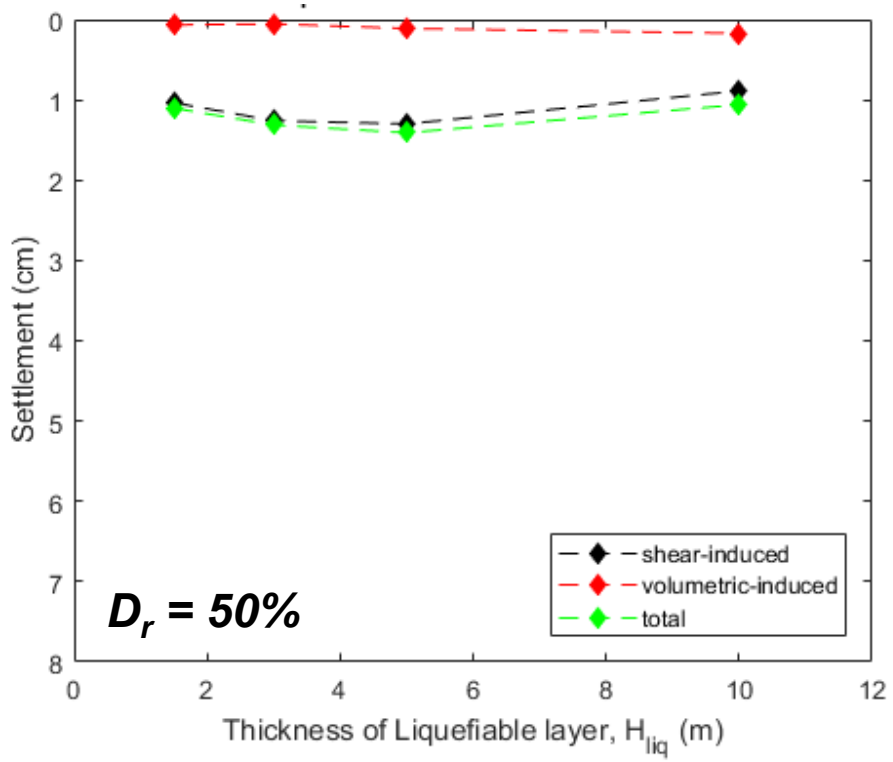


***Shear-Induced*** ***Volumetric-Induced*** ***Total***

Figure 6-6b

# Example Analyses Results for Cases with Non-liquefiable Crust

## Analyses Results with Crust

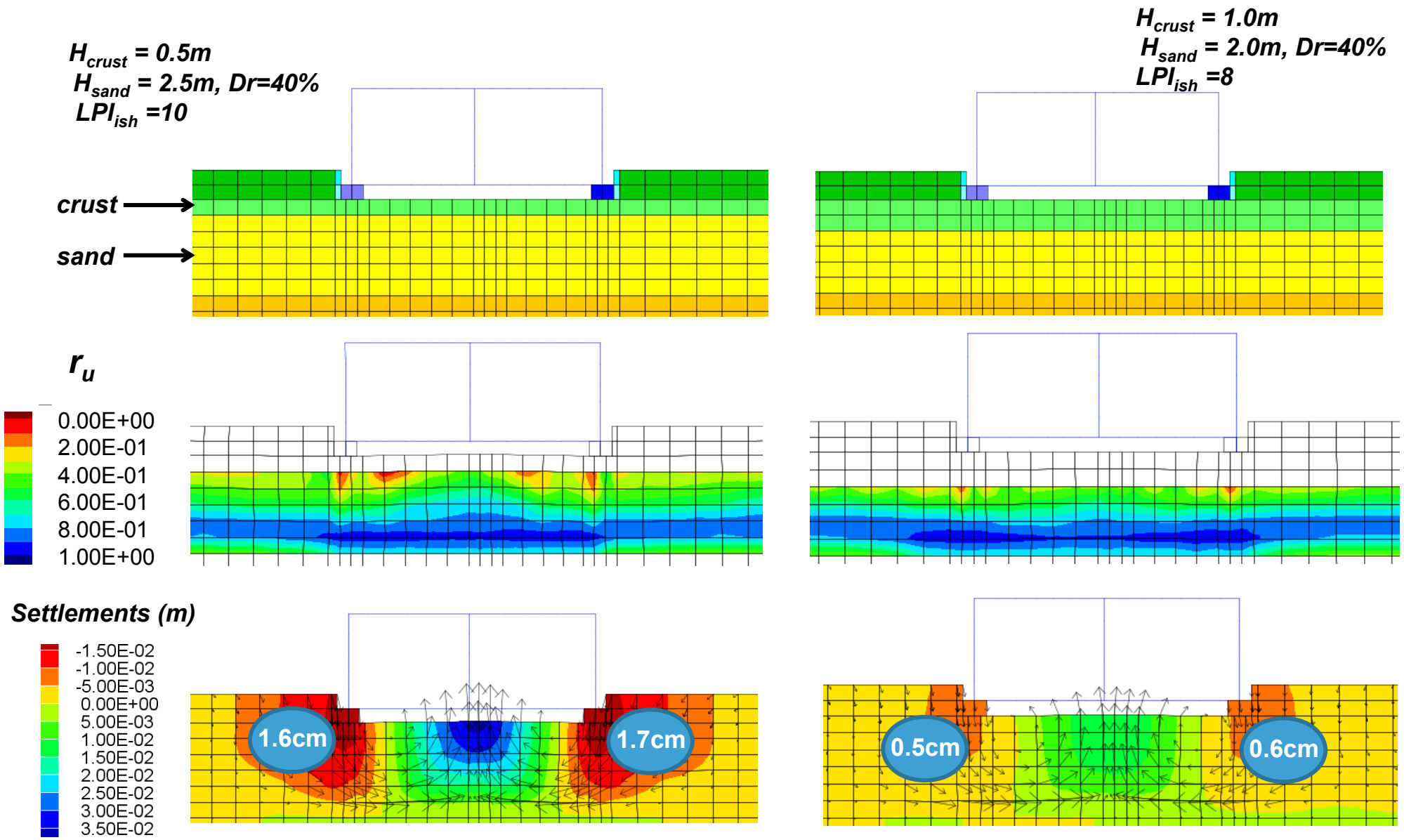


Figure 6-7a

# *Effect of Non-Liquefiable Crust Thickness*

## *Analyses Results*

***Effect of Crust Thickness***
***(B=0.7m, $D_r$=40%, q=36.7kPa)***

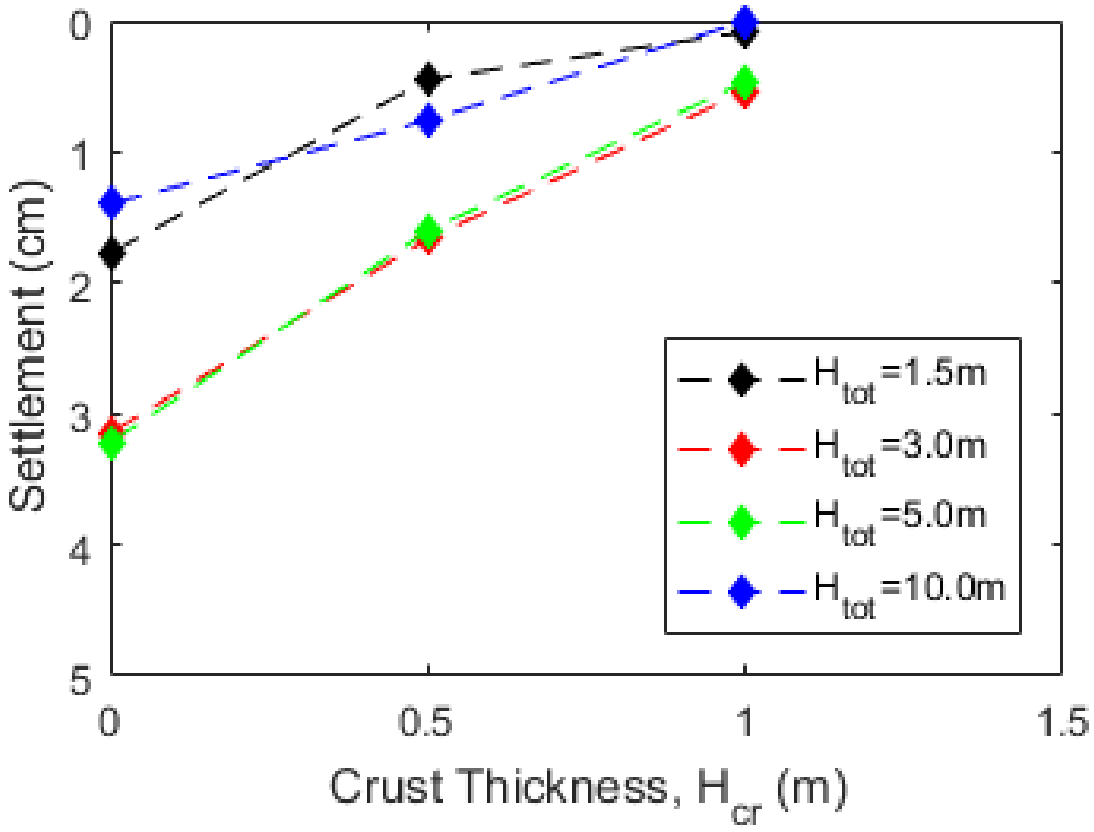


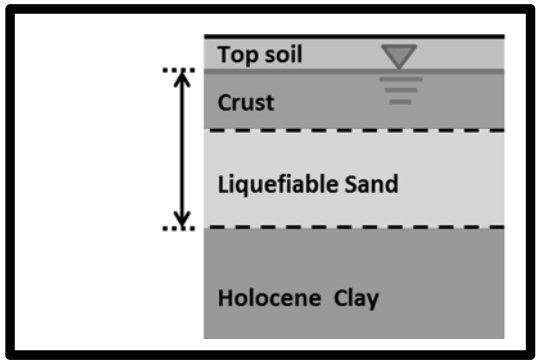


Figure 6-7b

# Post-Seismic Stability Check

## Post-Shaking Failure

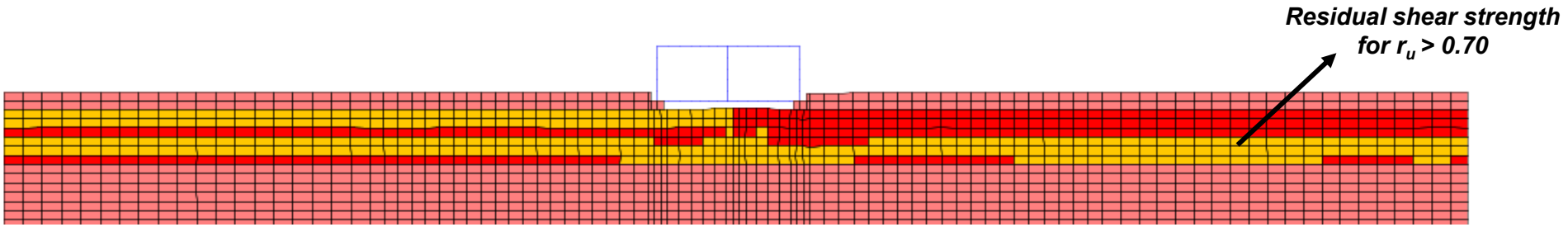


**Left Footing**

**Right Footing**

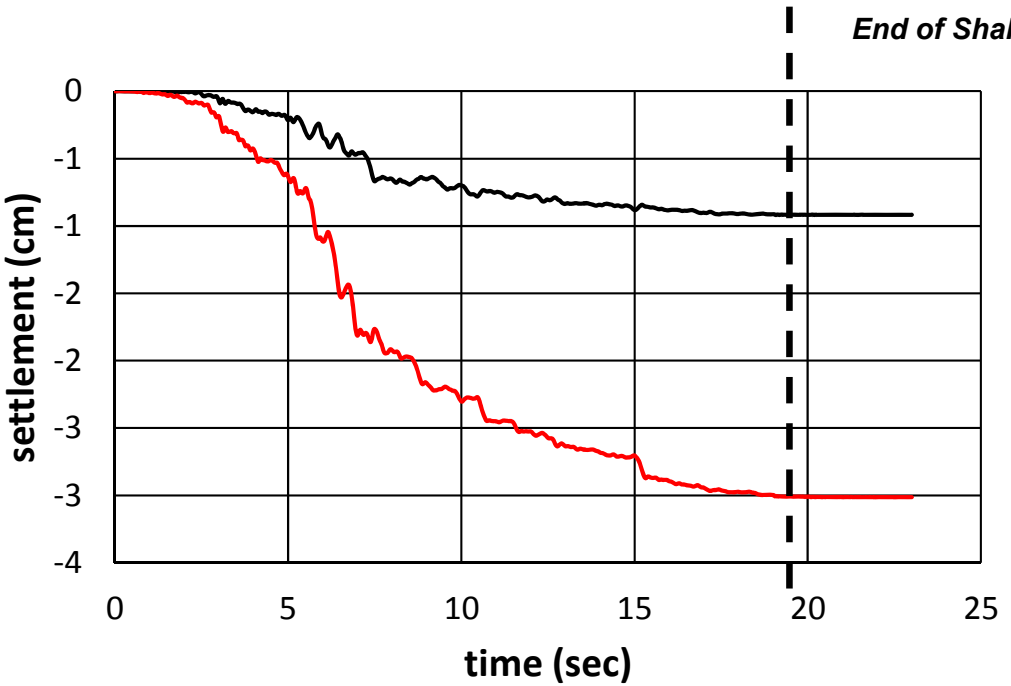


Figure 6-8

# Findings from others

## Bray and Macedo (2017) :

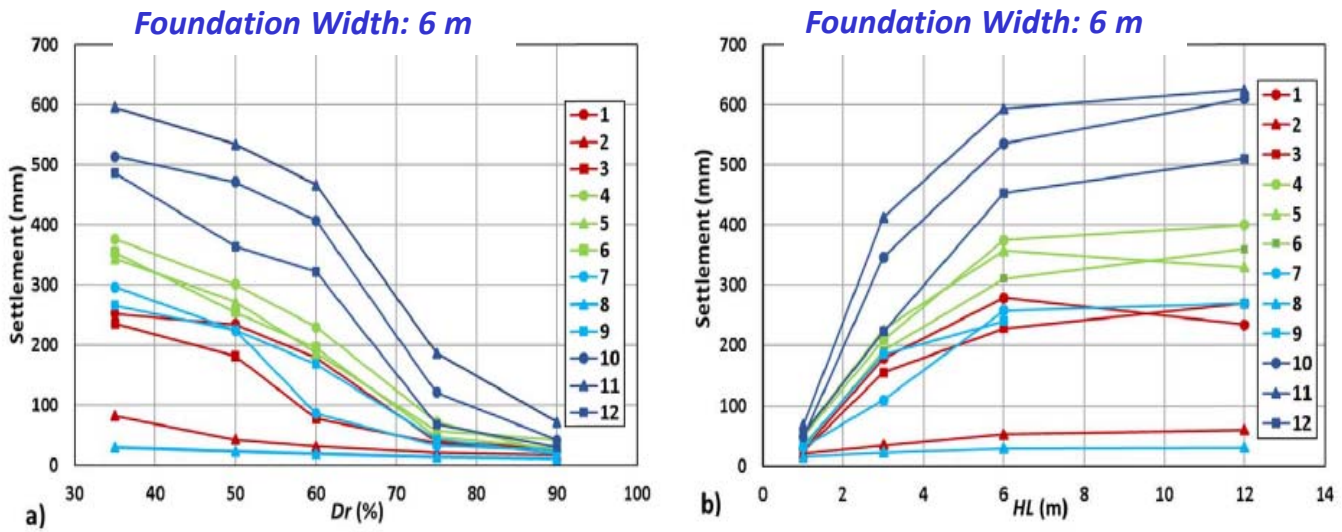


Fig. 5. Effects of liquefiable layer on building settlement (mm) for ground motions 1–12 (Table 2): (a) effects of relative density ($D_r$) for case with: $HL$ = 6 m, $Q$ = 80 kPa, $B$ = 12 m, $H$ = 12 m, and $HC$ = 2 m, and (b) effects of thickness of liquefiable layer ($HL$) for case with: $D_r$ of liquefiable layer = 50%, $B$ = 6 m, $Q$ = 80 kPa, $H$ = 12 m, and $HC$ = 2 m.

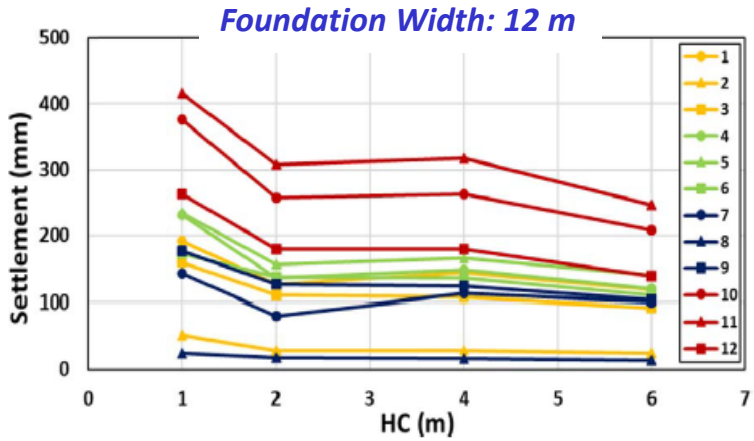


Fig. 6. Effects of crust thickness ($HC$) on building settlement (mm) for ground motions 1–12 (Table 2) for case with: $D_r$ of liquefiable layer = 50%, $HL$ = 3 m, $Q$ = 80 kPa, $B$ = 12 m, and $H$ = 12 m.

# Findings from others

*From Luque and Bray (2015)*

***Darfield event – CBD Case Study***

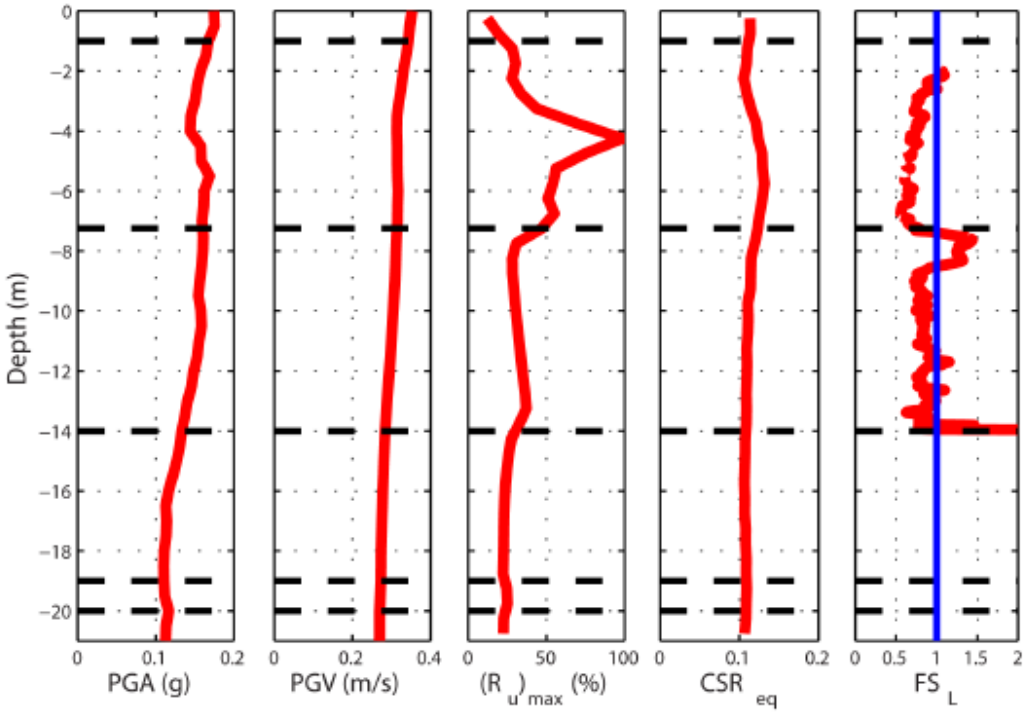


***Christchurch event – CBD Case Study***

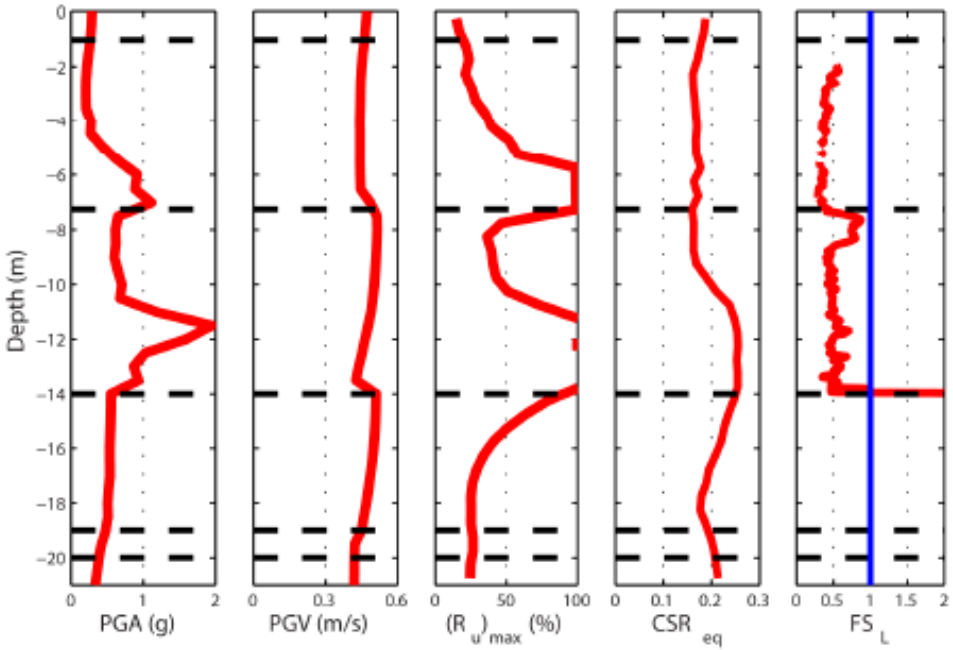


Figure 6-10

# *Effect of Input Motion Characteristics at -25 m NAP (IA, CAV, $CAV_{dp}$, $D_{5-75}$)*

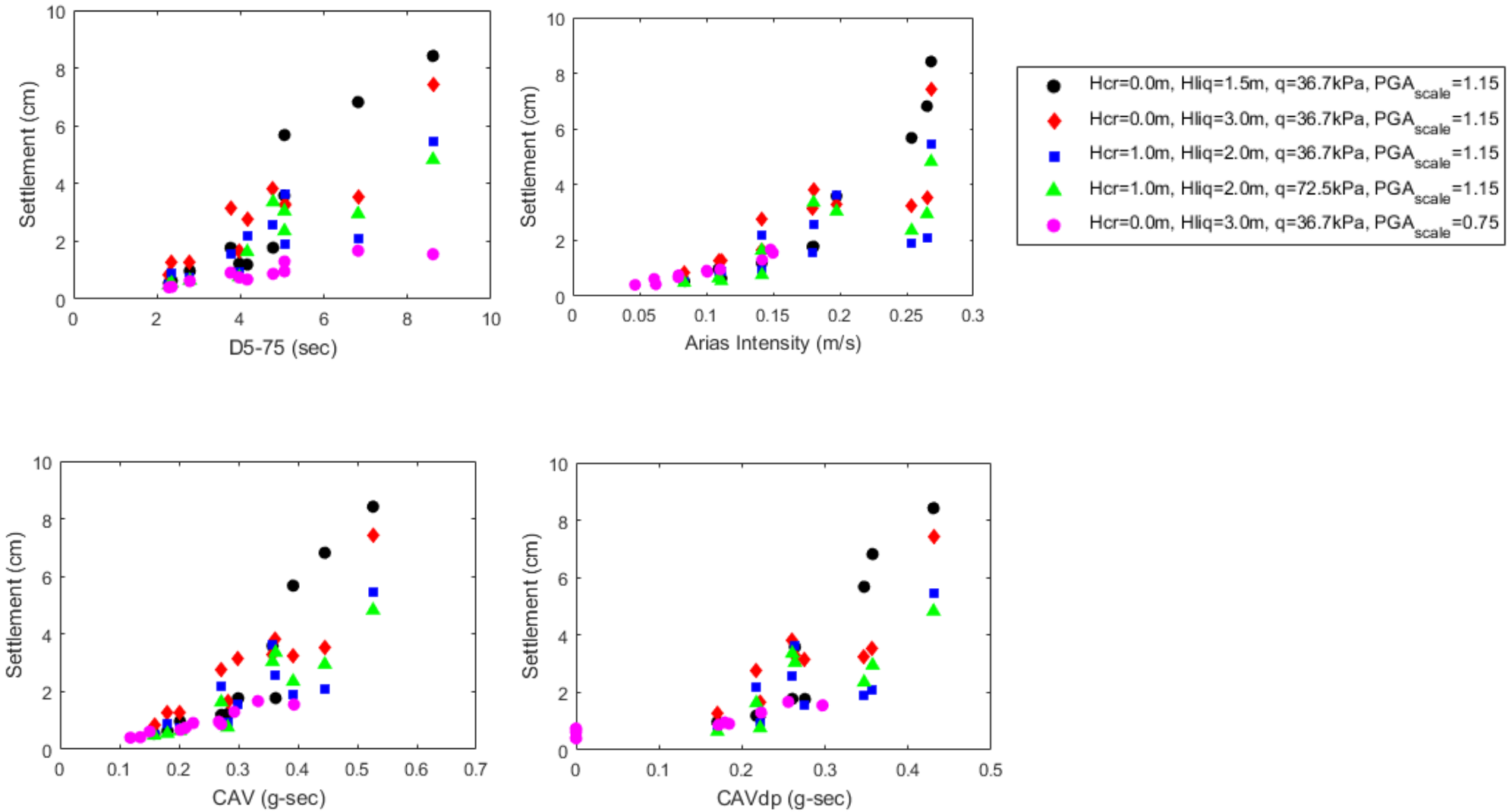


Figure 6-11a

# *Effect of Surface Motion Characteristics (IA, CAV, $CAV_{dp}$, $D_{5-75}$)*

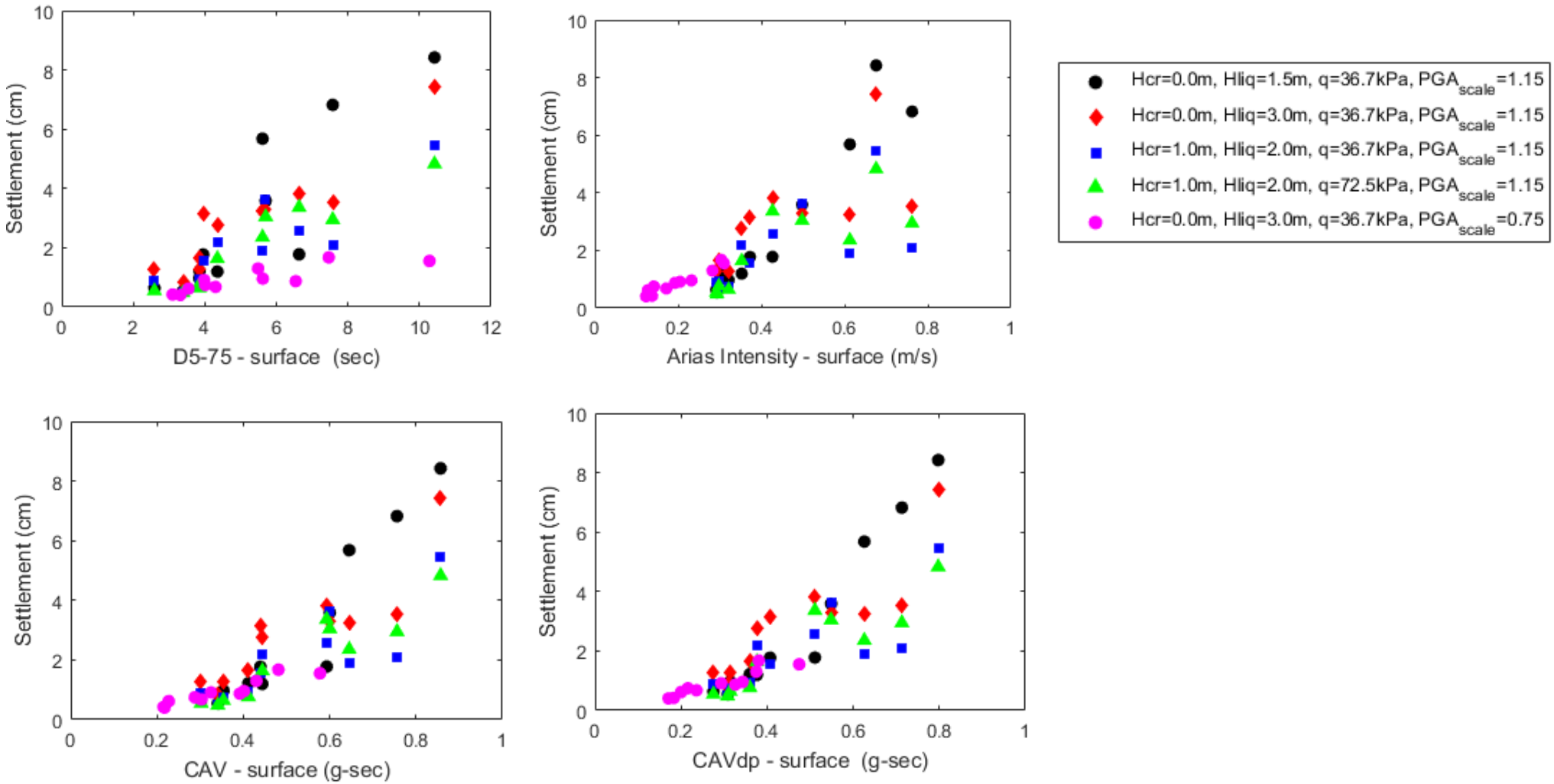


Figure 6-11b

# *Effect of Surface Motion Spectral Accelerations at Various Periods*

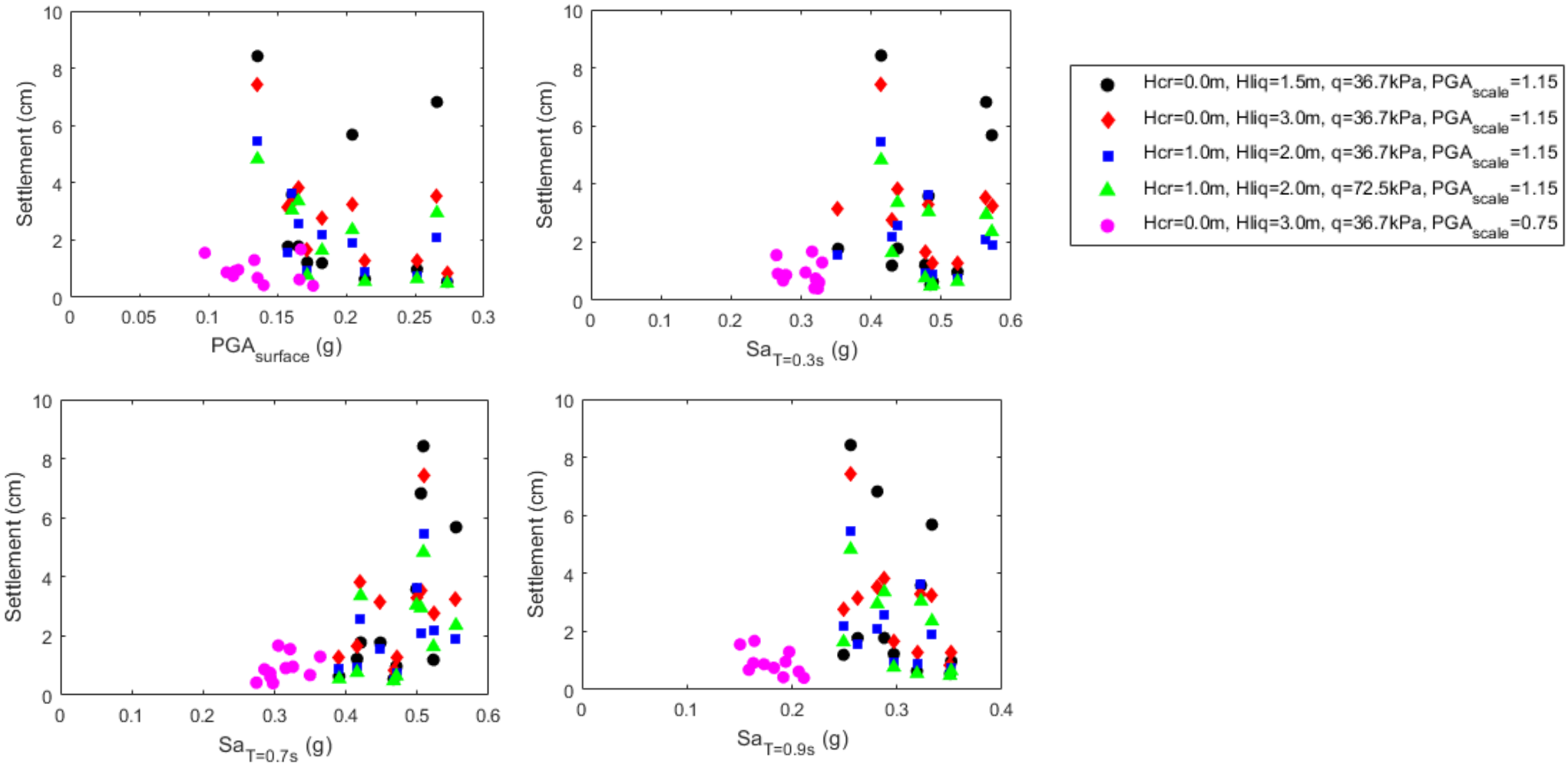


Figure 6-12

# Effect of Footing Width

## Effect of Footing Width, B

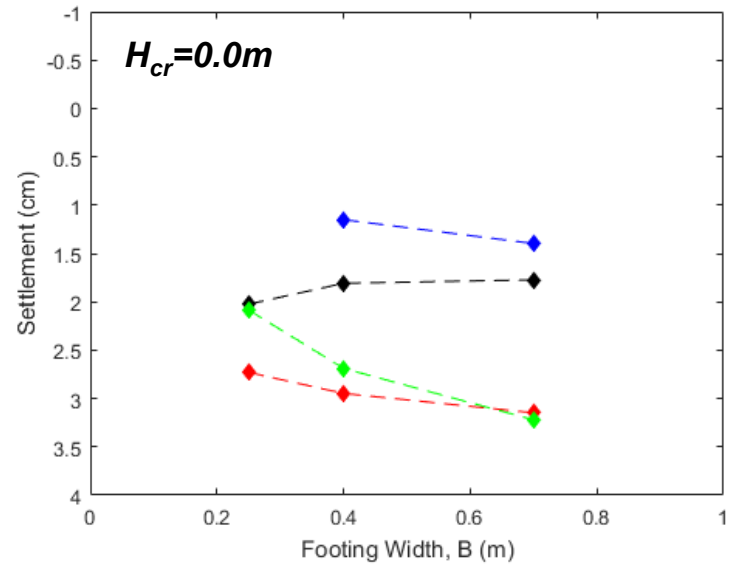


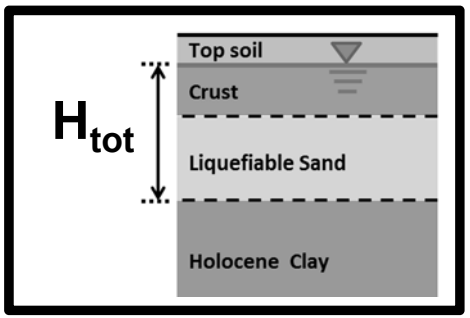


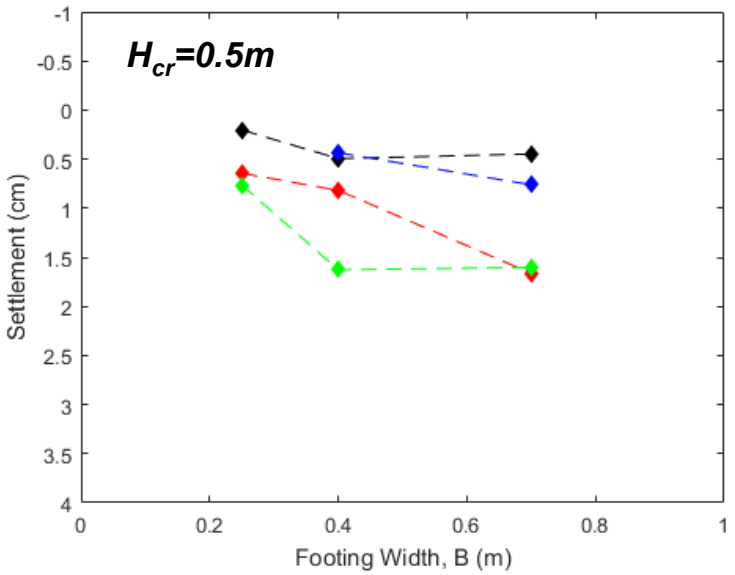


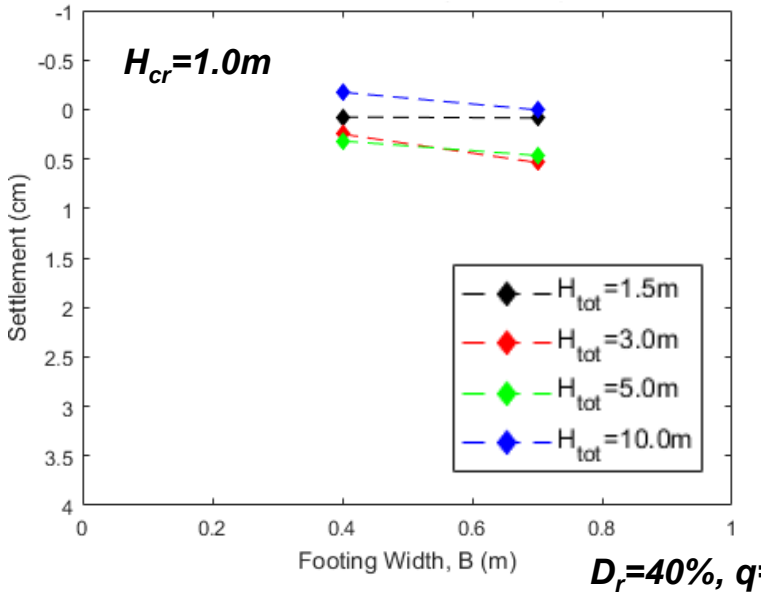


$D_r$=40%, q=36.7kPa, $c_u$=40kPa

Figure 6-13

# Effect of Footing Load, q

$D_r$=40%, B=0.7m, $H_{tot}$=3.0m, $c_u$= 40kPa

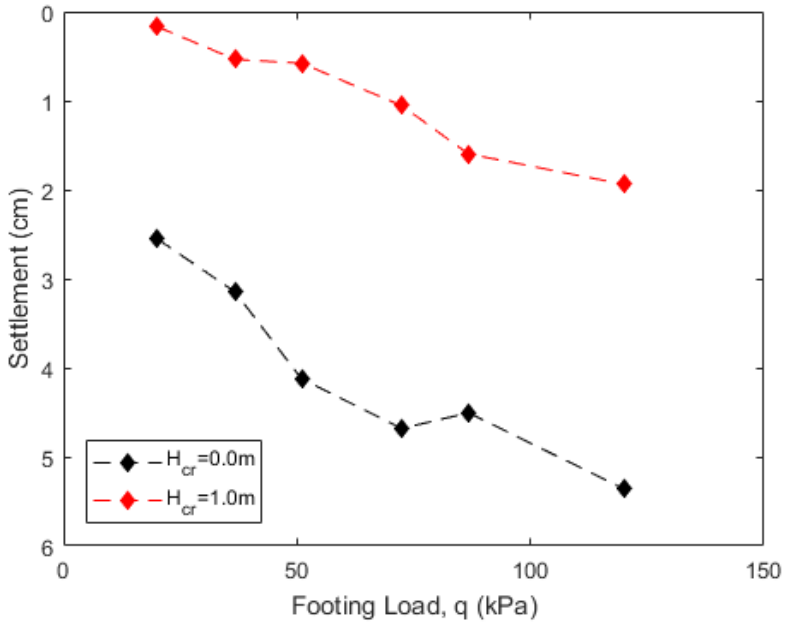


$D_r$=40%, B=0.4m, $H_{tot}$=3.0m, $c_u$= 40kPa

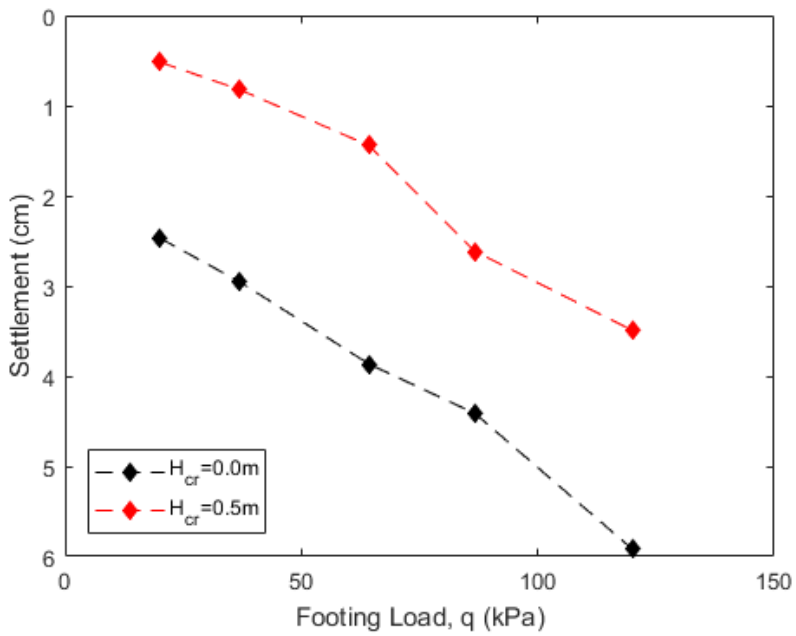


$D_r$=40%, B=0.7m,

Figure 6-14

# Effect of Crust Strength

## Effect of Crust Strength, $q_{ult,cr} / q$

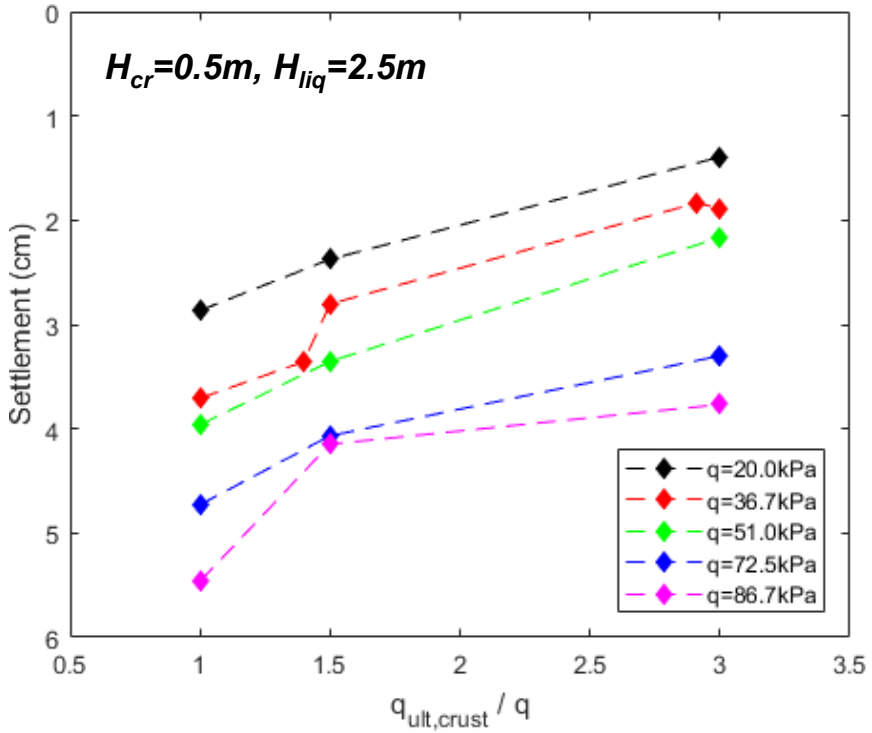


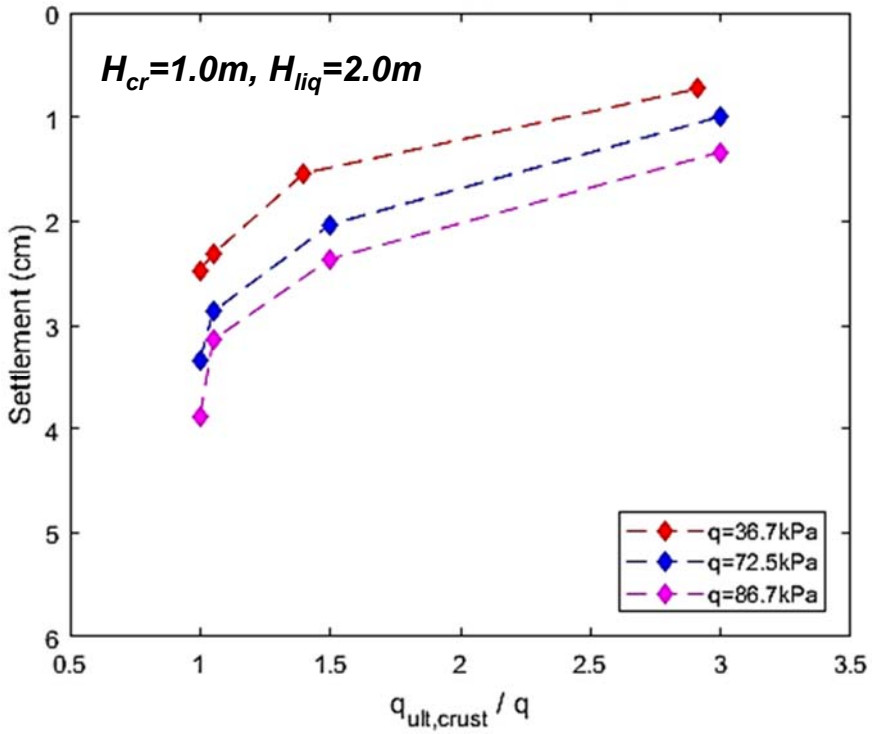


$D_r$=40%, B=0.7m

Figure 6-15

# *Sensitivity Analyses – Longitudinal Building Direction / Structural Period*

- ***Structural Period, $T_{str}$ = 0.11 sec & 0.22 sec (transverse direction)***
- ***Longitudinal building direction ($T_{str}$ = 0.13 sec)***

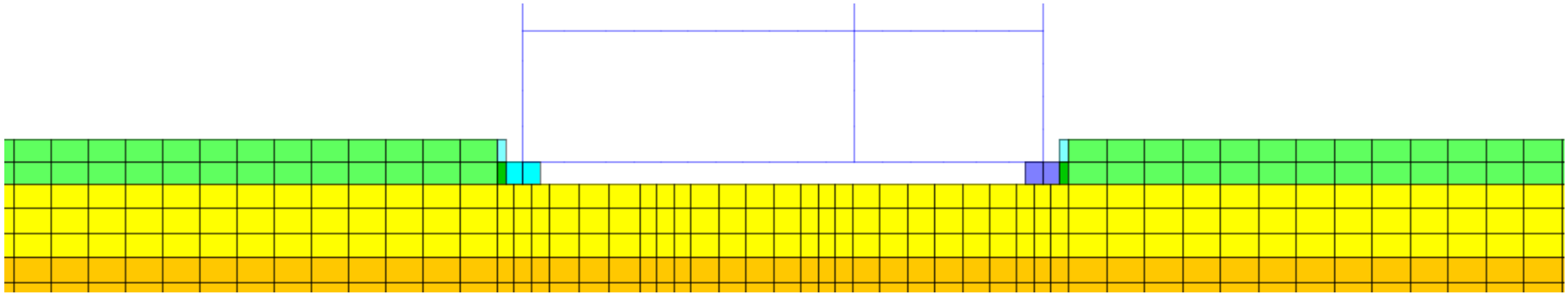

| ID | Thickness of Crust, $H_{cr}$ (m) | Thickness of Liquefiable Sand, $H_{sand}$ (m) | Relative Density, $D_r$ (%) | Frame | $T_{str}$ (sec) | $LPI_{ish}$ | Settlements (cm) | |
|---|---|---|---|---|---|---|---|---|
| | | | | | | Green et al (2018) | Left footing | Right footing |
| 1 | 0.0 | 3.0 | 40 | Transverse | 0.11 | 13 | 3.09 | 3.20 |
| 2 | 0.0 | 1.5 | 40 | Longitudinal | 0.13 | 8 | 4.37 | 3.82 |
| 3 | 0.0 | 3.0 | 40 | Transverse | 0.22 | 13 | 3.36 | 3.45 |

Figure 6-16

# Sensitivity Analyses – Effect of 20% Load Variability Between Footings

## Effect of Load Variability

**Left footing: q=36.7kPa** → **s = 2.95cm**

**Right footing: q = 1.2x36.7 = 44.04kPa** → **s = 3.75cm**

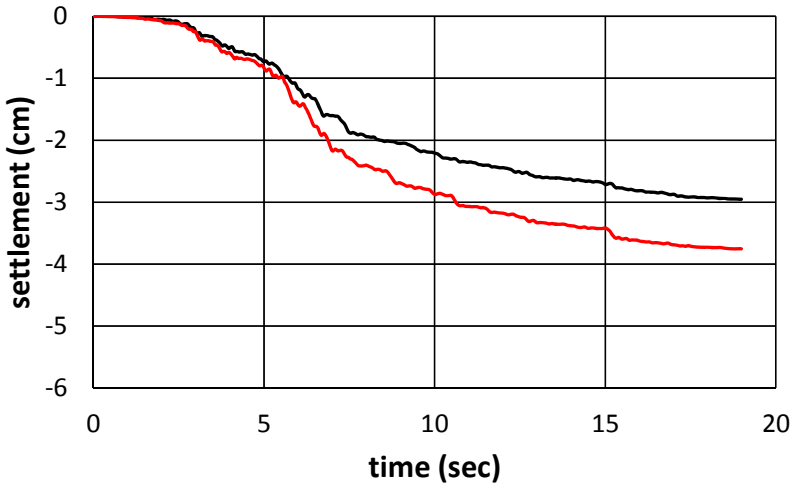


**Left footing: q=72.5kPa** → **s = 4.77cm**

**Right footing: q = 1.2x72.5 = 87.0kPa** → **s = 5.10cm**

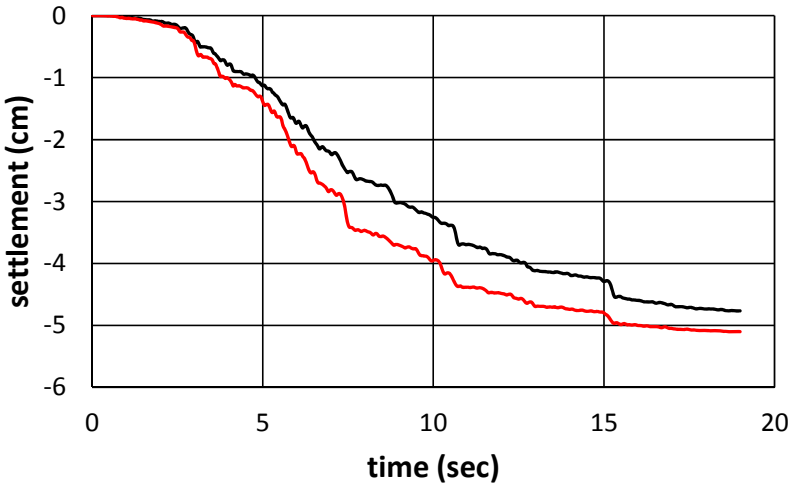


$D_r$=40%, B=0.7m, $H_{cr}$=0.0, $H_{liq}$=3.0m

Figure 6-17

## Scenario 1: Foundation on Clay

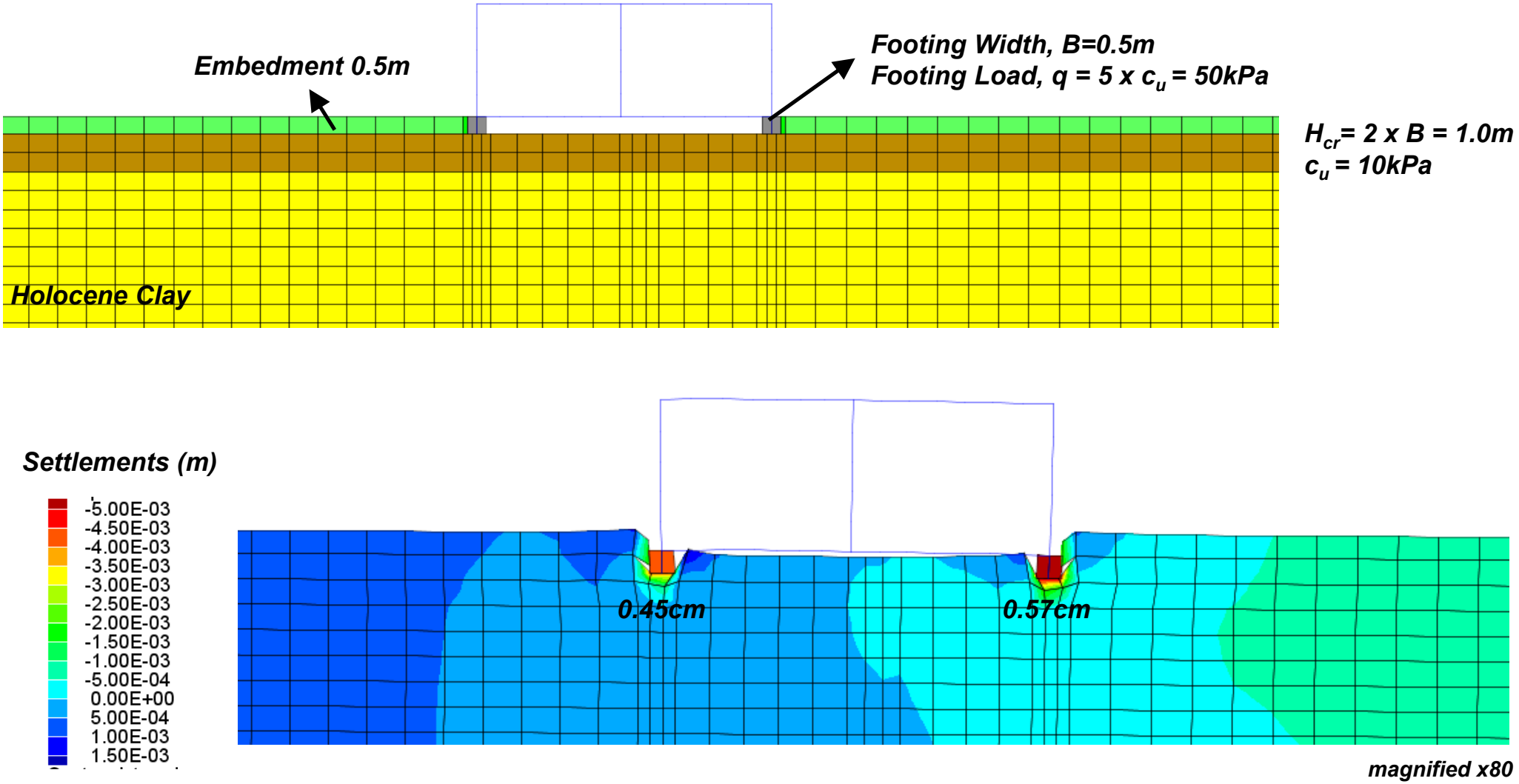


Figure 6-18

# Sensitivity Analyses – Foundation on Extremely Loose Sand

## Scenario 2: Foundation on Extremely Loose Sand (Case 1)

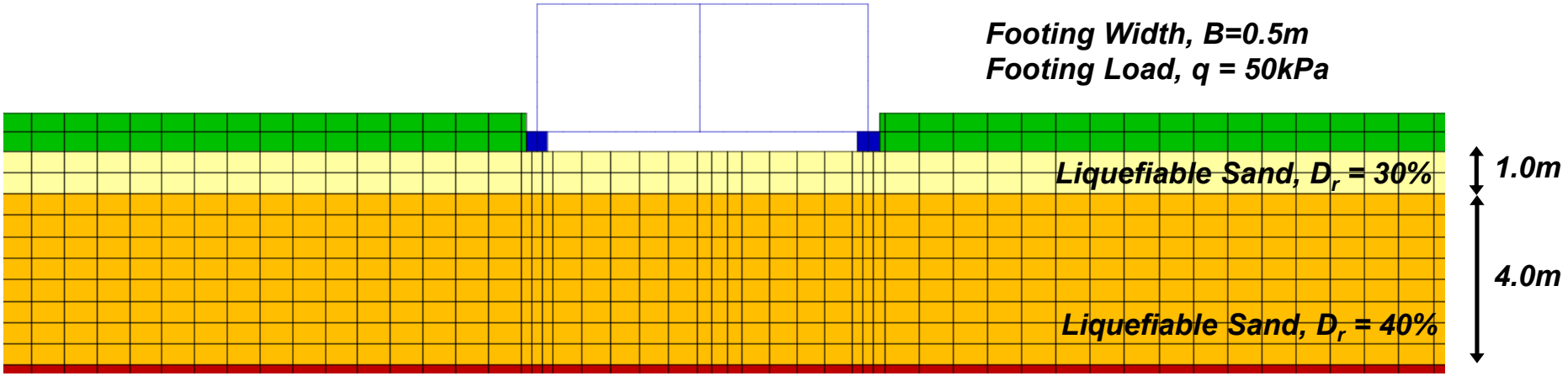


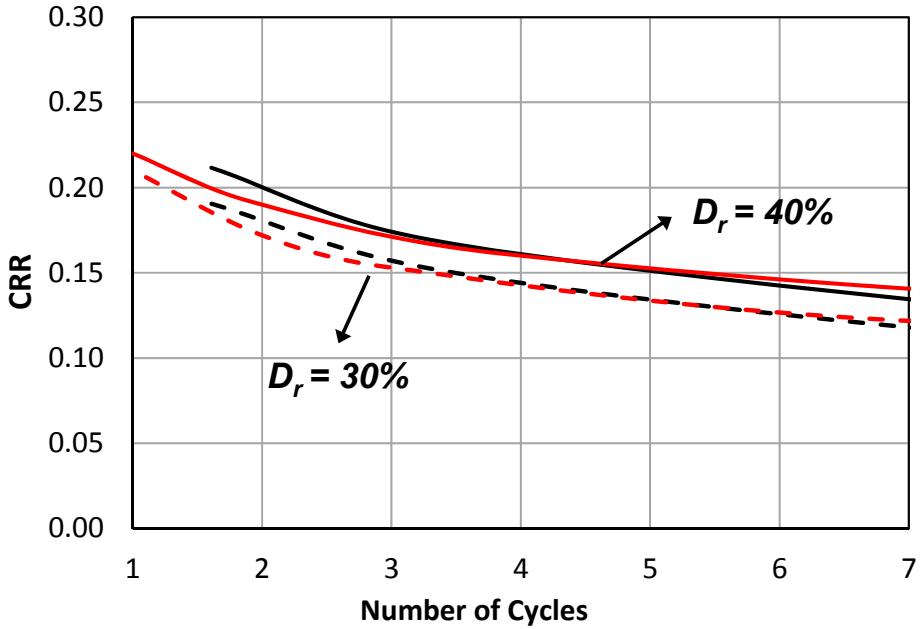


Green et al (2018)

PM4Sand

Figure 6-19a

# Sensitivity Analyses – Foundation on Extremely Loose Sand

## Scenario 2: Foundation on Extremely Loose Sand (Case 1)

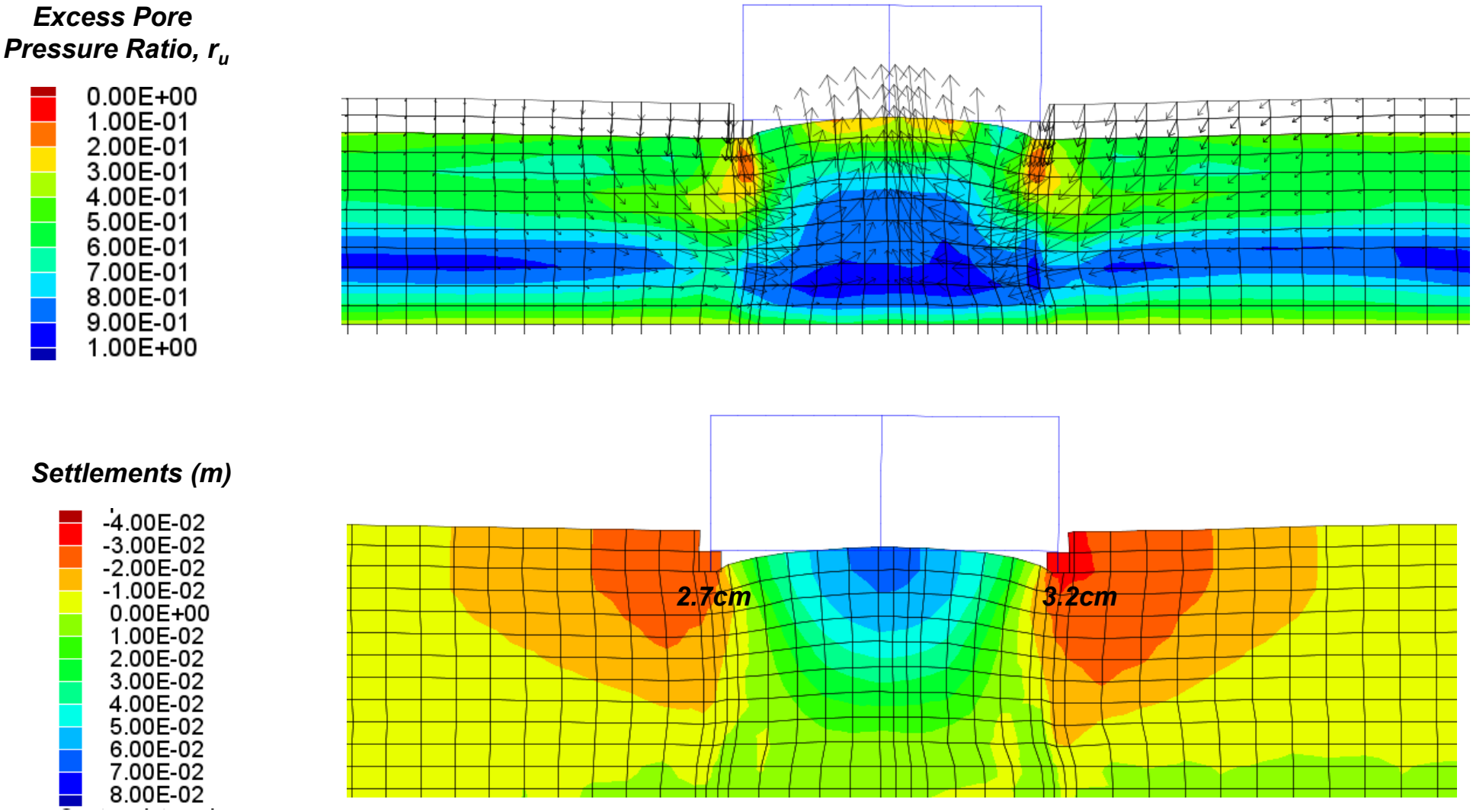


Figure 6-19b

# Sensitivity Analyses – Foundation on Extremely Loose Sand

## Scenario 2: Foundation on Extremely Loose Sand (Case 2)

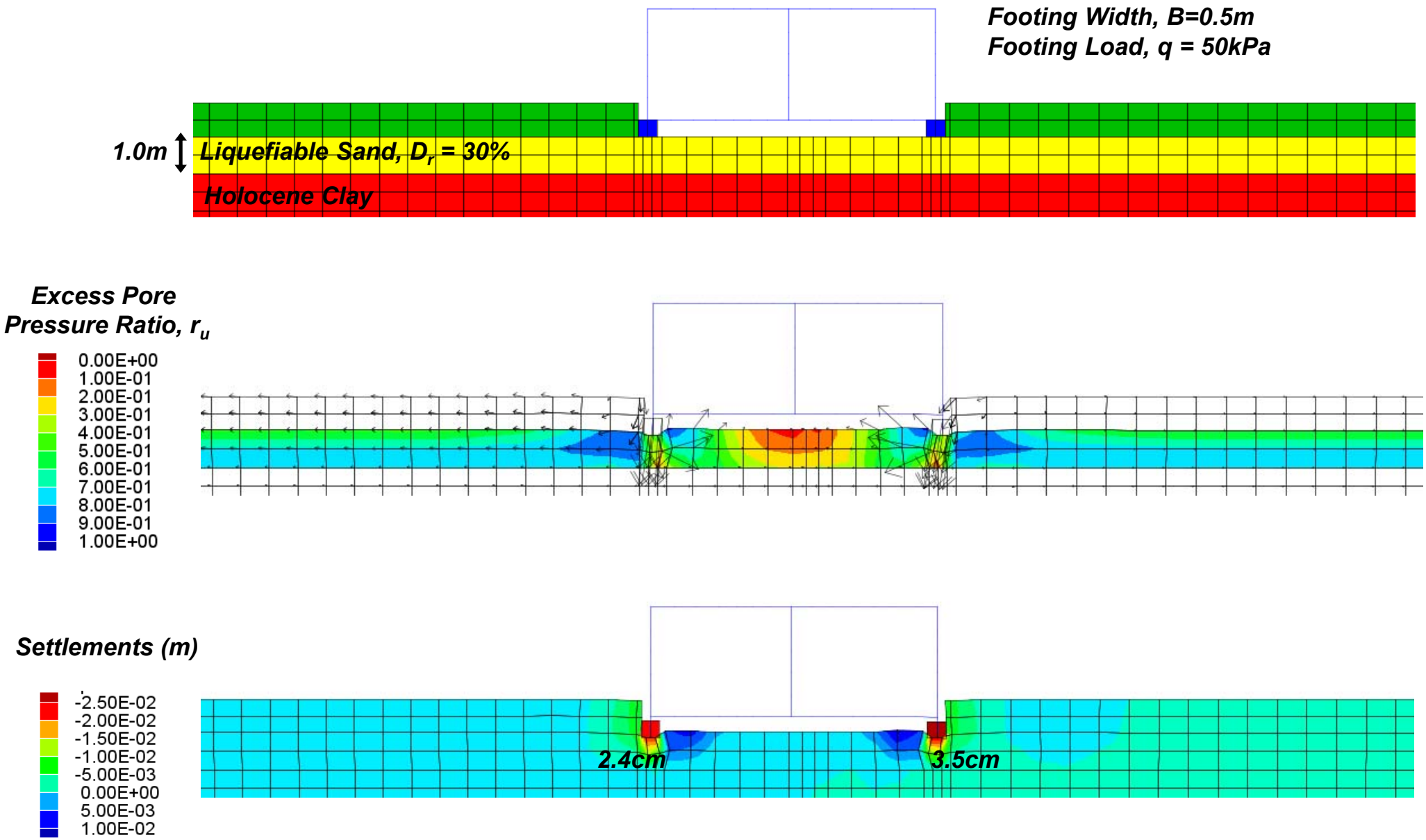


Figure 6-19c

# Sensitivity Analyses – Effect of Superstructure-Footing Connection

## Scenario 5: Superstructure-Footing Connection

*Footing Width, B=0.5m*

*Footing Load, q = 80kPa*

*Liquefiable Sand, $D_r$=40%, $H_{liq}$=5.0m*

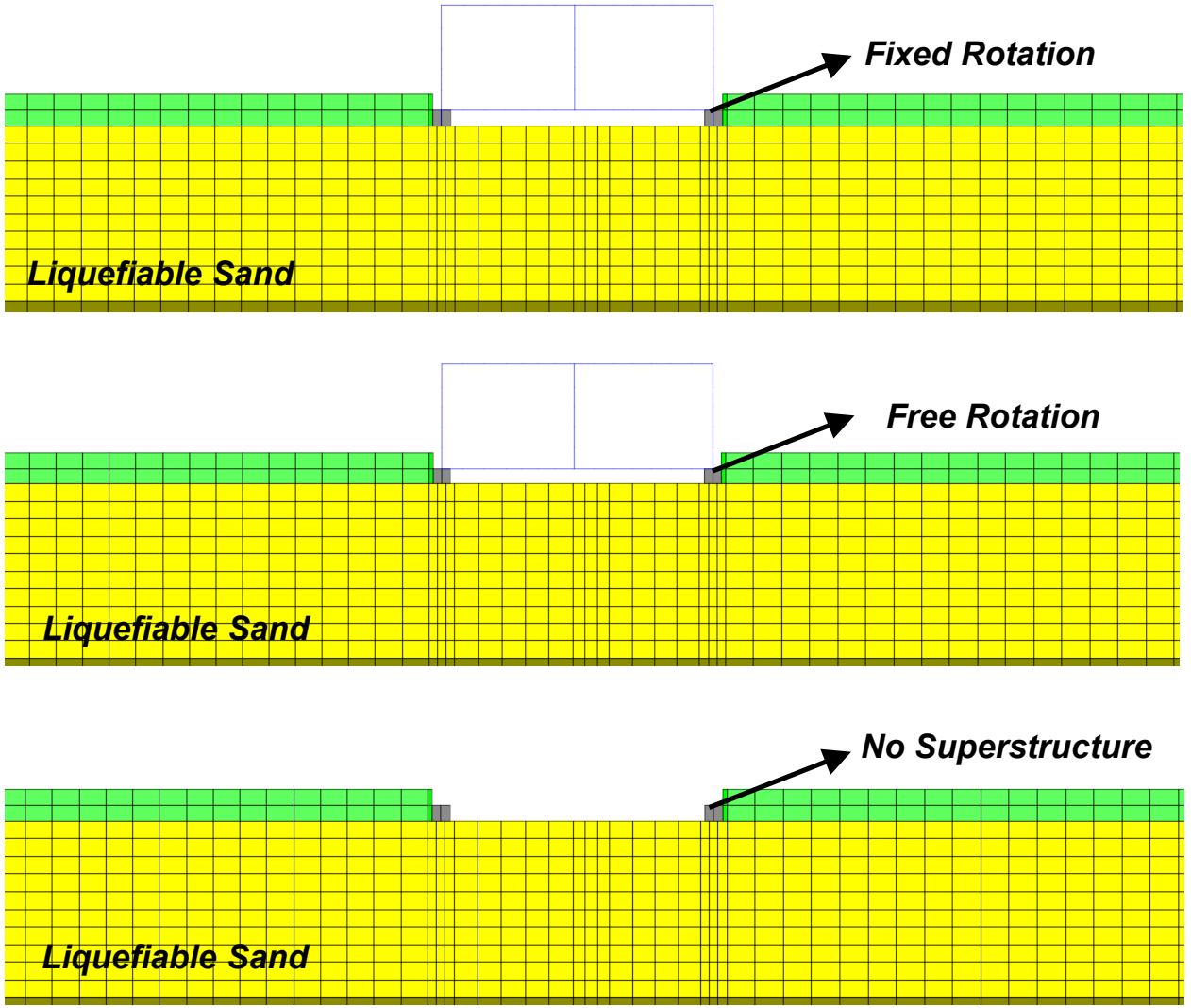


Figure 6-20a

# Sensitivity Analyses – Effect of Superstructure-Footing Connection

## Scenario 5: Superstructure-Footing Connection

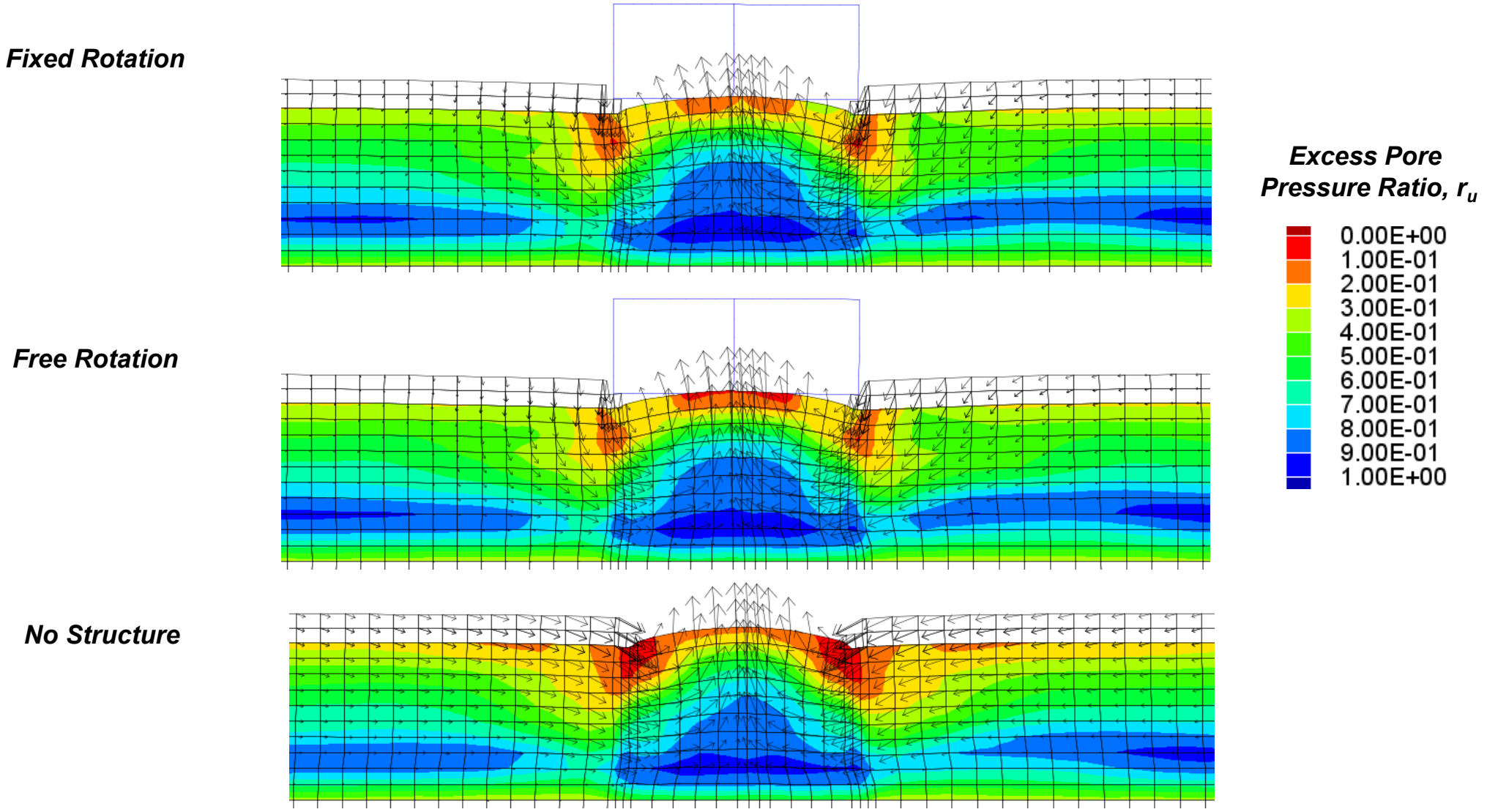


Figure 6-20b

# Sensitivity Analyses – Effect of Superstructure-Footing Connection

## Scenario 5: Superstructure-Footing Stiffness

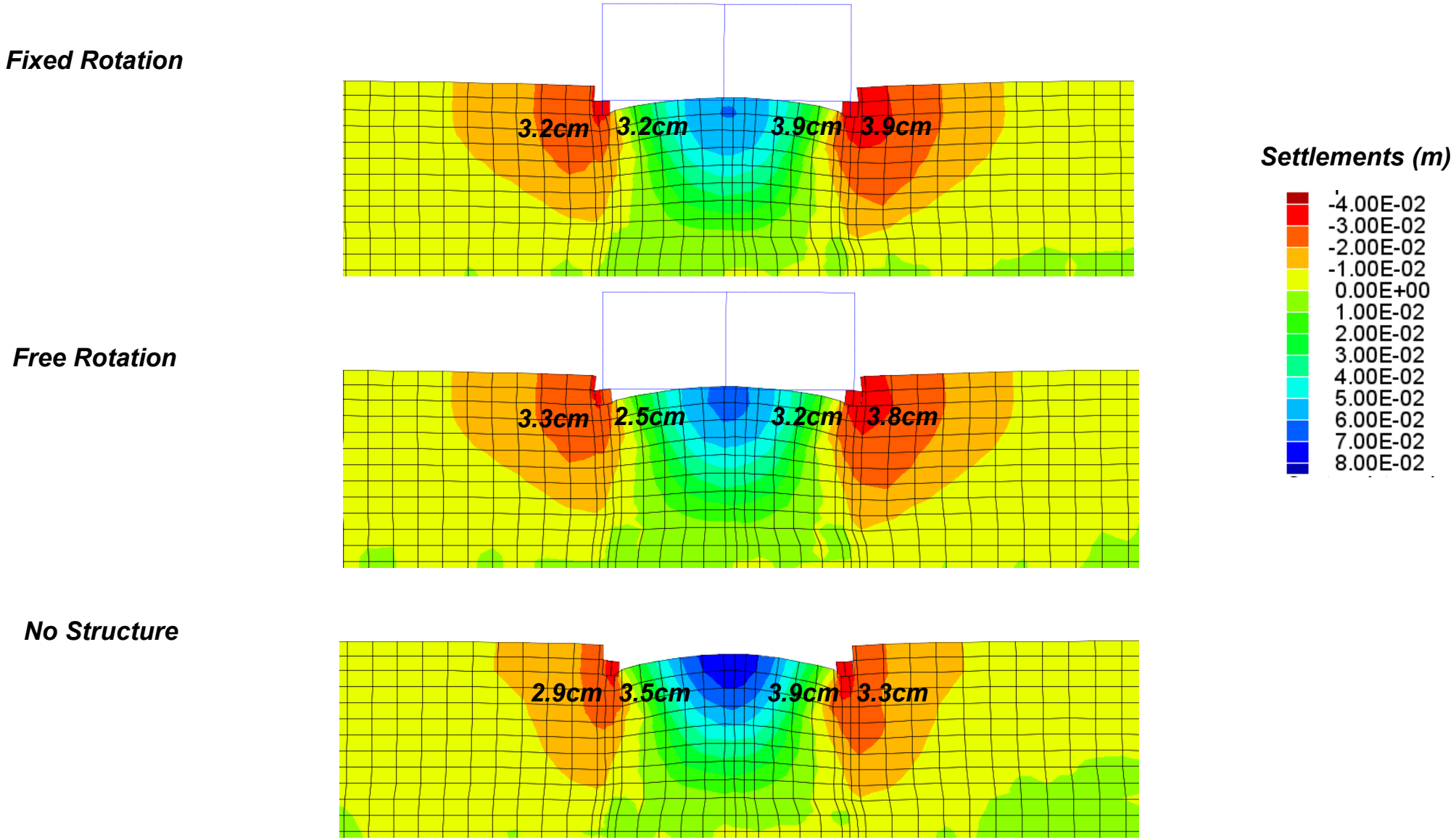


Figure 6-20c

# Sensitivity Analyses – Effect of Superstructure-Footing Connection

## Scenario 5: Superstructure-Footing Connection

**Fixed Rotation**

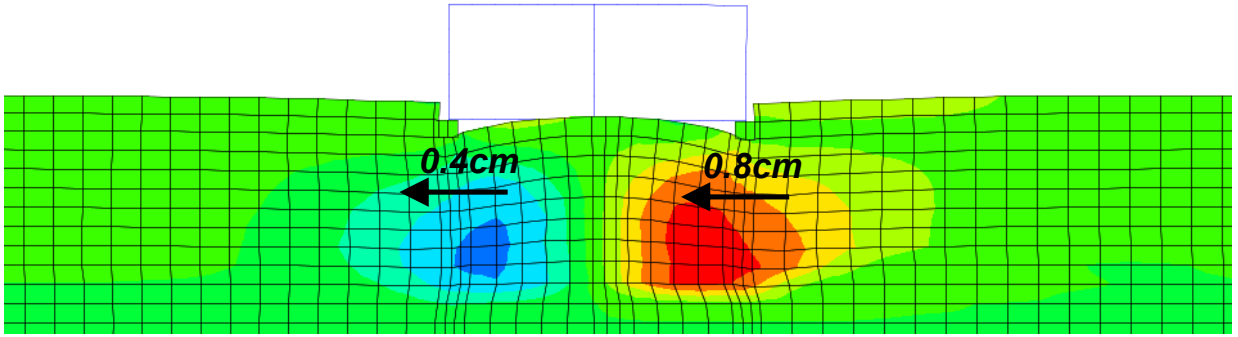


**Free Rotation**

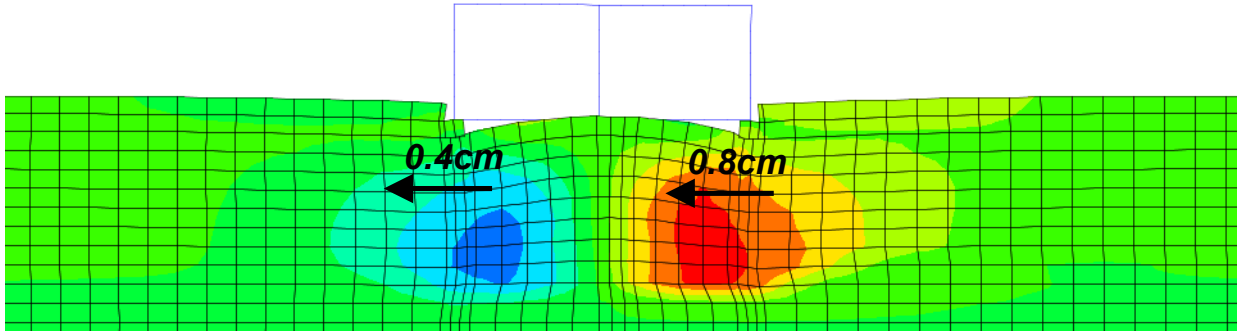


**No Structure**

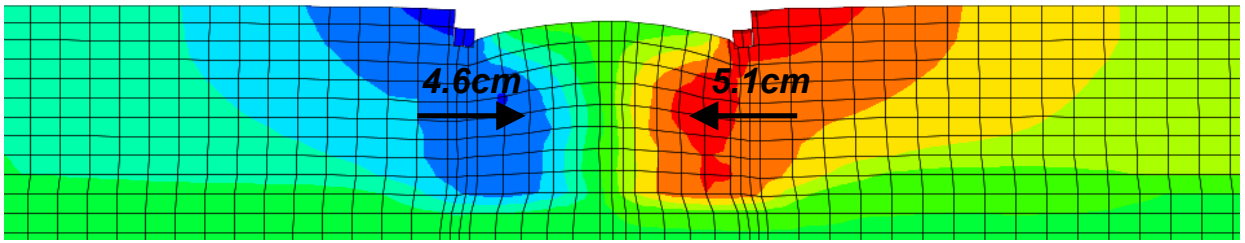


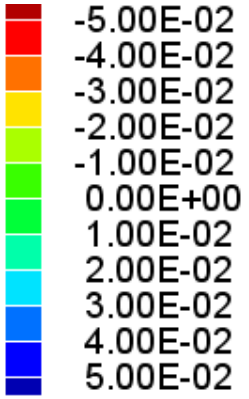


Figure 6-20d

# Sensitivity Analyses – Soil Variability Under Building

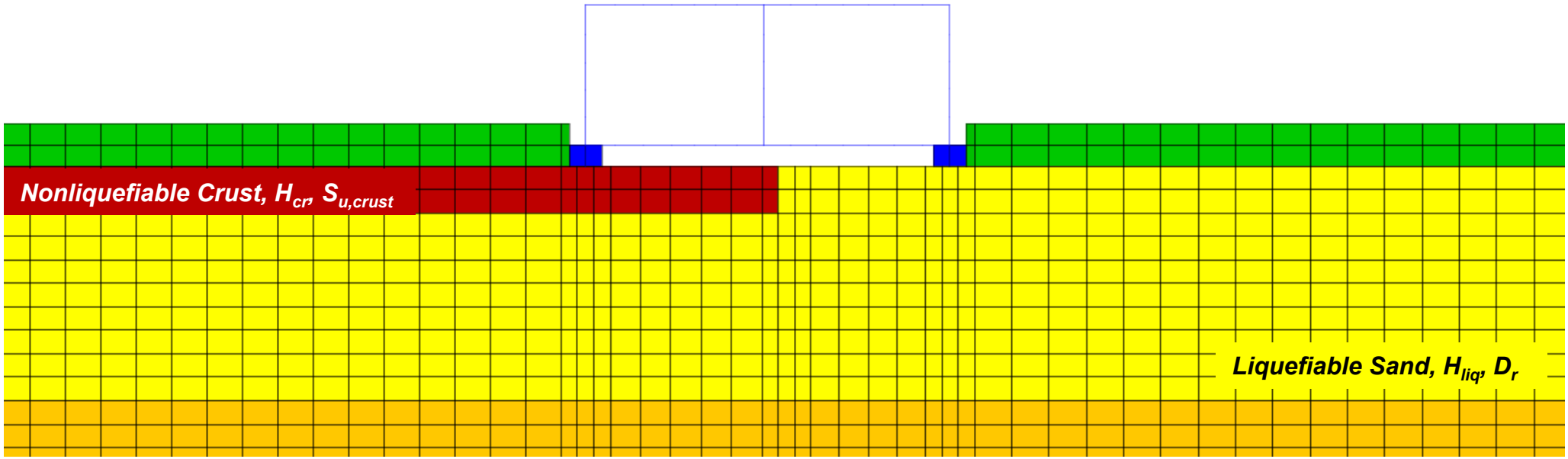


- *Footing width B=0.7m*
- *Footing load q=36.7kPa*
- *Crust thickness below left footing $H_{cr}$=1.0m, $S_{u,crust}$ = 40kPa*
- *Liquefiable Sand Relative Density, $D_r$=40%*
- *Liquefiable Sand thickness $H_{liq}$=1.5m, 3.0m & 5.0m*

Figure 6-21a

# Sensitivity Analyses – Soil Variability Under Building

- $D_r$=40%, $H_{crust}$=1.0m or $H_{liq}$=3.0m

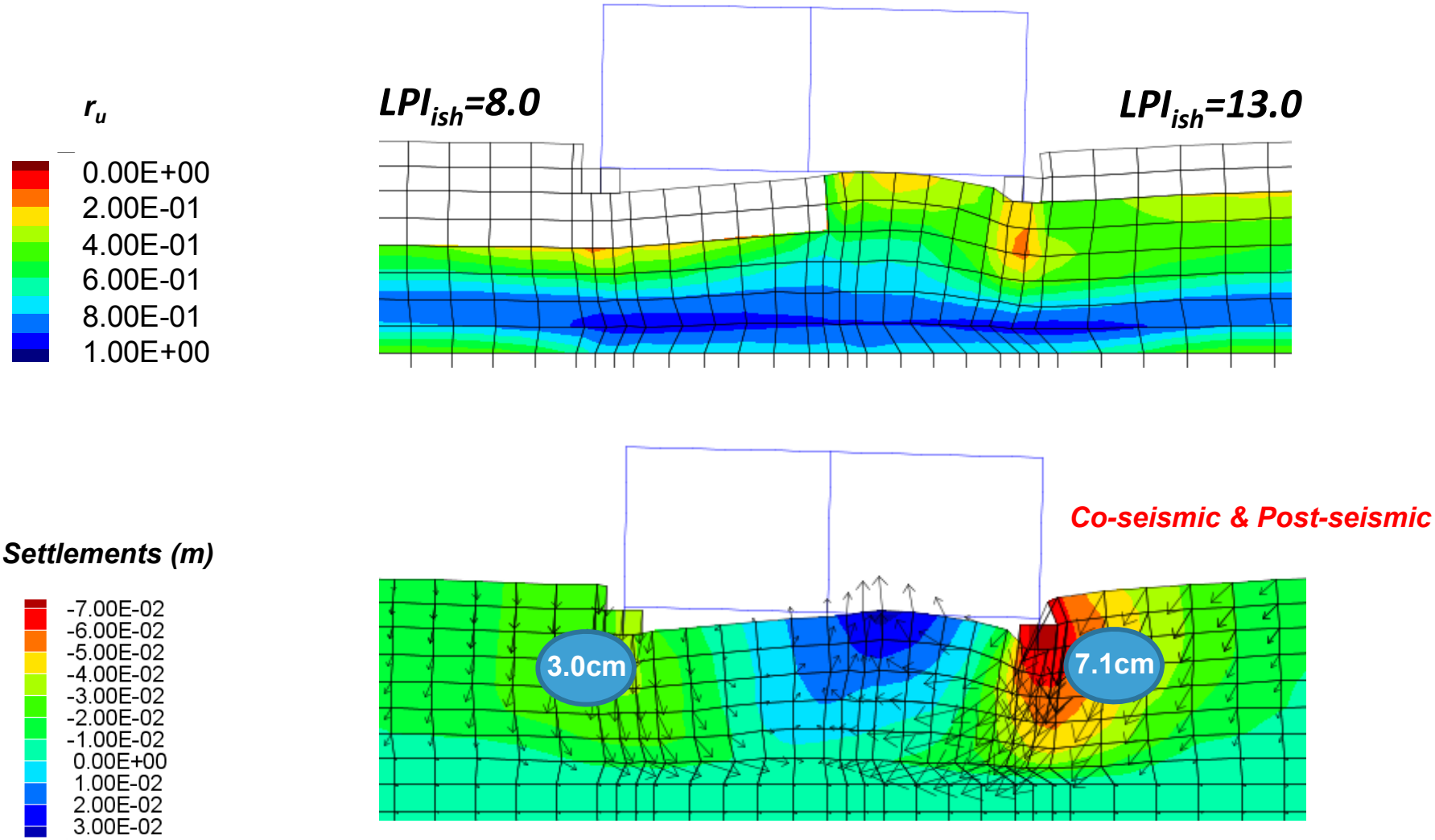


Figure 6-21b

# Sensitivity Analyses – Number of Storeys

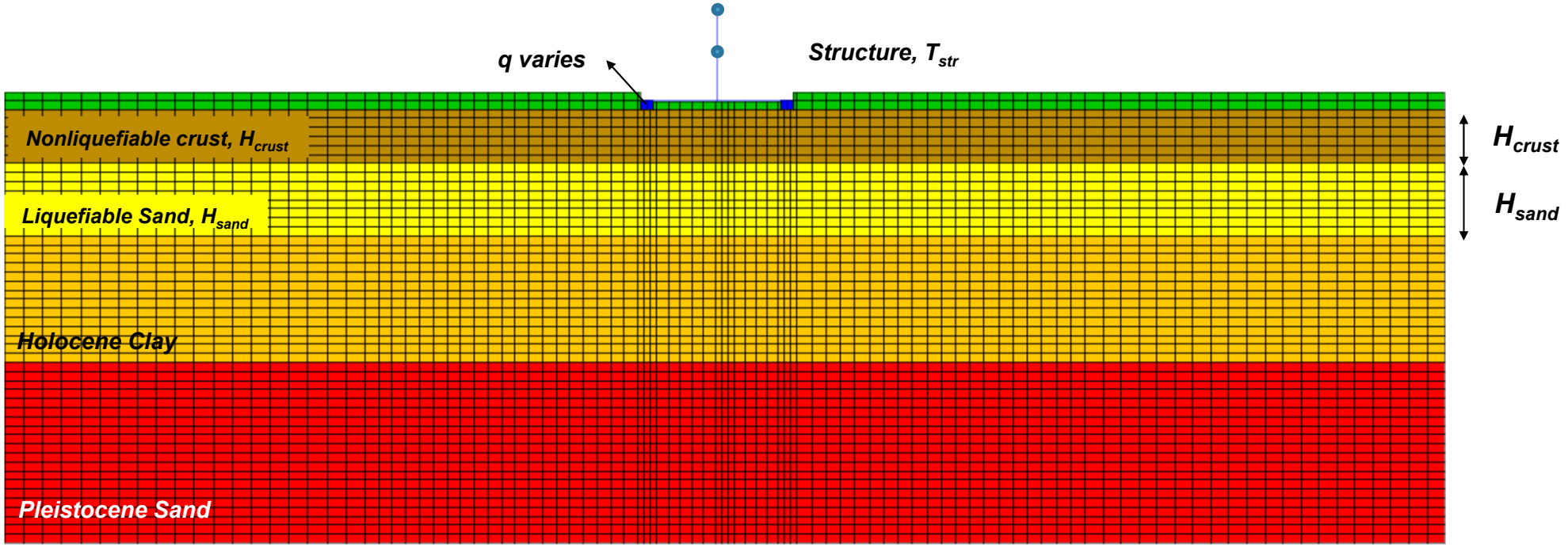


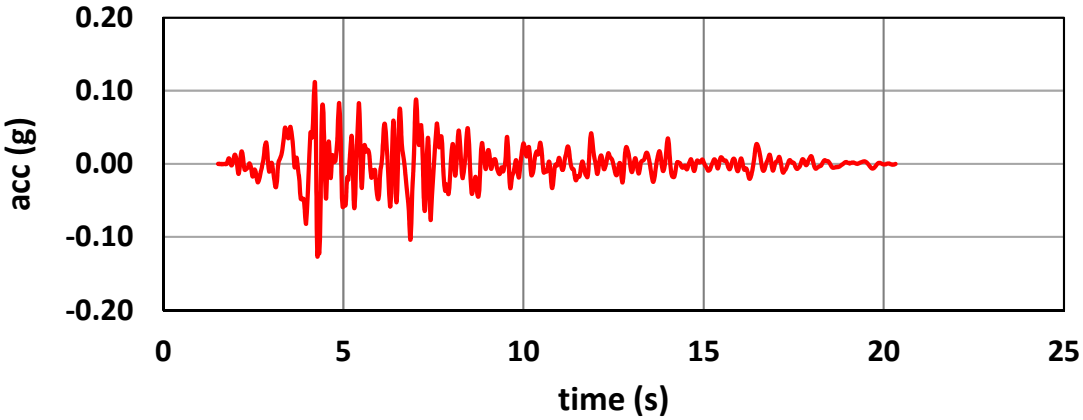


Figure 6-22

# Sensitivity Analyses – Number of Storeys

- $D_r$=40%, $H_{crust}$=0.0m or $H_{liq}$=3.0m

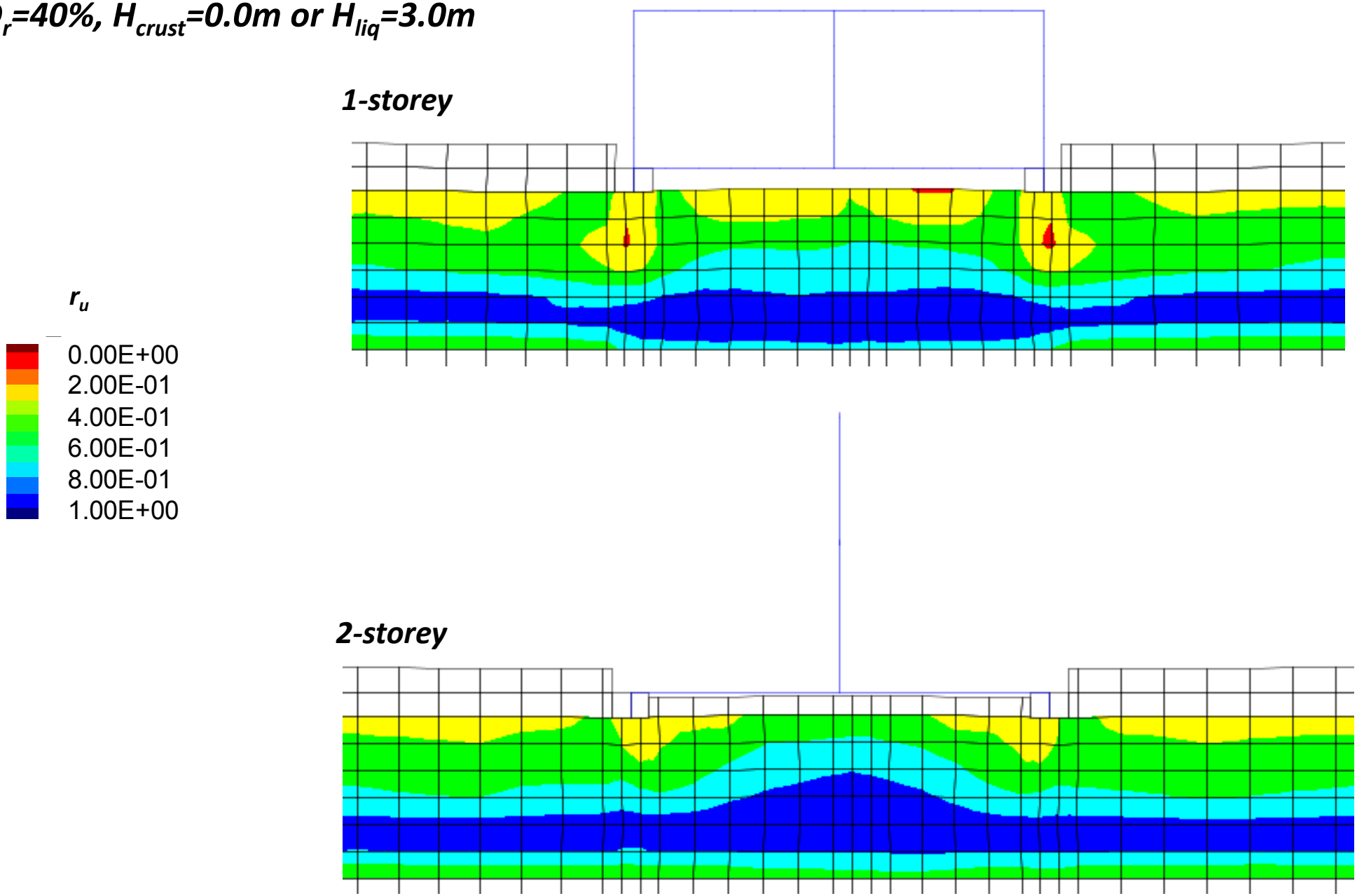


Figure 6-23a

# *Sensitivity Analyses – Number of Storeys*

- ***$D_r$=40%, $H_{crust}$=0.0m or $H_{liq}$=3.0m***

***1-storey***

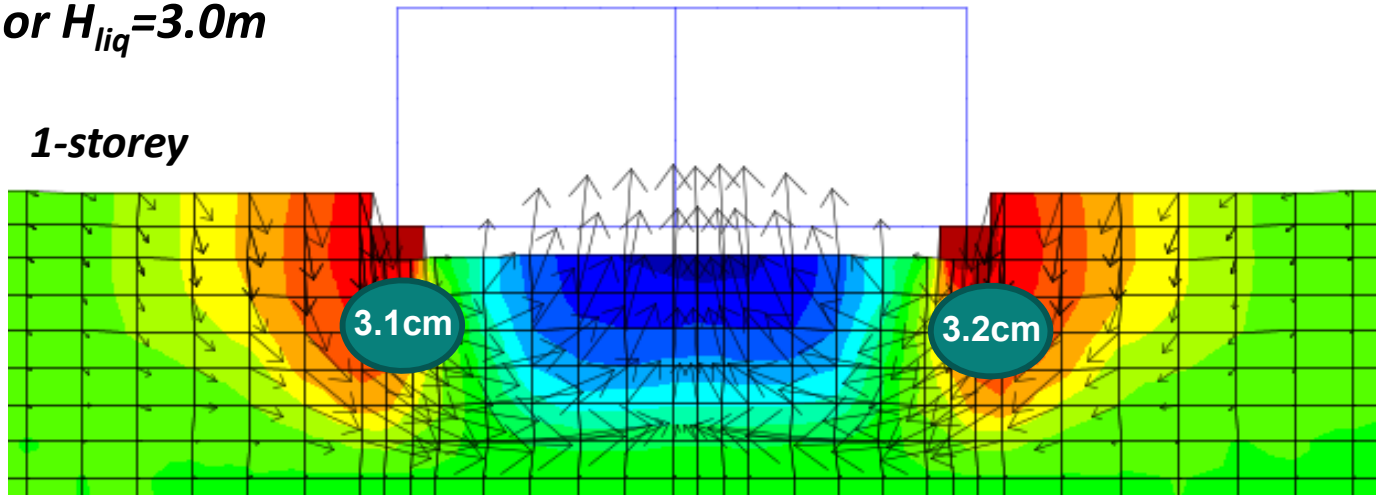


***Settlements (m)***

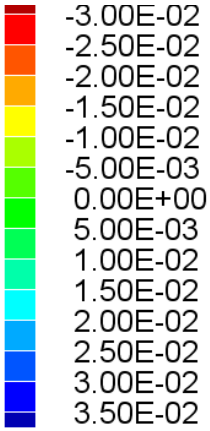


***2-storey***

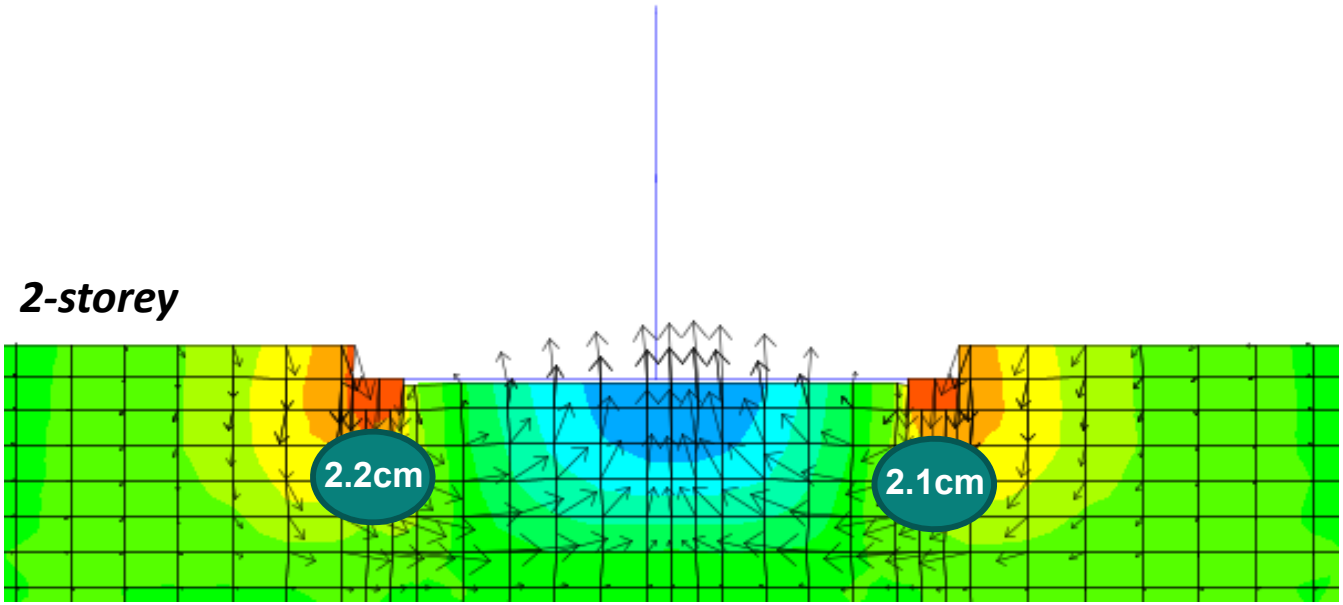


Figure 6-23b

# *Sensitivity Analyses – Number of Storeys*

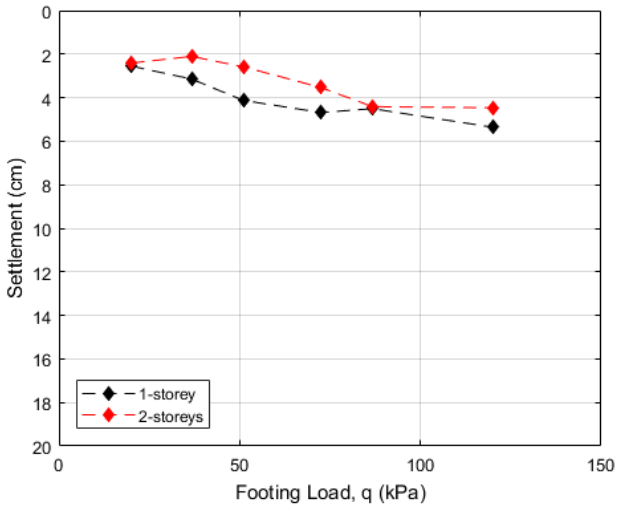


***$H_{cr}$=0.0m, $H_{liq}$=3.0m***

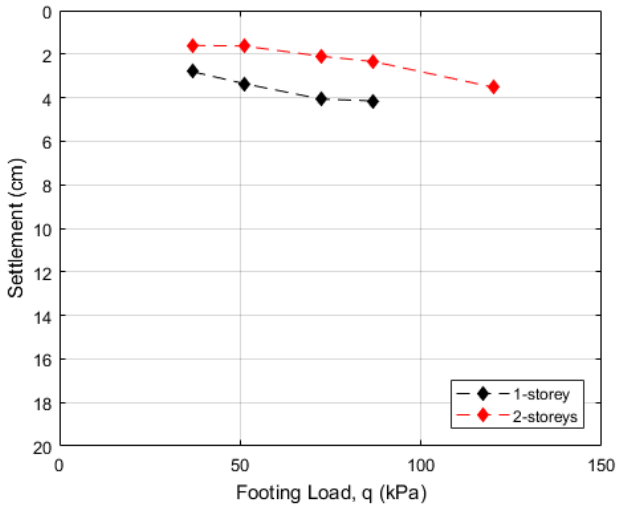


***$H_{cr}$=0.5m, $H_{liq}$=2.5m***

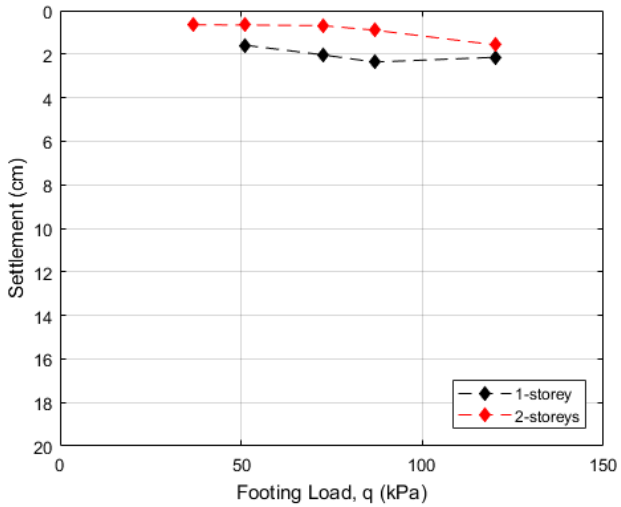


***$H_{cr}$=1.0m, $H_{liq}$=2.0m***

***$D_r$=40%, B=0.7m, $PGA_{scale}$=1.15, motion 4312**

Figure 6-24

# *Sensitivity Analyses – Structural Period*

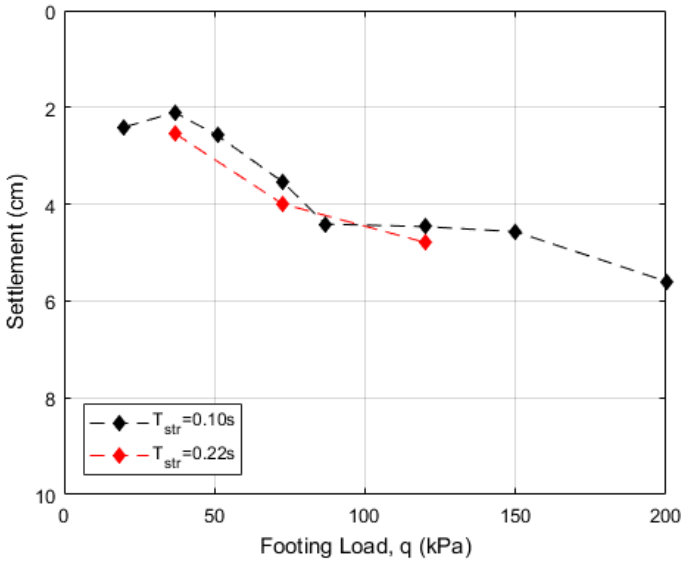


***$H_{cr}$=0.0m, $H_{liq}$=3.0m***

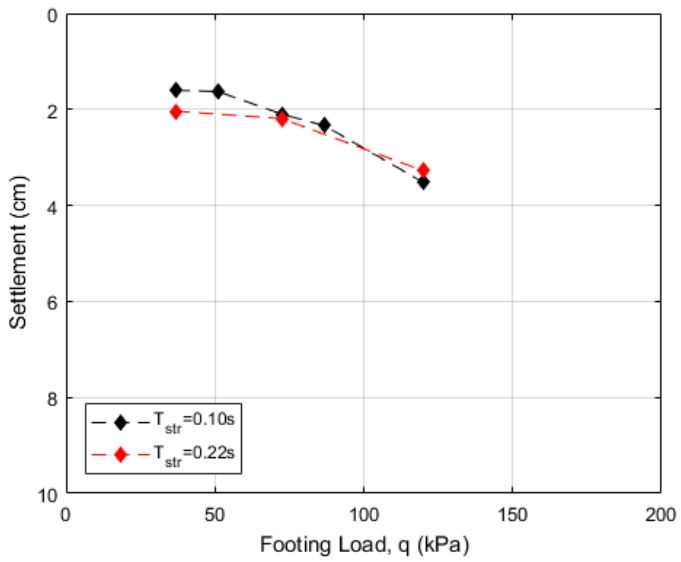


***$H_{cr}$=0.5m, $H_{liq}$=2.5m***

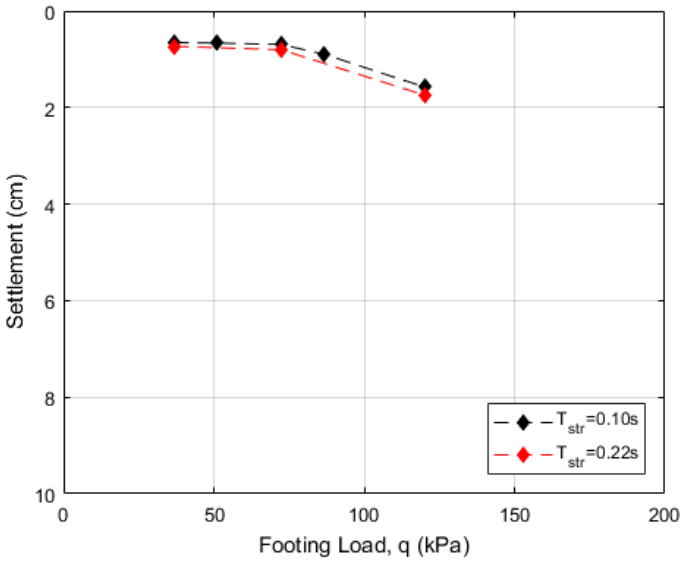


***$H_{cr}$=1.0m, $H_{liq}$=2.0m***

***$D_r$=40%, B=0.7m, D=0.9m $PGA_{scale}$=1.15, motion 4312**

Figure 6-25a

# *Sensitivity Analyses – Structural Period*

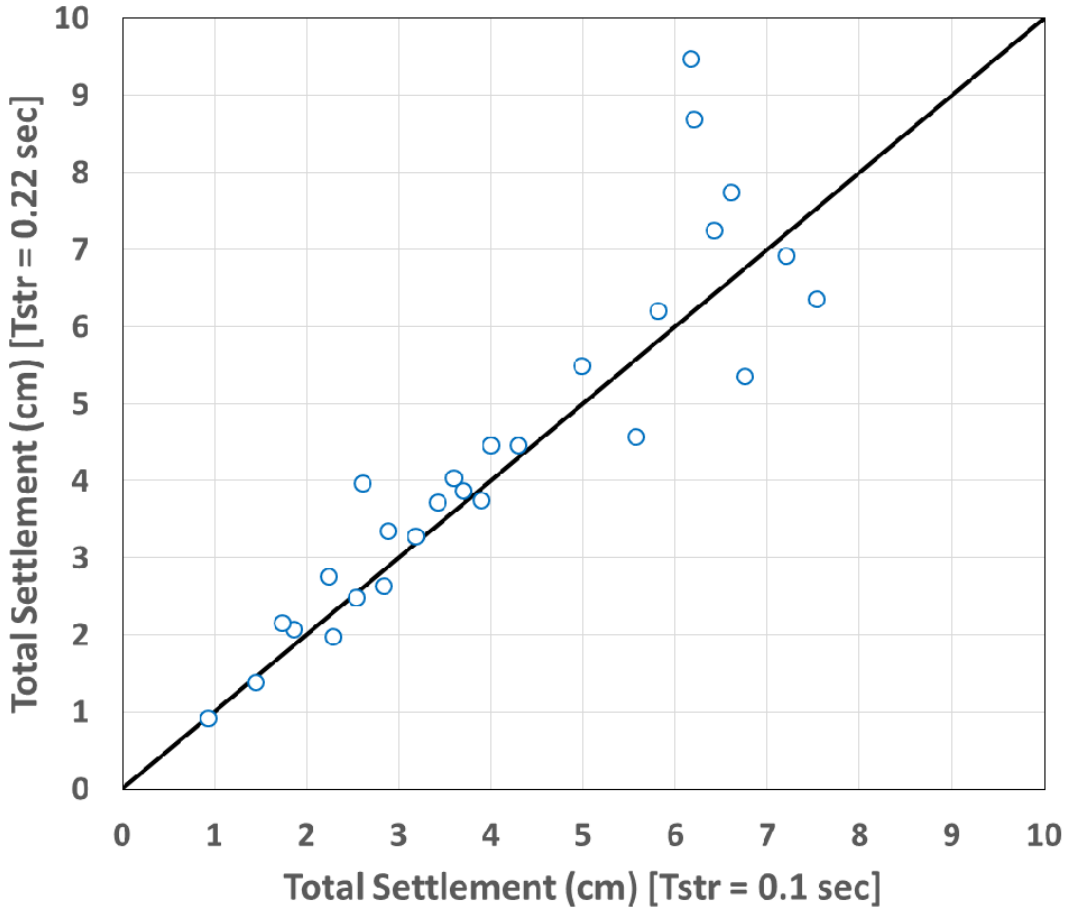


Figure 6-25b

# *Sensitivity Analyses – Number of Storeys*

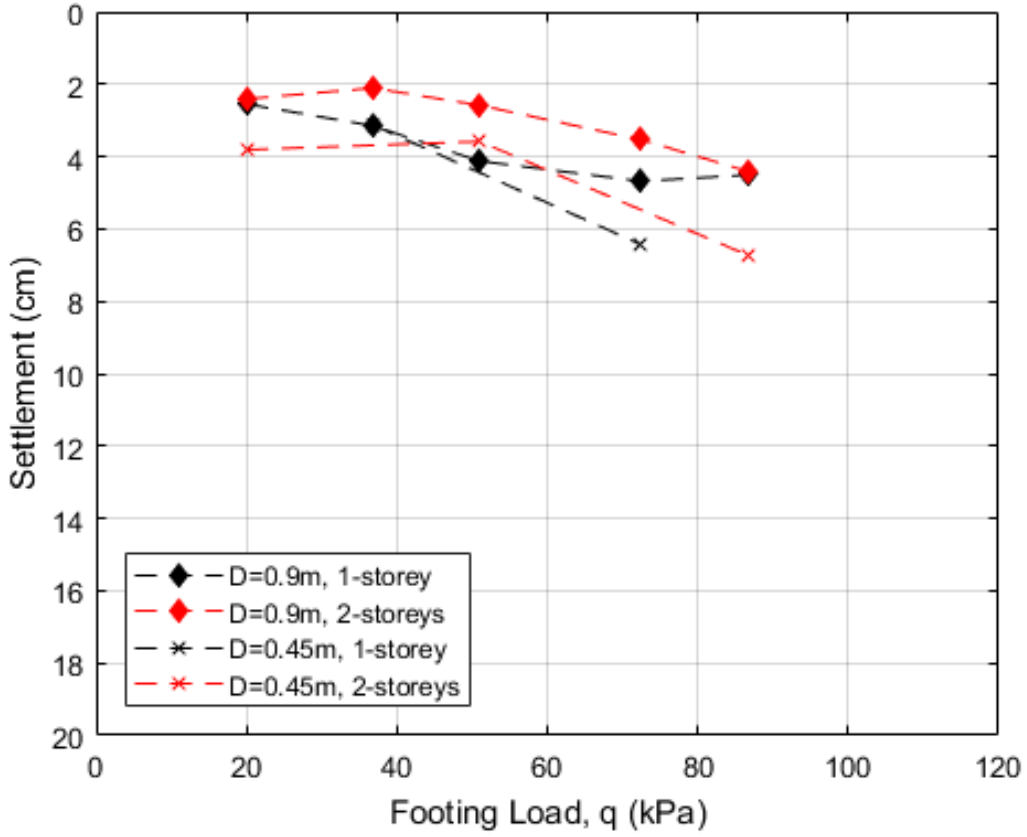


***$H_{cr}$=0.0m, $H_{liq}$=3.0m, $D_r$=40%, B=0.7m, $PGA_{scale}$=1.15, motion 4312**

Figure 6-26

# 7.0 EVALUATION OF BUILDING PERFORMANCE UNDER WORST-CASE SCENARIOS

## 7.1 BACKGROUND

The FLAC2D analyses described in Section 6.0 provide estimates of foundation settlement for a number of scenarios applicable to Groningen residential buildings. These analyses model the dynamics of the settlement process, capture the time-dependent generation, migration, and dissipation of shaking induced pore pressures, and the effects of shaking and pore pressure on soil strength and deformation. The FLAC2D analyses are plane-strain and assume that the section being analyzed extends out uniformly in the longitudinal direction. Consequently, the analyses do not provide a measure of building structural demand nor do they capture the restraint/load from adjacent sections (Figure 7-1).

In this section the impact of a worst-case scenario considering soil variability under the building foundations analyzed in a detailed 3D structural model developed by BICL incorporating Soil-Structure Interaction (SSI) effects through offset soils springs developed by Fugro.

## 7.2 OFFSET SOIL SPRING APPROACH

The offset soil spring approach has historically been used to capture SSI effects associated with displacement-limited soil movement around a structure. An example of such a problem is the assessment of pile foundations that penetrate through an unstable slope. In typical laterally loaded pile foundation analyses, the individual soil springs are developed from monotonic pushover type analyses where the individual pile segments are pushed into the surrounding soils. For the evaluation of piles that penetrate a slope, the individual lateral (p-y) soil springs are modified from those used in typical laterally-loaded pile evaluations by offsetting the load-deformation relative to the origin by the estimated magnitude of slope deformation at that depth. The offset spring is shown relative to a typical soil spring on Figure 7-2. The offset p-y springs thus serve to model:

- The lateral load applied on the pile by the soil flowing around the pile where the pile deformation is less than the movement of the surrounding soil; and
- The lateral resistance offered by soil on to the pile where the pile deformation exceeds the movement of the surrounding soil.

Once the individual offset springs have been developed they are connected to beam elements that represent the structural properties of the pile. The problem is then solved through structural analyses to estimate the deflected shape, and moments induced on the pile due to slope movement. The initial condition in the structural analyses is where the structure has zero displacement. In that condition all segments of the pile connected to offset springs experience a lateral load. The structure deflects under the applied load, continually shedding load in the sliding zone (modeled with offset springs) and gaining soil resistance in the underlying stable zones (springs with no offset or smaller offsets) as displacements increase.

Eventually equilibrium is reached where the stiffness of the pile is able to transfer load into the underlying stable soils. Since the springs model both load on the pile as well as soil resistance, the problem is self-solving with maximum movement of the structure limited to the maximum slope movement.

While the pile foundation problem described above is largely a static problem, the liquefaction-induced foundation settlement process is a dynamic problem with soil movement around the structure characterized by complex time-varying effective stress phenomena.

Consequently for the building SSI evaluations, the offset soil springs are calculated from a series of dynamic FLAC2D analyses, using the PM4Sand constitutive model for potentially liquefiable layers, with different levels of force (upward and downward) applied to the foundation in each analysis. The application of downward or upward force in the dynamic effective stress FLAC2D analyses respectively captures the effect of additional restraint or load from adjacent sections on the predicted final foundation settlement.

An example offset spring developed from a series of FLAC2D analyses is shown on Figure 7-3. The magnitude of the offset at the building vertical load (i.e. in this case 25 kN/m) is the displacement associated with an unrestrained FLAC2D analyses (similar to those described in Section 6.0). The application of downward force on to the foundation increases the predicted settlement. Similarly the application of upward force on the foundation decreases the predicted settlement until the point where the force becomes equal to the building dead load where the settlements predicted are equal to the free-field volumetric settlements (i.e. at 0 vertical load).

Offset springs were developed for the worst case scenario presented in Section 6.0 where a 1-m-thick crust is present under one footing while the other footing rests directly on a 3-m-thick, 40% relative density liquefiable sand layer (Figure 7-4). Each point on the springs shown on Figure 7-4 represents the foundation settlement (co-seismic and post seismic) from a dynamic analysis under a specific footing pressure. Since the springs are estimated from dynamic analyses, each set of springs is associated with a given input time history, in this case with motion 4312 and scaling factor 1.15.

The offset springs are then connected to the 3D detailed structural model of the building (Figure 7-5) and structural analyses are conducted to calculate the post-earthquake building deformations and associated structural demands. As discussed below an additional sensitivity analysis was considered where a y-multiplier of 2 was applied to the offset springs, thus doubling the ground deformation.

The structural analysis was conducted by BICL and are described below. Sensitivity of the results to assumptions regarding the spatial soil variability (i.e. location of crust/no crust under the building) that causes building distortion was also evaluated as discussed below.

## 7.3 3D DETAILED STRUCTURAL EVALUATIONS BY BICL

### 7.3.1 General approach

The general approach to estimating the differential settlements was to complete a structural analysis by applying the gravity structural loads (self-weight and live loads) onto a modelled representation of the building which was supported on the offset springs derived as outlined above. The analyses were completed without introducing inertial earthquake loads so can be considered representative of the settlements that might be expected to occur after the earthquake shaking has occurred and the pore water pressures have dissipated.

The differential settlements where taken as the maximum difference between the settlements determined from the analysis over the building footprint along critical wall lines.

As the objective was to determine the effect of the differential settlements on the building, the stresses and strains within the building structure were reviewed from the analyses to determine the expected damage within the building and, in particular, how this compared with the state of near collapse (NC).

The approach is indicated diagrammatically on Figure 7-5.

### 7.3.2 Computer structural model

The analyses were completed using the SAP structural analysis computer program.

The building structure was modelled using the equivalent frame approach. This is a standard technique used in analysing this type of structure (Pasticier et al. 2008) and models the walls and spandrel panels as centreline column and beam elements respectively. The effect of the element size (i.e. the distance from the equivalent frame centreline to the edge of the actual element) was accounted for by introducing rigid element offsets. This included the offset of the structural wall to the centreline of the strip footing.

The model was three dimensional and non-linear effects were modelled using nonlinear backbone models, typically introduced at the element ends. Only the structural elements that could potentially provide resistance against differential settlement were included in the model. This is considered to be a conservative assumption as it might be expected that some secondary elements (e.g. the roof) would provide some resistance to differential settlements. However, the conservatism introduced is considered to be acceptable.

Floor diaphragms were modelled as plate element interconnecting the tops of the walls at the height of the ground floor. The connection between the floor and the walls was pinned for rotations perpendicular to the wall face.

The flexural capacity of the brick foundation strip footings was modelled at the ends of the wall rigid element offsets but once exceeded was assumed to drop to zero to represent the effect of cracking of these unreinforced elements. The shear resistance was, however, assumed to be maintained. This is considered to be a reasonable assumption, particularly given the extent of cracking that was finally predicted.

A view of the model of the building is shown in Figure 7-6.

Secondary and non-structural elements were not included in the model. The effect of the differential settlements on state of NC (eg. rotation of floors on walls) is intended to be dealt with by considering the effect of the distortions between these elements after the analysis is complete. On the results collected to date, and described below, there is clearly insufficient distortion involved to cause an issue for these elements of the building in terms of the NC state.

Three different support cases were investigated. These are shown in Figure 7-7.

These were chosen to represent differential support conditions that could be expected to result in differential settlements of the building and distortions within the building structure. The settlement - load behaviour provided by areas of Crust and No Crust were modelled using the offset springs. Springs appropriate for each support condition (i.e. with crust or no crust) were introduced under relevant sections of the footings for each scenario. These are shown diagrammatically in Figure 7-7 where the green and red dotted lines indicated where the Crust and No Crust offset springs respectively were included

The analyses were allowed to run and the distortions within the building determined, including settlement of the footing and yielding of the structural elements. The results of these analyses are discussed below.

### 7.3.3 Analysis results

Analysis results are provided in Figures 7-8, 7-9 and 7-10 for each of the cases out lined above. In addition a sensitivity analysis was completed to determine the effect of halving

the soil spring stiffness (i.e. doubling ground deformation) for the same Crust /No crust division for Case 1. The results for this analysis is given in Figure 7-11.

For each case the figures indicate the predicted settlement and differential settlement along the critical wall, and the distortion within the building recorded as an inter-storey drift and the extent of yielding predicted within the structure.

For Cases 1, 2 and 3 maximum settlements of 75, 75 and 77 mm were predicted and the predicted differential settlements were 45, 45 and 30 mm respectively. These differential settlements were sufficient to cause stresses in excess of yield in the walls in a very few locations in the structure but, as noted on the figures, in all cases the level of yield was minor and consistent with maximum crack widths of less than 1 mm.

The level of cracking and the resulting inter-storey drifts are well below those that could be considered consistent with a NC state.

The sensitivity analysis performed by doubling ground deformation (Figure 7-11) indicates maximum settlements of 145 mm and differential settlements of 120 mm. As expected yielding is higher but the maximum nonlinear strains are still low at less than 10% of the yield strain. This is consistent with maximum crack widths of approximately 2 mm. As for Cases 1, 2 and 3 we believe that this indicates a state of stress well below NC.

# Section 7

## Structure in 3D

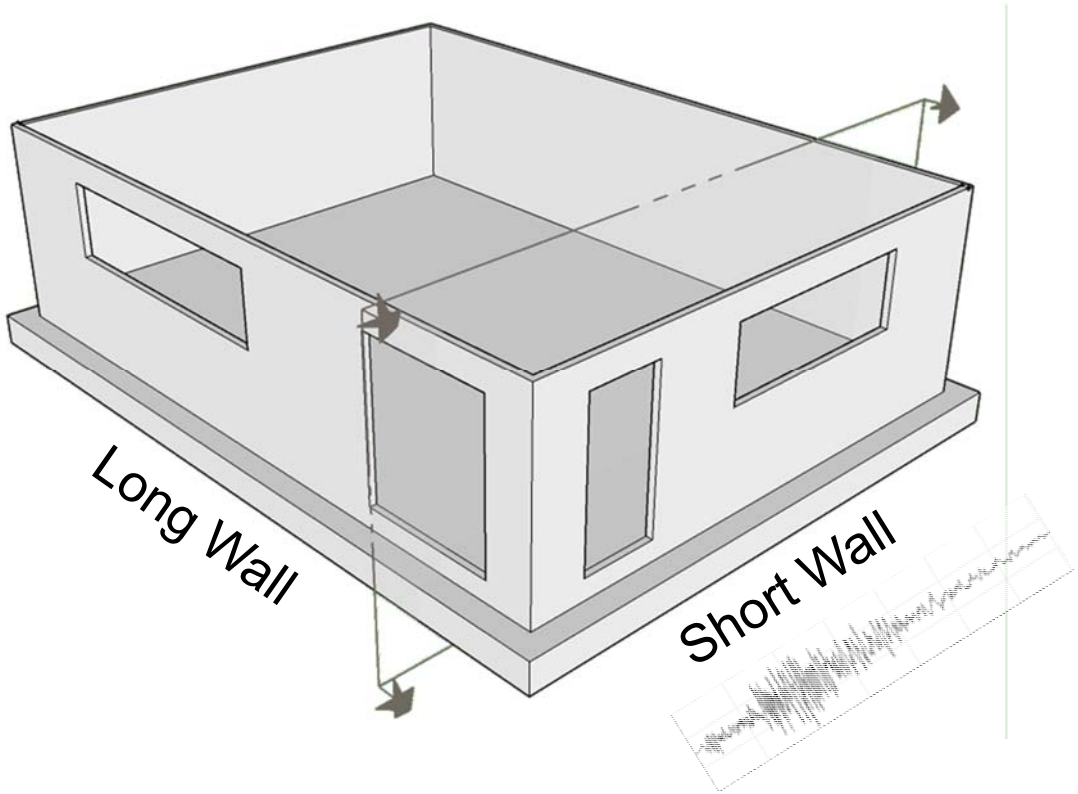


## Structure analysed in 2D

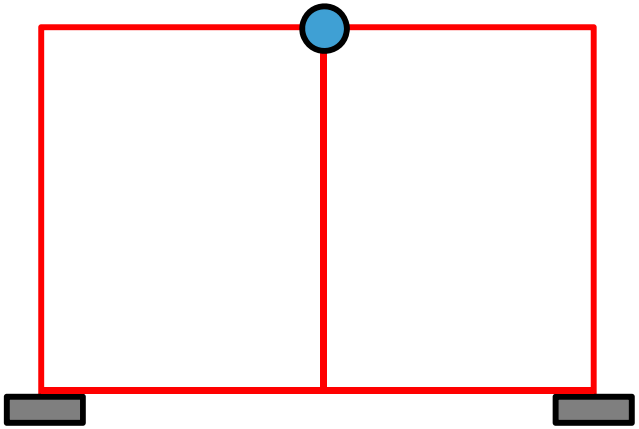

***Restraint/load from adjacent sections is not captured in 2D model***

Figure 7-1

# Offset Springs

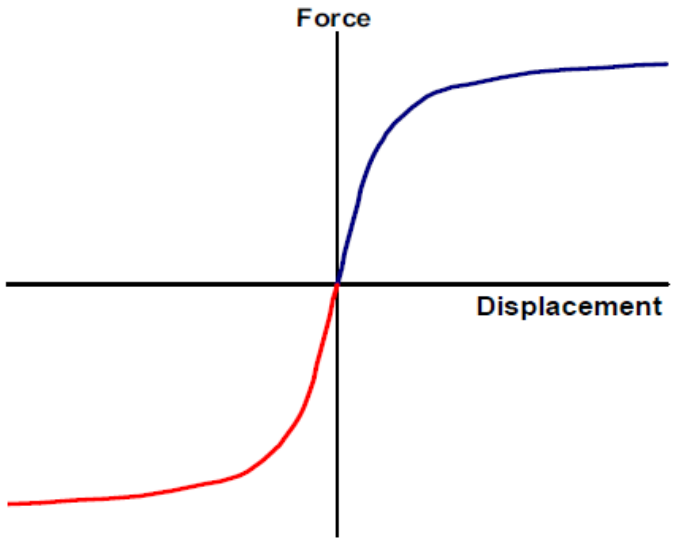


Typical Soil Spring

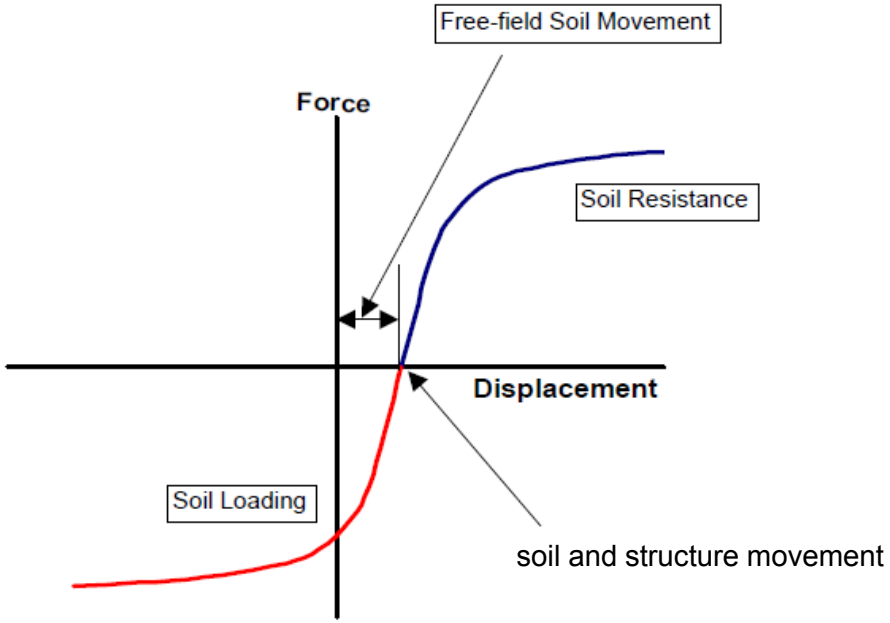


Offset Soil Spring

Figure 7-2

## Offset Spring for Footing Settlement

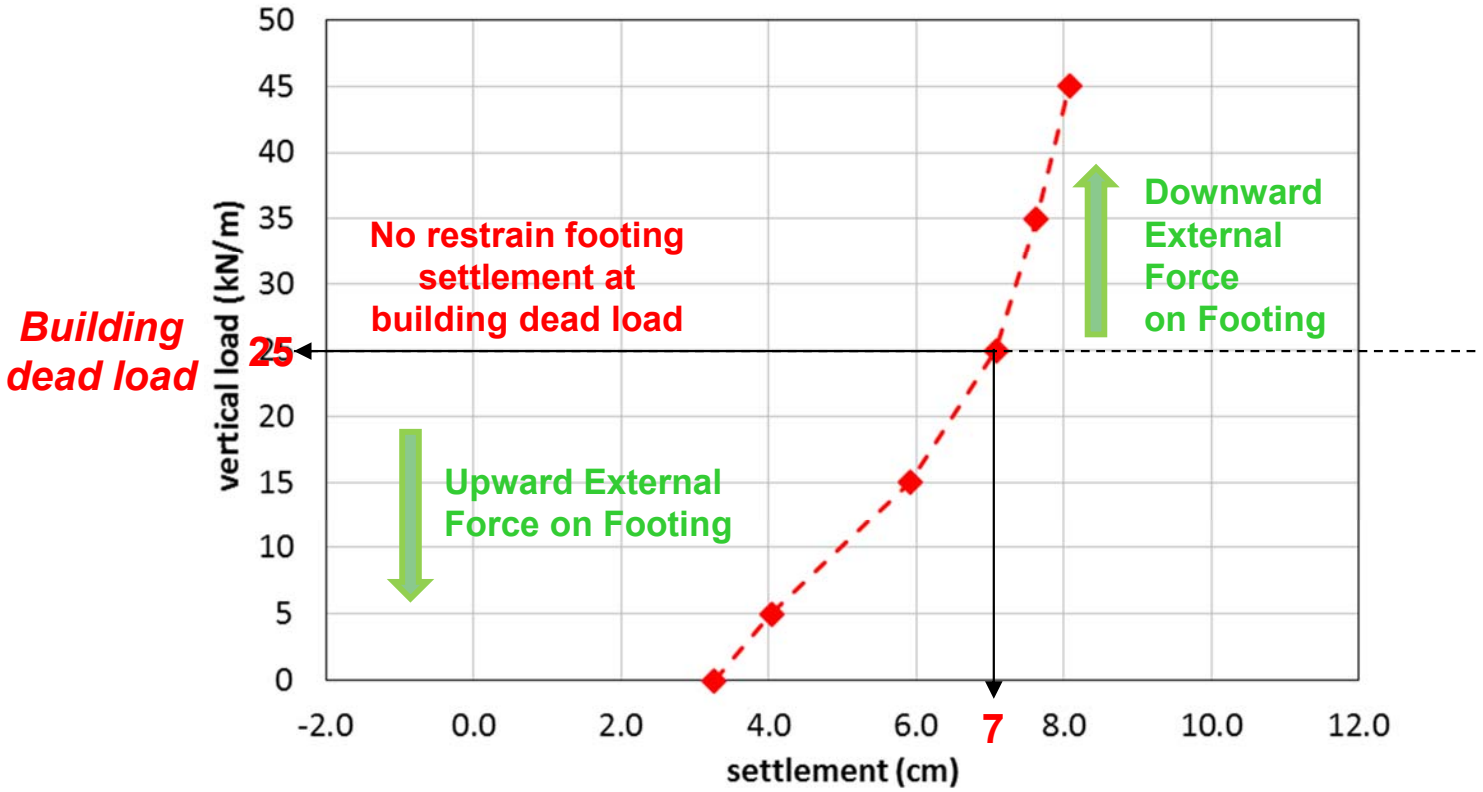


Figure 7-3

## Offset Springs for Differential Soil Conditions

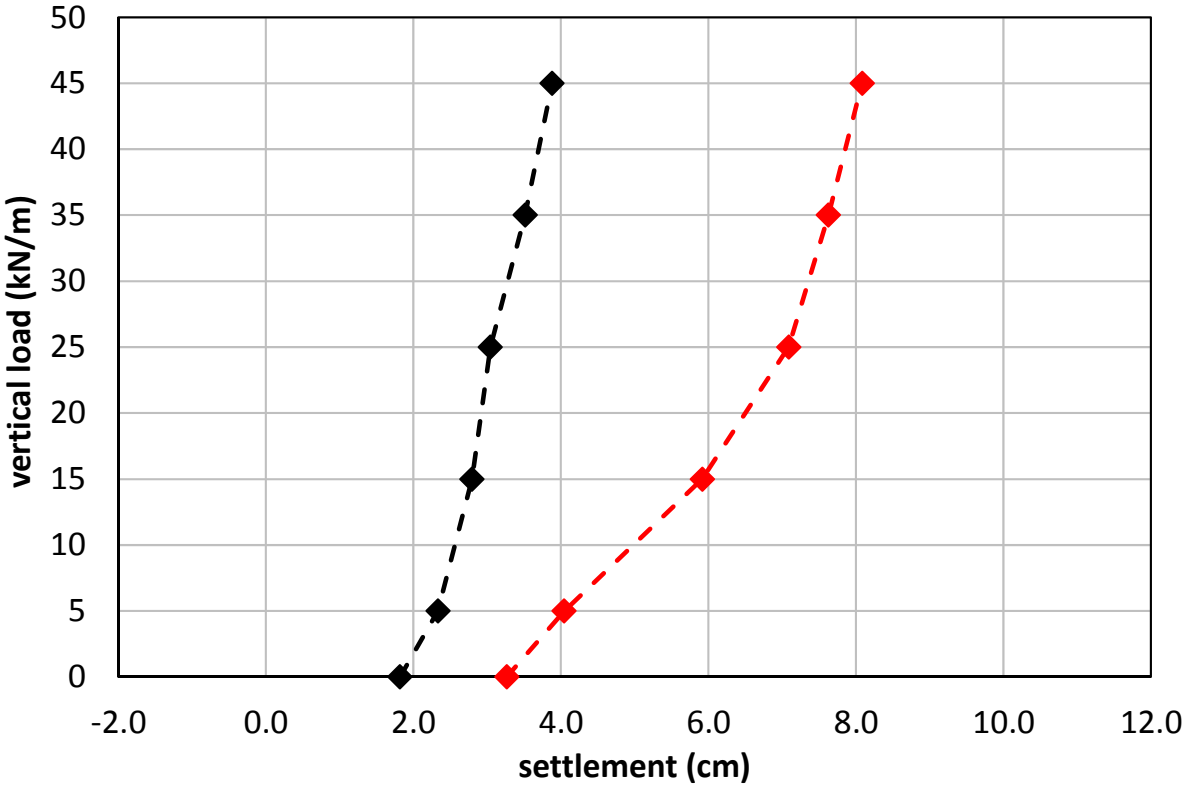


**Footing above crust**

**Footing above sand**

Figure 7-4

# General arrangement assumptions for differential settlement calculations

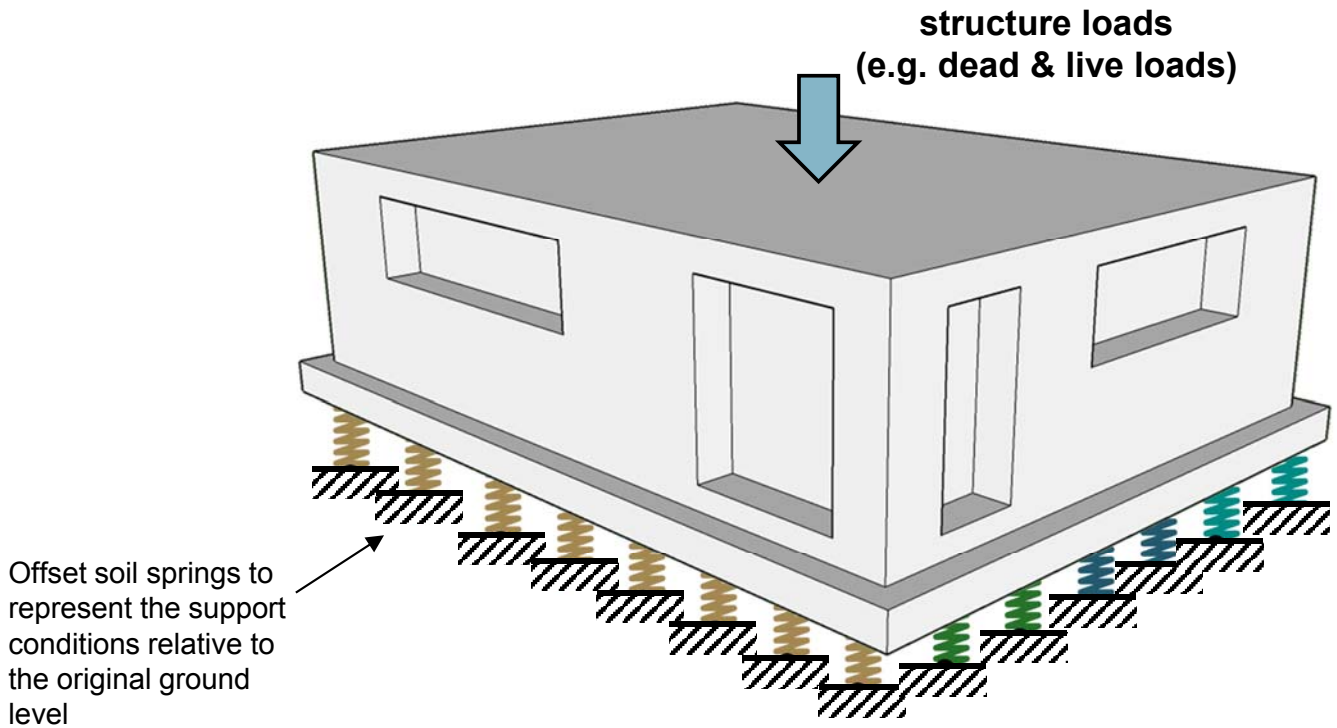


***Differential settlements are applied through the different springs (in terms of stiffness) along the perimeter of the building and this will impose strains on the superstructure***

Figure 7-5

# *General view of equivalent frame computer model*

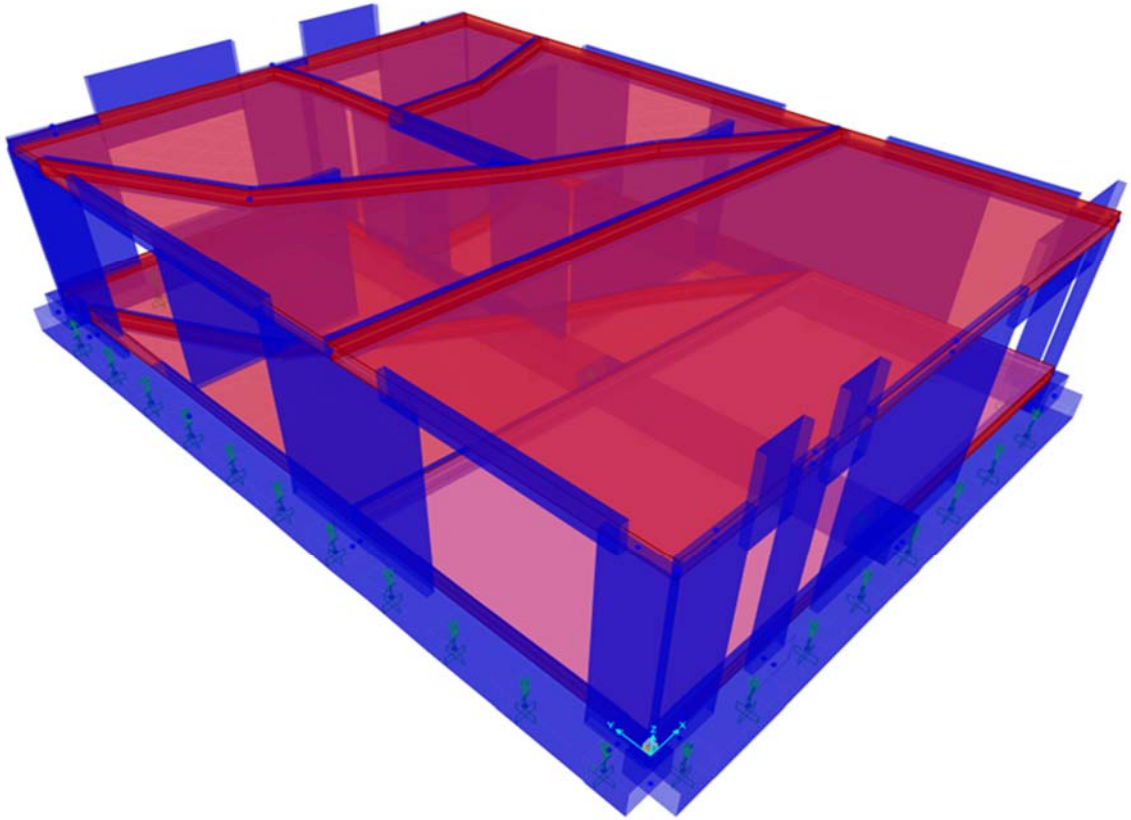

Figure 7-6

# *Differential Support Assumptions*

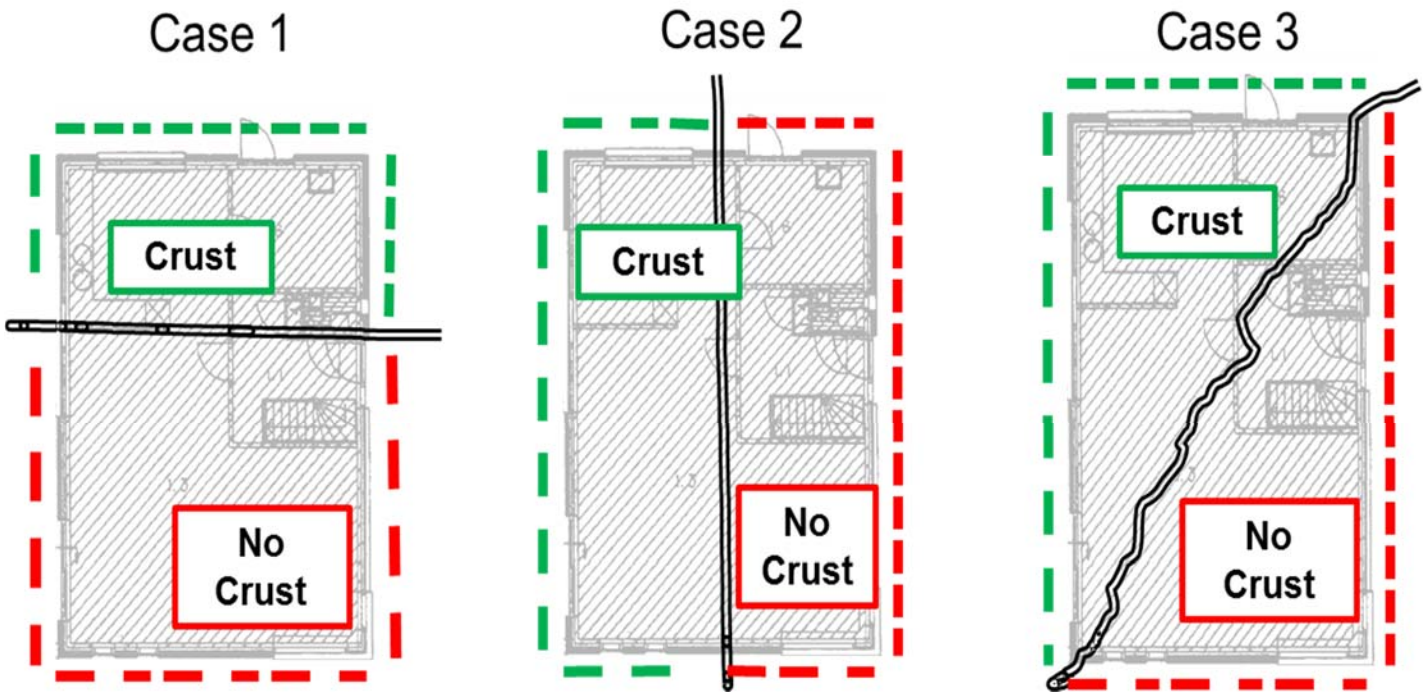


Figure 7-7

# *Settlement analysis results for Case 1 – Crust/No crust division across transverse direction*

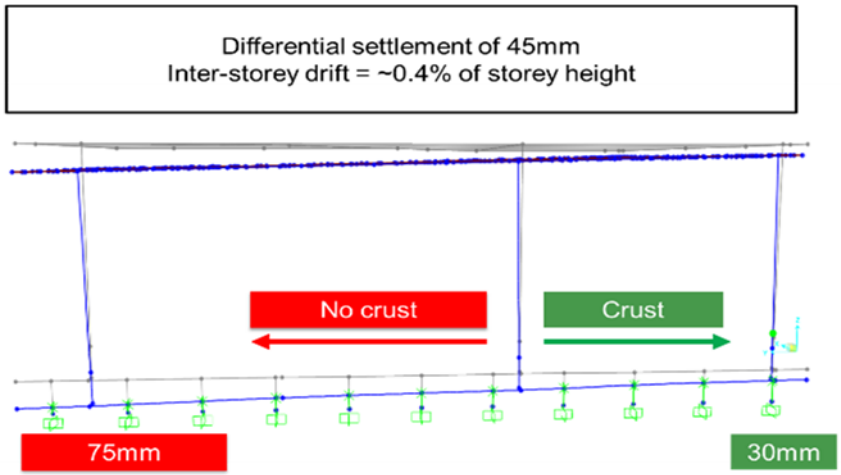


(a) Indicative settlements and differential settlements along longitudinal walls

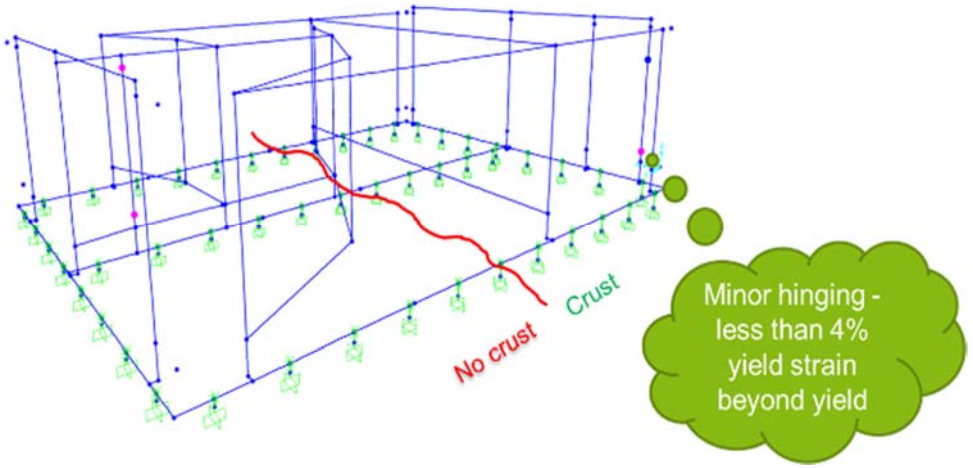


(b) Yeilding elements (shown as pink dots)

Figure 7-8

# *Settlement analysis results for Case 2 – Crust/No crust division along longitudinal direction*

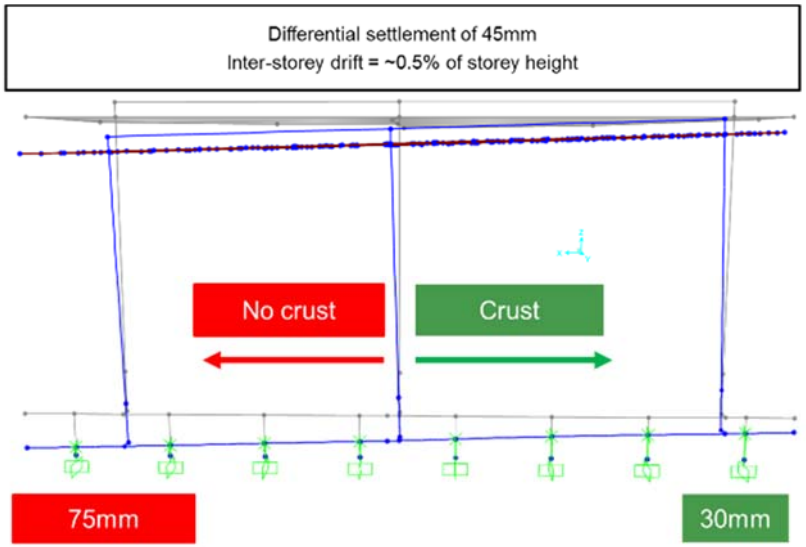


(a) Indicative settlements and differential settlements along transverse walls

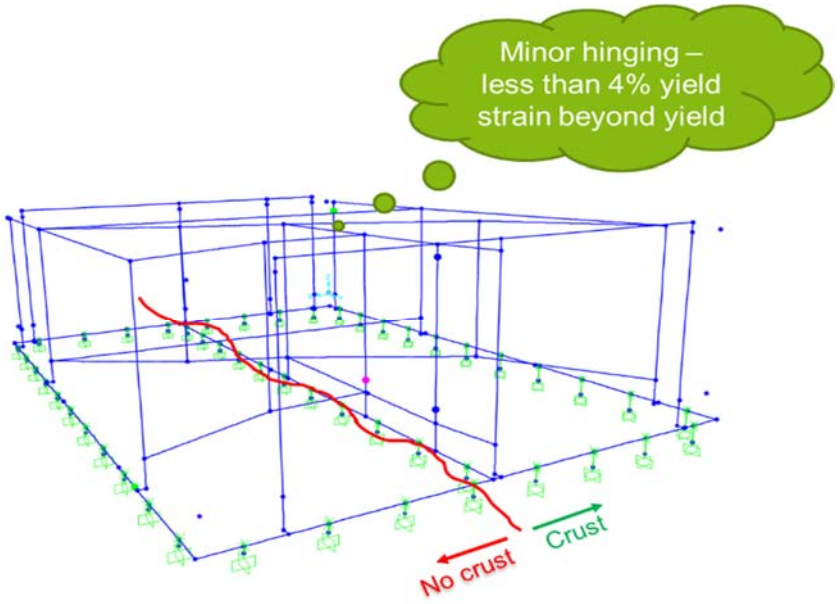


(b) Yilding elements (shown as pink dots)

Figure 7-9

# *Settlement analysis results for Case 3 – Crust/No crust division aligned diagonally*

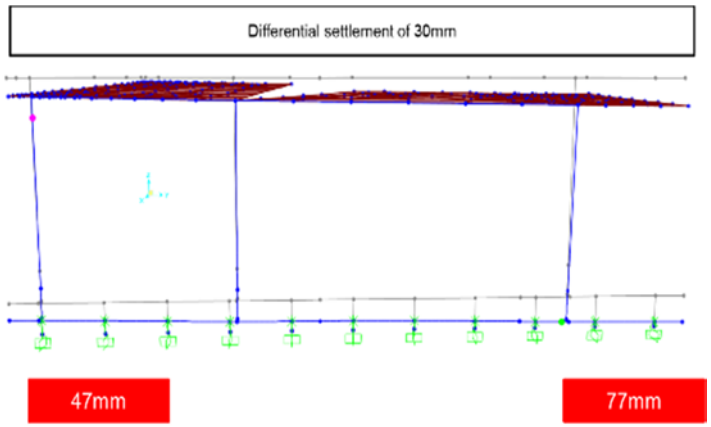


(a) Indicative settlements and differential settlements along the longitudinal wall over no crust

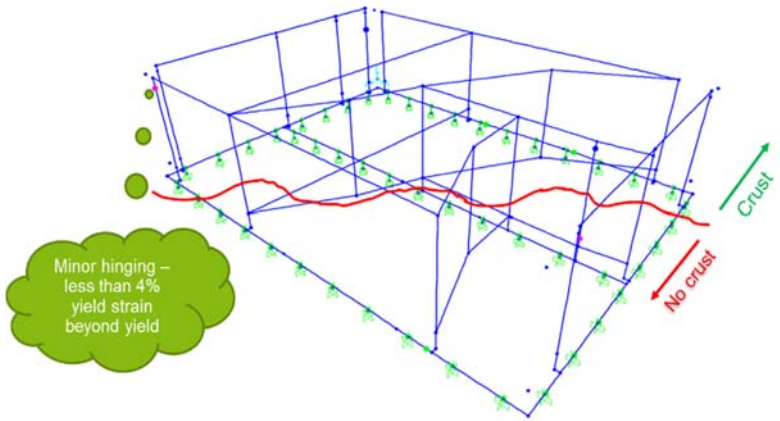


(b) Yilding elements (shown as pink dots)

Figure 7-10

## *Settlement analysis results for sensitivity Case 1 with soil spring stiffness reduced by a factor of two (doubling ground deformation) – Crust/No crust division across the transverse direction*

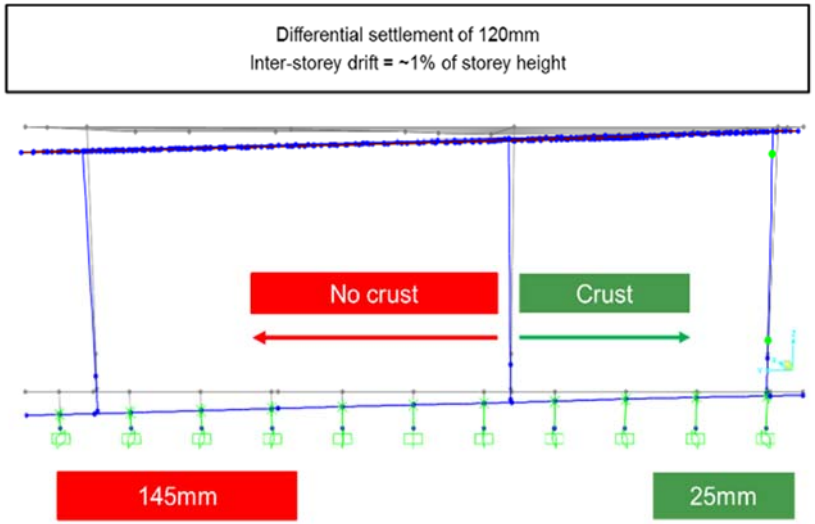


(a) Indicative settlements and differential settlements along the longitudinal wall over no crust

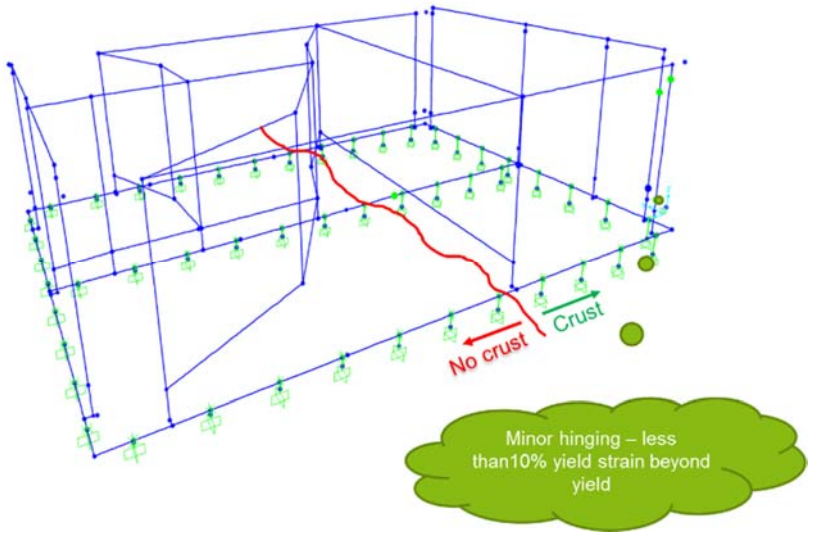


(b) Yilding elements (shown as light blue dots)

Figure 7-11

# 8.0 REGRESSION ANALYSES

## 8.1 BACKGROUND

The results of the parametric numerical analyses presented in Section 6.0 revealed that liquefaction-induced footing settlement is a function of several parameters related to the geometry of the footing, the stratigraphy and properties of the soil, and the seismic demand.

In an attempt to provide recommendations for evaluating building settlements at liquefiable sites, recent research (i.e. Bray and Macedo 2017) has led to simplified procedures in the form of equations derived from regression of numerical results. However, these efforts are focused on buildings resting on continuous rigid slab foundations (i.e. minimum footing widths of about 6 meters) under relatively large earthquake events (i.e. corresponding to magnitudes larger than $M_w$ 6) and therefore the basis of the recommended simplified procedures do not appear applicable to the vast majority of the buildings in Groningen area.

Following a similar approach, the results of the parametric study presented in this report were regressed to develop a design equation that can be used to derive estimates of liquefaction-induced settlements for typical residential buildings in Groningen.

## 8.2 REGRESSION ANALYSIS

Based on the trends identified between liquefaction-induced settlements and various parameters through the review of the numerical analyses results, and following the Bray and Macedo (2017) approach, several functional forms were investigated to represent the total footing settlement due to liquefaction (i.e. including both co-seismic shear-induced and post-seismic reconsolidation settlements). The functional form that was selected based on the quality of fit to the available numerical results is given by the following equation:

$$ln(s) = a_0 + a_1\, ln(Q) + a_2 B + a_3 H_{crust} + a_4\, ln\big(tanh\big(H_{liq}\big)\big) + a_5 Dr + a_6 l\, n(IM1) + a_7 l\, n(IM2) + \varepsilon$$

where $s$ is the total (co-seismic plus post-seismic) liquefaction-induced settlement of the footing [cm], $Q$ is the footing contact pressure (load) [kPa], $B$ is the width of the footing [m], $H_{crust}$ is the thickness of the non-liquefiable soil below the footing [m], $H_{liq}$ is the thickness of the liquefiable soil layer [m], $D_r$ is the relative density of the liquefiable soil [%], IM1 and IM2 are intensity ground motion parameters, $\alpha_0$ to $\alpha_7$ are the regression coefficients, and $\varepsilon$ is the error term in log units.

In order to select the most suitable intensity ground motion parameters for the regression model, several regression analyses were performed using the equation presented above and considering each time different intensity measure parameters or combinations of them. The examined intensity measures include ground motion parameters for the input ground motion at -25 m NAP (outcrop) as well as for the surface ground motion estimated from a total-stress site response analysis. Figure 8-1 summarizes the $R^2$ values obtained from the regressions considering each one of the intensity measure parameter. It is observed that Arias intensity of the input ground motion provides the best fit to the data while PGA at surface seems to be the least reliable predictor. Although Arias intensity (IA) and cumulative absolute velocity (CAV / $CAV_{dp}$) show better correlation with settlement, it was decided to use ground motion parameters that are readily available to the practitioners in Groningen through the v4 (or v5) GMM. For this reason, the significant duration $D_{5\text{-}75}$ at the ground surface and the 5%-damped spectral acceleration at 0.7sec period at the ground surface were selected for the regression model. The $R^2$ value obtained using these two intensity measure parameters is highlighted in Figure 8-1 (blue bar). Figure 8-2 compares the distribution of the residuals from

the regression using different intensity measures. It is observed that despite the slightly lower $R^2$ value, the regression using $D_{5\text{-}75}$ and $Sa_{T=0.7s}$ at the surface results in a rather normal distribution of residuals around zero, quite similar to those obtained using intensity measures with higher $R^2$ values.

In light of the above, the regression is performed with the equation below:

$$ln(s) = a_0 + a_1\, ln(Q) + a_2 B + a_3 H_{crust} + a_4\, ln\left(tanh\left(H_{liq}\right)\right) + a_5 Dr + a_6 l\, n(D_{5-75}) + a_7 l\, n(Sa_{T=0.7s}) + \varepsilon$$

where $D_{5\text{-}75}$ is the significant duration of the motion at the free-field ground surface [sec], $Sa_{T=0.7s}$ is the 5%-damped spectral acceleration at 0.7sec period at ground surface [g], $\varepsilon$ is the error term, and all the other parameters have been described above.

### 8.2.1 Regression Analyses on Single-storey House Analyses Results

The regression was initially performed with the numerical results from the analyses of the single-storey building and using the equation above. The single-storey house regression resulted in the following model coefficients: $\alpha_0 = 2.096$, $\alpha_1 = 0.308$, $\alpha_2 = 0.749$, $\alpha_3 = -0.353$, $\alpha_4 = 1.991$, $\alpha_5 = -0.031$, $\alpha_6 = 0.581$, and $\alpha_7 = 1.899$. The distribution of the regression residuals versus the predicted settlement values are shown on Figure 8-3(a). It is observed that the residuals vary symmetrically around zero, revealing a sufficiently good fit of the functional form to the data from the numerical analyses. The comparison of the predicted settlement values with the "actual" structure response (i.e. settlements calculated from the numerical analyses) is shown on the same figure, both in real and log units (graphs b and c, respectively). The concentration of the data points close to the diagonal in log units (graph c) supports the selection of a linear form to predict the logarithm of settlement.

Additional measures of the regression goodness are provided on Figure 8-4. Graph (a) presents a histogram of the residuals which seem to be normally distributed around zero. A fitted normal distribution plotted on top of the histogram (red line) verifies the hypothesis. The same conclusion is drawn from graph (c) which shows the cumulative frequency distribution of the residuals (blue x's) compared to the normal distribution (black dashed line). Graph (d) illustrates the symmetry of the distribution of residuals around their median value.

The error term $\varepsilon$ of the predicted total settlement was estimated from the variance of the residuals calculated from the regression analysis. The uncertainty in the estimate of footing total settlement, given a set of input parameters, is a normal random variable with $\mu = 0$ and $\sigma = 0.465$ in Ln units. In real units, this is translated to a multiplication factor $e^{\pm\lambda\sigma}$ applied to the mean settlement prediction in order to obtain the $\mu \pm \lambda\sigma$ settlement values. Figure 8-5 presents the 5-95% interval (dashed lines) of the predicted settlement values. An example that illustrates the range of the expected liquefaction-induced settlement is presented on the same figure [red whiskers]. Based on the regression of the available numerical results, if for a particular set of input parameters, the equation presented above predicts a mean total settlement of about 3 cm, the 90 percent confidence interval for settlements is between about 1.5 cm and 6.5 cm.

The regression presented above was based on the results from the numerical analyses of the single-storey structure. The impact of the two-storey building analysis results on the regression equation is examined below.

### 8.2.2 Regression Analyses Including Two-storey House Analyses Results

Review of the numerical analyses results of the two-storey building showed, in general, similar trends of settlement magnitude with the variables considered in the regression analysis

presented above. Based on this observation, it was presumed that the same functional form would apply to the two-storey building as well. As a first check, the ability of the equation derived based on single-storey house analyses results to “predict” settlements for two-storey houses was evaluated. Figure 8-6 presents the “actual” terraced house settlements estimated from the numerical analysis (y-axis) plotted against the “predictions” from the equation presented in Section 8.2.1 (x-axis). The vast majority of the points fall below the 1:1 curve (black line) indicating that the settlement prediction equation tends to overestimate settlements of the two-storey buildings. This trend is in agreement with the observation made from the review of the two-storey building analyses results that showed a tendency for terraced houses to settle less than the single-storey buildings.

Subsequently, the dataset used to derive the regression presented in Section 8.2.1 was extended to include the results from the numerical analyses of the terraced house and the full dataset was regressed to update the settlement prediction equation.

The regression performed with the numerical results from the analyses of both the single- and the two-storey buildings, and using the equation presented in Section 8.2.1 resulted in the following model coefficients: $\alpha_0 = 2.570$, $\alpha_1 = 0.200$, $\alpha_2 = 0.742$, $\alpha_3 = -0.454$, $\alpha_4 = 1.924$, $\alpha_5 = -0.031$, $\alpha_6 = 0.588$, $\alpha_7 = 1.900$, and $\sigma = 0.458$. The distribution of the regression residuals versus the predicted settlement values are shown on Figure 8-7(a). It is observed that the residuals vary symmetrically around zero, revealing a sufficiently good fit of the functional form to the data from the numerical analyses. The comparison of the predicted settlement values with the “actual” structure response (i.e. settlements calculated from the numerical analyses) is shown on the same figure, both in real and log units (graphs b and c, respectively). The concentration of the data points close to the diagonal in log units (graph c) supports the selection of a linear form to predict the logarithm of settlement.

Additional measures to evaluate regression goodness are provided on Figure 8-8. Graph (a) presents a histogram of the residuals which seem to be normally distributed around zero. A fitted normal distribution plotted on top of the histogram (red line) verifies the hypothesis. The same conclusion is drawn from graph (c) which shows the cumulative frequency distribution of the residuals (blue x’s) compared to the normal distribution (black dashed line). Graph (d) illustrates the symmetry of the distribution of residuals around their median value.

Figure 8-9 presents the 5-95% interval (dashed lines) of the predicted settlement values. An example that illustrates the range of the expected liquefaction-induced settlement is presented on the same figure [red whiskers]. If the equation presented above predicts a mean total settlement of about 3 cm, the expected settlement ranges from about 1.5 cm to 6.5 cm with a 90% confidence interval.

Figure 8-10 summarizes the differences in the regression analysis including or not the two-storey building results. Including the terraced house analyses suggest a slightly smaller influence of load and liquefiable layer thickness on settlements and a slightly larger influence of crust thickness. However, for all practical purposes, no significant impact was identified.

# Section 8

# Selection of Intensity Measure

## $R^2$ value for different intensity measures

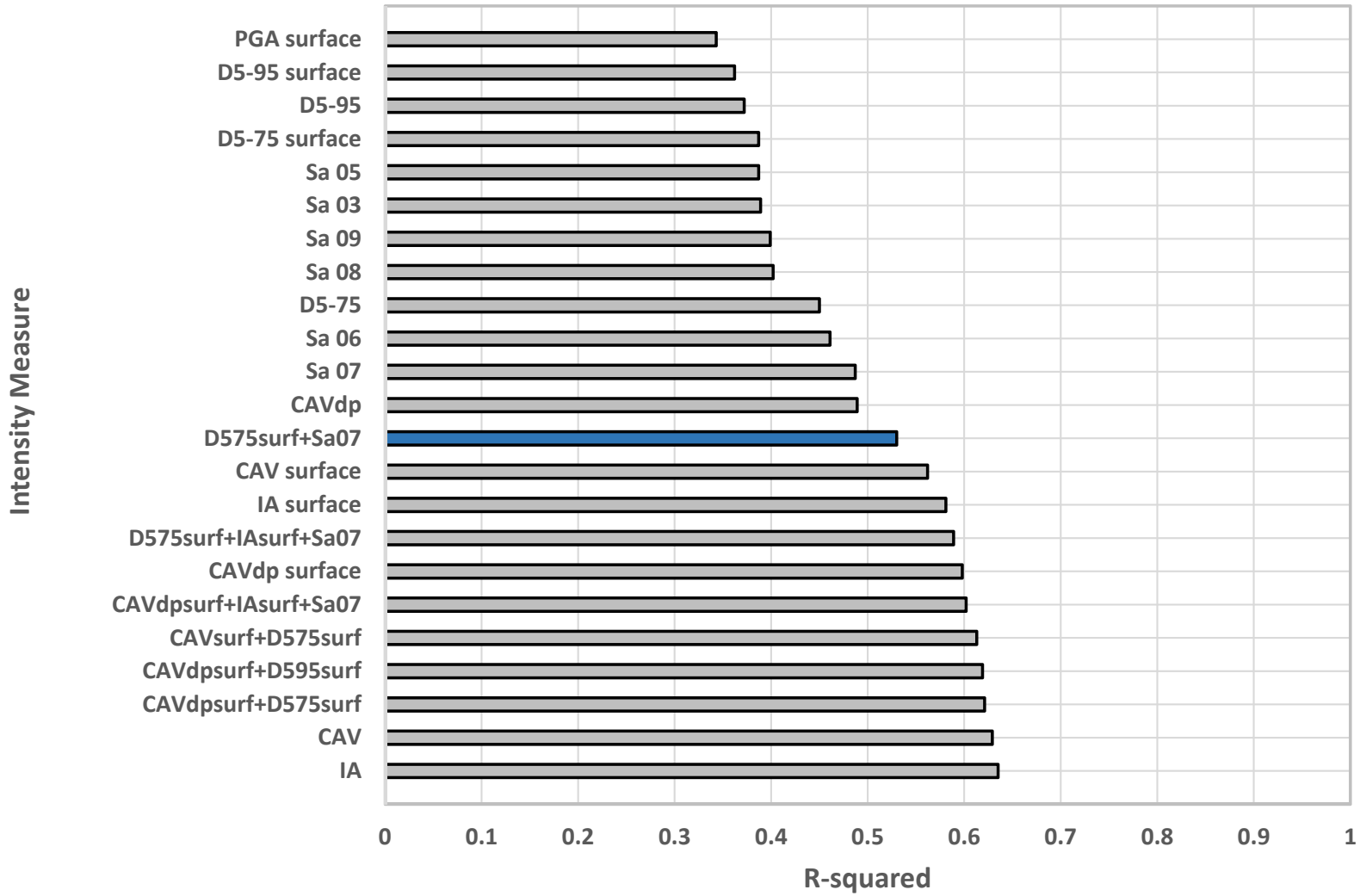


Figure 8-1

# Selection of Intensity Measure

$D_{5\text{-}75,surf} + Sa_{T=0.7s,surf}$

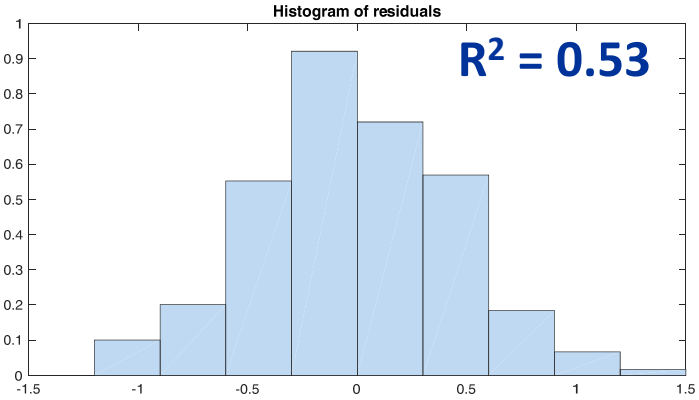


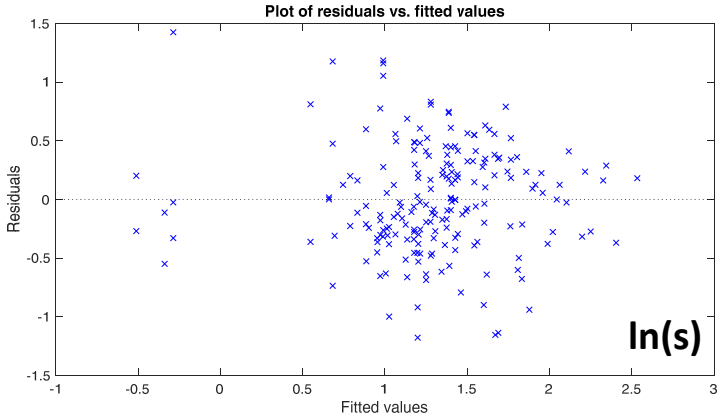


$I_{a,\ surface}$

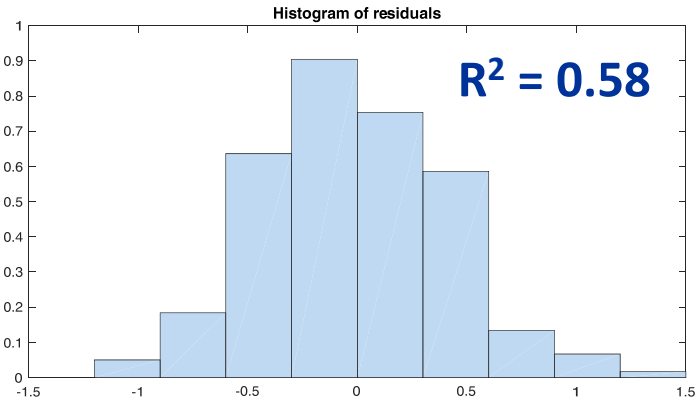


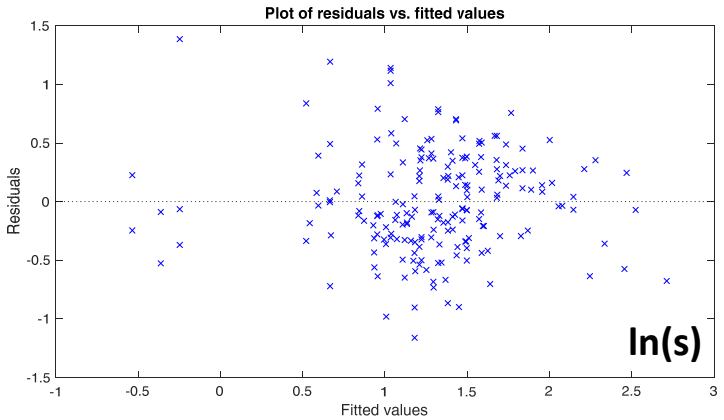


$CAVdp_{surface}$

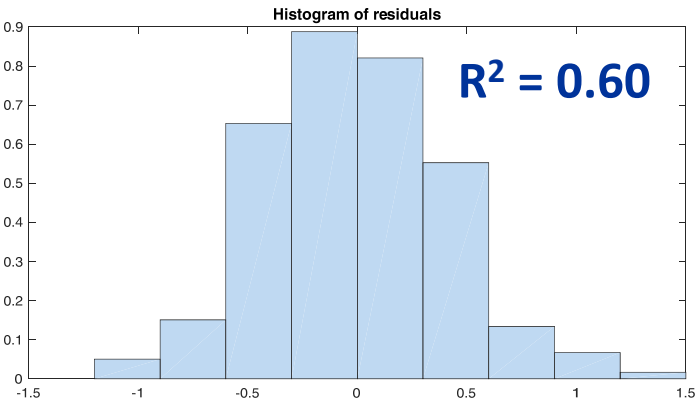


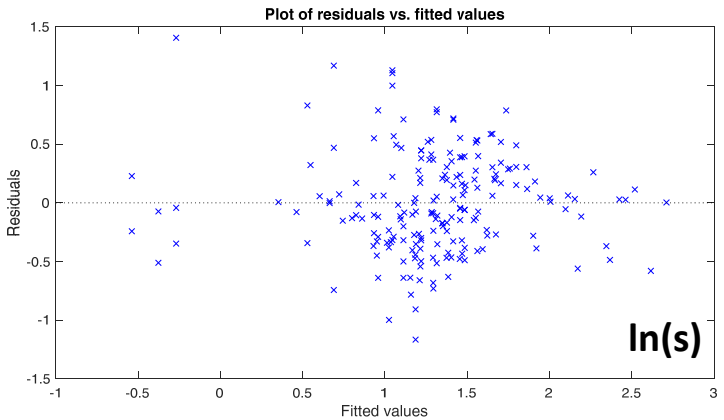


Figure 8-2

# *Multiple Linear Regression*

$$\ln(s) = a_0 + a_1 \ln(Q) + a_2 B + a_3 H_{crust} + a_4 \ln\left(\tanh\left(H_{liq}\right)\right) + a_5\, Dr + a_6 \ln(D_{5-75}) + a_7 \ln(Sa_{T=0.7s})$$

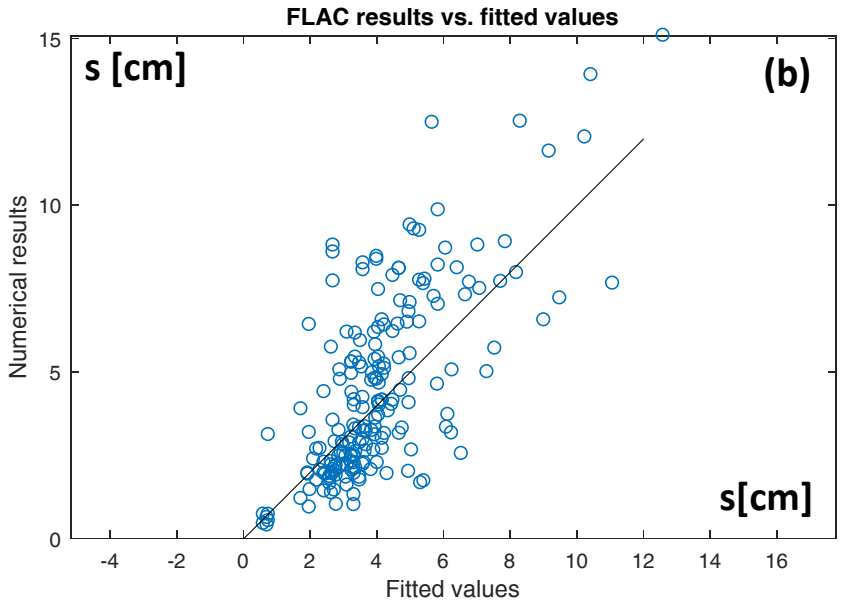


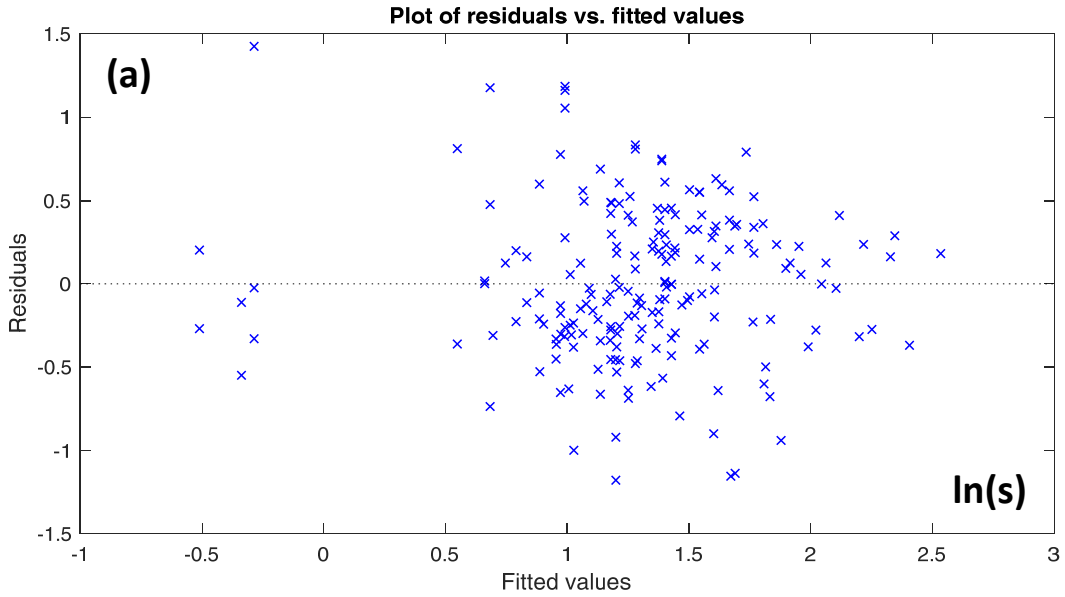


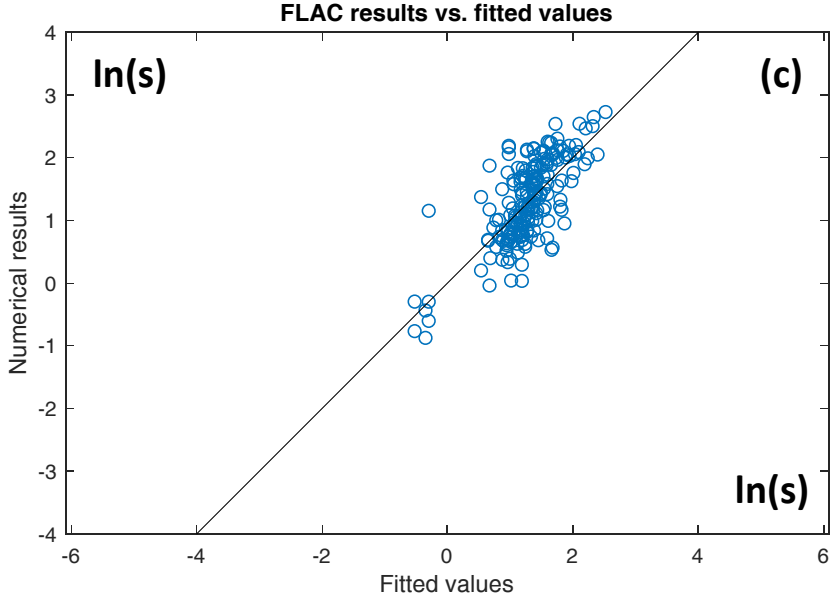


Figure 8-3

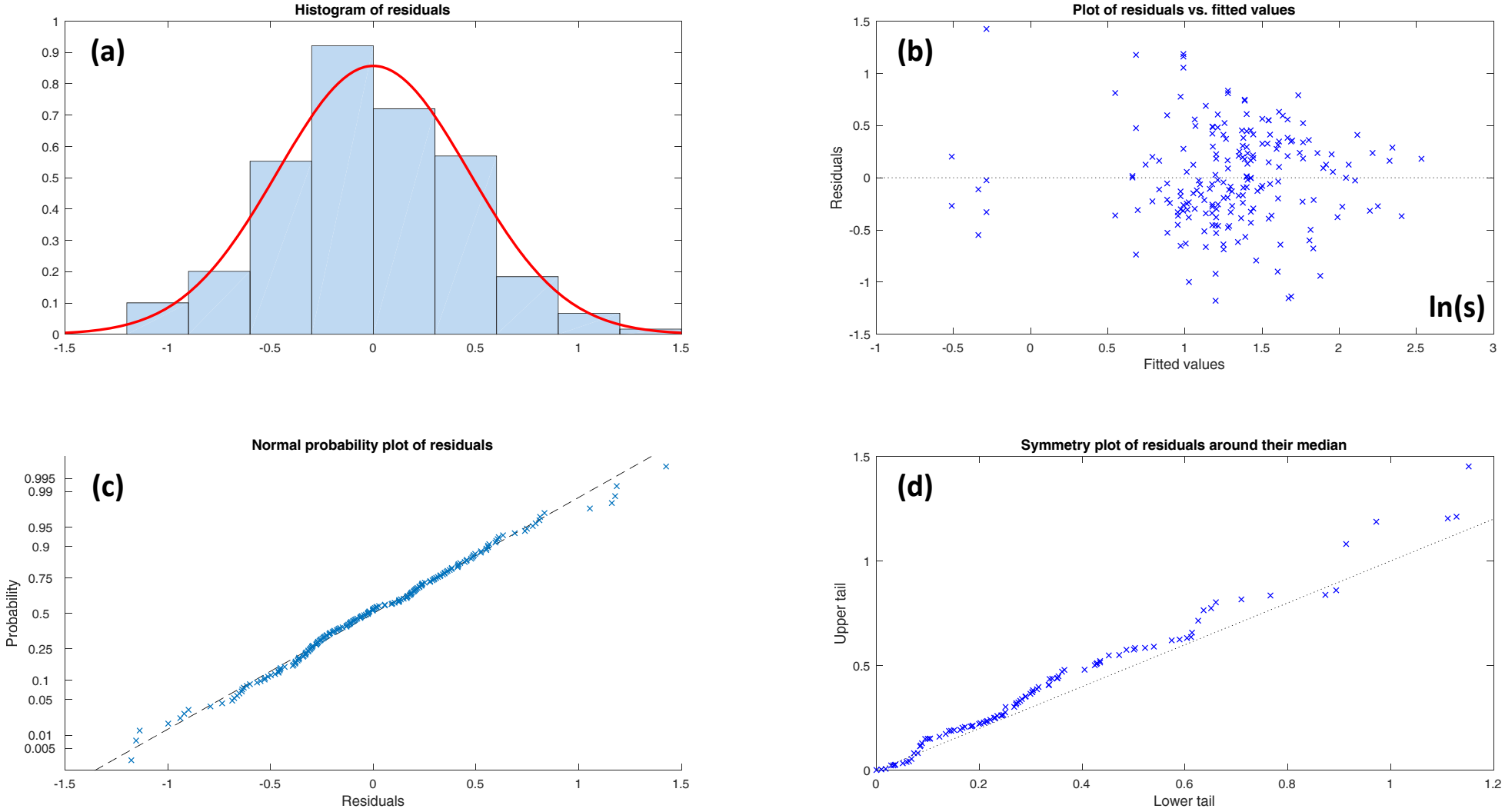
Histogram of residuals
(a)
Plot of residuals vs. fitted values
(b)
Residuals
Fitted values
ln(s)
Normal probability plot of residuals
(c)
Probability
Residuals
Symmetry plot of residuals around their median
(d)
Upper tail
Lower tail

Figure 8-4

# *Uncertainty in settlement estimate*

$$\ln(s) = a_0 + a_1 \ln(Q) + a_2 B + a_3 H_{crust} + a_4 \ln\left(\tanh\left(H_{liq}\right)\right) + a_5\, Dr + a_6 \ln(D_{5-75}) + a_7 \ln(Sa_{T=0.7s}) + \varepsilon$$

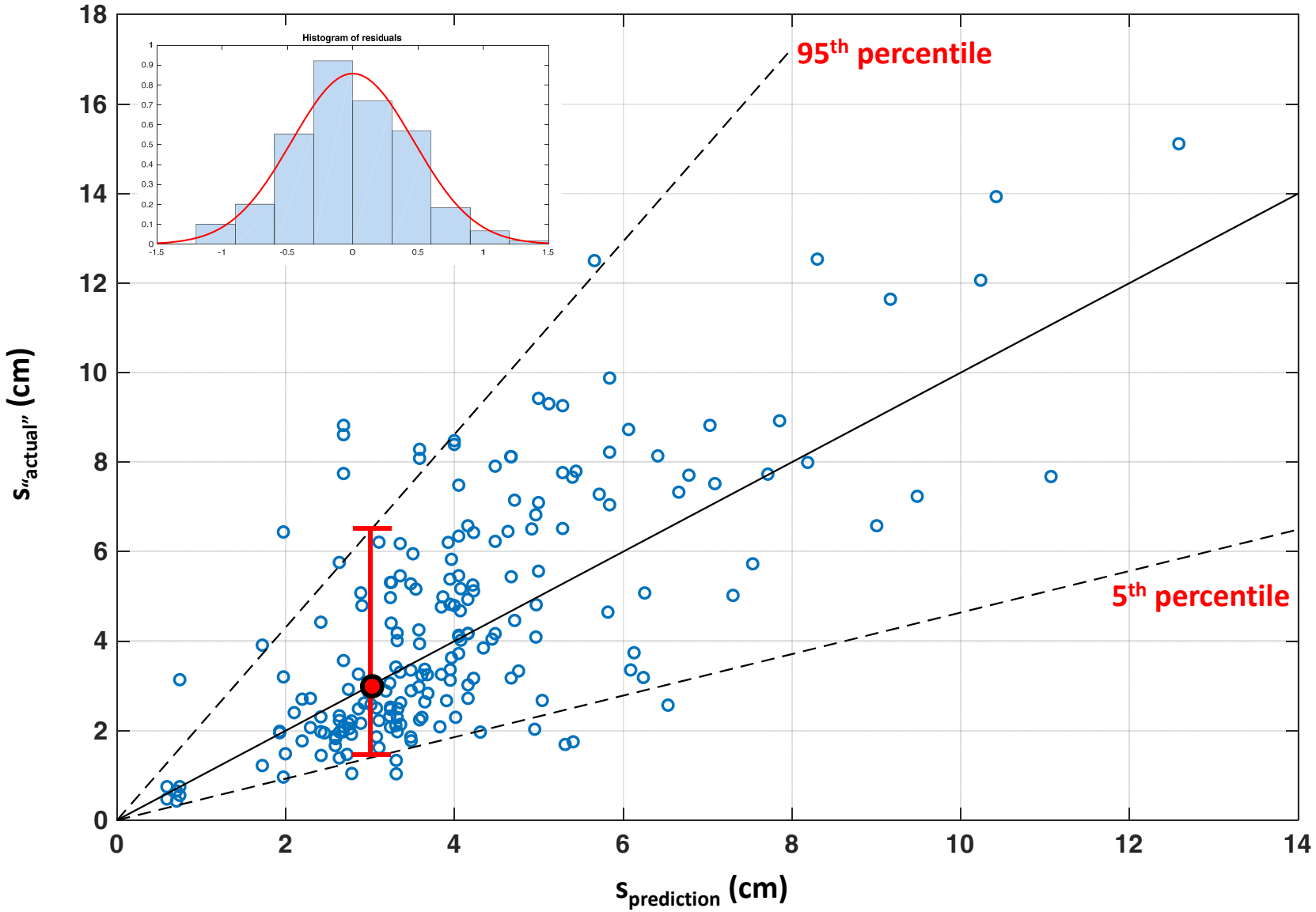


Figure 8-5

# Regression – 2-storey building settlements

***2-storey building calculated settlements vs. regression equation predictions***

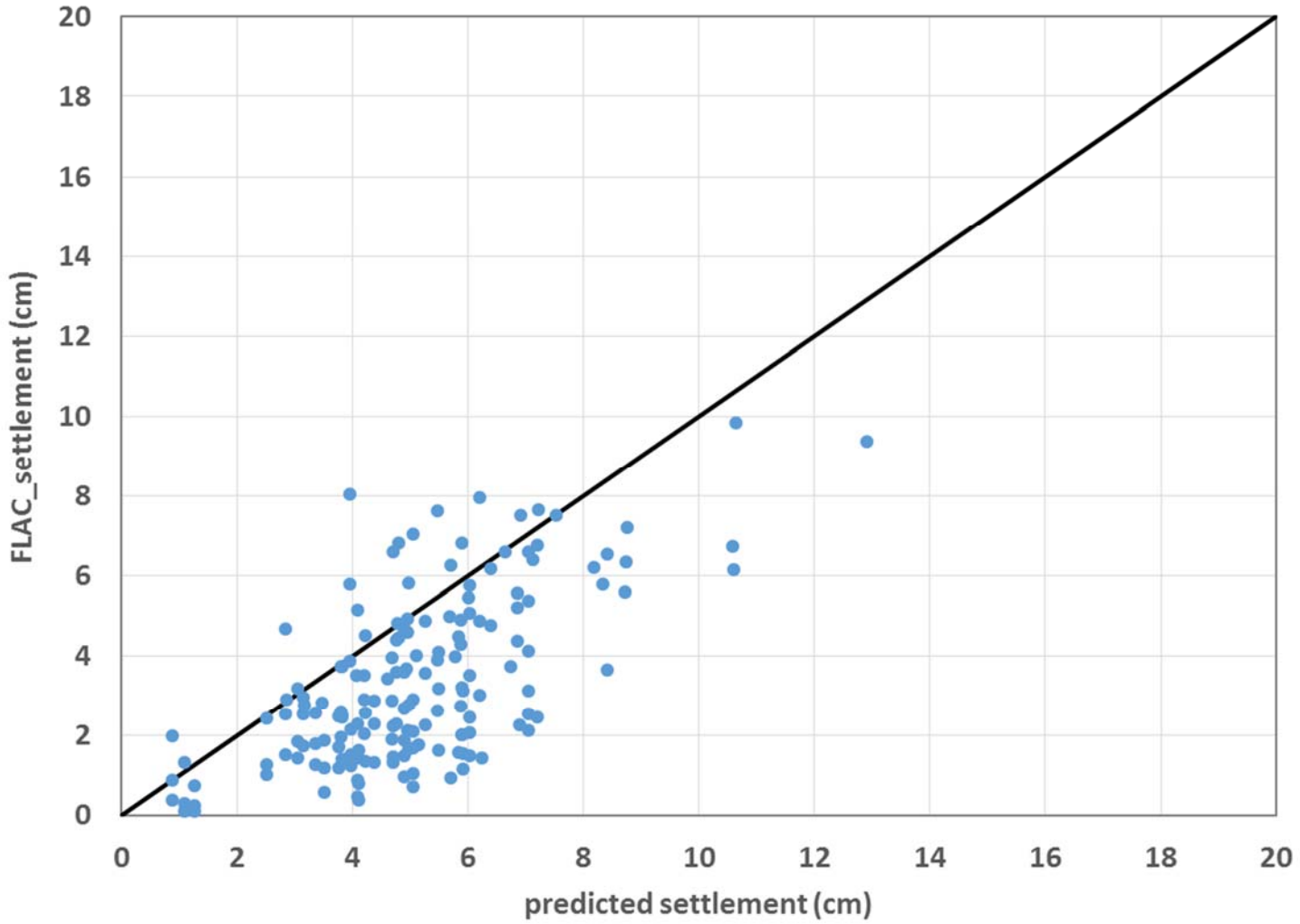


Figure 8-6

# Multiple Linear Regression

## Including 2-storey building settlements

$$\ln(s) = a_0 + a_1 \ln(Q) + a_2 B + a_3 H_{crust} + a_4 \ln\left(\tanh\left(H_{liq}\right)\right) + a_5\, Dr + a_6 \ln(D_{5-75}) + a_7 \ln(Sa_{T=0.7s})$$

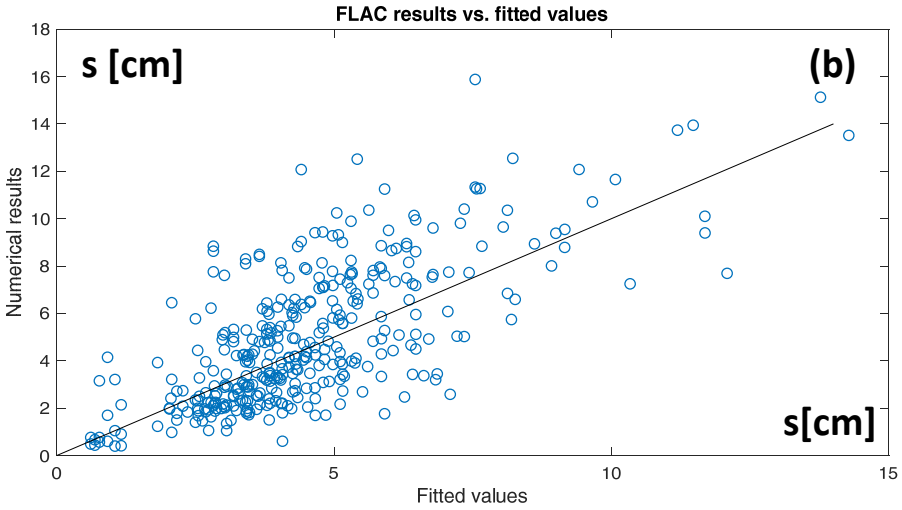


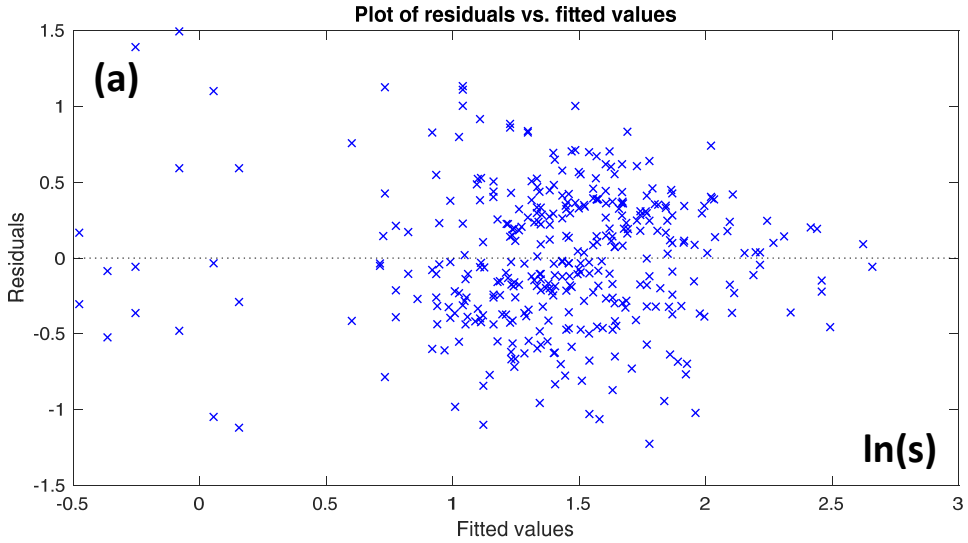


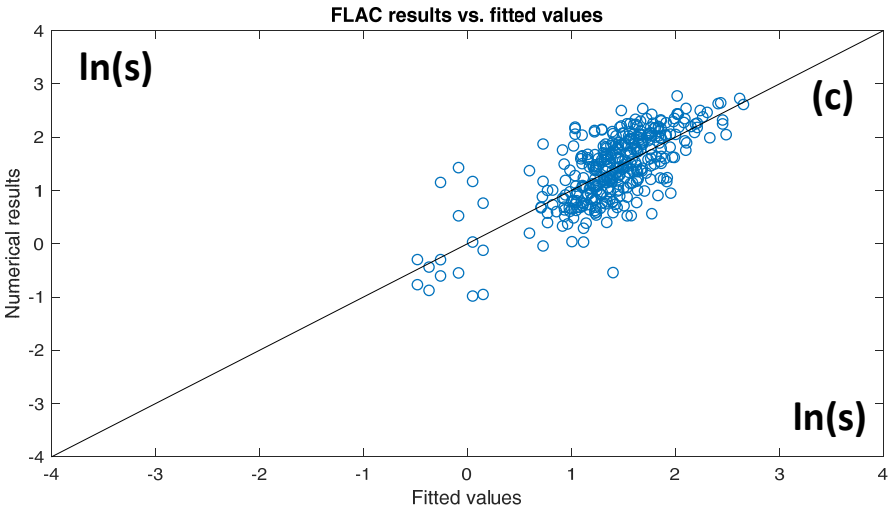


Figure 8-7

# Multiple Linear Regression

## Including 2-storey building settlements

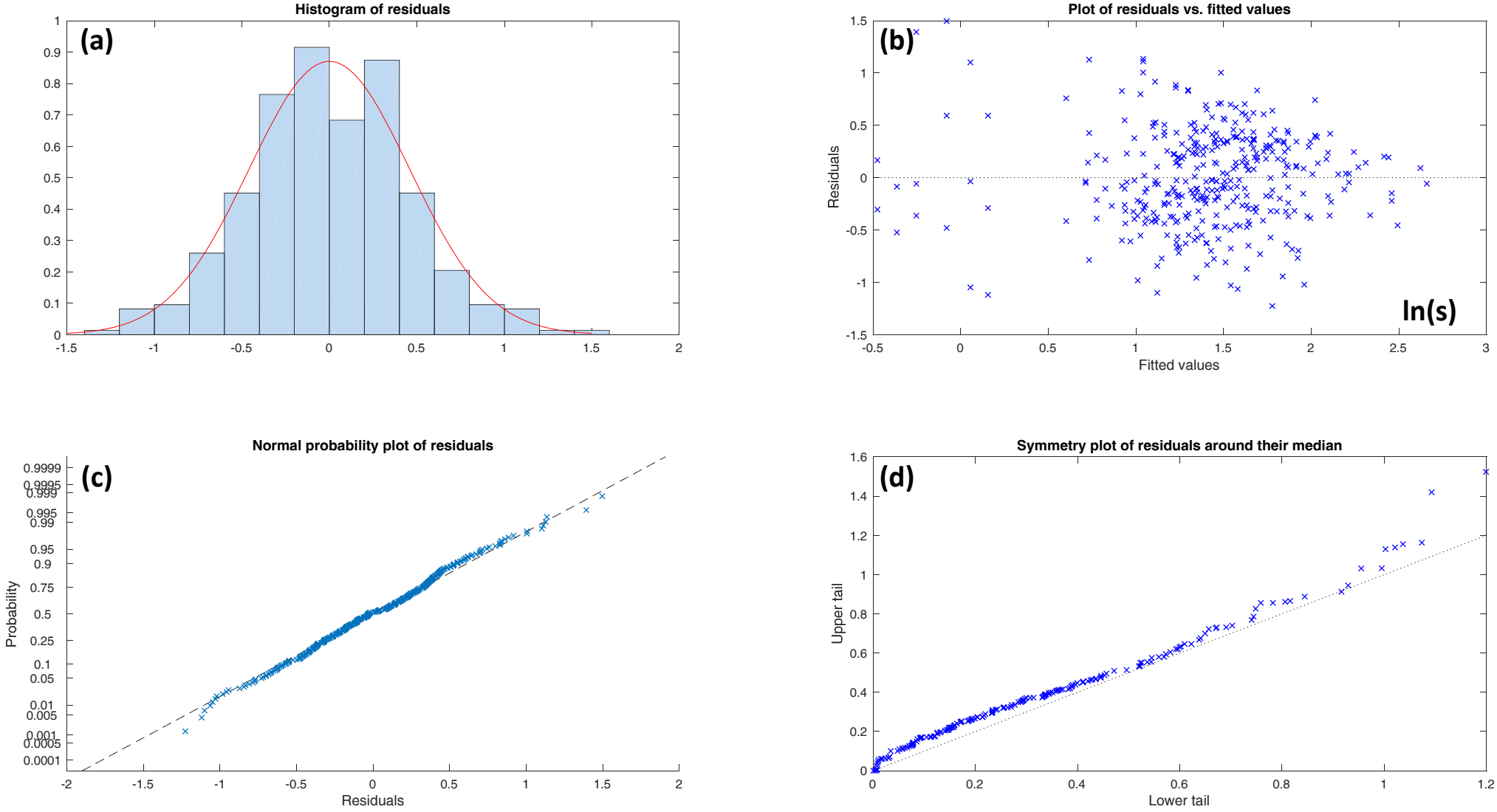


Figure 8-8

# *Uncertainty in settlement estimate*

$$\ln(s) = a_0 + a_1 \ln(Q) + a_2 B + a_3 H_{crust} + a_4 \ln\left(\tanh\left(H_{liq}\right)\right) + a_5\, Dr + a_6 \ln(D_{5-75}) + a_7 \ln(Sa_{T=0.7s}) + \varepsilon$$

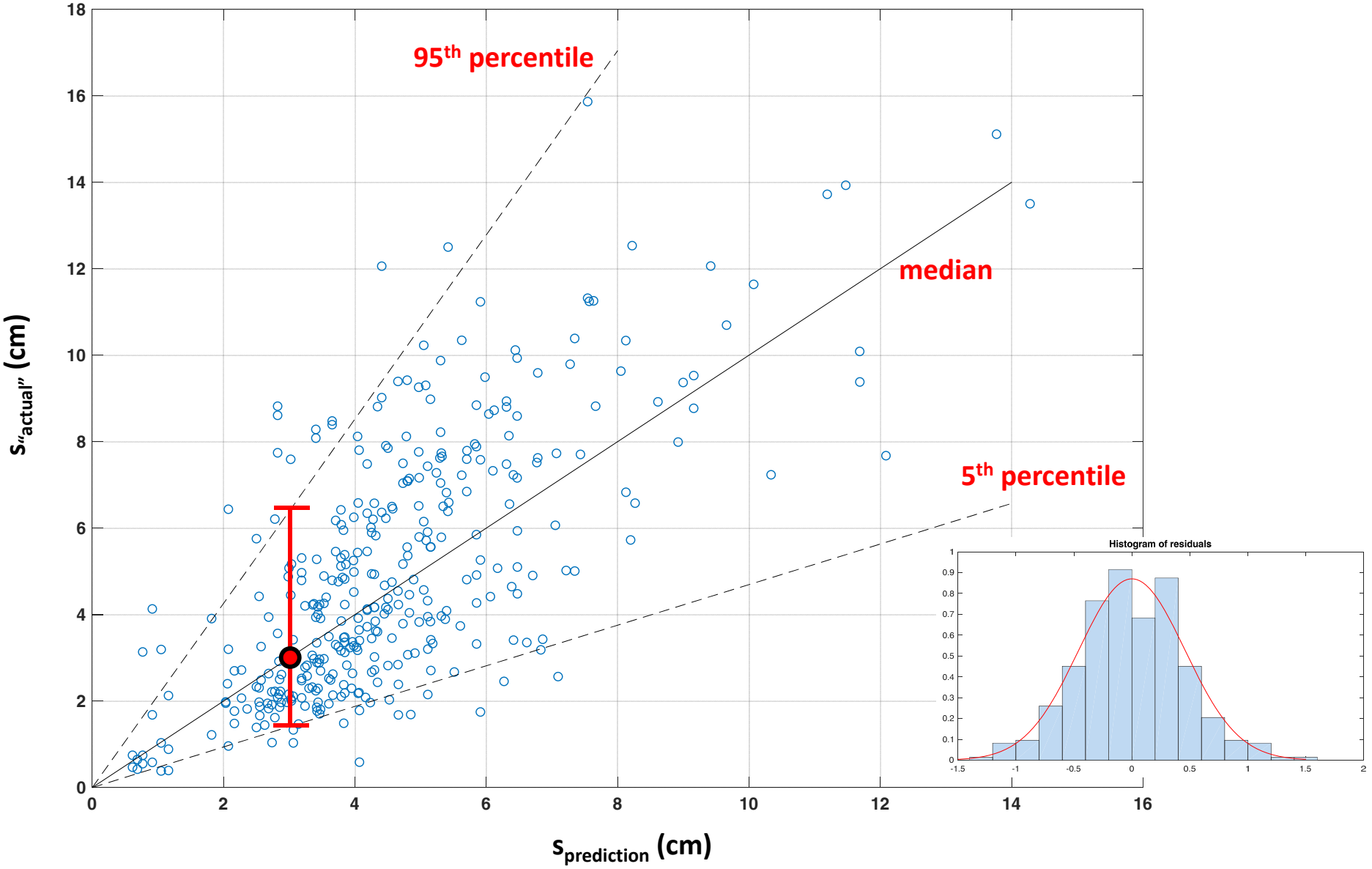


Figure 8-9

# Settlement Prediction Equation

$$\ln(s) = a_0 + a_1 \ln(Q) + a_2 B + a_3 H_{crust} + a_4 \ln\left(\tanh\left(H_{liq}\right)\right) + a_5 Dr + a_6 \ln(D_{5-75}) + a_7 \ln(Sa_{T=0.7s}) + \varepsilon$$

| Regression | α0 | α1 | α2 | α3 | α4 | α5 | α6 | α7 | σ |
|---|---|---|---|---|---|---|---|---|---|
| initial | 2.096 | 0.308 | 0.749 | -0.353 | 1.991 | -0.031 | 0.581 | 1.899 | 0.465 |
| updated | **2.570** | **0.200** | **0.742** | **-0.454** | **1.924** | **-0.031** | **0.588** | **1.900** | **0.458** |

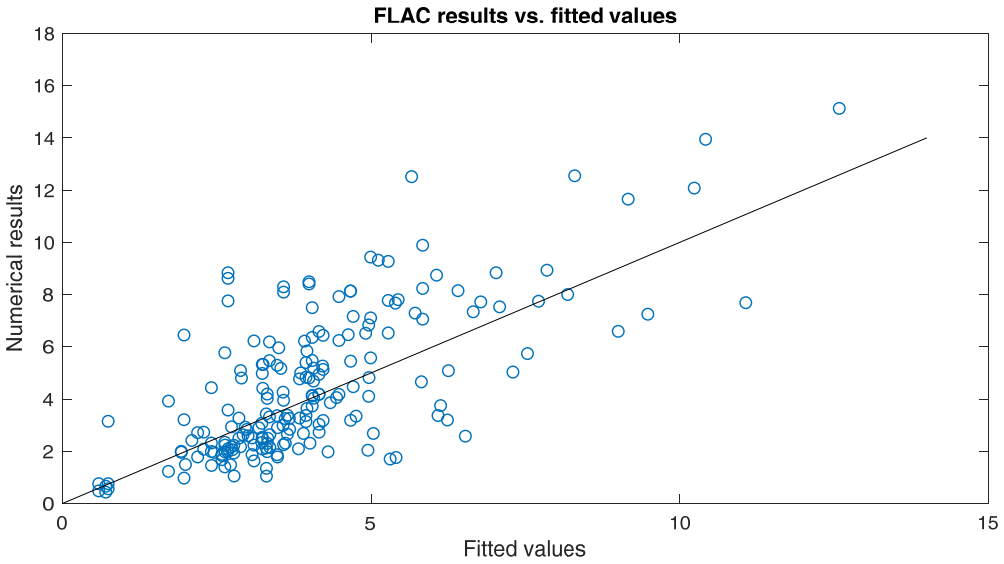


initial (without 2-storey building results)

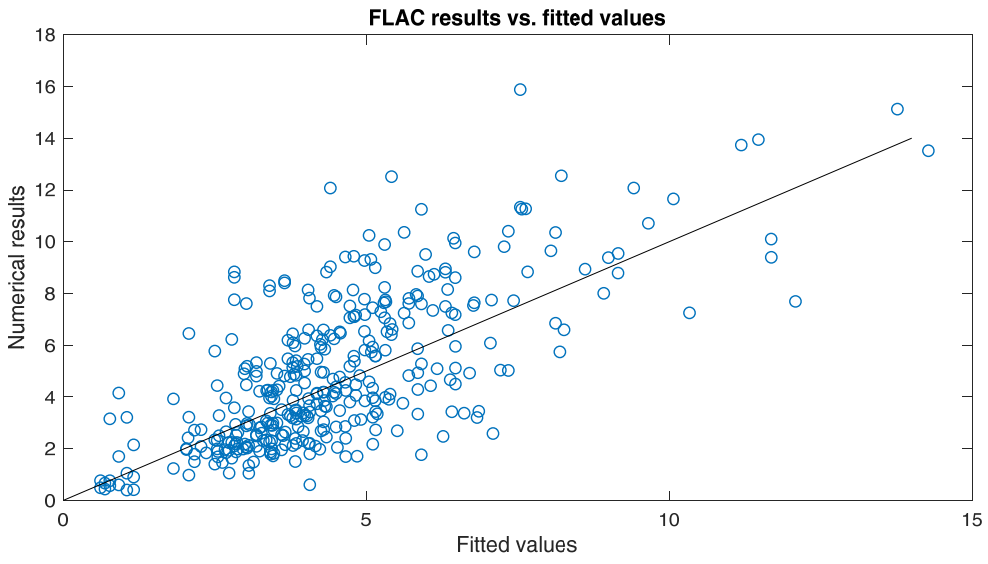


updated (including 2-storey building results)

Figure 8-10

## 9.0 REFERENCES


Abrahamson, N.A. (2003) RSPMATCH Software, time dependent spectral matching method software

Andrus R.D., Mohanan N.P., Piratheepan P., Ellis B.S., Holzer T.L. (2007). Predicting shear-wave velocity from cone penetration resistance. Proceedings, 4th International Conference on Earthquake Geotechnical Engineering, Thessaloniki, Greece

BICL (2018). NAM Groningen Foundation Assessment- Geotechnical Assessment of 188 Williams St, Kaiapoi, New Zealand. Report, 14 February 2018.

Bommer JJ, Dost B, Edwards B, Kruiver PP, Meijers P, Ntinalexis M, Polidoro B, Rodriguez-Marek A, Ruigrok E, Spetzler J and Stafford PJ (2017a) V4 Ground-Motion Model (GMM) for Response Spectral Accelerations, Peak Ground Velocity, and Significant Durations in the Groningen Field. Report to NAM, Version 2, 3 June 2017, 540 pp

Boulanger, R. W., and Ziotopoulou, K. (2015) "PM4Sand (version 3): A sand plasticity model for earthquake engineering applications." Report No. UCD/CGM-15/01, Center for Geotechnical Modeling, Department of Civil and Environmental Engineering, University of California, Davis, CA, March, 112 p.

Boulanger, R. W., Seed, R. B., Chan, C. K., Seed, H. B., and Sousa, J. B., (1991) "Liquefaction Behavior of Saturated Sands under Uni-Directional and Bi-Directional Monotonic and Cyclic Simple Shear Loading", Geotechnical Engineering Report No. UCB/GT/9108, University of California, Berkeley, August

Boulanger, R.W. and Idriss, I.M. (2014). "CPT and SPT Based Liquefaction Triggering Procedures." Report No. UCD/CGM-14/01. Center for Geotechnical Modeling, Dept. of Civil and Environmental Engineering, University of California, Davis.

Bradley BA. (2012) Strong ground motion characteristics observed in the 4 September 2010 Darfield, New Zealand earthquake. Soil Dynamics and Earthquake Engineering 42: 32-46. http://dx.doi.org/10.1016/j.soildyn.2012.06.004.

Bradley, B.A. (2013). "A New Zealand-Specific Pseudospectral Acceleration Ground-Motion Prediction Equation for Active Shallow Crustal Earthquakes Based on Foreing Models." Bulletin of the Seismological Society of America. Vol. 103, No. 3, pp. 1801-1822, June 2013.

Bray, J.D., and Dashti, S. (2014). Liquefaction-Induced Building Movements. Bulletin of Earthquake Engineering, Springer, Vol. 12(3), 1129-1156, DOI: 10.1007/s10518-014-9619-8.

Bray, J.D., and Luque R. (2017) Seismic performance of a building affected by moderate liquefaction during the Christchurch earthquake, Soil Dynamics and Earthquake Engineering 102, 99-111

Bray, J.D., and Macedo, J. (2017). Simplified procedure for estimating liquefaction-induced building settlement, Proceedings of the 19th International Conference on Soil Mechanics and Geotechnical Engineering, Seoul

Brown, L.J. and Weeber, J.H. (1992). "Geology of the Christchurch Urban Area." Scale 1:25000. Institute of Geological and Nuclear Sciences geological map 1.

Cetin O. K., Youd L. T., Seed R.B., Bray J. D., Sancio R., Lettis W., Yilmaz T. M., Durgunoglu T. H. (2002) Liquefaction-induced ground deformations at Hotel Sapanca during

Kocaeli (Izmit),Turkey earthquake, Soil Dynamics and Earthquake Engineering 22 (2002) 1083–1092

Chakrabortty P., Popescu R., and Philips R. (2010) Liquefaction of Heterogeneous Sand: Centrifuge Study, Geotechnical Testing Journal, Vol. 33, No.4

Cubrinovski M., Green R., Allen J., Ashford S., Bowman E., Bradley BA., Cox B., Hutchinson T., Kavazanjian E. and Orense R. (2010) Geotechnical reconnaissance of the 2010 Darfield (New Zealand) earthquake.Commissioned by University of Canterbury. 173pp. http://hdl.handle.net/10092/5124.

Dafalias, Y. F., and Manzari, M. T. (2004) "Simple plasticity sand model accounting for fabric change effects." Journal of Engineering Mechanics, ASCE, 130(6), 622-634

Darendeli, M. (2001). "*Development of a new family of normalized moduli reduction and material damping curves*." Ph.D. thesis, University of Texas at Austin.

Dashti, S. and Bray, J.D. (2013). Numerical Simulation of Building Response on Liquefiable Sand. Bulletin of Earthquake Engineering, J. Geotech. Geoenviron. Engng, DOI: 10.1061/(ASCE)GT.1943-5606.0000853.

Dashti, S., Bray, J.D., Pestana, J.M., Riemer, M.R. and Wilson, D. (2010). Mechanisms of seismically-induced settlement of buildings with shallow foundations on liquefiable soil. J. Geotech. Geoenviron. Engng. 136

Elgamal, A., Lu, J., and Yang, Z. (2005). "Liquefaction-induced settlement of shallow foundations and remediation: 3D numerical simulation." J. Earthquake Eng., 9(1), 17–45.

Fugro (2016) Evaluation of Dynamic Stability, Eemshaven-Delfzijl Levee, The Netherlands, Prepared for NAM, December

Fugro (2017) Evaluation of Dynamic Stability Using Code Calibrated Design Parameters, Sections 3-4 Eemskanaal Levee, The Netherlands, Prepared for NAM, October

Fugro (2018) Evaluation of Dynamic Shallow Foundations Settlements of Existing Residential Buildings in Groningen on Clays with Relatively Low Strengths, Project Memorandum prepared for NPR TG2, April 30

Giannakou, A., Travasarou, T., and Chacko, J. (2012) "Numerical Modeling Of Liquefaction-Induced Slope Movements" GeoCongress, Oakland, CA

Giannakou, A., Travasarou, T., Ugalde, J., Chacko, J., and Byrne, P. (2011) "Calibration Methodology for Liquefaction Problems Considering Level and Sloping Ground Conditions", 5th International Conference on Earthquake Geotechnical Engineering, Chile

Green R. (2018) Groningen-Specific Liquefaction Evaluation – Summary

Green R. (2018) Back-Calculating Laboratory Liquefaction Curves from Groningen-Specific Simplified Liquefaction Evaluation Procedure - Summary

Idriss I. M., and Boulanger R. W. (2008) Soil Liquefaction During Earthquakes, Earthquake Engineering Research Institute

Ishihara, K. and Yoshimine, M. (1992) Evaluation of settlements in sand deposits following liquefaction during earthquakes: Soils and Foundations, 32(1), p.173-188

Ishihara, K., Yasuda, S., and Nagase, H. (1996), “Soil characteristics and ground damage,” Special Issue of Soils and Foundations, January, 109-118

Itasca Consulting Group Inc. (2016) “Fast Lagrangian Analysis of Continua (FLAC2D)” version 8.0

Jongejan R., Chacko J., Giannakou A., Drosos V., Tasiopoulou P. (2017) A Code Calibrated Method for Seismic Stability Assessments of the Embankments along Eemscanal, Final Report, July 31, 2017

Kammerer, A.M., Wu, J., Pestana, J.M., Riemer, M., and Seed, R.B., (2000) "Cyclic Simple Shear Testing of Nevada Sand for PEER Center Project 2051999," Geotechnical Engineering Report, UCB-GT-2000-01, Dept. of Civil and Environmental Engineering, University of California, Berkeley

Kottke, A.R., Wang, X., and Rathje, E.M. (2013) “Technical Manual for Strata), Geotechnical Engineering Center, Department of Civil, Architectural, and Environmental Engineering, University of Texas

Lilhanand, K., and Tseng, W.S. (1988) Development and Application of Realistic Earthquake Time Histories Compatible with Multiple Damping Response Spectra. 9th World Conf. Earthquake Engineering, Tokyo, Japan, Vol. II, p. 819-824

Liu, L., and Dobry, R. (1997). “Seismic response of shallow foundation on liquefiable sand.” J. Geotech. Geoenviron. Eng., 123(6), 557–567.

Luque R. and Bray, J.D. (2015) Dynamic Analysis of a Shallow-Founded Building in Christchurch during the Canterbury Earthquake Sequence, 6th International Conference on Earthquake Geotechnical Engineering 1-4 November 2015 Christchurch, New Zealand

Markham C., Macedo J. and Bray J. (2014). Evaluating Fully Nonlinear Effective Stress Site Response Analyses using Records from the Canterbury Earthquake Sequence. U.S.G.S. Report, Award Number: G13AP00029, Department of Civil and Environmental Engineering, University of California, Berkeley.

Mayne, P.W., and Rix, G.J. 1995. Correlations between cone tip resistance and shear wave velocity in natural clay. Soils and Foundations, 35 (2): 107 – 110

Mejia LH and Dawson EH (2006) Earthquake Deconvolution in FLAC. Proc. 4th International FLAC Symposium in Numerical Modeling in Geomechanics, Minneapolis MN

NPR 9998 (2017) Practical Guideline NPR 9998 Assessment of structural safety of buildings in case of erection, reconstruction and disapproval – Basic rules for seismic actions: induced earthquakes, June

Pasticier L, Amadio C, Fragiacomo M (2008) Non-linear seismic analysis and vulnerability evaluation of a masonry building by means of the SAP2000 V.10 code, Journal of Earthquake Engng Struct. Dyn. 2008; 37:467–485

Shahir, H., and Pak, A. (2010). “Estimating liquefaction-induced settlement of shallow foundations by numerical approach.” Comput. Geotech., 37(3), 267–279.

Sriskandakumar, S. (2004) "Cyclic Loading Response of Fraser River Sand for Validation of Numerical Models Simulating Centrifuge Tests," M.A.Sc Thesis, Department of Civil Engineering, The University of British Columbia, Vancouver

Tasiopoulou P., Drosos V., Giannakou A., Georgarakos P., Chacko J., de Wit S., and Zuideveld-Venema N. (2018) Dynamic Performance Assessment of the Eemskanal Levee in Groningen, 16th European Conference on Earthquake Engineering, Thessaloniki, 18-21 June *(accepted)*

Tasiopoulou P., Giannakou A., Chacko J. and de Wit S. "Evaluation of Liquefaction Triggering Resistance and Deformation Accumulation in Laminated Sand and Clay Deposits", Theme Lecture, 3rd International Conference on Performance-based Design in Earthquake Geotechnical Engineering, July 16-19, 2017

Tasiopoulou P., Giannakou A., Chacko J., and de Wit S. (2018) Liquefaction Triggering and Post-liquefaction Deformation of Laminated Deposits, Journal of Soil Dynamics and Earthquake Engineering *(accepted)*

Tasiopoulou, P., Taiebat, M., Tafazzoli, N., and Jeremić, B.(2015), "On validation of fully coupled behavior of porous media using centrifuge test results". Coupled Systems Mechanics, 4 (1), 37-65.

Taylor M.L., Cubrinovski M. and Bradley B.A. (2013). Cyclic strength testing of Christchurch sands with undisturbed samples. Proc. of NZSEE Conference, 26-28 April 2013, Wellington, New Zealand.

Vaid, Y. P., and Chern, J. C. (1985) "Cyclic and Monotonic Undrained Response of Saturated Sands, Advances in the Art of Testing Soils under Cyclic Conditions", ASCE, NY, 120-47

Vaid, Y. P., and Finn, W. D. L. (1979) "Static shear and liquefaction potential", J Geotechnical Div., ASCE 105(GT10), 1233-246

Wu, J. (2002) "Liquefaction Triggering and Post-Liquefaction Deformation of Monterey 0/30 Sand Under Uni-Directional Cyclic Simple Shear Loading," Doctoral Dissertation, Civil and Environmental Engineering, UC. Berkeley

Yasuda (2012) Characteristics of liquefaction in Tokyo Bay area by the 2011 Great East Japan Earthquake, Soils and Foundations, Volume 52, Issue 5, October, Pages 793-810

Ziotopoulou, K., and Boulanger, R. W. (2013) "Calibration and implementation of a sand plasticity plane-strain model for earthquake engineering applications." Journal of Soil Dynamics and Earthquake Engineering, 53, 268-280, dx.doi.org/10.1016/j.soildyn.2013.07.009

Ziotopoulou, K., and Boulanger, R. W. (2013) "Numerical Modeling Issues In Predicting Post-Liquefaction Reconsolidation Strains And Settlements." 10th International Conference on Urban Earthquake Engineering March 1-2, 2013, Tokyo Institute of Technology, Tokyo, Japan

# APPENDIX A

# SPECTRALLY MATCHED GROUND MOTIONS AT NS_B

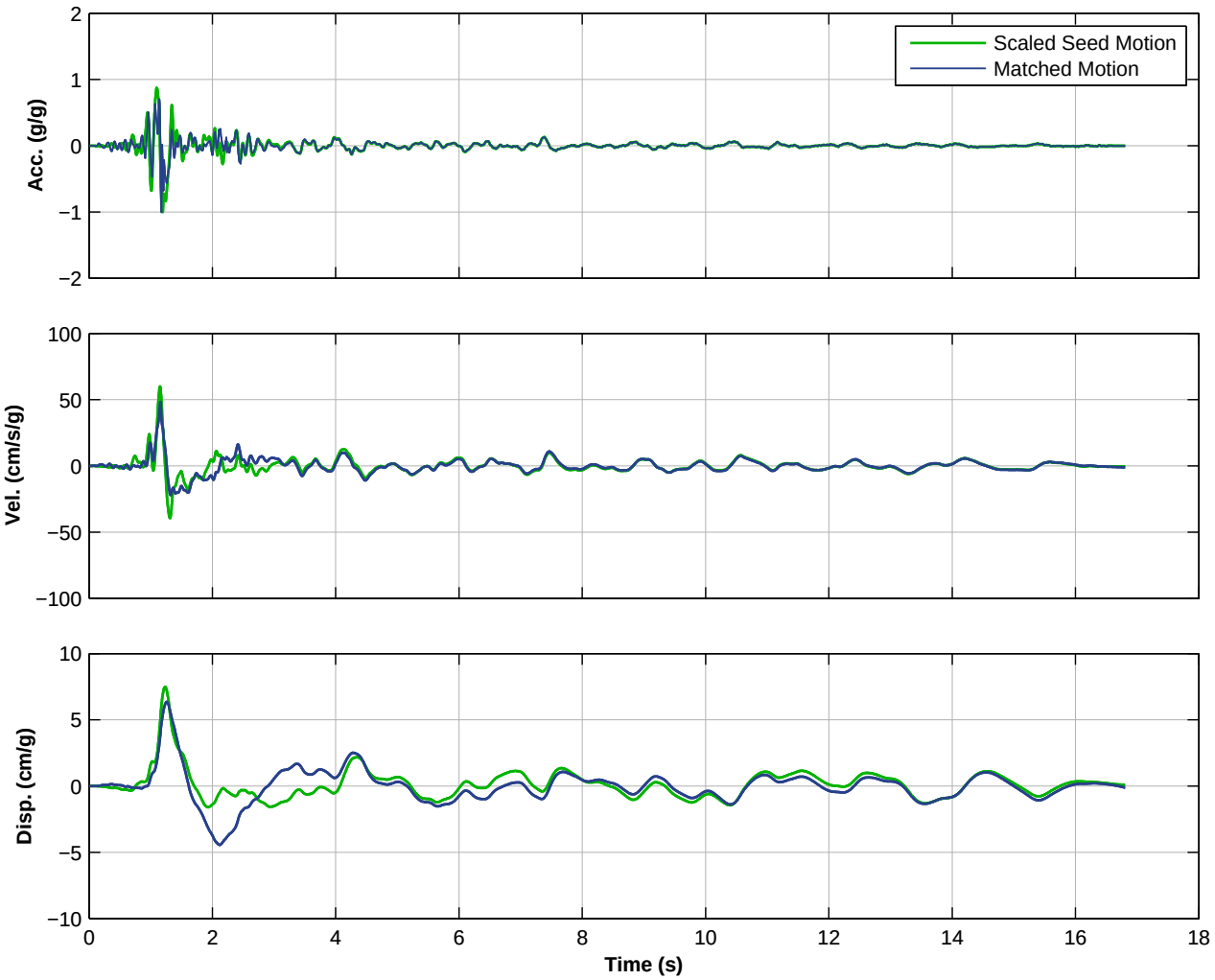


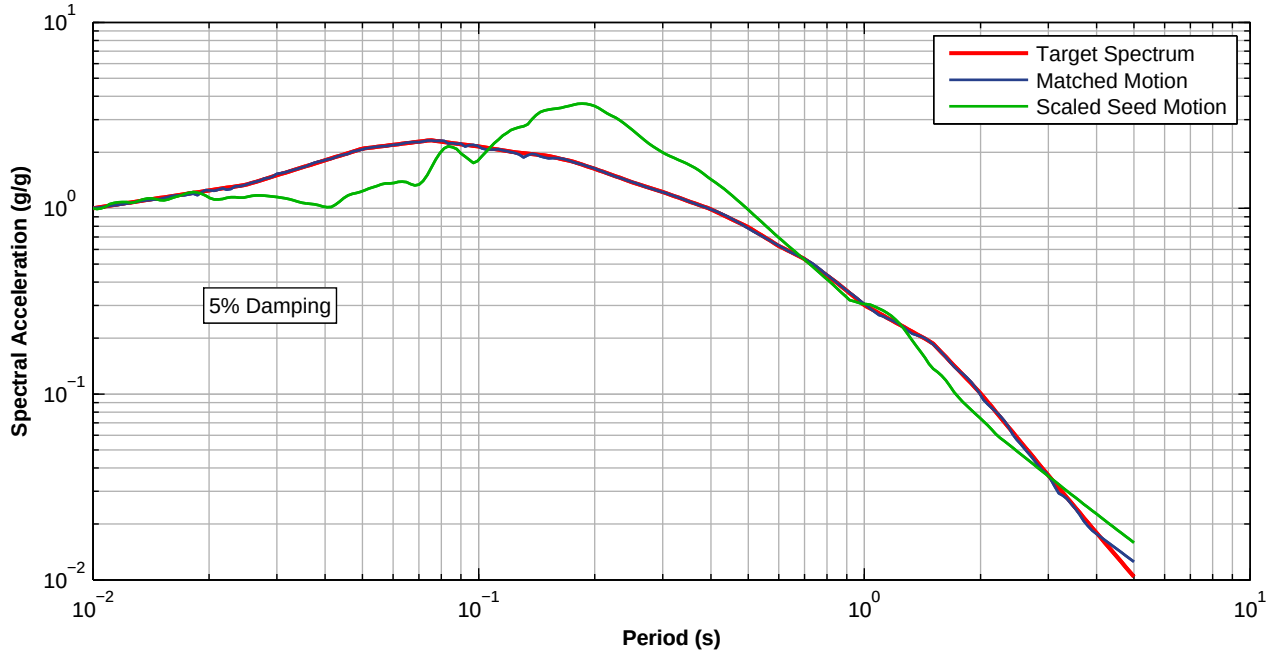


**SPECTRALLY MATCHED SULPHUR BATHS (TEMP) MOTION, 090 COMPONENT**
**1983 COALINGA−07, USA**

Eemskanaal Levee Project
Groningen, The Netherlands

FIGURE A−2a

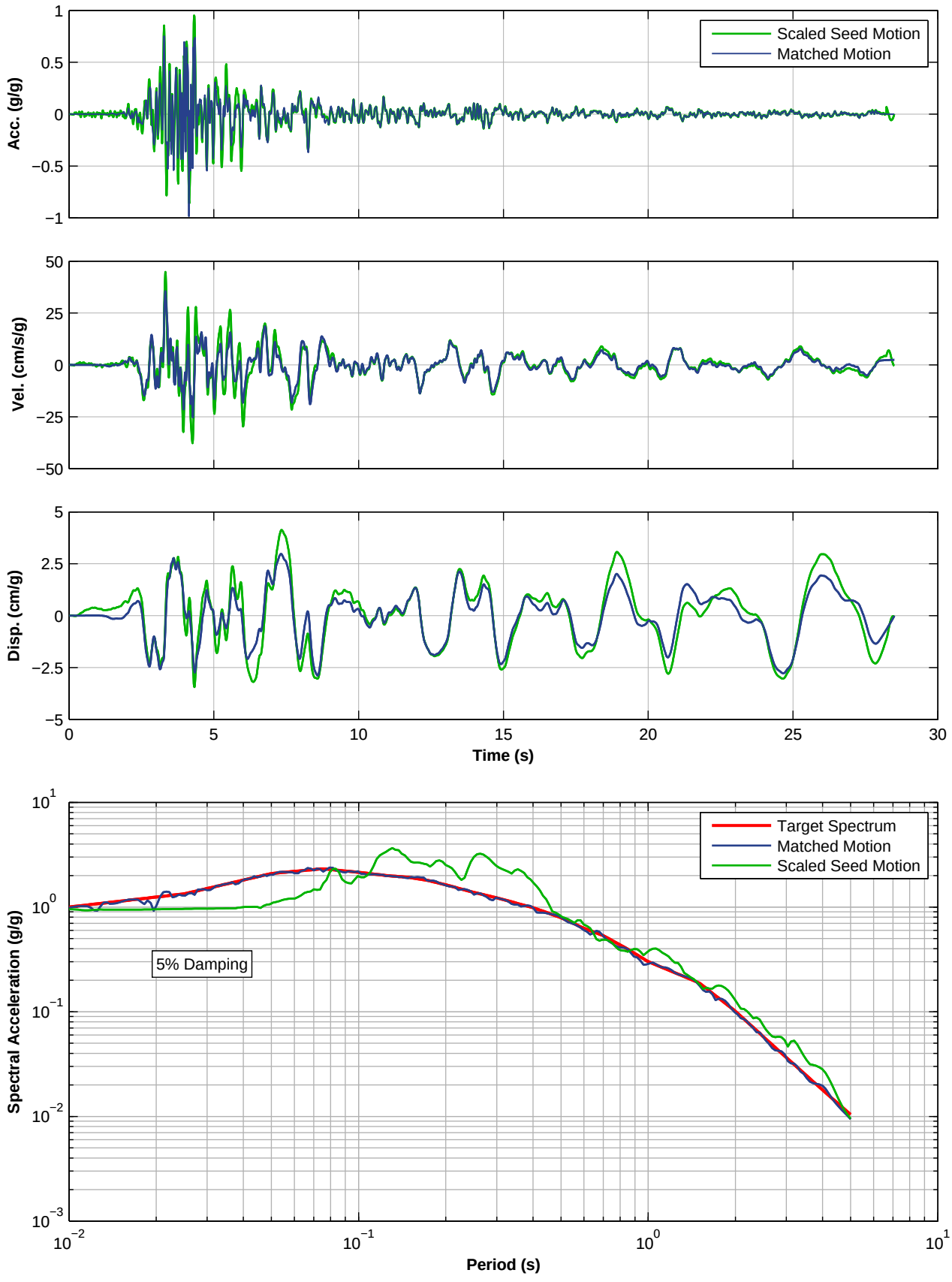


**SPECTRALLY MATCHED ATHENS 2 (CHALANDRI) MOTION, N36 COMPONENT 1999 ANO LIOSIA, GREECE**

Eemskanaal Levee Project
Groningen, The Netherlands

FIGURE A−2b

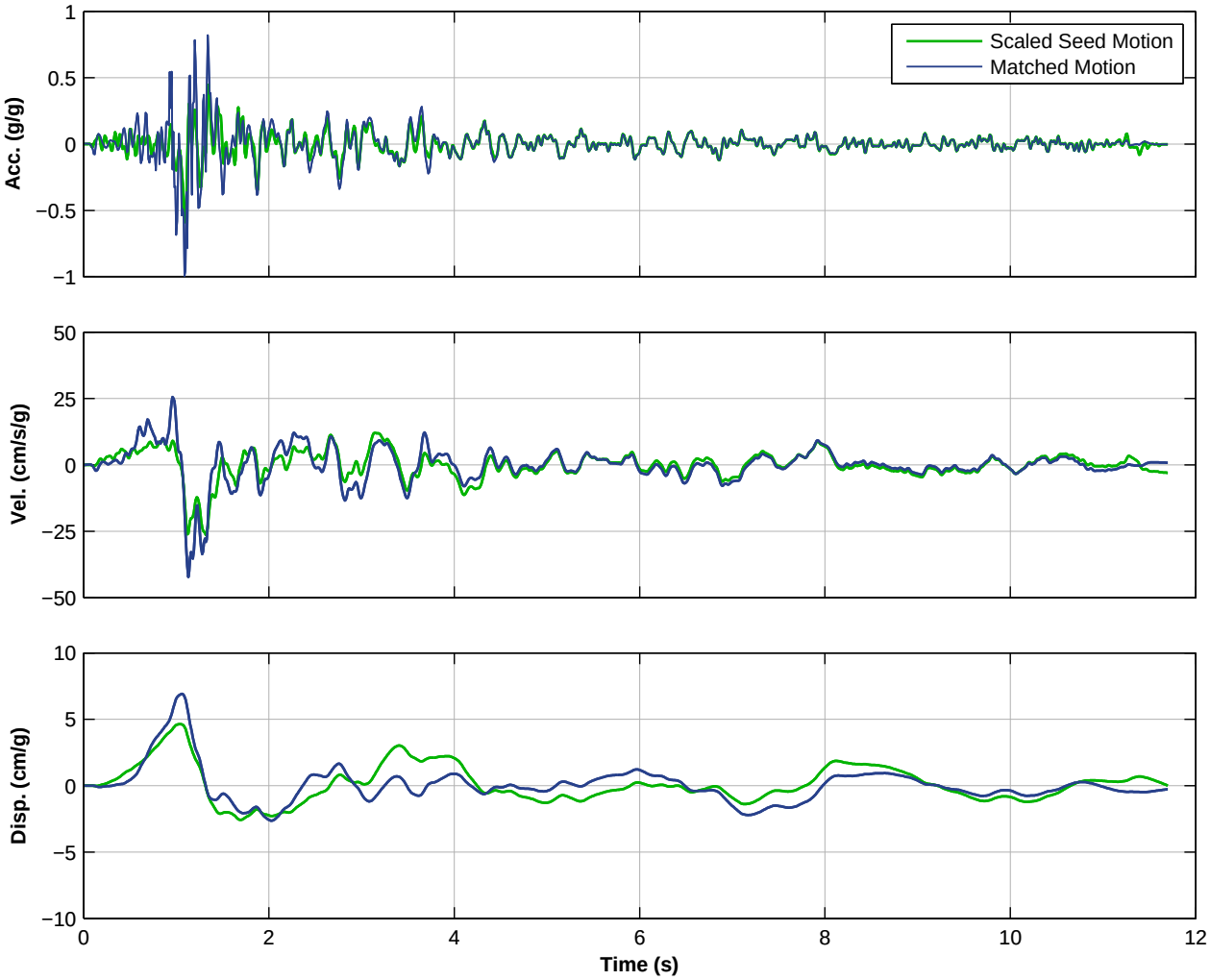


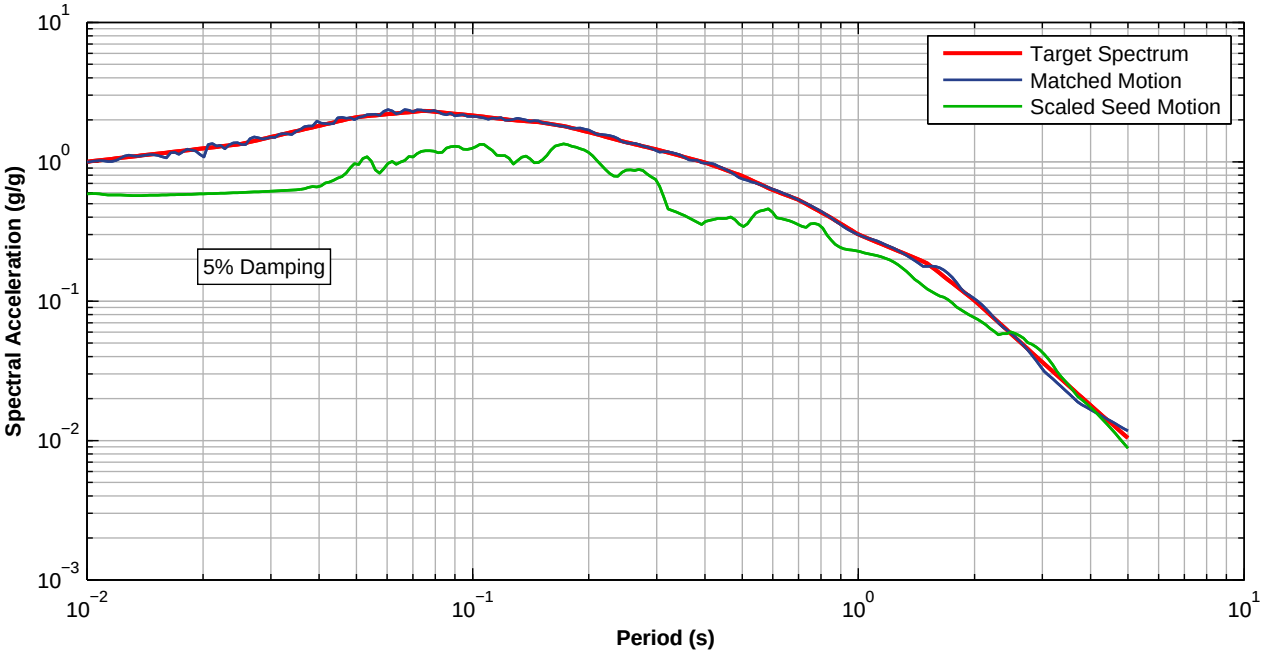


**SPECTRALLY MATCHED KALAMATA − OTE BUILDING MOTION, LONG COMPONENT**
**1986 KALAMATA (AFTERSHOCK), GREECE**

Eemskanaal Levee Project
Groningen, The Netherlands

FIGURE A−2c

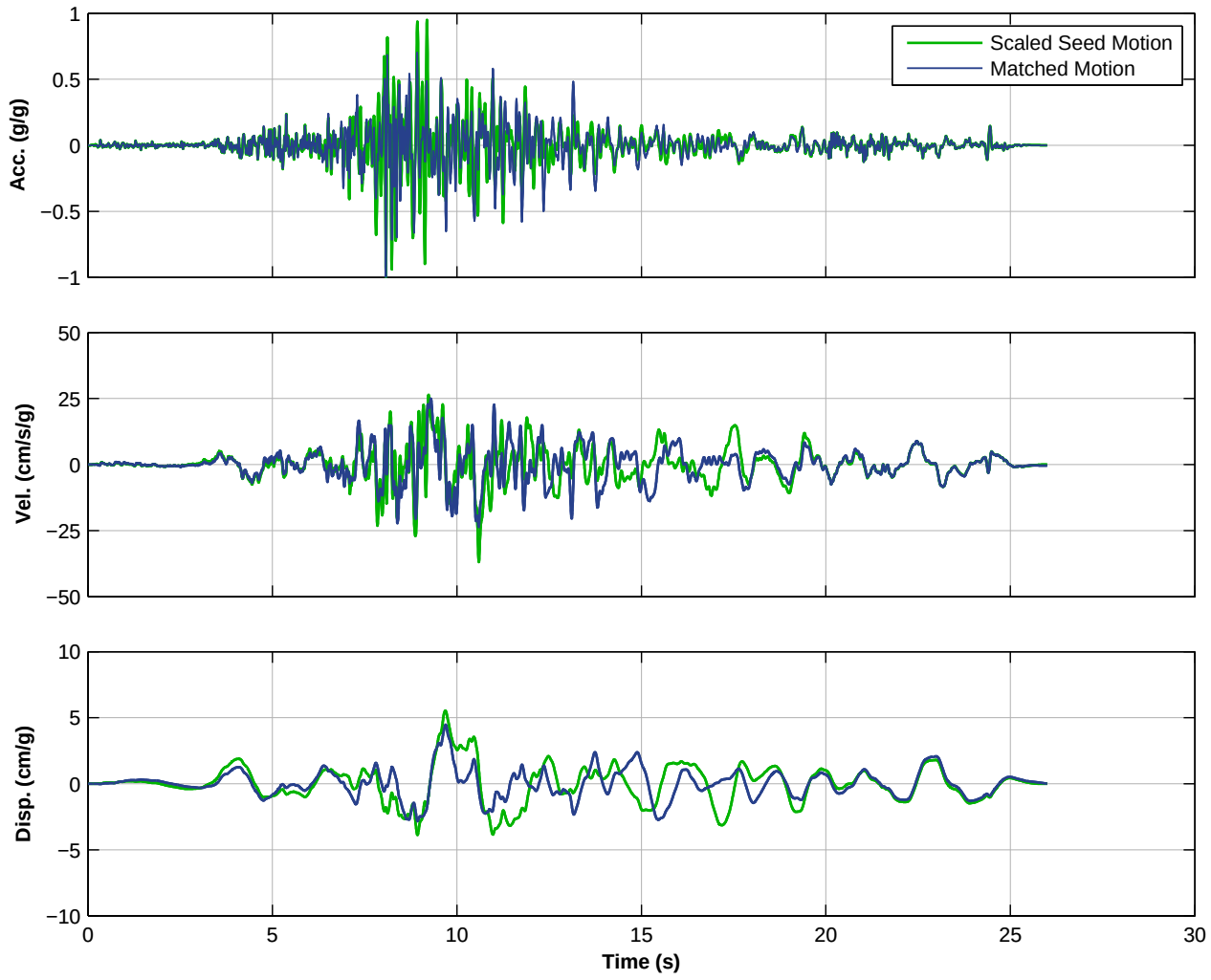


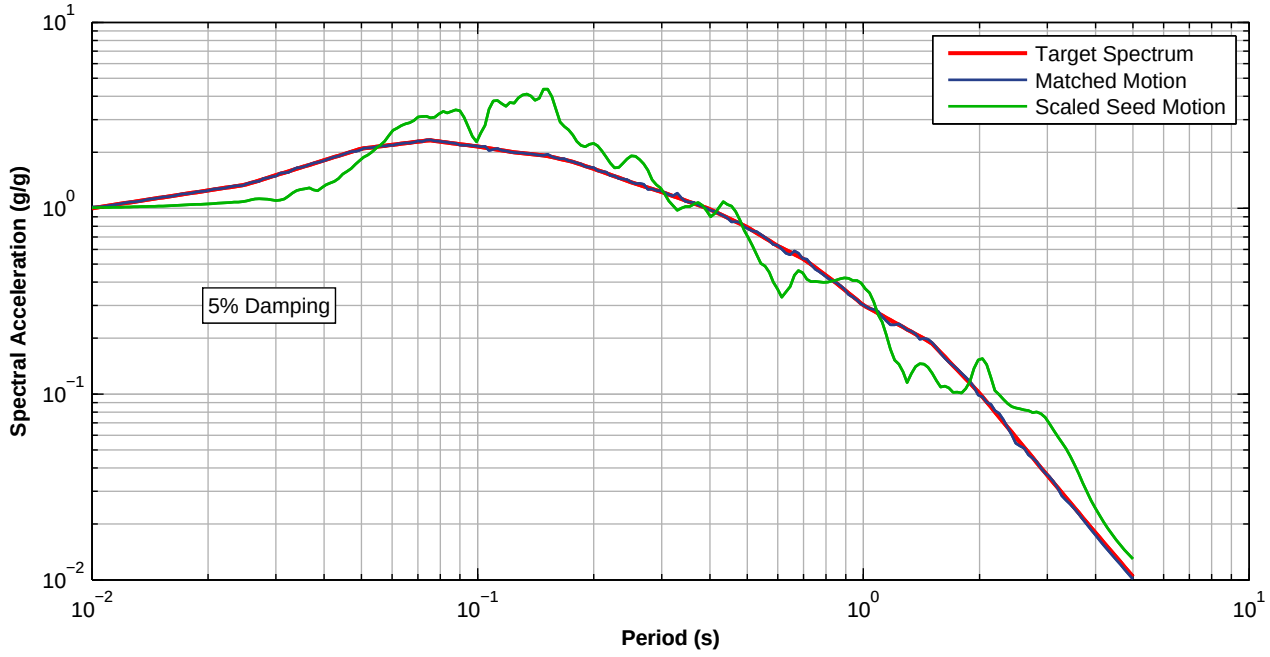


**SPECTRALLY MATCHED TCU 137 MOTION, N COMPONENT**
**1999 CHI−CHI − 02, TAIWAN**

Eemskanaal Levee Project
Groningen, The Netherlands

FIGURE A−2d

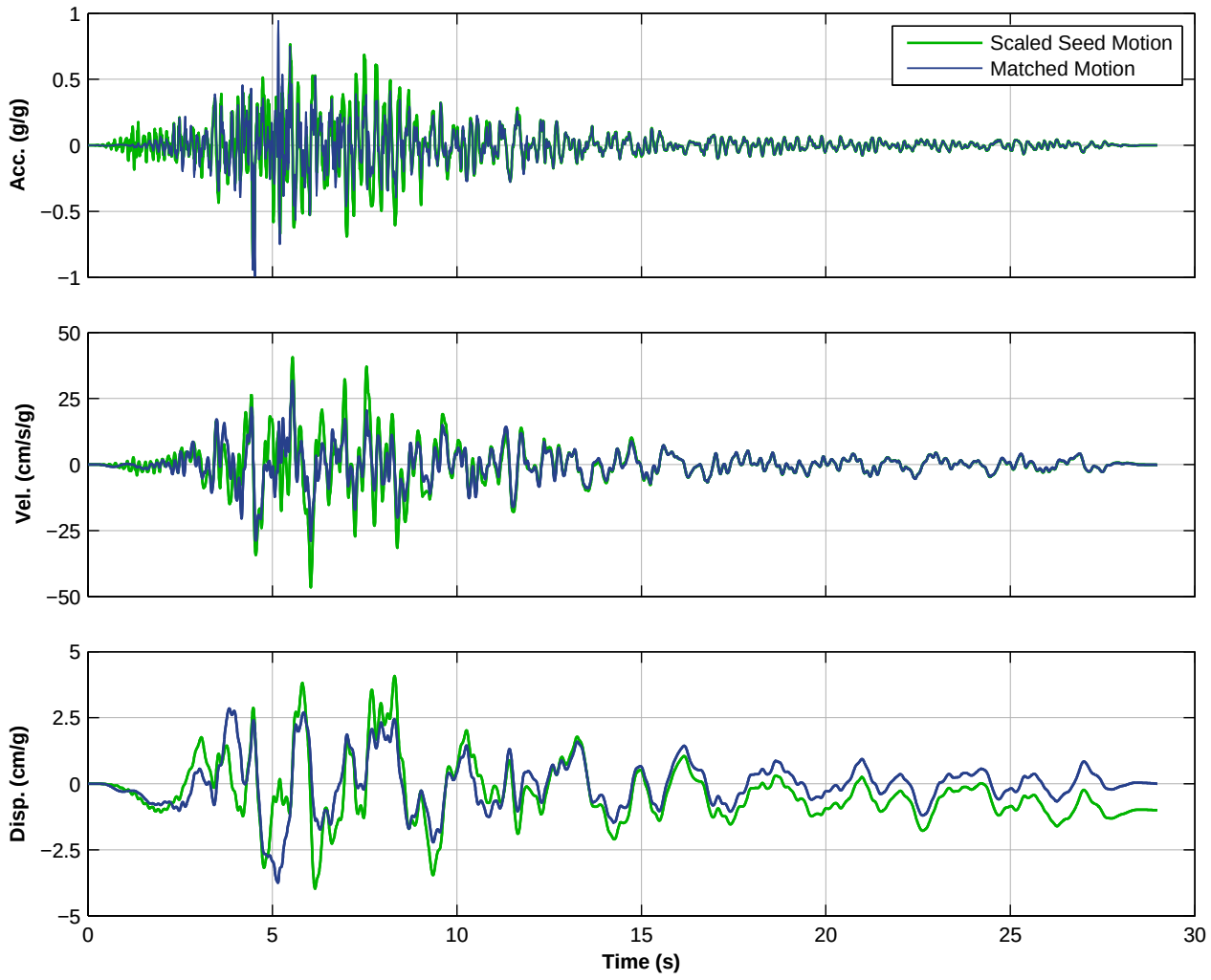


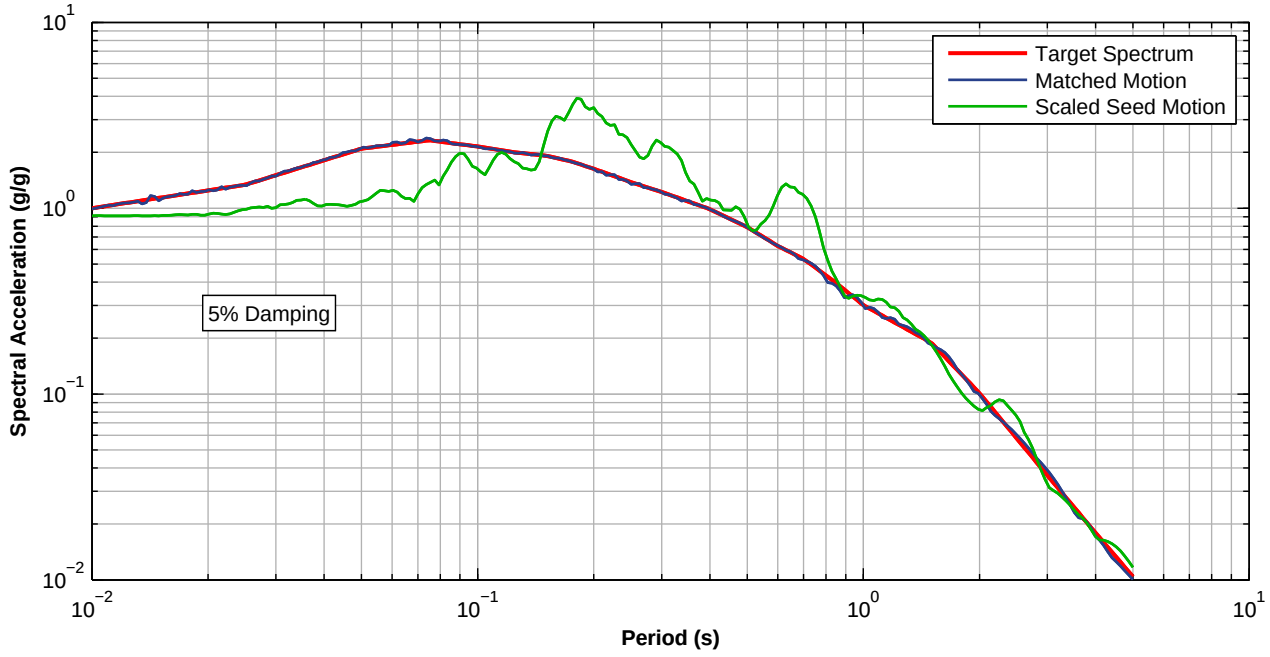


**SPECTRALLY MATCHED NASO MOTION, 090 COMPONENT**
**1978 BASSO TIRENO, ITALY**

Eemskanaal Levee Project
Groningen, The Netherlands

FIGURE A−2e

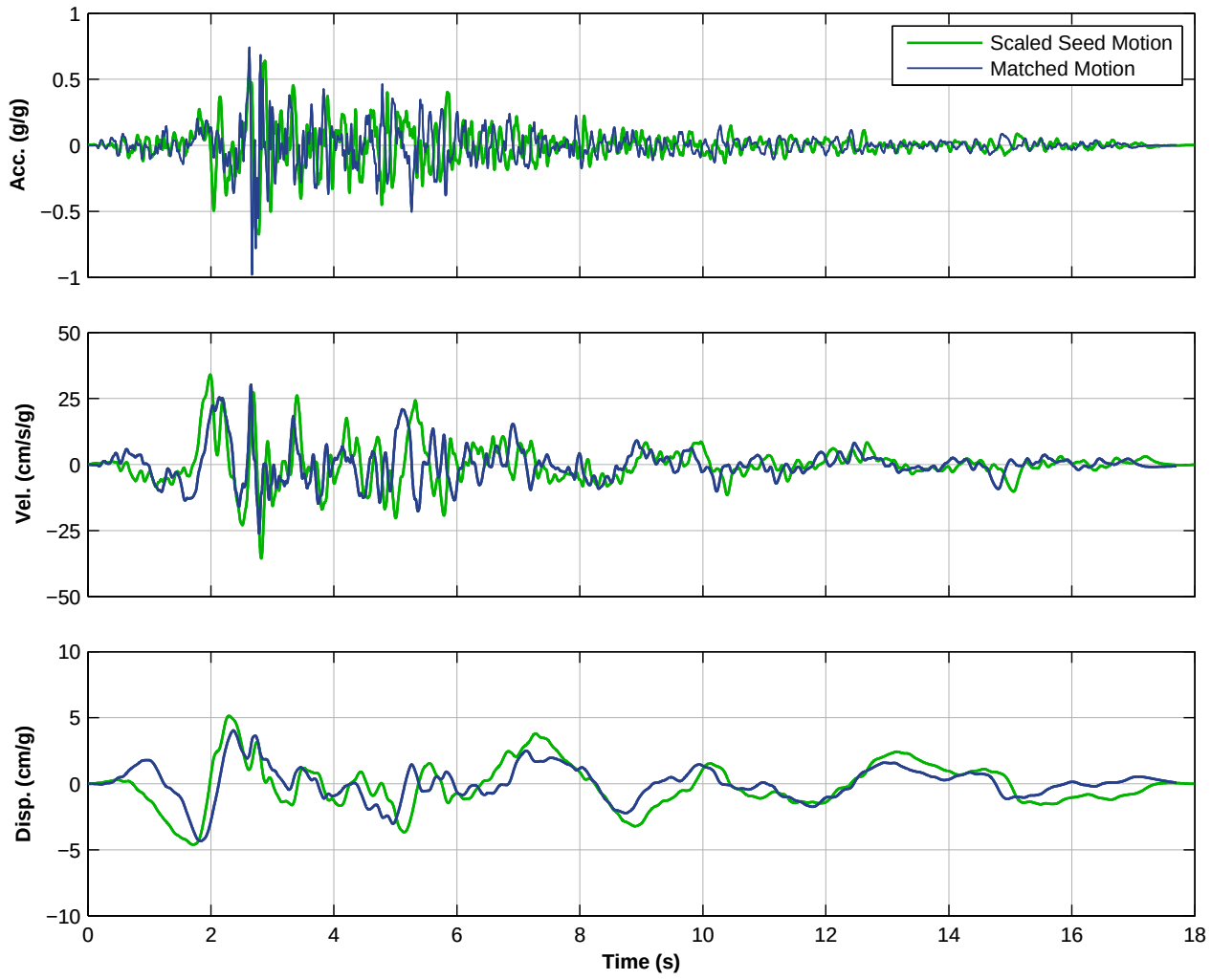


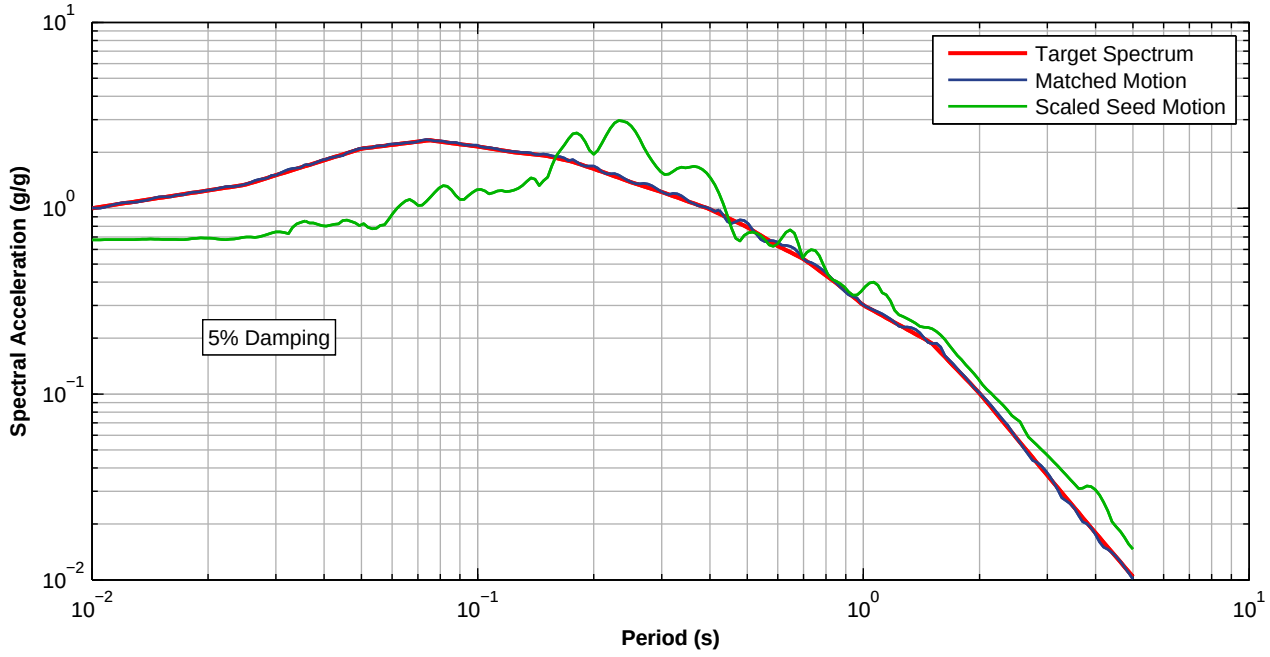


**SPECTRALLY MATCHED GUBBIO MOTION, 090 COMPONENT**
**1984 UMBRIA−03, ITALY**

Eemskanaal Levee Project
Groningen, The Netherlands

FIGURE A−2f

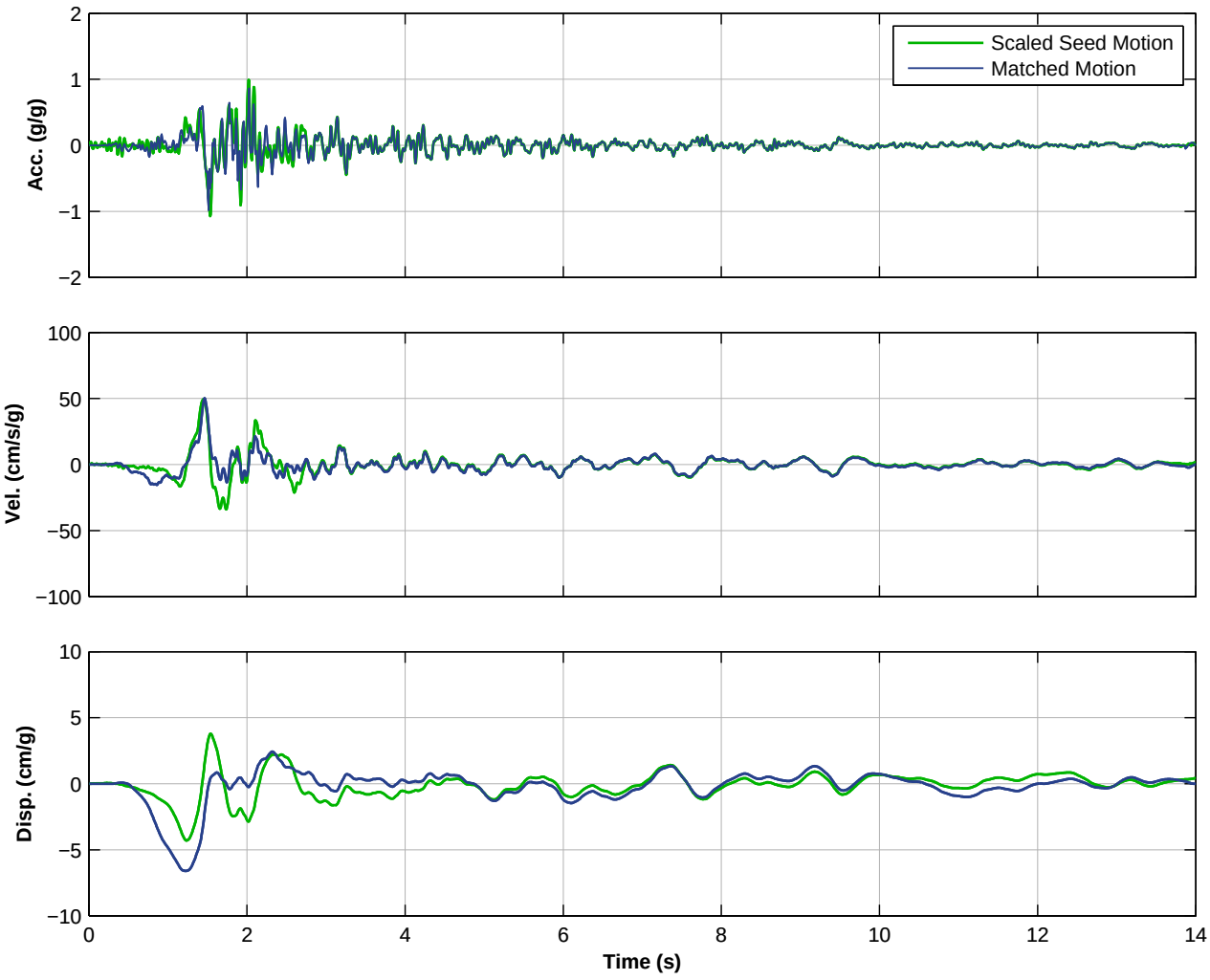


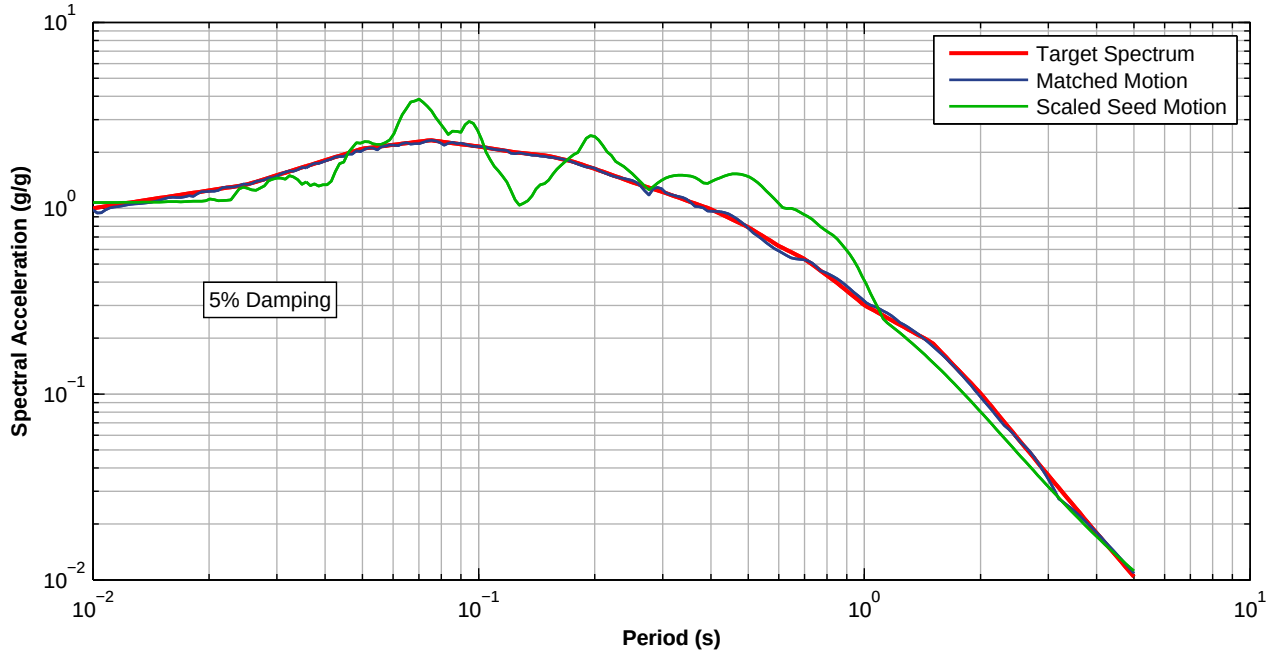


**SPECTRALLY MATCHED NOCERA UMBRA − SALMATA MOTION, 270 COMPONENT**
**1997 UMBRIA MARCHE (AFTERSHOOCK 1), ITALY**

Eemskanaal Levee Project
Groningen, The Netherlands

FIGURE A−2g

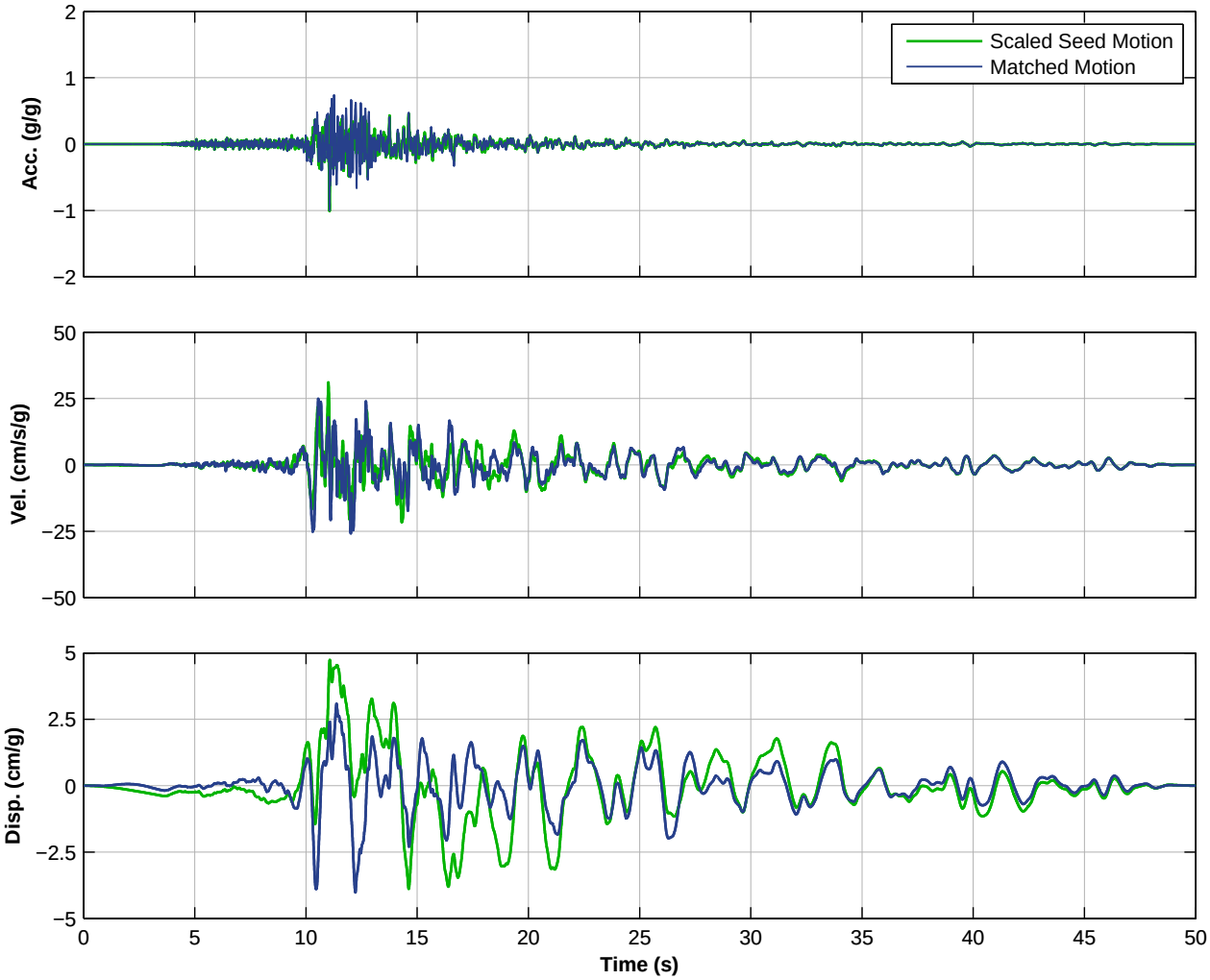


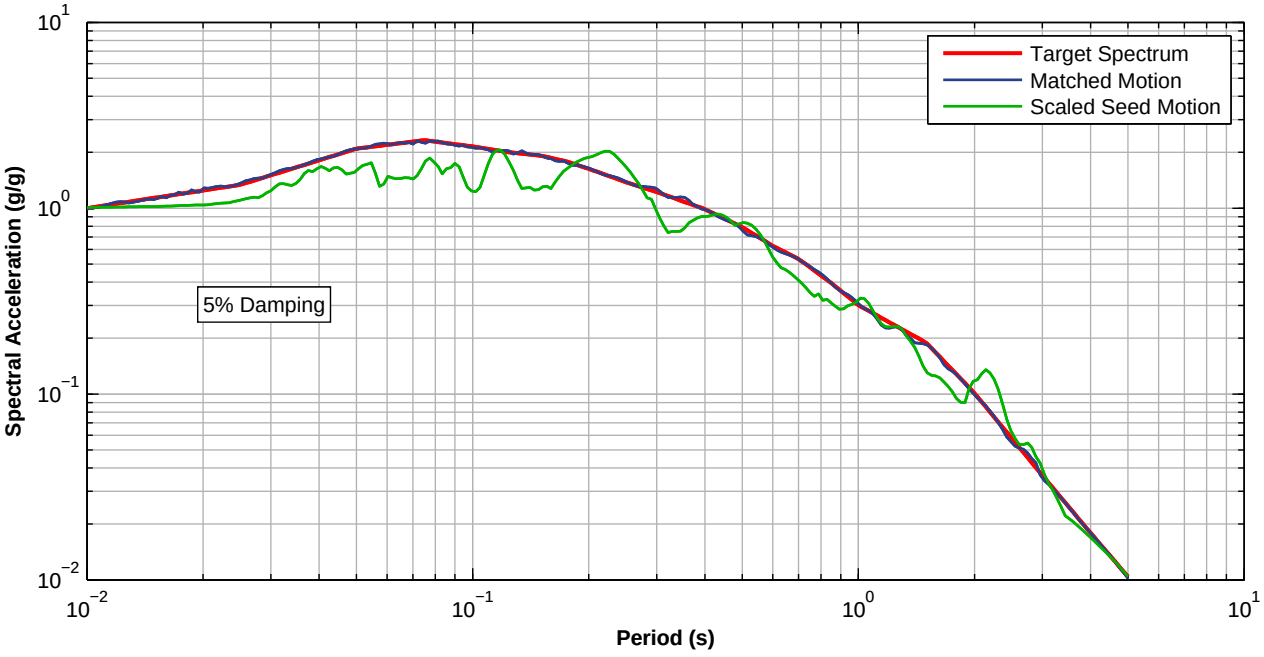


**SPECTRALLY MATCHED SULMONA MOTION, N COMPONENT**
**2009 L'AQUILA (AFTERSHOCK 1), ITALY**

Eemskanaal Levee Project
Groningen, The Netherlands

FIGURE A−2h

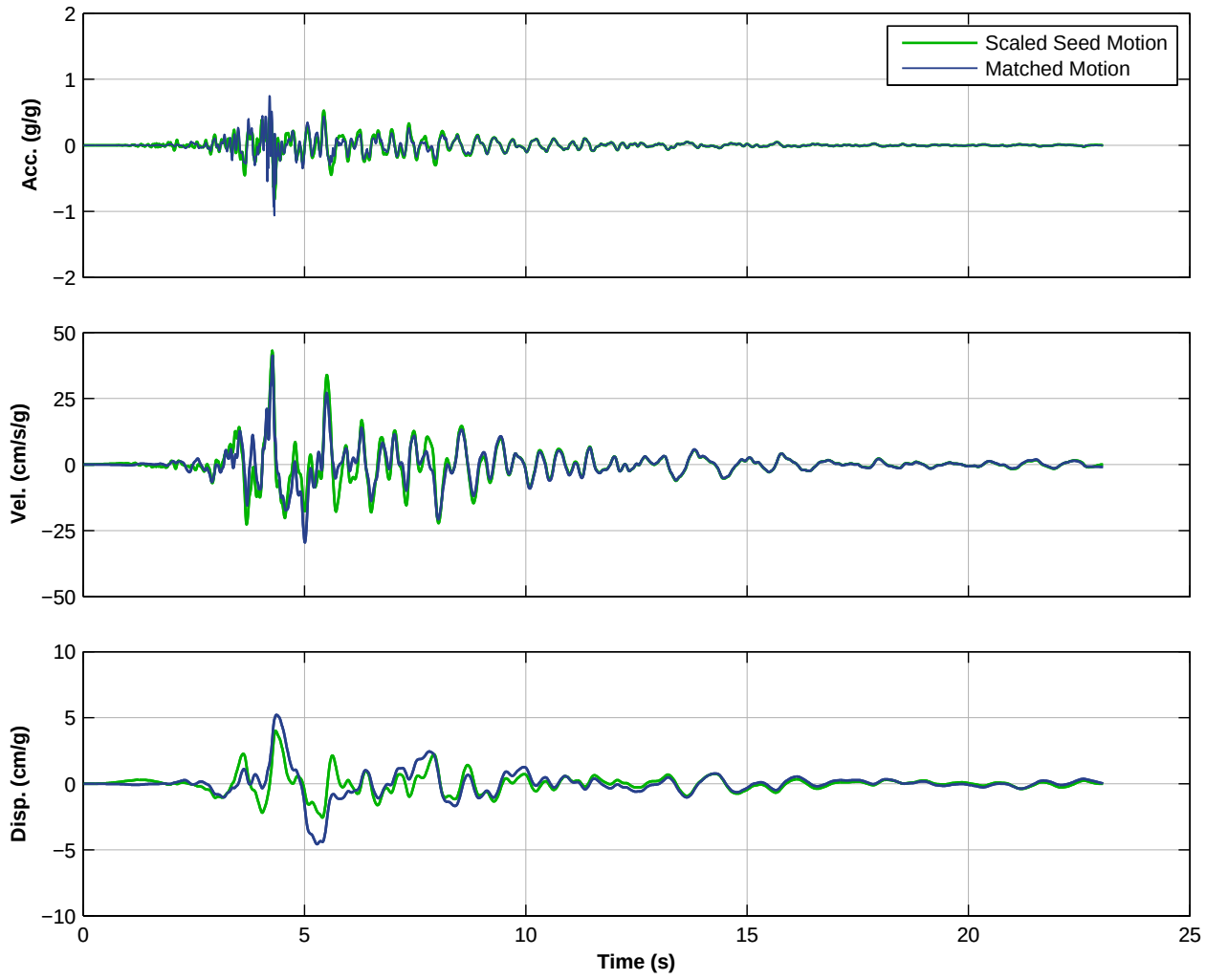


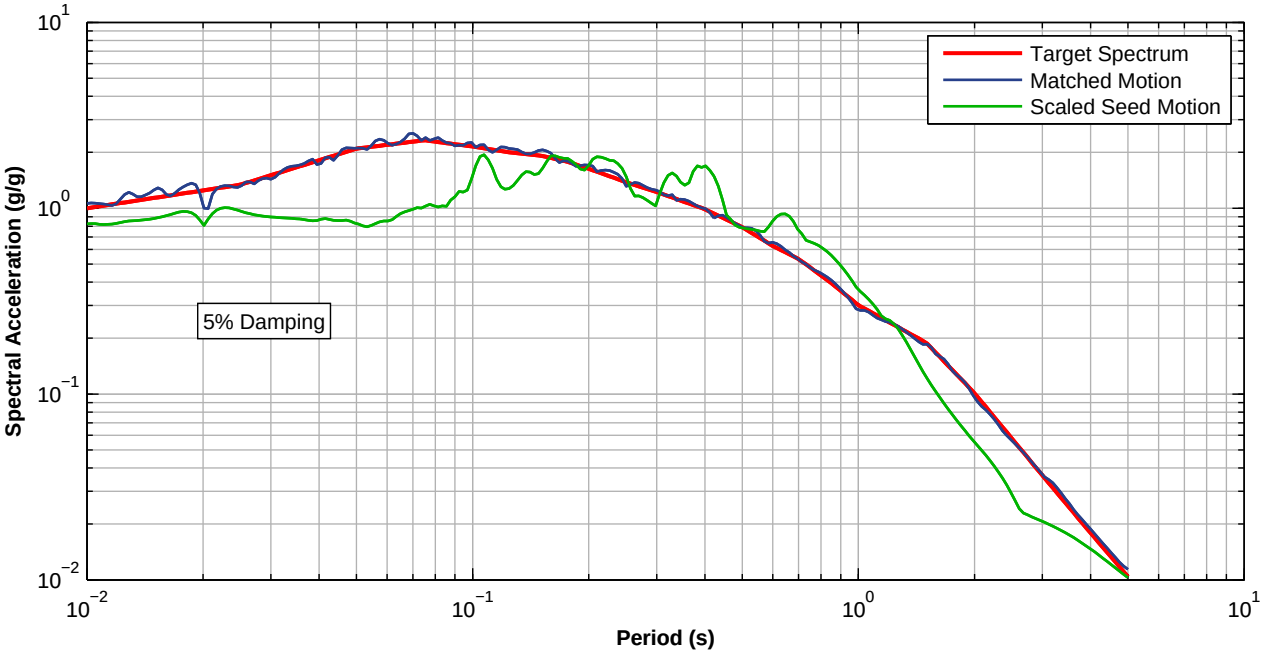


**SPECTRALLY MATCHED KARPERO TOWN HALL MOTION, NS COMPONENT**
**1995 KOZANI (AFTERSHOCK), GREECE**

Eemskanaal Levee Project
Groningen, The Netherlands

FIGURE A−2i

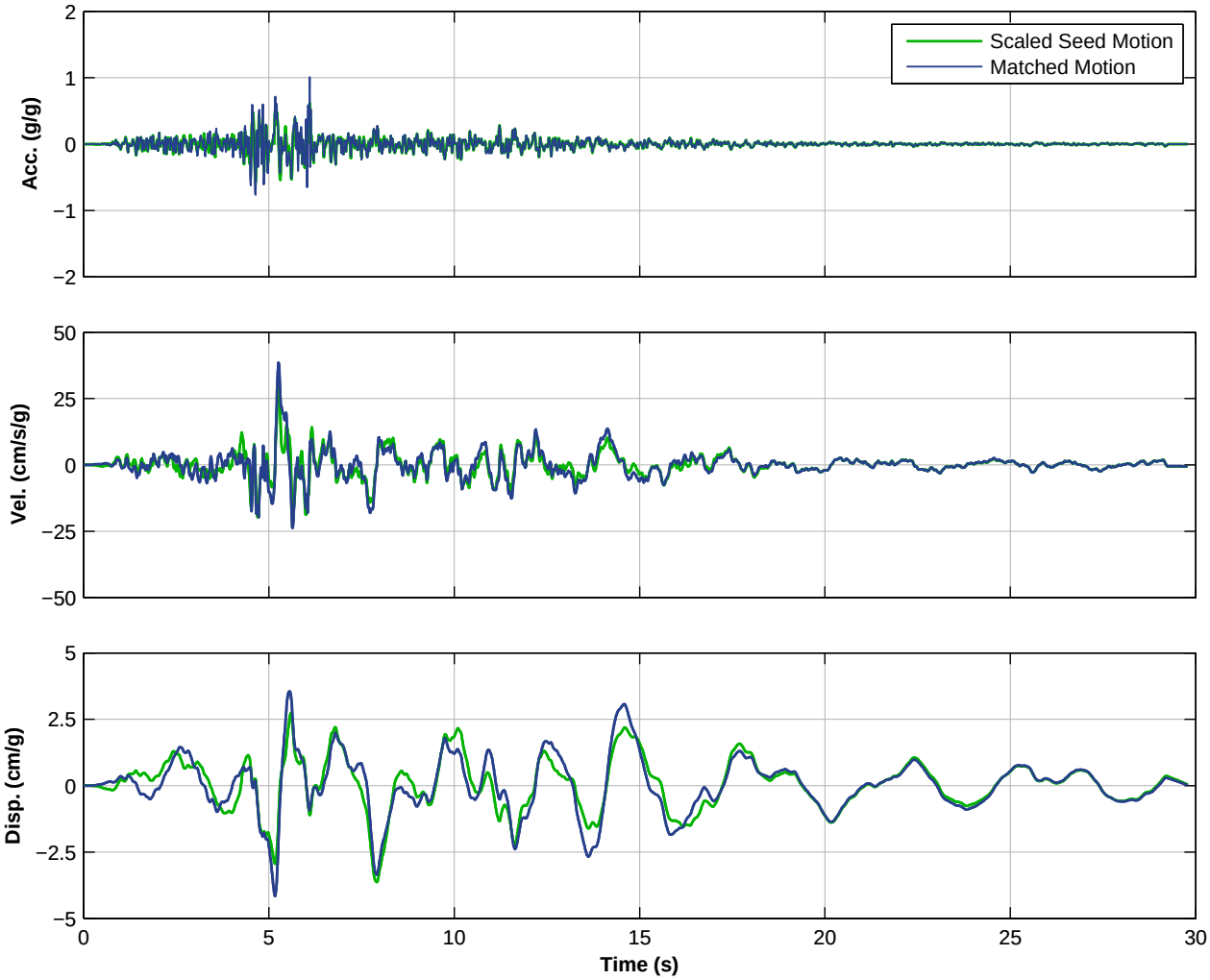


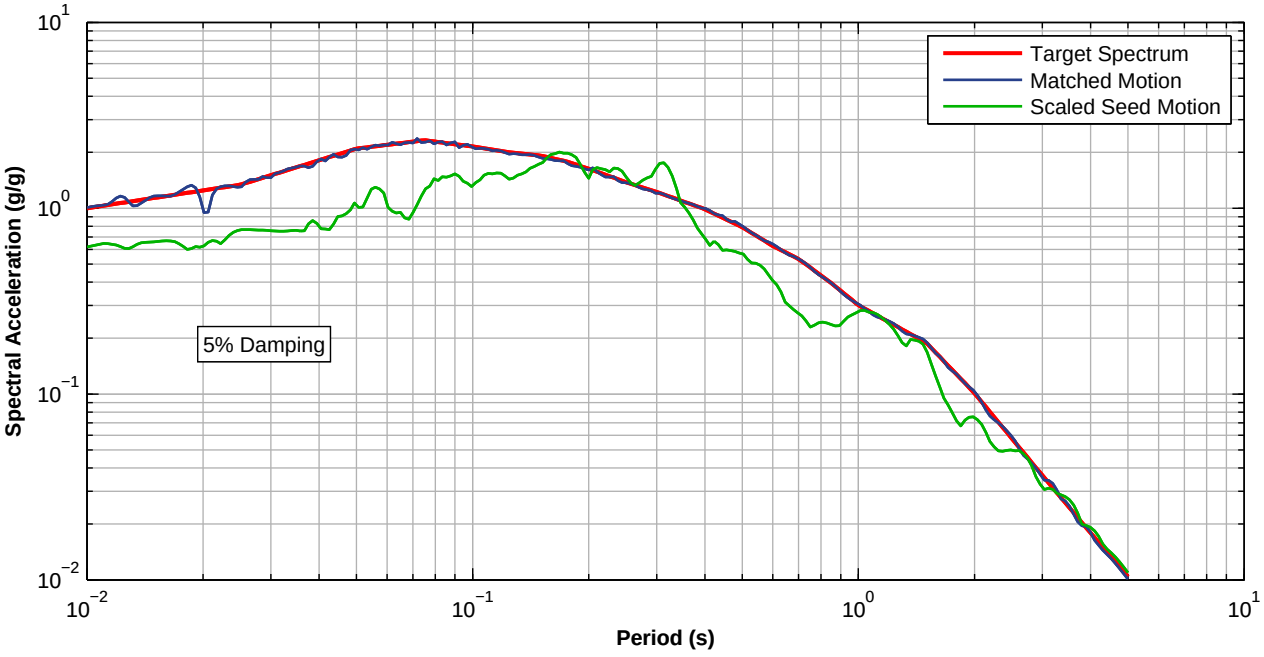


**SPECTRALLY MATCHED LDEO STATION NO. C1059 BV MOTION, EW COMPONENT**
**1999 IZMIT (AFTERSHOCK), TURKEY**

Eemskanaal Levee Project
Groningen, The Netherlands

FIGURE A−2j

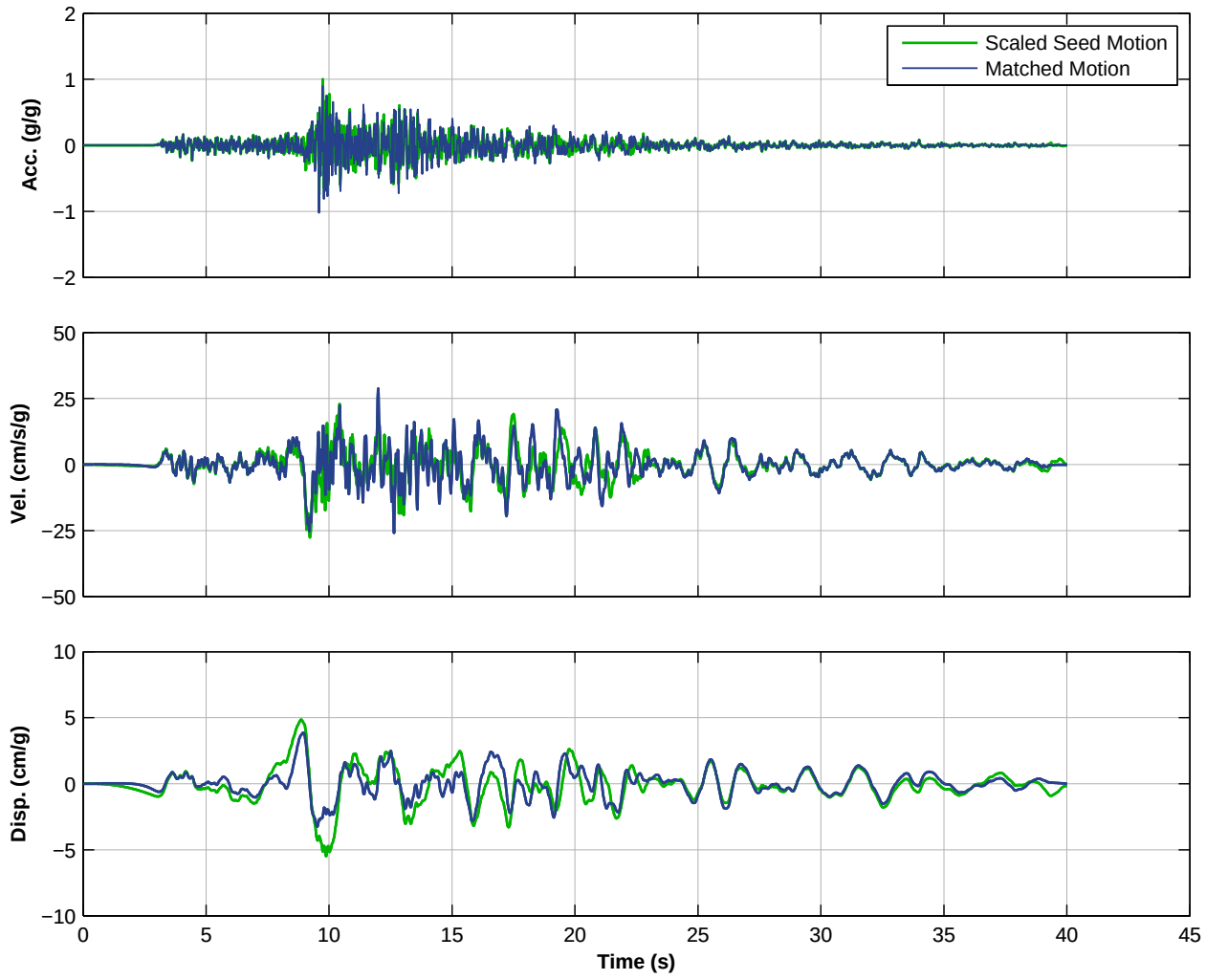


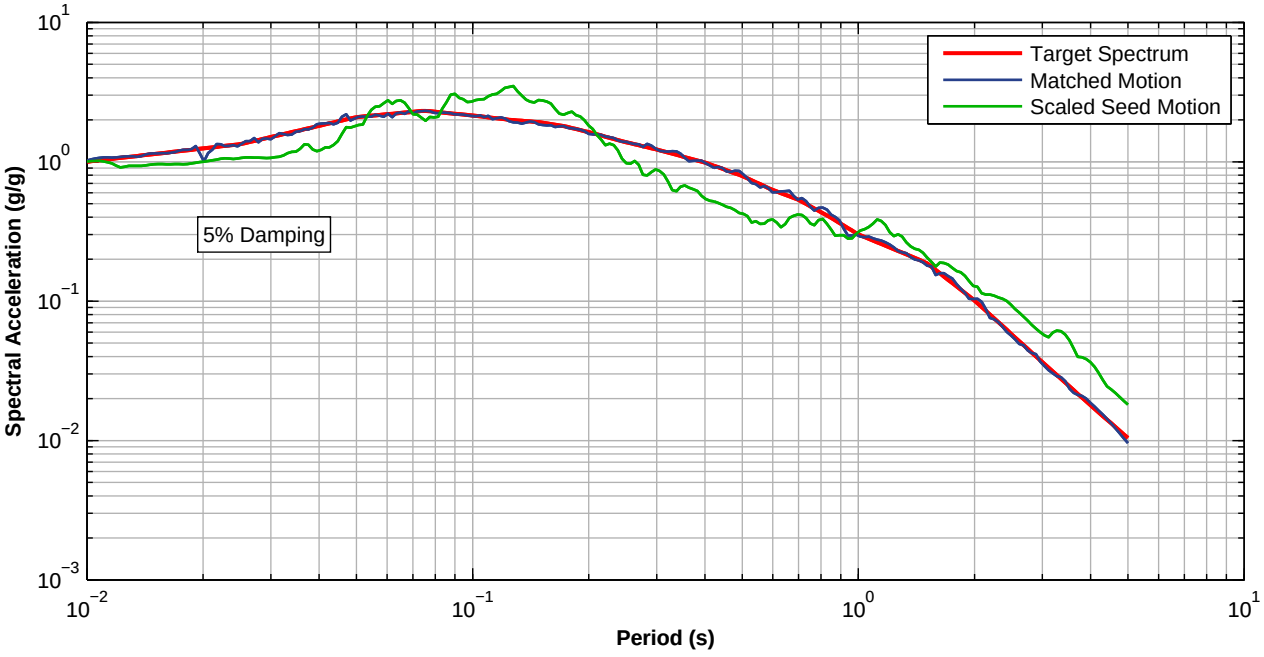


**SPECTRALLY MATCHED CHILAO FLAT RNGR STA. MOTION, E COMPONENT**
**2008 14383980 EQ., USA**

Eemskanaal Levee Project
Groningen, The Netherlands

FIGURE A−2k